INTERMETALLICS AND ALLOYS FOR FUEL CELL APPLICATIONS

A Dissertation

Presented to the Faculty of the Graduate School

of Cornell University

in Partial Fulfillment of the Requirements for the Degree of

Doctor of Philosophy

by

Tanushree Ghosh

February 2010

INTERMETALLICS AND ALLOYS FOR FUEL CELL APPLICATIONS

Tanushree Ghosh, Ph. D.

Cornell University 2010

In the search of better catalysts for fuel cells, synthesis of several intermetallic compounds and alloys as nanoparticles has been investigated. In order to obtain these materials as catalysts for fuel cells, chemical co-reduction of precursors in the absence of surfactants with suitable reducing agents has been chosen as the method of synthesis. This work was done in collaboration with combinatorial groups and electrochemists for identifying potential catalysts and electrochemically evaluating them.

Starting with PtPb, the scope of this method has been extended to obtain Pt intermetallic compounds and alloys with metals across the periodic table with sodium naphthalide as the reducing agent. The sodium napthalide method has been compared side by side with the sodium borohydride method for metals which can be reduced by both. Other reducing agents have also been explored.

PtPb synthesis using sodium naphthalide has been investigated in detail as a case study. Factors affecting room temperature crystallization of PtPb and contributing to low activity observed previously have been identified and addressed by changing the Pt precursor and post reduction work-up. Extending to Pt-Ti, additional factors, which need to be considered for highly reactive metals have been identified. Each of the parameters involved (metal precursor, reducing agent, reducing agent and precursor concentrations, reaction solvent, stirring time, reaction temperature, post reaction

washed and annealing) have been analyzed in depth for co-reduction of Pb, Ti and the elements lying in between in reactivity. The observations and inferences in each case have been discussed. Alloy and intermetallic phases of Pt with Ni, Mn, Cr, V, Cd and Hg have been synthesized as nanoparticles. Powder X-ray diffraction, SEM and TEM (scanning and transmission electron microscopy respectively) imaging, surface area measurements (using BET isotherm) and energy dispersive X-ray analysis (EDX) have been performed on all phases mentioned above. In some cases, IR, TGA (thermogravimetric analysis) and MS (mass spectroscopy) studies have also done on these phases in-order to identify contaminants.

Several of these phases have shown significant activity for oxidation of formic acid. The electrochemical evaluations have been discussed.

Challenges encountered in obtaining these materials clean with the sodium napthalide method have been discussed and are being addressed with other reducing agents like nBuLi.

Lastly, in collaboration with the Adzic group in the Brookhaven National Laboratories, activity of PtPb for the oxygen reduction reaction in both nascent and modified form (with monolayer of Pt deposited by underpotential deposition) has been studied. Pd alloys and intermetallic compounds with Pb and Fe have also been synthesized, characterized and similarly evaluated. All these materials were found to active and stable catalysts for the oxygen reduction reaction. Initial experiments were done with Pt_3Cr and PtNi.

BIOGRAPHICAL SKETCH

The author was born on 19th October, 1981 in Kolkata, India. She received her school education from Bhartiya Vidya Bhavan (BGKV), Kolkata and graduated with a degree in science in 1999. She did her Bachelor (with Honors) in Chemistry from the prestigious Presidency College, Kolkata. It is here, that her interest in science and her philosophy of life started taking shape. Graduating from Presidency in 2002, she went on to the Indian Institute of Technology, Kanpur (IIT Kanpur) to receive a Masters in Chemistry. She worked with Prof. Manas Ghorai for her Masters research and received the award for the best Masters Research work in Chemistry, in 2004. She also worked as a summer intern at the Indian Association for the Cultivation of Science (IACS), Kolkata, with Prof. Shankar Prasad Bhattacharya in the summer of 2003. After completing her Masters from IITK in 2004 she joined Cornell University to pursue a Ph. D. in Chemistry. At that point, her field of interest and research background was organic chemistry and on completing course work in Cornell, she joined Prof. David B. Collum's research group to work with Lithium enolates. However, she increasingly started to feel the need to coincide her goals in life with her research, by directing the latter towards solving some of the issues she cared deeply about. After working for a year with Prof. David B. Collum, she decided to switch research groups, and decided to join Prof. Francis J. DiSalvo's group to help in the efforts to solve the energy and climate crisis. There, she spent the last four years exploring synthesis of Pt alloy and intermetallic compounds as nanoparticles, and their applications in fuel cell catalysis. She presented at several conferences (including Gordon Fuel Cell conference 2007, AIChE 2007 and ACS 2009) and received the 2008 outstanding student award from the International Precious Metal Institute (IPMI).

In 2008, she also worked in Prof Radoslav Adzic's research group at the Brookhaven National Laboratories for a period of three months. During her years in Cornell, she volunteered for Asha for Education; a worldwide organization facilitating education of underprivileged children in India. She was involved with several projects and schools in India, held several different posts in the organization and was the co-ordinator of its Cornell chapter for a year. Her work with Asha completed her experience in Cornell and contributed significantly towards her personal development. After receiving her Ph.D. from Cornell, she'll start working with Intel Corporation in Chandler, Arizona. She will continue working with Asha and plans to join other humanitarian efforts, to champion the causes of the underprivileged.

To Chotomama and Chotoma.

ACKNOWLEDGEMENTS

As I start writing this section, I feel very overwhelmed thinking about all the things that I'd like to say to all the people who helped me get here, and knowing that I will not be able to say it all.

First and foremost, I would like to thank Prof. Francis J. DiSalvo, for being my advisor. Going through my graduate school years in his group, I have developed great appreciation for his depth of knowledge and his sympathetic demeanor towards his students. Having him as my advisor always made me feel like I have someone with whom I could share all my problems. I feel extremely fortunate, to have had him as my Ph.D. advisor, and as I go through life, I will try my best to take forward everything he has taught me.

I would also like to express my gratitude towards Prof. Radoslav Adzic, whom I worked with in the fall of 2008. His devotion to his research and his concern for his students (which I experienced several times while working with him for only 3 months) has touched me deeply. I am also thankful to him for giving me an opportunity to work in the Brookhaven National Laboratory, which was an invaluable experience for me.

I would like to thank my minor advisors, Prof. Hector D. Abruña, Prof. Ulrich Wiesner and Prof. Bruce vanDover (who had kindly agreed to act in place of Prof. Wiesner during my dissertation defense, given Prof Wiesner's scheduling conflict for the same). I feel extremely fortunate to have had the opportunity to work with such brilliant, accomplished and caring professors.

I don't know how to best acknowledge Dr. Paul F. Mutolo's help during my years in the DiSalvo group. He was a friend to whom I could go to for every advice, from

(resume and career advice to address research blues). Without Paul's guidance during some very difficult times, I don't think I could have made through.

I have had the very good fortune of having very committed undergraduate students working with me, Marilyn Weiss and Jennifer McInnis. I would especially like to thank Jenny, for when she started working with me, I myself was learning the techniques (since I came from an organic background into a solid state/material science group). She was more like a friend, who made going through the woes and frustrations of those initial days much easier.

I would like to thank the past and present DiSalvo group members, namely Neal Abrams, Liliana Viciu, Jesse Reiherzer, Heather Edvenson, Mark Dreibelbis, Yongkwan Dong, Raymond Burns, Minh Nguyen, Hao Chen, whom I have known and worked with for the past four years for their support. I would specially like to thank Dr. Hideki Abe, Dr. Chandrani RoyChowdhury, Dr. Brian Leonard, Dr. Akira Miura and Chinmayee Subban for their help. I would also like to thank Dr. Futoshi Matsumoto and Dr. Qin Zhou for doing the electrochemical experiments with my samples and Dr. Miomir B. Vukmirovic at the Brookhaven National laboratories for completing some of the work I started there.

I would like to thank Kelly Case for her sympathetic help whenever I was in need and CCMR facility managers: Mick Thomas and John Grazul for help with SEM and TEM microscopy. I would like to specially thank Mick Thomas for patiently teaching me everything I wanted to know about electron microscopy.

The work described in this dissertation would not have been possible without the insights provided by our collaborating groups in the CFCI. I would like to thank all the members of the CFCI not only for their contributions to my research, but for also teaching me the value of collaborative efforts and teamwork.

I would now like to acknowledge people in my life, back in India, who gave me unconditional love, believed in me and felt proud no matter what I did: my grandparents (Chotoma, Chotodadabhai, Borodadabhai and Thakuma), my uncles (Mejomama, Chotomama and Gopalmama) and Anjupisi, my aunt. Since this is probably the only opportunity I will get to thank them in print, I would like to do so, even though I am at loss for words to convey the depth of my gratitude.

I would like to mention my friends, especially Kalyan Sadhu, Soumik, Saikat, Shantanu, Ananda, Amrita, Anusua, Chris, Maxim, Ashima and Jolita and would like to thank them for being there for me, always.

Lastly, I would like to mention my parents, my sister, Ashish, my husband (whom I met and married while doing my Ph.D. at Cornell) and my mother and father–in-law. Their presence in my life has inspired me to keep going whenever I have felt the urge to quit. I will not try to thank them, as I could not possibly thank them enough. But I will thank god, for surrounding me with all the wonderful people I have mentioned above.

TABLE OF CONTENTS

LIST OF FIGURES

LIST OF TABLES

Chapter 1

INTRODUCTION

1.1 Origin of the project

Advancement in fuel cell technologies for practical applications requires, amongst other things, highly efficient catalysts for cathode and anode reactions. In the quest for more efficient anode reactions with carbon containing fuels, it was observed that some ordered intermetallic compounds, are efficient CO tolerant catalysts even in bulk form[1]. The efficiency of Bi sub-monolayers on stepped Pt single crystals in mitigating CO poisoning of the Pt surface during formic acid oxidation (HCOOH) was demonstrated by Dr. Sean P. Smith, a then graduate student in Prof. Hector D. Abruna's research group in the Department of Chemistry and Chemical Biology, Cornell University, in this doctoral work[2-4]. This work suggested a very wide, and at that time, a completely unexplored class of new materials based on ordered intermetallic compounds that could be promising in addressing fuel cell challenges. This laid the foundation for the Cornel Fuel Cell Institute (CFCI). Established in 2002 by Professors F. J. DiSalvo and H. D. Abruna in order to address material challenges posing impediments in the practical realization of fuel cell technologies, the institute has now grown to include eight research groups working in collaboration with industry and national laboratories (BNL). In addition to work that has repeatedly demonstrated improved performance of bulk PtPb and PtBi towards formic acid and methanol oxidation and their tolerance to CO poisoning, extensive synthesis work has also been done in the DiSalvo group by previous group members: Dr. Laif Alden, Dr. Hideki Abe and Dr. Chandrani Roy Chowdhury to obtain these materials in

nanoparticle form. Electrochemical evaluation was performed on these materials by Dr. Futoshi Matsumoto[5-7]. Obtaining homogenous nanoparticles of specific composition and structure is vital in order to achieve high surface areas and high activities from a small amount of material (keeping in mind the cost and size issues in real fuel cells).

However, the synthesis of these materials as compositionally and dimensionally uniform nanoparticles (both alloys and intermetallic compounds) is a complex problem owing to the many factors that need to be controlled during the synthesis process. In addition the electrocatalysts require clean uncontaminated surfaces. This prevents us from using surfactants (removal of surfactants would require extensive post reaction washes which in turn work against size and composition control). This work delves into the details of understanding and controlling the above mentioned challenges, explores quite a few alternative approaches and demonstrates the potential of these materials not only as anode catalysts, but as cathode catalysts for the oxygen reduction reaction.

The key concepts essential for understanding this research are briefly discussed in the following sections.

1.2 Fuel Cells

1.2.1 Need for fuel cells

The combined effect of depletion of fossil fuel reserves and global warming is a strong motivation for researchers to look into renewable, efficient and clean energy sources. Fuel cells may be able to address the need for more efficient conversion of chemical to electrical energy, since they are not Carnot engines and in principle can

convert the chemical free energy of reaction at nearly 100 % efficiency[8]. Although real fuel cells with 50-60% efficiencies at their operating point and 10 to 100 kW outputs are already realizable, cost and durability issues are the largest barriers to commercial use[3, 9]. These issues can only be addressed by improved materials (membranes, catalysts and catalyst supports)[10].

1.2.2 Concept and construction

Fuel cells and batteries are close relatives. Both have two electrodes – anode and cathode, separated by an ionically conducting medium. In batteries the reactants are included in the packaging. In fuel cells the reactants are supplied from an external power source. Fuel cells produce electricity as long as they are supplied with reactants (the fuel and the oxidant), by converting the energy from chemical reaction directly into electricity. The term 'fuel' used above is generally hydrogen or sometimes other small molecules that are oxidized at the fuel cell anode. The oxidant (oxygen) is reduced at the fuel cell cathode. Taking the simple example of reaction between hydrogen and oxygen:

$$2H_2 + O_2 \rightarrow 2H_2O \qquad \text{(Eqn. 1)}$$

At the atomic scale, hydrogen-hydrogen and oxygen-oxygen bonds are broken while hydrogen-oxygen bonds are formed through re-configuration of the electrons. The energy difference from the processes is released as heat. Since the entire process is extremely fast, this energy is recoverable only as heat. This is the case in combustion engines, where heat is released by combustion of the fuel, which in the above case would be hydrogen. However, this heat energy then needs to be converted into

electricity via intermediate steps. The basic laws of thermodynamic limit the fraction of heat energy that can be converted to other forms of energy (mechanical, electrical, etc) to $(T_h - T_c)/T_h$, where T_h is the temperature of the heat source and T_c is the temperature of the heat sink (usually cooling water). The remainder of the heat is rejected into the heat sink. Fuel cells by-passes the heat step by spatially separating the fuel and the oxidant so that the electron transfer happens over an extended length scale, and the electrons moving from the fuel to the oxidant species can be directly harnessed as electrical current. Figure 1.1 gives a simplified diagram of a hydrogen oxygen fuel cell. The spatial separation between the oxidation of the fuel and the reduction of the oxidant is achieved by using an electrolyte, and the electrons flow through the external circuit.

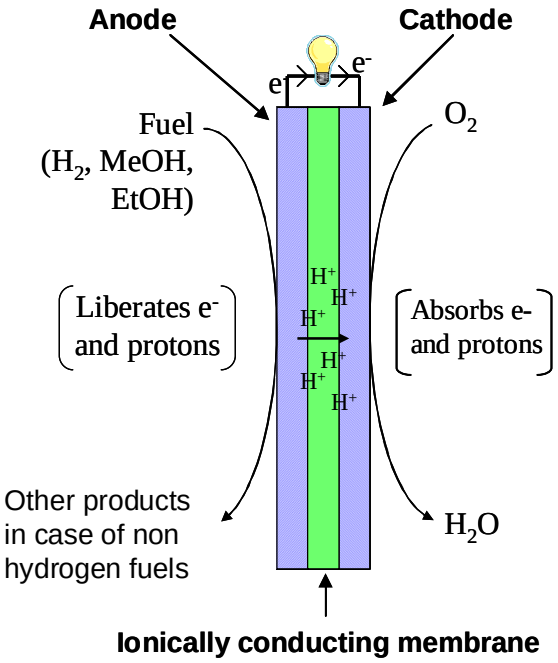

Figure 1.1: A simplified schematic diagram of a fuel cell.

Fuel Cells cannot convert all the enthalpy of reaction (heat at constant temperature and pressure) to electricity. Rather, a small amount, $T\Delta S$ (where T denotes absolute temperature), is rejected as heat. As shown in equation 2:

$$E^0 = \frac{\Delta G^0}{nF} = \frac{\Delta H^0 - T\Delta S^0}{nF} \qquad \text{(Eqn. 2)}$$

where E^0 is the cell potential at standard conditions, ΔG^0 is the free energy of reaction, ΔH^0 is the enthalpy of reaction and ΔS^0 is the entropy change in the reaction. T, n and F are the absolute temperature, number of moles of electrons transferred in the redox reaction and the Faraday constant respectively. ΔG^0 (= nFE^0) is the thermodynamically obtainable electricity from a fuel cell. At room temperature, the difference between ΔH (the heat of reaction) and ΔG (the free energy of reaction) is small, on the order of 5-10%.

Depending on the electrolyte the fuel cells are categorized into five major types. These types differ in materials used, temperature range of operation, fuel tolerance and performance. Table 1.1 gives a summary of different types of fuel cells and their major characteristics.

Table 1.1: Types of fuel cell technologies[11].

Fuel Cell Type	**Electrolyte**	**Conducting Ion**	**Operation Temperature**	**Features**
Polymer Fuel: high purity H_2	$CF(CF_2)_nOCF_2SO_3^{2-}$	H^+ (hydrated)	60-80	High power density, Pt catalyst, must be kept wet, poisoned by CO
Direct methanol Fuel: CH_3OH	$CF(CF_2)_nOCF_2SO_3^{2-}$	H^+ (H_2O, CH_3OH)	60-120	Medium power density, low efficiency, high Pt content
Alkaline Fuel: H_2	KOH	OH^-	90	High power density, Pt catalyst, cannot tolerate CO
Phosphoric acid Fuel: H_2	H_3PO_4	H^+	200	Medium power density, Pt catalyst, less CO sensitive
Molten carbonate Fuel: H_2	Li_2CO_3/K_2CO_3	CO_3^{2-}	650	Low power density, Ni catalyst, needs CO_2 recycle
Solid oxide Fuels: H_2, CH_4	$Zr_{0.98}Y_{0.08}O_{1.96}$	O^{2-}	700-1000	Medium -high power density, No CO sensitivity

1.2.3 Challenges and research

The simplistic picture of fuel cells portrayed in the above section has numerous hidden challenges. The major steps in the process include: reactant transport, electrochemical reaction, ionic and electronic transfer (through the electrolyte and the electrode respectively) and product removal. The first and the last step require fast and continuous supply of fuel and oxidant and removal of the reaction products. A combination of flow field plates and porous electrodes are employed to achieve these goals. For example, in PEMFCs (polymer electrolyte membrane fuel cells) 'flooding' by product liquid water blocks oxygen from entering pores. Since electrochemical reactions are necessarily heterogeneous (can take place only at the electrode electrolyte interface), the current produced by the fuel cell is directly proportional to the total surface area where the reactants, the electrode and the electrolyte can meet. Since high power densities are necessary for most applications, high current densities are necessary. High currents mean a high reaction rate. Choosing a proper catalyst is important to achieve fast reaction kinetics. This poses a critical challenge, especially for low temperature fuel cells. Proper designing of the reaction zones is also vital. The electrolytes in fuel cells have to be made as thin as possible to lower the resistance of the ionic medium by minimizing the distance over which ionic conduction needs to occur.

Of the different types of fuel cells described in the previous section, PEM (polymer electrolyte membrane) fuel cells have been of central interest, since they can be operated at close to ambient temperature range (-20 ^{o}C to 80 ^{o}C) and are therefore, the most practical for commercialization of this technology in automobiles and portable electronics.

Hence, we confine ourselves to discussions pertinent to PEM fuel cells. The major challenge impeding the success of the fuel cell technology lies on developing new materials for membranes, catalyst supports and electrocatalysts. The electrocatalyst is specific to the fuel used in the anode. The simplest fuel is hydrogen, while small, single carbon molecules like formic acid and methanol are also being considered. The next sections discuss in details each of these areas: membranes and electrocatalysts (including catalyst supports). Here, we will briefly state some other issues faced with hydrogen fuel cells which caused people to look elsewhere for fuels.

1.2.3.1 Other issues with hydrogen fuel cells

Hydrogen as fuel is very attractive, since its use in fuel cells for energy production would give zero carbon emissions. Of course, the hydrogen would have to be generated in a carbon free manner, perhaps using solar energy to split water. Also, the oxidation rate of hydrogen on a Pt anode catalyst is very fast, generating high current densities under fuel cell operating conditions. These factors make hydrogen the fuel of choice for fuel cell vehicles as they can be twice as efficient as conventional internal combustion engine technologies and can also incorporate other technologies for increasing efficiency [12]. However, generation of clean hydrogen, along with its storage and production are the some of the issues plaguing this seemingly ideal solution. Current hydrogen fed fuel cells need to be accompanied either with reforming units, or hydrogen storage tanks (which typically have low capacity) as energy storage density for hydrogen is poor compared to liquid hydrocarbons[13]. Power densities express how much power can be produced per unit volume (volumetric power density) or per unit mass (gravimetric power density). Combustion engines and batteries have higher power densities than hydrogen fuel cells. Especially in volumetric power density, the

later lags far behind[10]. Currently there are three principle hydrogen storage technologies available: high pressure gas storage, cryogenic storage of liquid hydrogen near 20 K and hydride storage[14].Given the interest in hydrogen as a fuel, serious research efforts are continuing to improve gravimetric and volumetric energy densities for hydrogen storage. These efforts include approaches like compression and liquefaction. Material approaches to hydrogen storage involve materials like metal hydrides, metal organic frameworks, clathrates, chemical hydrides and nanoscale carbons in which hydrogen can be chemisorbed or chemically bonded to atoms in the bulk providing high gravimetric and volumetric hydrogen density. Metal hydrides and complex hydrides are being investigated for both reversible and irreversible hydrogen storage with recent approaches to improve their hydrogenation and dehydrogenation properties[15]. The US DOE has set 90 g/kg and 81 g/L as standards for hydrogen storage to be attained by 2015 to implement wide-scale application of hydrogen technology in transport[16]. Current hydrogen production technologies involve electrochemical or chemical generation of hydrogen. Electrochemical generation of hydrogen involves electrolysis and the resulting hydrogen can be very clean and carbon monoxide free. This method has been used for on-board production of hydrogen in buses (electrolysis of KOH)[17]. However, the maximum energy efficiency of the whole cycle (electric energy –hydrogen- electric energy) is only 30 %. Much higher efficiencies can be obtained with batteries (e.g. 80 % for lead acid batteries)[18, 19]. Chemical production of hydrogen on-board vehicles (predominantly from methanol or ethanol) is less useful as the carbon monoxide content is high in spite of best research efforts till date[17]. CO is known to poison the electrocatalyst by adhering to the catalytic sites. Chemical hydrogen production at fueling stations can be much better regulated and much more efficient removal of carbon monoxide can be achieved. However, in case of on-site production of hydrogen at fueling stations,

issues with storage and fueling safety arise. The bottom line for 'clean hydrogen' technology rests on the clean generation of hydrogen; however, with current technologies production of hydrogen from renewable sources is much more costly than hydrogen production from fossil fuels. Research is ongoing to explore a number of more efficient hydrogen production technologies. These include photochemical and photoelectrochemical routes using solar energy, thermolysis using nuclear reactor waste heat or solar concentrators, electrolysis using low carbon electricity and catalytic and chemical conversion routes from biomass. Hydrogen production is projected to become much more cost competitive by 2030[20].

1.2.3.2 Major issues with MeOH and other fuel cells

The issues with hydrogen as a fuel (discussed above) have caused researchers to explore other fuels. Methanol and other alcohols and other small molecules like formic acid have come up as viable options. However, not unexpectedly, each of these comes with issues of their own, requiring research for new electrocatalysts compatible with the fuel. Indeed, a particular fuel (for example formic acid), might be suitable for a particular application (such as for cell phones and other portable electronics).

Methanol has advantages over hydrogen in being a liquid fuel at normal temperatures which has high solubility in aqueous electrolytes and can be stored and transported easily. It also has a high theoretical energy density, about 50 % of that of gasoline[21]. However, methanol suffers from disadvantages of its own, like toxicity (toxic in both liquid and vapor form) and flammability. Most importantly, unlike hydrogen, MeOH is not a renewable fuel. Other alcohols (e.g. ethanol) can be generated from biomass and are preferable in this respect to methanol. Looking into thermodynamics and kinetic for the alcohols, reversible energy efficiency for alcohols is much better than

H_2/O_2 fuel cell (which is only 0.83% at 25 ^oC), approaching unity for the lighter alcohols[21]. However, slow kinetics is an issue with all these fuels given their complex multi-step and multi-electron oxidation[21]. This gives rise to high anodic overpotentials, particularly with the heaviest alcohols. However, research efforts have lead to development of electrocatalysts (particularly bi or multi metallic electrocatalysts) which can significantly improve the kinetics. For example, $Pt_{0.50}/Ru_{0.50}$ alloys decrease the overpotential for MeOH oxidation by 0.2 V compared to pure Pt. The second metal often plays a role in oxidizing the strongly adsorbed intermediate species, such as carbon monoxide, generated during the multi-step mechanisms. For formic acid oxidation, good catalysts are known to promote an alternative mechanism for oxidation thus improving efficiency[22]. Efficiency can also be increased by increasing the operating temperature. However, that requires development of new membrane materials, as traditionally used Nafion membranes are not durable above 120 ^oC to 140 ^oC. The research efforts with electrocatalysts and membranes for DMFCs and such are discussed in the catalyst and membrane section respectively. With Methanol fuel cells, MeOH crossover through Nafion type membranes cause depolarization (voltage loss) of the cathode. This issue, once again, can be tackled only through development of new membrane materials. Also, methanol tolerant cathode catalysts (having no effect on MeOH oxidation) are being developed by some groups to counter the cathode polarization problem. Some of this effort is discussed in the catalysts for fuel cell cathodes section. In summing up, for methanol fuel cells, slow oxidation kinetics with even the best electrocatalysts, catalyst poisoning by adsorbed intermediates (primarily CO for MeOH oxidation) and MeOH crossover are major challenges, which can only be overcome by development of new and improved catalysts (mainly anode electrocatalysts although as mentioned above, MeOH tolerant cathode catalysts could also help) and membranes (with low MeOH

crossover, higher temperature of operation) materials. The issue of slow anode kinetics is also pertinent to other small molecule fuel cells. Developing better (higher efficiency, lower cost) anode catalysts for MeOH and other small molecule oxidation is the primary focus of this work, though we have also explored the potential of our materials in other areas of fuel cell catalysis.

1.3 Membranes

Several different kinds of membrane have been studied for PEM fuel cell applications. Modifications to membranes for hydrogen PEM fuel cells, which are primarily comprised of perfluorosulfonic acid polymers, have been explored in order to accommodate the additional requirements for methanol fuel cells[23]. Standard membrane requirements are high proton/ion conductivity, high mechanical and thermal and chemical durability, and low cost. For methanol fuel cells other requirements include low methanol crossover, low Ru crossover (the anode catalyst for MeOH contains Ru), high temperature operation (for improved kinetics of methanol oxidation and improved electrode tolerance to CO poisoning) and increased lifetime (Nafion membranes have insufficient durability under DMFC conditions for commercial applications). Table 1.2 gives the four major classifications of the different types of membranes. The first two groups consist of fluorinated commercial membranes (including Nafion, most commonly used) and have issues like high methanol cross over and stability in limited temperature ranges. The properties of these membranes are improved by adding organic-inorganic and/or acid –base constituents to produce composite membranes (which comprise the third and fourth group). For example, methanol cross over (MCO) is reduced by modifying the fluorinated and non-flourinated membranes by adding inorganic constituents. Non-

flourinated hydrocarbon membranes were developed for their higher durability and lifetime (especially for high temperature operations)[24]. Addition of inorganic constituents to hydrocarbon membranes also improves their stability[25]. The proton conductivity of the membranes is most commonly improved through the use of additives[26-34]. Membranes with higher proton conductivity than Nafion include membranes modified by addition of inorganic compounds like SiO_2, MoPh (molybdophosphoric acid) and ZrP[21, 23]. Membranes with lowest MCO ratio are poly(1-methylpyrrole) modified Nafion and membranes developed by companies 3P energy and Pall[21]. AMPS (asymmetric based acrylic) membranes have best thermal stability[35]. In summing up, for hydrogen fuel cells, Nafion (perfluorosulfonic acid based) membranes dominate, while for DMFCs, several different alternatives arise, each with its own advantages and disadvantages[21].

Table 1.2: Different types of membrane[23].

1	Nafion Membranes
2	Non-Nafion fluorinated membranes
3	Composite fluorinated membranes Organic-inorganic composite, Acidic-basic composite
4	Composite non-flourinated membranes Organic-inorganic composite, Acidic-basic composite

1.4 Fuel Cell catalysis: avenues and advances

1.4.1 Catalysts for fuel cell anodes

For hydrogen fuel cells, research efforts in catalysis are predominantly concentrated in developing better cathode catalysts. Pt is currently serving well as the anode catalyst producing high power densities with hydrogen as the fuel. In the future, however, keeping in mind the cost and availability of Pt, the need for other catalysts might arise. Also, catalysts tolerant to CO could allow the use of 'dirty' hydrogen, eliminating the need to generate squeaky clean hydrogen. We'll mostly discuss the catalysts for methanol and other small molecules in this section. In order to improve both cost and activity, alloying (often non-noble metal) has proved to be a successful strategy for the development of new catalysts for methanol and other small molecule oxidation. CO is more often than not an intermediate in these oxidative processes and causes catalyst poisoning by adhering to the Pt surface. A second metal can provide oxygenated species at lower potentials for oxidative removal of the adsorbed CO. Pt alloys of Ru, Os, Sn, W, Mo etc. have been investigated, of which Pt-Ru (1:1) alloys have been found to be the most active and is the current commercially used catalyst in DMFCs[36-38]. Optimization of catalyst activity by exploring different catalyst preparation methods and techniques to support these catalysts are ongoing[39], as is the search for less expensive (non-noble metal) catalysts[40] and more durable catalyst supports (discussed in a later section). In fact, in recent years, the focus of research for improved catalysts for small molecule oxidation have been on enhancement of Pt-Ru based materials. These efforts include advancement in nanotechnology leading to synthesis of 3-5 nm particle catalysts[41, 42], surface structure elucidation of the catalysts and refining catalyst composition. However, serious issues still remain with Pt-Ru

alloys as catalysts (like phase separation and Ru leaching under real working fuel cell conditions). Exploring intermetallics as alternative catalysts for small molecule oxidation to counter the shortcomings of Pt-Ru alloy catalysts have been the primary goal of the DiSalvo and other research groups in the CFCI and was a major force behind its establishment in 2002. These issues with Pt-Ru alloy catalysts and previous research in the group with intermetallics will be discussed in greater detail in the alloys vs intermetallics and following sections. Not unexpectedly, the motivation for this work arises in continuation of work done in the group previously.

1.4.2 Catalysts for fuel cell cathodes – the oxygen reduction reaction.

The slow kinetics of the oxygen reduction reaction (ORR) have always been the most critical challenge to overcome and the most limiting factor in the energy conversion efficiency of state-of-the-art fuel cells. Starting with noble metals, the catalytic activities of noble metals towards ORR has been explored for both bulk and nanoparticle materials. Pt and Pt alloys expectedly lead the pack. Of other materials investigated, Cu/Ru and Au (111) surfaces have shown promising results. Au(111) electrodes modified with 1/3 ML Cu, 1/3 ML Ag and Bi(2X2) have shown a two fold increase in the reduction current in alkaline media[43]. Bimetallic catalysts have also been explored[44], of which, Pd/Co on glassy carbon have shown high ORR activities. The Adzic group in the Brookhaven National Laboratories has done significant work in exploring the electrocatalytic activity of metal surfaces modified by underpotential deposition of other metals. They have also introduced a new class of electrocatalysts for the ORR based on the deposition of a monolayer of Pt on different late transition metals like Au, Pd, Ir, Rh and Ru. Pd – M binary alloys and even ternary ones have been shown to have high activity by Adzic[45-47] and other research groups[48]. They have

then combined the two techniques: Pt, Pd, or sub Pt (part of the Pt replaced by a late transition metal) monolayers on Pt or Pd alloys to obtain high activity catalysts with lower Pt loadings[49, 50]. Some of the other noble metal nanoparticulate systems found to be promising include TiO_2 nanoparticles coated with Au monolayers[51], Pd nanoparticles on carbon nanotubes, an Ag/C system[52] and a Ru containing Cheverel phase $Ru_2Mo_4Se_8$[53]. Transition metal N_4-macrocycles like porphyrin complexes (which catalyze oxygen reduction under physiological conditions) and other structurally similar transition metal complexes have also been extensively explored for ORR activities[54-59]. Of the non-noble metal catalysts explored for ORR, Cu [60], Ni [61] and metal oxides like TiO_2 on a Ti surface[62] are worth mentioning. Other metal oxides including spinel, perovskite and pyrochlore structures show high ORR activity in alkaline media[63-65]. In acid media however, they fare poorly in terms of activity and stability, indeed most of them dissolve at low pH. Transition metal compounds and non-metallic counter ions derived from the chalcogenides have also shown remarkable activity towards ORR in the recent years[66-77]. As discussed previously, MeOH tolerant catalysts for ORR are very important for DMFCs as a viable route for countering the MeOH crossover problem. Researchers have shown that the mass activity of Pt in MeOH oxidation decreases significantly with a decrease in particle size from 4.6 nm to 2.3 nm[78]. Accordingly, several preparatory routes have been proposed and explored to synthesize Pt and Pt alloy electrocatalysts as finer particles[79]. Pt/Fe-C and Pt/Co-C have also been reported to be MeOH tolerant electrocatalysts[80, 81]. Of the transition metal chalcogenides, RuSe has shown the most promise as a selective ORR catalyst. The above discussion does not include all those materials being explored as potential ORR catalysts, but a complete review is beyond the scope of this modest section. This thesis mostly originated and mostly evolves around anode (non hydrogen) catalysts; however, we have successfully explored the potential of our materials towards the

ORR in collaboration with the Adzic group in BNL. This work is discussed in Chapter 7.

1.4.3 Catalyst supports

Catalyst support strategies are necessary to achieve high dispersion of the nanoparticles, resulting in stable nanoparticles and increasing utilization of the catalyst surface. Desirable properties for catalyst supports include good electrical conductivity and stability under fuel cell operating conditions. Corrosion of catalyst support causing decline in catalyst activity remains a major challenge. Carbon materials have been a popular choice as catalyst supports given their electrical conductivity, relative kinetic stability in acidic and basic media and high surface area. Different types of carbon blacks have been extensively explored as catalyst supports. Properties of the carbon support (like pore size distribution and surface functional groups of the carbon blacks) have been shown to significantly affect the properties and performance of the supported catalysts[82-86]. Issues like metal nanoparticles sinking into micropores of the support resulting in low activity of the supported catalyst arise from some synthesis techniques. The metal catalyst utilization in a supported catalyst is decided by the electrochemically accessible active area and not the carbon specific surface area but depends on the porosity and pore size distribution in the support. Optimum catalyst loadings also depend on these factors, since even with high loadings of Pt (or other catalyst nanoparticles), activity can be reduced by catalyst particles getting trapped in pores inaccessible to reactants or the Nafion ionomer (electrolyte in PEM fuel cells)[87]. Ketjen black and Vulcan XC-72 are two of the most commonly used carbon blacks. Recently, a lot of attention has been given to nanostructured carbon (most predominantly to different types of carbon nanotubes) and mesoporous carbon

materials[88]. Both single walled (SWNT) and multi walled (MWNT) carbon nanotubes with supported Pt have been shown to give much higher current densities for methanol oxidation than bulk Pt electrodes[89, 90]. This increased activity is attributed to larger surface area and lower overpotential for MeOH oxidation on carbon nanotubes. Although promising, issues like CNT synthesis, loading of catalysts and electrode preparation with CNT supported catalysts need to be further sorted out. Mesoporous materials like mesoporous carbon and mesoporous oxides which are electrically conducting are other materials for catalyst supports being explored extensively. The DiSalvo and Weisner groups in the Cornell Fuel Cell Institute have done a significant amount of work exploring the latter materials. For all the supported materials discussed in this work, Vulcan XC-72 was the support used.

1.5 Catalysts for oxidation of small molecules: background

1.5.1 Alloys vs intermetallics

Materials made from two or more metallic elements can be classified into two major sub-types: alloys and intermetallics. The former refers to a material in which the elemental crystal structure of one of the constituent elements is adopted, but with random site occupancy of each element on the atomic positions. Alloys are also referred to as “solid solutions” given the analogy of solutes dissolving into solution. Intermetallics on the other hand, are true compounds between the constituent elements; having crystal structures with specific sites assigned for the atoms of each constituent element (Figure 1.2 a, b). Alloys typically form between similar elements, while dissimilar elements tend to form intermetallics, similarity here referring to characteristics like size, electronegativity and number of valence electrons.

Intermetallics have more negative free energy of formation than alloys. The enthalpy contribution to the free energy of formation of alloys is not very high, since the work function difference between elements forming alloys is not very large[91]. For many alloys, the entropy of mixing times temperature at room temperature is only a few kilojoules[92]. For example, the ΔG_f of a PtRu 1:1 alloy (current industry standard for anode catalysis in DMFCs) is about -2 kJ/mol of alloy atoms according to theoretical calculations[91]. Intermetallics however, have much higher ΔG_fs since they form between elements with dissimilar electronegativities, which result in large bond enthalpies that contribute significantly to the free energy of formation. PtBi and PtPb are calculated to have ΔG_fs of -63 kJ/mol and -51 kJ/mol, respectively[91]. Hence alloys are less stable thermodynamically and are likely to be more susceptible towards surface rearrangement and phase separation, both known to be issues with PtRu alloy catalyst under fuel cell operating conditions. Also, random site occupancy of alloys results in many different co-ordinations around an individual Pt atom. This limits the 'good' catalysis sites available only to certain regions. For example, the sites with Pt directly adjacent to Ru are believed to be the 'good' catalysis sites in the PtRu alloy: Ru is believed to exist in partially oxidized state (possibly Ru-OH) providing oxygen for oxidation of CO molecules (a reaction intermediate in MeOH oxidation which requires to be oxidized to CO_2) adsorbed on the adjacent Pt atoms[93]. In an alloy, such sites would be found only in regions rich in both elements. The intermetallics on the other hand, with their regular repeating array of surface atoms would ensure homogeneity of the 'good' sites, if they are active. Real catalysts will have multiple crystal planes exposed (either because it is polycrystalline or in nanoparticle form). Therefore, some variation in activity across the surface of the entire sample is expected as different crystal surfaces of a material (e.g. Pt) are well known to show markedly different electrochemical behavior[94-96]. This variation would be found in

both alloys and intermetallics, but the potential advantage that intermetallics could have over alloys if their structure is retained under real catalysis conditions is evident.

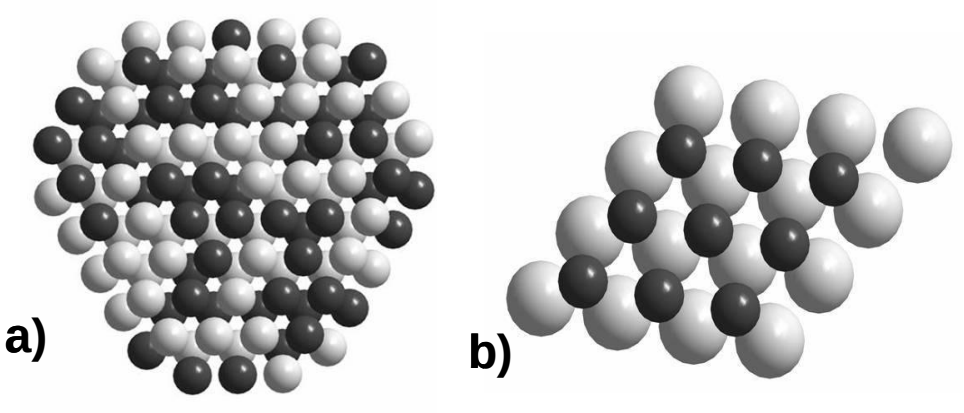

Figure 1.2: a) A possible random arrangement of the 111 surface of Pt-Ru alloy, black spheres represent Pt atoms and grey spheres represent Ru atoms. b) The 001 surface of PtPb intermetallic, black spheres represent Pt atoms and grey spheres represent Pb atoms.

1.5.2 Synthesis of intermetallics as nanoparticles

1.5.2.1 Need for nano-materials

Demand for nano-materials of elemental metals and their alloys are on the rise owing to their remarkable properties. Due to the high surface area of the nanomaterials, the ratio of surface to bulk atoms is very high, making these materials ideal for catalytic application. Also, since most catalysts contain precious metals, the cost comes down significantly when using nanomaterials as higher activity can be obtained from smaller amounts of the catalyst. High surface area nanoparticles are vital for fuel cells in order

to generate the necessary current densities while keeping the cost relatively low. Lastly, the catalytic properties of a material can be drastically altered when it is in nanoparticle form. Au nanoparticles are well known to be able catalyze certain chemical reactions[97] even though in bulk it cannot. It is thus entirely possible that an intermetallic/alloy in nanoparticle form would have markedly different (and hopefully improved!) catalytic properties compared to that same material in bulk.

1.5.2.2 Issues with syntheses

Synthesis of any material as nanoparticles brings some tricky issues into the picture – nucleation of the desired phase and control of size distribution. Adding the terms 'intermetallic compounds' and 'catalyst materials' to the equation further complicates the issue. The former requires nucleation for the specific ordered crystal structure and the later requires the route followed to be devoid of surfactants (often used in solution phase nanoparticle synthesis for maintaining the size distribution by preventing particle agglomeration). The issues with intermetallic nanoparticle synthesis will be discussed in further detail in the next chapter, for now we concentrate on nanoparticle synthesis and extrapolate additional needs for nanoparticles to be used as catalyst materials.

Most conventional methods to make metal nanoparticles by mechanically grinding the material in bulk are unable to reproducibly achieve small particle sizes with narrow size distributions. Particle sizes below about 0.5 μm are difficult to achieve by grinding. Therefore, the synthetic strategy used in this work was to prepare nanoparticles by nucleation and growth, a "bottom up" approach, rather than a "top down" approach. Also, traditional solid state methods involve reactions at very high temperatures to obtain the desired phases also result in particle growth by sintering,

and hence usually cannot be employed for obtaining nanomaterials. Metal nanoparticles for catalytic applications have been prepared by various techniques[98, 99] such as metal vapor deposition, controlled decomposition (usually thermally, photochemically or sonochemically) of zero- or low-valent metal containing precursors, electrochemical reduction, or chemical reduction of metal precursors from solution. The most common technique to make metal nanoparticles remains chemical reduction and precipitation from aqueous or organic solutions[98, 100-104]. Metal cations are reduced by a chemical reducing agent to their zero-valent state in solution where they nucleate and grow into nanoparticles as long as they do not react with the solvent or other included or generated species. The three distinct steps in this event are: reduction, nucleation and growth. In the ideal case of reduction of a metal cation precursor (in absence of interference from any included or generated species), M^{x+} is reduced to M^0. Nucleation occurs when a critical number of M^0 atoms agglomerate so that the rate of growth is larger than the rate of dissolution. After nucleation, the nanoparticle will continue to grow via one or more mechanisms: addition of more metal atoms (alternatively M^{x+} can also attach to the growing cluster and can then be reduced to give M_n), Ostwald ripening and oriented attachment of metal crystallites. The latter requires aligned attachment of the crystallites, unaligned attachment is agglomeration. Generally, fast nucleation and slow growth means smaller nanoparticles and slow nucleation and fast growth means larger nanoparticles, hence the balance of these two rates is vital for achieving the desired size distribution.

Next, the issue of stabilizing the synthesized nanoparticles has to be considered. Metal nanoparticles suspended in solution fuse together to diminish their total surface energy. To keep the metal particles from agglomerating, a repulsive interaction needs to be introduced. The stabilization methods employed can be steric, electrostatic or a combination of both. A steric approach means adding a bulky substance that

chemisorbs or physisorbs to the nanoparticle surface. As two such nanoparticles are brought into close contact with one another, configurational constraints of the adsorbed molecules will keep them apart physically and prevent them from agglomerating. If the particles have sufficiently large surface charge, electrostatic repulsion between the double layers around the particles keeps them from agglomerating. This is the principle of electrostatic stabilization methods. Surface charge can be generated by controlling the pH of the solution and/or by adding charged ligands and their counter ions. Electrostatic stabilization is primarily employed only in polar media. Supporting the nanoparticles by bonding the nanoparticles to the surface of another material also keeps them apart. For example, the Pt and PtRu nanoparticles in fuel cell applications are usually carbon supported[88].

For application of the nanoparticles as catalyst materials, the stabilization issue creates an inherent conflict. The reason for preparing these catalytic materials as nanoparticles is to maximize the surface area of the material so that it is catalytically available. Agglomeration can greatly diminish the surface area per unit mass. However, the stabilizers used to prevent agglomeration and retain the high surface area of these nanoparticles invariably coat the surface of the nanoparticles, which usually prevents the reactants from accessing the surface and prevents catalysis from occurring (i.e. the surface is “poisoned”). Preparing catalyst nanoparticles so that they bind to the surface of a supporting material is one way to prevent agglomeration and maintain a relatively high active surface area. To achieve this, solution phase synthesis techniques need to be first explored for unsupported materials and then extended to trapping them on a support during synthesis. In this work, the support material explored was always Vulcan (Carbon black) keeping the fuel cell applications in mind.

1.5.2.3 Previous work in the group in synthesis and characterization of catalyst nanomaterials

The idea of exploring Pt intermetallics as potential catalysts for small molecules oxidation was inspired in part by the doctoral research of Sean P. E. Smith in Prof. Abruna's group showing the favorable effects of Bi sub-monolayer on stepped Pt single crystal surfaces for the oxidation of formic acid. The increased activity and observed mitigation of CO poisoning, combined with the possible advantages of intermetallics as catalysts led to the desire to synthesize and explore Pt intermetallics as nanoparticles. In the past years since then, significant work has been done in the DiSalvo groups towards understanding the syntheses of intermetallics as nanomaterials. Unlike the syntheses of bulk materials, which has been explored in detail by many solid state chemists, the synthesis of these materials as nanoparticles, for reasons discussed in detail in the previous sections, pose a much greater challenge. The first studies explored the synthesis of PtPb and PtBi nanoparticles by chemical co-reduction using $NaBH_4$ as the reducing agent. Later the syntheses were extended to reactions using sodium napthalide as the reducing agent in search of a stronger reducing agent which could encompass broader range of metals. PtPb is the most explored case of the two. Using $NaBH_4$ as the reducing agent in MeOH solvent, Dr. Chandrani RoyChowdhury, a previous group member was able to synthesize single phase PtPb, Pt_3Pb, PtBi and PtSn as aggregated nanoaparticles with domain sizes between 8-15 nm. These materials were characterized by powder X-ray diffraction, BET surface area measurements, scanning and ultra high vacuum scanning transmission electron microscopy (SEM and UHV-STEM) and energy dispersive X-ray analysis (EDX). Some of these compounds have been found to be active towards the oxidation of small organic molecules such as formic acid, methanol and ethanol.

PtPb exhibited impressive tolerance towards carbon monoxide and sulfur-containing poisons. Chandrani also showed in her work with $NaBH_4$ that choice of precursors and synthesis technique has a profound effect on the electrochemical activity of the products. For example, PtPb prepared using $Pb(MOEEAA)_3$ (where MOEEAA = 2-[2-(2-methoxyethoxy)ethoxy]acetic acid[7] was found to have much higher current density for formic acid oxidation than PtPb prepared from $Pb(C_2H_3O_2)_2$ (lead acetate)[5]. Borohydride reduction was found to give much cleaner end products compared to the other techniques (primarily sodium napthalide reduction) to be discussed below. The ability to carry out the reduction in aqueous or alcohol media is an advantage of the borohydride method. There are typically a wide variety of precursors and consequent side products that are soluble in protic solvents. This is a challenge we are still trying to overcome with the organic solvents required for sodium napthalide reductions. In order to obtain enhanced surface area and prevent particle aggregation, the borohydride reduction technique was extended to the synthesis of supported PtPb nanoparticles on commercially available carbon black: Vulcan. Initial work on the synthesis of ternary phases as nanopowders was also done using sodium borohydride as a reducing agent. Moving on to sodium napthalide, Dr. Laif Alden, in his doctoral research, targeted the synthesis PtPb and PtBi nanoparticles with sodium napthalide as the reducing agent. His work showed that unlike with sodium borohydride, thermal energy needed to be provided by in-situ heating for crystallization/growth of the PtPb phase. The difference between this two is indistinguishable by XRD since the broad pattern obtained could be either due to amorphous material, from an alloy with a broad composition, or from extremely small crystalline particles. Reaction temperature, method of injection, stirring time after injection and the method of exposure to air following work-up influenced the properties of the products (most notably, the domain sizes of the PtPb particles). Particle domain size was found to saturate after a certain

temperature and stirring time. These results, along with lower activity of PtPb particles synthesized by sodium napthalide reduction compared to those from borohydride reduction lead to an initial hypothesis that the sodium napthalide method might not be generating clean particles. This dissertation was started with the goal of understanding the underlying factors affecting the synthesis and properties of these particles. Improved method for sodium naphthalide reduction to synthesize PtPb nanoparticles with higher activities is discussed in detail in Chapter 2. The insights obtained were used to explore the limits of sodium napthalide reduction in order to obtain products containing more electropositive elements and establish general guidelines for doing so (Chapter 3 and 4). As work progressed, other reducing agents (Chapter 5) were explored in order to address the challenges inherent to sodium napthalide reduction. It should be mentioned here, that methods like grignard reduction, the polyol process and hydrazine reduction had already been explored by the researchers mentioned above[105, 106]. The results from those are not pertinent to this work and won't be discussed here. Lastly, as will be discusses in Chapter 3 in detail, Dr. Hideki Abe, a post doctoral researcher in the DiSalvo group, had initiated exploring the potential of sodium napthalide reduction for synthesizing Pt-Ti phases[6] and synthesized ordered (Pt_3Ti) and disordered phases which showed promising activity towards MeOH and formic acid oxidation.

Lastly, the role of the combinatorial sub-group in the CFCI in helping to choose compositions is important to note. In order to expedite the search for remarkable catalyst materials, a combinatorial method was developed using sputtering of different materials as thin films, followed by electrochemical testing of the film to rapidly screen for active catalysts. Often the synthesis of nanoparticles of a particular phase was driven by combinatorial screening results given our ultimate goal of developing more efficient catalysts. This is why systems such as Pt-Ti and later Pt-Cd and Pt-Hg

(Chapter 6) were explored in otherwise seemingly random (non-periodic or non-systematic) ways.

REFERENCES

1. Casado-Rivera, E.; Gal, Z.; Angelo, A. C. D.; Lind, C.; DiSalvo, F. J.; Abruna, H. D., Electrocatalytic oxidation of formic acid at an ordered intermetallic PtBi surface. *Chemphyschem* **2003,** 4, (2), 193-199.

2. Smith, S. P. E.; Abruna, H. D., Structural effects on the oxidation of HCOOH by bismuth modified Pt(111) electrodes with (110) monatomic steps. *Journal of Electroanalytical Chemistry* **1999,** 467, (1-2), 43-49.

3. Smith, S. P. E. Sensitivity to surface structure and composition of the electrocatalytic oxidation of formic acid at bismuth modified, single crystal platinum electrodes. 2000.

4. Smith, S. P. E.; Ben-Dor, K. F.; Abruna, H. D., Poison formation upon the dissociative adsorption of formic acid on bismuth-modified stepped platinum electrodes. *Langmuir* **2000,** 16, (2), 787-794.

5. Alden, L. R.; Roychowdhury, C.; Matsumoto, F.; Han, D. K.; Zeldovich, V. B.; Abruna, H. D.; DiSalvo, F. J., Synthesis, characterization, and electrocatalytic activity of PtPb nanoparticles prepared by two synthetic approaches. *Langmuir* **2006,** 22, (25), 10465-10471.

6. Abe, H.; Matsumoto, F.; Alden, L. R.; Warren, S. C.; Abruna, H. D.; DiSalvo, F. J., Electrocatalytic performance of fuel oxidation by Pt3Ti nanoparticles. *Journal of the American Chemical Society* **2008,** 130, (16), 5452-5458.

7. Roychowdhury, C.; Matsumoto, F.; Zeldovich, V. B.; Warren, S. C.; Mutolo, P. F.; Ballesteros, M.; Wiesner, U.; Abruna, H. D.; DiSalvo, F. J., Synthesis, characterization, and electrocatalytic activity of PtBi and PtPb nanoparticles prepared by borohydride reduction in methanol. *Chemistry of Materials* **2006,** 18, (14), 3365-3372.

8. Lamy, C. L., Leger, J. M., Srinivasan, S., *Direct Methanol Fuel Cells: From a Twentieth Century Electrochemist's Dream to a Twenty-first Century Emerging Technology*. New York: Kluwer Academic/Plenum: 2001; Vol. 34.

9. Shah R. K., K., S.J. In *Fuel cell science, engineering and technology* American Society of Mechanical engineers, Rochester, NY, 2003; Rochester, NY, 2003; p 538

10. O'Hayre, R.; Cha, S.; Colella, W.; Prinz, F. B., *Fuel Cell Fundamentals*. John Wiley and Sons, Inc.,: New York, 2006.

11. www.sc.doe.gov/bes/hydrogen.pdf.

12. www.fueleconomy.gov.

13. Schlapbach, L.; Zuttel, A., Hydrogen-storage materials for mobile applications. *Nature* **2001,** 414, (6861), 353-358.

14. Funck R, V. W., Lamm A, Gasteiner H A, *Handbook of fuel cells*. John Wiley and Sons Ltd.: 2003; Vol. 3.

15. Graetz, J., New approaches to hydrogen storage. *Chemical Society Reviews* **2009,** 38, (1), 73-82.

16. www.1.eere.energy.gov/vehiclesandfuels/pdfs/program/hydrogen_storage_roadmap.pdf.

17. Janssen, L. J. J., Hydrogen fuel cells for cars and buses. *Journal of Applied Electrochemistry* **2007,** 37, 1383-1387.

18. Rand, D. A. J.; Woods, R.; Dell, R. M., *Batteries for electric vehicles* Research studies press Ltd., Taunton, Wiley England, 1998.

19. Linden, D., *Handbook of batteries and fuel cells*. Mc Graw-Hill Book Company: New York, 1984; Vol. 26.

20. www.hyways.de/doc/Brochures_and_flyers/HyWays_Roadmaps_FINAL_22FEB2008.pdf.

21. Lamy, C.; Lima, A.; LeRhun, V.; Delime, F.; Coutanceau, C.; Leger, J. M., Recent advances in the development of direct alcohol fuel cells (DAFC). *Journal of Power Sources* **2002,** 105, (2), 283-296.

22. Zhou, W. P.; Lewera, A.; Larsen, R.; Masel, R. I.; Bagus, P. S.; Wieckowski, A., Size effects in electronic and catalytic properties of unsupported palladium nanoparticles in electrooxidation of formic acid. *Journal of Physical Chemistry B* **2006,** 110, (27), 13393-13398.

23. Neburchilov, V.; Martin, J.; Wang, H. J.; Zhang, J. J., A review of polymer electrolyte membranes for direct methanol fuel cells. *Journal of Power Sources* **2007,** 169, (2), 221-238.

24. Roziere, J.; Jones, D. J., Non-fluorinated polymer materials for proton exchange membrane fuel cells. *Annual Review of Materials Research* **2003,** 33, 503-555.

25. Ponce, M. L.; Prado, L.; Silva, V.; Nunes, S. P. In *Membranes for direct methanol fuel cell based on modified heteropolyacids*, 2004; 2004; pp 383-391.

26. Kim, Y. M.; Park, K. W.; Choi, J. H.; Park, I. S.; Sung, Y. E., A Pd-impregnated nanocomposite Nafion membrane for use in high-concentration methanol fuel in DMFC. *Electrochemistry Communications* **2003,** 5, (7), 571-574.

27. Ma, Z. Q.; Cheng, P.; Zhao, T. S., A palladium-alloy deposited Nafion membrane for direct methanol fuel cells. *Journal of Membrane Science* **2003,** 215, (1-2), 327-336.

28. Dimitrova, P.; Friedrich, K. A.; Stimming, U.; Vogt, B. In *Modified Nafion((R))-based membranes for use in direct methanol fuel cells*, 2002; 2002; pp 115-122.

29. Antonucci, P. L.; Arico, A. S.; Creti, P.; Ramunni, E.; Antonucci, V. In *Investigation of a direct methanol fuel cell based on a composite Nafion (R)-silica electrolyte for high temperature operation*, 1999; 1999; pp 431-437.

30. Tazi, B.; Savadogo, O. In *Parameters of PEM fuel-cells based on new membranes fabricated from Nafion (R), silicotungstic acid and thiophene*, 2000; 2000; pp 4329-4339.

31. Yang, C.; Srinivasan, S.; Arico, A. S.; Creti, P.; Baglio, V.; Antonucci, V., Composition Nafion/zirconium phosphate membranes for direct methanol fuel cell operation at high temperature. *Electrochemical and Solid State Letters* **2001,** 4, (4), A31-A34.

32. Vaivars, G.; Mokrani, T.; Hendricks, N.; Linkov, V., Inorganic membranes based on zirconium phosphate for fuel cells. *Journal of Solid State Electrochemistry* **2004,** 8, (11), 882-885.

33. Park, Y. S.; Yamazaki, Y., Novel nafion/hydroxyapatite composite membrane with high crystallinity and low methanol crossover for DMFCs. *Polymer Bulletin* **2005,** 53, (3), 181-192.

34. Tricoli, V.; Nannetti, F., Zeolite-Nafion composites as ion conducting membrane materials. *Electrochimica Acta* **2003,** 48, (18), 2625-2633.

35. Pei, H. Q.; Hong, L.; Lee, J. Y., Embedded polymerization driven asymmetric PEM for direct methanol fuel cells. *Journal of Membrane Science* **2006,** 270, (1-2), 169-178.

36. Schmidt, T. J.; Gasteiger, H. A.; Behm, R. J., Methanol electrooxidation on a colloidal PtRu-alloy fuel-cell catalyst. *Electrochemistry Communications* **1999,** 1, (1), 1-4.

37. Narayanan, S. R.; et al. In Fuel Cell Seminar, Orlando, FL., 1996; Orlando, FL., 1996.

38. Costamagna, P.; Srinivasan, S. In *Quantum jumps in the PEMFC science and technology from the 1960s to the year 2000 Part I. Fundamental scientific aspects*, 2001; 2001; pp 242-252.

39. Liu, H. S.; Song, C. J.; Zhang, L.; Zhang, J. J.; Wang, H. J.; Wilkinson, D. P., A review of anode catalysis in the direct methanol fuel cell. *Journal of Power Sources* **2006,** 155, (2), 95-110.

40. Zhang, L.; Zhang, J. J.; Wilkinson, D. P.; Wang, H. J., Progress in preparation of non-noble electrocatalysts for PEM fuel cell reactions. *Journal of Power Sources* **2006,** 156, (2), 171-182.

41. Gasteiger, H. A.; Markovic, N. M.; Ross, P. N., H-2 and Co Electrooxidation on Well-Characterized Pt, Ru, and Pt-Ru .1. Rotating-Disk Electrode Studies of the Pure Gases Including Temperature Effects. *Journal of Physical Chemistry* **1995,** 99, (20), 8290-8301.

42. Long, J. W.; Stroud, R. M.; Swider-Lyons, K. E.; Rolison, D. R., How to make electrocatalysts more active for direct methanol oxidation - Avoid PtRu bimetallic alloys! *Journal of Physical Chemistry B* **2000,** 104, (42), 9772-9776.

43. Vigier, F.; Coutanceau, C.; Leger, J. M.; Dubois, J. L., Polyoxymethylenedimethylether (CH3-O-(CH2-O)(n)-CH3) oxidation on Pt and Pt/Ru supported catalysts. *Journal of Power Sources* **2008,** 175, (1), 82-90.

44. Siroma, Z.; Fujiwara, N.; Loroi, T.; Yamazaki, S.; Senoh, H.; Yasuda, K.; Tanimoto, K., Transient phenomena in a PEMFC during the start-up of gas feeding

observed with a 97-fold segmented cell. *Journal of Power Sources* **2007,** 172, (1), 155-162.

45. Adzic, R. R. In DOE Hydrogen and Fuel Cell Review Meeting, Philadelphia, PA., 2004; Philadelphia, PA., 2004.

46. Shao, M. H.; Sasaki, K.; Adzic, R. R., Pd-Fe nanoparticles as electrocatalysts for oxygen reduction. *Journal of the American Chemical Society* **2006,** 128, (11), 3526-3527.

47. Shao, M. H.; Huang, T.; Liu, P.; Zhang, J.; Sasaki, K.; Vukmirovic, M. B.; Adzic, R. R., Palladium monolayer and palladium alloy electrocatalysts for oxygen reduction. *Langmuir* **2006,** 22, (25), 10409-10415.

48. Vigier, F.; Coutanceau, C.; Leger, J. M.; Dubois, J. L., *Journal of Power Sources* **2009,** 175, 82.

49. Shao, M. H.; Sasaki, K.; Liu, P.; Adzic, R. R., Pd3Fe and pt monolayer-modified Pd3Fe electrocatalysts for oxygen reduction. *Zeitschrift Fur Physikalische Chemie-International Journal of Research in Physical Chemistry & Chemical Physics* **2007,** 221, (9-10), 1175-1190.

50. Nilekar, A. U.; Xu, Y.; Zhang, J. L.; Vukmirovic, M. B.; Sasaki, K.; Adzic, R. R.; Mavrikakis, M., Bimetallic and ternary alloys for improved oxygen reduction catalysis. *Topics in Catalysis* **2007,** 46, (3-4), 276-284.

51. Stiehl, J. D.; Kim, T. S.; McClure, S. M.; Mullins, C. B., Evidence for molecularly chernisorbed oxygen on TiO_2 supported gold nanoclusters and Au(111). *Journal of the American Chemical Society* **2004,** 126, (6), 1606-1607.

52. Demarconnay, L.; Coutanceau, C.; Leger, J. M., Electroreduction of dioxygen (ORR) in alkaline medium on Ag/C and Pt/C nanostructured catalysts - effect of the presence of methanol. *Electrochimica Acta* **2004,** 49, (25), 4513-4521.

53. Vante, N. A.; Tributsch, H., Energy-Conversion Catalysis Using Semiconducting Transition-Metal Cluster Compounds. *Nature* **1986,** 323, (6087), 431-432.

54. Chang, C. J.; Loh, Z. H.; Shi, C. N.; Anson, F. C.; Nocera, D. G., Targeted proton delivery in the catalyzed reduction of oxygen to water by bimetallic Pacman porphyrins. *Journal of the American Chemical Society* **2004,** 126, (32), 10013-10020.

55. Winnischofer, H.; Otake, V. Y.; Dovidauskas, S.; Nakamura, M.; Toma, H. E.; Araki, K., Supramolecular tetracluster-cobalt porphyrin: a four-electron transfer catalyst for dioxygen reduction. *Electrochimica Acta* **2004,** 49, (22-23), 3711-3718.

56. Yoshimoto, S.; Inukai, J.; Tada, A.; Abe, T.; Morimoto, T.; Osuka, A.; Furuta, H.; Itaya, K., Adlayer structure of and electrochemical O-2 reduction on cobalt porphine-modiried and cobalt octaethylporphyrin-modifled Au(111) in HClO4. *Journal of Physical Chemistry B* **2004,** 108, (6), 1948-1954.

57. Collman, J. P.; Shiryaeva, I. M.; Boulatov, R., Effect of electron availability on selectivity of O-2 reduction by synthetic monometallic Fe porphyrins. *Inorganic Chemistry* **2003,** 42, (16), 4807-4809.

58. Chang, C. J.; Chng, L. L.; Nocera, D. G., Proton-coupled O-O activation on a redox platform bearing a hydrogen-bonding scaffold. *Journal of the American Chemical Society* **2003,** 125, (7), 1866-1876.

59. Chang, C. J.; Deng, Y. Q.; Shi, C. N.; Chang, C. K.; Anson, F. C.; Nocera, D. G., Electrocatalytic four-electron reduction of oxygen to water by a highly flexible cofacial cobalt bisporphyrin. *Chemical Communications* **2000**, (15), 1355-1356.

60. Kolovos-Vellianitis, D.; Kammler, T.; Kuppers, J. In *Interaction of gaseous hydrogen atoms with oxygen covered Cu(100) surfaces*, 2001; 2001; pp 166-170.

61. Lescop, B.; Jay, J. P.; Fanjoux, G., Reduction of oxygen pre-treated Ni(111) by H-2 exposure: UPS and MIES studies compared with Monte Carlo simulations. *Surface Science* **2004,** 548, (1-3), 83-94.

62. Mentus, S. V., Oxygen reduction on anodically formed titanium dioxide. *Electrochimica Acta* **2004,** 50, (1), 27-32.

63. Efremov, B. N.; Tarasevich, M. R., Kinetics and Mechanisms of the Electroreduction and Evolution of Oxygen on Cobalt Spinels. *Soviet Electrochemistry* **1981,** 17, (11), 1392-1398.

64. Tamura, H.; et. al. In Electrodes of Conducting Metallc Oxides, Part A, Amsterdam, 1981; Trasatti, S., Ed. Elsevier: Amsterdam, 1981.

65. Goodenough, J. B.; Shukla, A. K.; Paliterio, C.; Jamieson, K. R.; Hamnett, A.; Manoharan, R. 8422546, 1985.

66. Tributsch, H.; Bron, M.; Hilgendorff, M.; Schulenburg, H.; Dorbandt, I.; Eyert, V.; Bogdanoff, P.; Fiechter, S., Methanol-resistant cathodic oxygen reduction catalysts for methanol fuel cells. *Journal of Applied Electrochemistry* **2001,** 31, (7), 739-748.

67. Bron, M.; Bogdanoff, P.; Fiechter, S.; Dorbandt, I.; Hilgendorff, M.; Schulenburg, H.; Tributsch, H., Influence of selenium on the catalytic properties of ruthenium-based cluster catalysts for oxygen reduction. *Journal of Electroanalytical Chemistry* **2001,** 500, (1-2), 510-517.

68. Duron, S.; Rivera-Noriega, R.; Poillerat, G.; Solorza-Feria, O., Kinetic study of oxygen electro-reduction on RuxSy(CO)(n) based catalyst in 0.5 M H2SO4. *Journal of New Materials for Electrochemical Systems* **2001,** 4, (1), 17-23.

69. Alonso-Vante, N.; Bogdanoff, P.; Tributsch, H., On the origin of the selectivity of oxygen reduction of ruthenium-containing electrocatalysts in methanol-containing electrolyte. *Journal of Catalysis* **2000,** 190, (2), 240-246.

70. Sebastian, P. J.; Rodriguez, F. J.; Solorza, O.; Rivera, R., Development of PEM (Proton Exchange Membrane) fuel cell using carbon supported Mo-Ru-Se electrodes. *Journal of New Materials for Electrochemical Systems* **1999,** 2, (2), 115-119.

71. Duron, S.; Rivera-Noriega, R.; Leyva, M. A.; Nkeng, P.; Poillerat, G.; Solorza-Feria, O., Oxygen reduction on a RuxSy(CO)(n) cluster electrocatalyst in 0.5 M H2SO4. *Journal of Solid State Electrochemistry* **2000,** 4, (2), 70-74.

72. Rodriguez, F. J.; Sebastian, P. J., MoxSey-(CO)(n) electrocatalyst prepared by screen-printing and sintering. *International Journal of Hydrogen Energy* **2000,** 25, (3), 243-247.

73. Solorza-Feria, O.; Citalan-Cigarroa, S.; Rivera-Noriega, R.; Fernandez-Valverde, S. M., Oxygen reduction in acid media at the amorphous Mo-Os-Se carbonyl cluster coated glassy carbon electrodes. *Electrochemistry Communications* **1999,** 1, (12), 585-589.

74. Reeve, R. W.; Christensen, P. A.; Hamnett, A.; Haydock, S. A.; Roy, S. C., Methanol tolerant oxygen reduction catalysts based on transition metal sulfides. *Journal of the Electrochemical Society* **1998,** 145, (10), 3463-3471.

75. Trapp, V.; Christensen, P.; Hamnett, A., New catalysts for oxygen reduction based on transition-metal sulfides. *Journal of the Chemical Society-Faraday Transactions* **1996,** 92, (21), 4311-4319.

76. Fischer, C.; Alonsovante, N.; Fiechter, S.; Tributsch, H., Electrocatalytic Properties of Mixed Transition-Metal Tellurides (Chevrel-Phases) for Oxygen Reduction. *Journal of Applied Electrochemistry* **1995,** 25, (11), 1004-1008.

77. Alonsovante, N.; Schubert, B.; Tributsch, H., Transition-Metal Cluster Materials for Multi-Electron Transfer Catalysis. *Materials Chemistry and Physics* **1989,** 22, (3-4), 281-307.

78. Maillard, F.; Martin, M.; Gloaguen, F.; Leger, J. M., Oxygen electroreduction on carbon-supported platinum catalysts. Particle-size effect on the tolerance to methanol competition. *Electrochimica Acta* **2002,** 47, (21), 3431-3440.

79. Petrow, H. G.; Allen, R. J. 3992331, 1976.

80. Grgur, B. N.; Markovic, N. M.; Lucas, C. A.; Ross, P. N., Electrochemical oxidation of carbon monoxide: from platinum single crystals to low temperature fuel cells catalysts. Part I: Carbon monoxide oxidation onto low index platinum single crystals. *Journal of the Serbian Chemical Society* **2001,** 66, (11-12), 785-797.

81. Toda, T.; Igarashi, H.; Uchida, H.; Watanabe, M., Enhancement of the electroreduction of oxygen on Pt alloys with Fe, Ni, and Co. *Journal of the Electrochemical Society* **1999,** 146, (10), 3750-3756.

82. Rao, V.; Simonov, P. A.; Savinova, E. R.; Plaksin, G. V.; Cherepanova, S. V.; Kryukova, G. N.; Stimming, U., The influence of carbon support porosity on the activity of PtRu/Sibunit anode catalysts for methanol oxidation. *Journal of Power Sources* **2005,** 145, (2), 178-187.

83. Mastragostino, M.; Missiroli, A.; Soavi, F., Carbon supports for electrodeposited Pt-Ru catalysts for DMFCs. *Journal of the Electrochemical Society* **2004,** 151, (11), A1919-A1924.

84. Park, G. G.; Yang, T. H.; Yoon, Y. G.; Lee, W. Y.; Kim, C. S., Pore size effect of the DMFC catalyst supported on porous materials. *International Journal of Hydrogen Energy* **2003,** 28, (6), 645-650.

85. Anderson, M. L.; Stroud, R. M.; Rolison, D. R., Enhancing the activity of fuel-cell reactions by designing three-dimensional nanostructured architectures: Catalyst-modified carbon-silica composite aerogels. *Nano Letters* **2002,** 2, (3), 235-240.

86. Uchida, M.; Fukuoka, Y.; Sugawara, Y.; Ohara, H.; Ohta, A., Improved preparation process of very-low-platinum-loading electrodes for polymer electrolyte fuel cells. *Journal of the Electrochemical Society* **1998,** 145, (11), 3708-3713.

87. Rao, V.; Simonov, P. A.; Savinova, E. R.; Plaksin, G. V.; Cherepanova, S. V.; Kryukova, G. N.; Stimming, U. In *The influence of carbon support porosity on the activity of PtRu/Sibunit anode catalysts for methanol oxidation*, 2005; 2005; pp 178-187.

88. Chan, K. Y.; Ding, J.; Ren, J. W.; Cheng, S. A.; Tsang, K. Y., Supported mixed metal nanoparticles as electrocatalysts in low temperature fuel cells. *Journal of Materials Chemistry* **2004,** 14, (4), 505-516.

89. Girishkumar, G.; Vinodgopal, K.; Kamat, P. V., Carbon nanostructures in portable fuel cells: Single-walled carbon nanotube electrodes for methanol oxidation and oxygen reduction. *Journal of Physical Chemistry B* **2004,** 108, (52), 19960-19966.

90. Che, G. L.; Lakshmi, B. B.; Martin, C. R.; Fisher, E. R., Metal-nanocluster-filled carbon nanotubes: Catalytic properties and possible applications in electrochemical energy storage and production. *Langmuir* **1999,** 15, (3), 750-758.

91. Miedema, A. R.; Dechatel, P. F.; Deboer, F. R., Cohesion in Alloys - Fundamentals of a Semi-Empirical Model. *Physica B & C* **1980,** 100, (1), 1-28.

92. Gaskell, D. R., *Introduction to Metallurgical Thermodynamics.* 2nd ed.; Hemisphere publishing corp.: New York, 1981.

93. Hogarth, M. P.; Ralph, T. R., *Platinum Metals Review* **2002,** 46, 146-164.

94. Ross, P. N., Hydrogen Chemisorption on Pt Single-Crystal Surfaces in Acidic Solutions. *Surface Science* **1981,** 102, (2-3), 463-485.

95. Motoo, S.; Furuya, N., Electrochemistry of Platinum Single-Crystal Surfaces .1. Structural-Change of the Pt (111) Surface Followed by an Electrochemical Method. *Journal of Electroanalytical Chemistry* **1984,** 172, (1-2), 339-358.

96. Oudar, J.; Marcus, P.; Clavilier, J., Electrochemistry at Well-Defined Metal-Surfaces. *Journal De Chimie Physique Et De Physico-Chimie Biologique* **1991,** 88, (7-8), U1247-U1247.

97. Chen, M.; Cai, Y.; Yan, Z.; Goodman, D. W., On the origin of the unique properties of supported Au nanoparticles. *Journal of the American Chemical Society* **2006,** 128, (19), 6341-6346.

98. Cushing, B. L.; Kolesnichenko, V. L.; O'Connor, C. J., Recent advances in the liquid-phase syntheses of inorganic nanoparticles. *Chemical Reviews* **2004,** 104, (9), 3893-3946.

99. Roucoux, A.; Schulz, J.; Patin, H., Reduced transition metal colloids: A novel family of reusable catalysts? *Chemical Reviews* **2002,** 102, (10), 3757-3778.

100. Deivaraj, T. C.; Chen, W. X.; Lee, J. Y., Preparation of PtNi nanoparticles for the electrocatalytic oxidation of methanol. *Journal of Materials Chemistry* **2003,** 13, (10), 2555-2560.

101. Komarneni, S.; Li, D. S.; Newalkar, B.; Katsuki, H.; Bhalla, A. S., Microwave-polyol process for Pt and Ag nanoparticles. *Langmuir* **2002,** 18, (15), 5959-5962.

102. Pileni, M. P., Mesostructured fluids in oil-rich regions: Structural and templating approaches. *Langmuir* **2001,** 17, (24), 7476-7486.

103. Ahmadi, T. S.; Wang, Z. L.; Green, T. C.; Henglein, A.; ElSayed, M. A., Shape-controlled synthesis of colloidal platinum nanoparticles. *Science* **1996,** 272, (5270), 1924-1926.

104. Alivisatos, A. P., Semiconductor clusters, nanocrystals, and quantum dots. *Science* **1996,** 271, (5251), 933-937.

105. Alden, L. R. Synthesis of platinum intermetallic compounds for fuel cell anode catalysts. Cornell University, 2006.

106. Roychowdhury, C. Intermetallic nanoparticles for fuel cell applications: syntheses and characterization studies. Cornell University, 2008.

Chapter 2

PtPb NANOPARTICLES BY SODIUM NAPTHALIDE REDUCTION: OPTIMIZATION OF PROPERTIES

In the introduction section, we mentioned the advances in syntheses of intermetallics as nanoparticles for fuel cell catalysts. The challenges were found to be higher on switching to sodium napthalide as the reducing agent from sodium borohydride, presumably due to the cleaner overall system in the later case (solvents and easily washable side products form precursors). As we will see in this and the forthcoming chapters, these conditions (precursors, reaction solvent, work-up techniques and solvents) play a major role in deciding the chemical composition of the alloy or intermetallic compounds targeted. Hence, it was important to explore, understand and control these factors for a familiar phase (like PtPb)[1, 2] and optimize its properties. Sodium borohydride reduction is a very useful method for metals it can reduce. However, sodium borohydride cannot be used for reducing all metals across the periodic table. As our goal is not to limit ourselves in our search for new catalyst materials, understanding and modifying reductions with sodium napthalide, a much stronger reducing agent, becomes imperative for widespread application of the chemical reduction method. This chapter is adapted from a paper published in the *Journal of Nanoparticle Research.*

2.1 Introduction

The need for more efficient and alternative energy sources to cope with the issues arising from fossil fuel usage is becoming more and more evident. One potential technology for higher efficiency is direct fuel cells operating near room temperature. So called direct fuel cells use small molecules as the fuel source, completely oxidizing the fuel to CO_2 and H_2O[3]. Fuel cells are not heat engines so their efficiency is not bound by Carnot cycle limitations, but rather the entire free energy of a redox reaction can (in principle) be converted to electrical energy. Real fuel cells with efficiencies of about 50-60% at their operating point with 10-50 kW outputs are already realizable[4]. Cost and durability/longevity factors, however, still keep these fuel cells from being practically usable, which is inhibiting their introduction into the market. Nevertheless, the potential of polymer electrolyte membrane fuel cells (PEMFCs) in the transportation market and as small portable power sources are being explored by many. The basic components of the fuel cell, including the electrocatalyst, present a challenge for most fuel cell technologies. The common industry standard for the anode electrocatalyst is still Pt (for H_2 as a fuel) or a 1:1 PtRu alloy (for MeOH as a fuel) usually in the form of 3-5 nm particles supported on carbon to achieve high surface areas and generate the high current densities needed[5]. The use of nanoparticles also diminishes the amount (and therefore cost) of Pt used.

Recently, the authors and their collaborators have shown that high performance electrocatalysts can be obtained from the family of Pt based ordered intermetallic compounds[6-11]. Two of these intermetallics, PtBi and PtPb have, indeed, shown not only higher tolerance to S and CO poisoning (surface poisoning of the catalyst by CO is a pertinent issue when carbon containing fuels are considered) but also superior electrocatalytic activity toward formic acid oxidation compared to Pt, 1:1 PtRu and

Pd[1, 2, 6, 7, 9, 10, 12]. However, the electrocatalytic activity, along with the size and surface properties of the nanoparticles were found to be highly dependent on the details of the synthesis methods. Initially, sodium borohydride was used as a reducing agent for preparing PtPb and PtBi intermetallics[1, 2, 7], but in order to explore intermetallics of metals with a wider range of reduction potentials as anode electrocatalysts, stronger reducing agents needed to be considered. Also, it is important to prepare the particles by a number of different chemical routes to investigate the role of synthesis in determining the surface composition, morphology, impurity contamination and subsequently, electrochemical activity of the nanoparticles.

PtPb nanoparticle syntheses using sodium napthalide as the reducing agent and dimethyl(1,5-cyclooctadiene)platinum and lead(II)2-ethylhexanoate as the precursors was also undertaken previously in the group[2, 12], and interestingly, the domain size of the nanoparticles was found to be dependent on stirring time and reaction temperature. For reductions done at room temperature, crystallization of the nanoparticles to give an identifiable PtPb phase by XRD was observed only when the particles rapidly warmed by surface oxidation when exposed to air quickly post synthesis. Higher reaction temperatures and stirring times were seen to be necessary[13] for increased crystal domain sizes. These observations indicated a 'barrier' to crystallization of the PtPb nanoparticles that required a thermal treatment. Some observations suggested that the presence of organics from the precursors (or the reducing agent) bound to the nanoparticle surfaces (or even inside the nanoparticles) contributed to this crystallization 'barrier'. Varying the platinum precursors and studying the resulting nanoparticles is one way to explore this phenomenon. Also, if these organics are the main inhibitors of crystallization, quantification of the amount of organics in or on the nanoparticles, and possible correlation with particle domain sizes would be revealing. Moreover, finding precursors with ligands having smaller binding affinity to platinum

would be useful for further syntheses of Pt based intermetallics. Another important issue with these solution based syntheses is the solubility of platinum and other metal precursors. Using sodium napthalide as the reducing agent limits solvent options to tetrahydrofuran (THF) or glymes. The platinum precursor (dimethyl(1,5-cyclooctadiene)platinum), though considerably soluble in THF, has fairly low solubility in diglyme (a THF substitute for higher temperature reactions). Comparable solubility of both metal precursors in the reaction solvent is highly desirable for the purpose of co-reduction of metals with widely different reduction potentials. Hence, higher solubility is a desirable attribute for the platinum precursors to be investigated. The above research led us to a plausible mechanistic picture of the processes that occur in the synthesis of intermetallic nanoparticles from solution by chemical co-reduction of the precursors (Scheme 2.1).

We started our investigation by synthesizing a number of Pt precursors having 1,5-cycloctadiene derivatives in place of the 1,5-cyclooctadiene (hoping that alkyl based derivatives would make the molecule less symmetric and more soluble) and screened them primarily based on their solubility in THF and diglyme. We also started working with platinum acetylacetonate (obtained commercially) following our quest for a platinum precursor with ligands having lower affinity for platinum (on the basis of Pt-L bond enthalpies)[14].

Scheme 2.1: Key issues in intermetallic nanoparticle syntheses by chemical co-reduction of precursors.

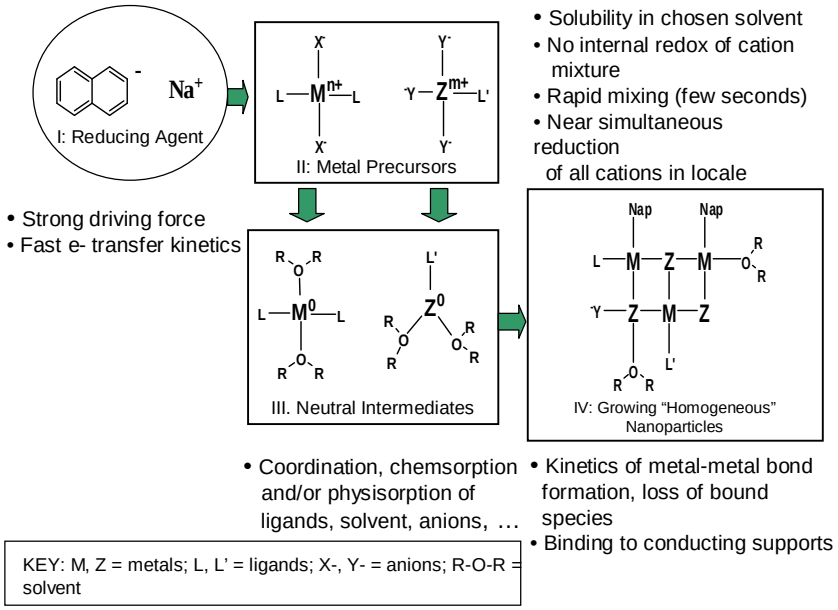

We used the precursors having considerable solubility in THF and diglyme (Table 2.1) to synthesize PtPb. We also explored different synthetic strategies with platinum acetylacetonate (the most soluble one of all). Interestingly, the resulting nanoparticle domain sizes showed different behavior with different synthesis or annealing temperature as well as different electrocatalytic activities depending on the method of synthesis employed. It was also possible to identify some organic groups from the precursor in the products. Quantitative studies further revealed a clear correlation between the amount of organics and crystal domain sizes supporting our hypothesis about organic interference in PtPb nanoparticle crystallization. Sodium was also detected in the nanoparticles product, but could be removed by a water wash. However,

evidence suggested that sodium may also play a role in the crystallization dynamics. Organic and sodium contamination in the products could be mitigated by modification of the method of solvent removal after reduction. Thermogravimetric analyses and IR studies of the particles confirmed the presence of organics. At the same time, organics from the reducing agent/lead precursors have not yet been detected. SEM and TEM images of the nanoparticles prepared from Pt acetylacetonate offered evidence of the change in nature and composition of the particles crystallizing when the reaction temperature was increased. Although the particles are always agglomerated (expected, since stabilizers/surfactants were not employed), crystal grain boundaries were observable as the smallest features in the images (with domain sizes corresponding to those measured from XRD of the particles). CBED and SAED studies confirmed the crystalline nature of these particles.

Table 2.1: Solubility of different Pt precursors in THF and diglyme.

Compound	Solubility in mmol/ml	
	in THF	in Diglyme
$PtMe_2$	0.108	0.045
$PtCl_2$	0.006	–
$PtCl_2$-	0.011	0.010
$PtCl_2$-	0.002	0.002
$Pt(acac)_2$	0.049	0.041

More interestingly, the PtPb nanoparticles prepared from platinum acetylacetonate had the highest electrocatalytic activity (mass activity normalized to the BET surface area)

compared to nanoparticles previously synthesized using sodium napthalide or sodium borohydride as reducing agents. In each case however, different precursors were used[1, 2, 12].

2.2 Experimental

2.2.1 Platinum precursors

All materials used were at least reagent grade. All platinum precursors, except platinum acetylacetonate and platinum hexafluoroacetylacetonate (Aldrich), were synthesized in the laboratory starting from Pt (Englehard, 99.9 %). Platinum (1g, 5.13 mmol) was dissolved in 20 ml of aqua-regia (3 parts of 12 M HCl with 1 part of 12 M HNO_3), and stirred in an open flask at 120 ^oC for 30 min. The resulting orange solution was cooled down to room temperature and solid KCl (0.848 g, 11.4 mmol) was added. The resulting mixture was cooled in an ice bath for 30 min, and the yellow precipitate was collected by suction filtration, washed with chilled water, ethanol and diethyl ether. XRD showed the dried precipitate to be pure K_2PtCl_6. The K_2PtCl_6 was reduced to K_2PtCl_4 with H_2SO_3 (commercially obtained from Aldrich) following a standard reduction procedure[15]. The K_2PtCl_4 was dissolved in glacial acetic acid (Aldrich) and water (purified with a Millipore Milli Q system) in a 12.5:8 by volume solution, and then 1,5-cycloctadiene, or 3-methyl 1,5-cycloctadiene or 3,4-dimethyl 1,5-cyclooctadiene (all from Aldrich) was added to obtain the corresponding platinum organic dichloride compound. Platinum acetate was synthesized by refluxing platinum tetrachloride (0.406 g, 1.21 mmol) and silver acetate (0.1 g, 0.6 mmol) for 3 hrs in 24 mL glacial acetic acid and worked up following a reported procedure[16]. However, we found that washing the final product with acetone improved its purity. A

recrystallization of the product from acetone was also attempted. However, the attempt failed due to the high solubility of platinum acetate in acetone. Platinum acetate was found to decompose to platinum metal (which precipitated out) when its solution in acetone was heated to just 60 ^{o}C. Thus, all reactions with this precursor were carried by injecting the precursors into reducing agent at room temperature, heating up only later, if necessary.

2.2.2 Napthalide reduction

Materials: Naphthalene was purchased from Fisher. Sodium metal and diglyme were purchased from Aldrich. THF and diglyme were freshly distilled over sodium prior to use. Lead(II)2-ethylhexanoate was purchased from STREM Chemicals Inc. Because of the high viscosity of lead(II)2-ethylhexanoate, 0.05M stock solutions were prepared by dissolving 2.496 g in 100 mL THF.

2.2.3 Synthesis of PtPb nanoparticles

A solution of sodium napthalide was prepared by weighing out stoichiometric amounts of naphthalene (0.1923 g, 1.50 mmol) and sodium metal (0.0345g, 1.50 mmol) in an argon atmosphere glovebox and loading these reactants into a flask containing 50 mL diglyme or THF. The flask was sealed and removed from the glovebox and stirred overnight under argon to produce a dark green sodium napthalide solution.

Platinum acetylacetonate (0.0988 g.0.25 mmol) was dissolved in a 5.0 mL aliquot of a 0.05 M stock solution of lead(II)2-ethylhexanoate in diglyme (0.25 mmol lead(II)2-ethylhexanoate). Meanwhile, an argon purged flask containing the freshly prepared sodium napthalide was connected to a water cooled condenser. If the reaction was to

be carried out above room temperature, the flask was heated to the desired reaction temperature in an oil bath. The aliquot of metal precursors was injected into the dark green sodium napthalide solution which immediately became black and opaque. The solution was stirred for 30 minutes. If the reaction mixture was heated (either before – labeled series 1, or immediately after the reduction step - labeled series 2) the mixture was stirred for 10 minutes at temperature and then cooled to ambient by removing the oil bath. The solvent and any volatile side products were carefully pumped out of the flask using first static followed by dynamic vacuum, leaving a black residue. Once the flask was pumped down to a suitably low pressure (~ 200 m Torr), 40 mL of degassed ethanol were added to the flask, which was then sonicated in an immersion bath sonicator for 10 min. The contents of the flask were then transferred to a centrifuge tube with a cannula and centrifuged (2K rpm, 10 min). The supernatant (colored yellow) was removed and 40 mL of hexanes were distilled into the black precipitate. The tube was sonicated for 10 min and centrifuged again. The supernatant (usually colorless) was removed and the black precipitate was dried under vacuum. The tube was then backfilled with argon, and was left overnight with a needle in the septum to allow slow exposure of the nanoparticles to air. Another series (labeled series 3) of reactions were done in which the preparation of reducing agent and injection of precursors were done in the above mentioned way. Following the injection, the flask was heated up to the desired temperature using an oil bath (it took approximately 10 - 15 min for the bath to reach the desired reaction temperature). Once the desired temperature was reached, the flask was stirred for 10 min and the solution was allowed to cool to 40 ^{o}C. The reaction mixture was cannula transferred into a centrifuge tube and was centrifuged for 10 min at 2K rpm. The diglyme was syringed off leaving a black residue. 40 mL of degassed ethanol were added to the flask, which was then sonicated in an immersion bath sonicator for 10 min. The contents of the flask were

then transferred to a centrifuge tube with a cannula and centrifuged (2K rpm, 10 min). The supernatant was removed with a syringe following which; the usual washings and slow exposure to air were carried out. Table 2 gives a summary of each of the series described above.

2.2.4 Characterization

X-ray powder diffraction powder patterns (Scintag XDS 2000) were taken of the black PtPb nanoparticles to confirm the composition and structure of the intermetallic phase. The particle morphology and size was studied by scanning electron microscopy (SEM) using a LEO-1550 Field emission SEM (FSEM). Energy dispersive X-ray analysis (EDX) was also done on the particles on the same instrument. For EDX analysis, unless otherwise specified, particles in dry powder form were used on GaAs wafers. A JEOL 8900 EPMA Microprobe was used for preliminary EDX on most of the PtPb samples. Scanning TEM images and convergent beam electron diffraction (CBED) data were collected on a VG HB501UX UHV STEM. Dry particles, in powdered form dispersed on ultra thin TEM grid, were used for STEM and SEM images. TEM images and selected area electron diffraction (SAED) were taken on a JEOL 1200EX TEM on microtomed (60 nm) sections of the nanoparticles dispersed on an ultrathin TEM grid. To measure the surface area of the samples, a Micromeritics ASAP 2020 was used to collect a partial adsorption isotherm at liquid nitrogen temperature (-196 ^{o}C) with krypton as the adsorption gas over the pressure range (P/P_0) range of 0.06 and 0.5. Prior to measurements, the sample was degassed under vacuum at room temperature for 48 h. The specific surface area was determined according to the Brunauer-Emmett-Teller (BET) method in the relative pressure range of 0.08 to 0.185.

2.2.5 Electrocatalytic activity

The electrocatalytic activity of the PtPb nanoparticles for the oxidation of formic acid was examined. Prior to each experiment, a suspension of the nanoparticle catalyst was prepared as follows: to 4 mg of the dried nanoparticle sample were added 3.98 mL of distilled water and 1 mL of isopropyl alcohol (Aldrich). Additionally, 20 μL of a 5% w/w Nafion solution in alcohols (Aldrich, EW: 1100) and water were added to this mixture. The resulting mixture was sonicated in a bath type ultrasonicator, for 15 min. Each nanoparticle suspension described above was coated onto a 3 mm diameter glassy carbon (GC) electrode. The electrode had been previously polished with diamond paste (METADI-Buehler, $\varnothing$ = 1 μm) and ultrasonicated in Millipore water (18 MΩ cm^{-1}, Millipore Milli-Q) for 10 min. The electrode was then rinsed with Millipore water and allowed to dry in air. 70 μg cm^{-2} of the nanoparticles (6.1 μL of nanoparticle suspension) were coated onto the clean glassy carbon electrode. The electrode was then spin dried at 600 rpm under a nitrogen gas atmosphere.

Before studying fuel oxidation, electrochemical pretreatment of nanoparticle coated electrodes is sometimes necessary to obtain optimal activity[17, 18]. A partially optimized procedure involved generating hydrogen by holding the nanoparticle ink coated electrode at -0.7 V vs. Ag/AgCl for 40 min in 0.1 M H_2SO_4.

Formic acid oxidation on the nanoparticle-coated GC electrode was examined in a solution of 0.5M formic acid (Mallinckrodt, 88% analytical reagent)/0.1M sulfuric acid at a sweep rate of 10 mVs^{-1}. All solutions were prepared with Millipore water and deaerated with prepurified nitrogen for at least 10 min before each experiment. The measurements were conducted at room temperature. All potentials are referenced to a sodium chloride saturated Ag/AgCl electrode without regard for the liquid junction.

2.3 Results and discussion

2.3.1 Investigating platinum precursors

The platinumdichloride(1,5-cyclooctadiene) derivatives synthesized were compared with the commercially obtained platinum acetylacetonate with respect to solubility in diglyme and THF (Table 2.1). The solubility of (3,4-dimethyl-1,5-cycloctadiene)platinumdichloride was lower than (3-methyl-1,5-cycloctadiene)platinumdichloride in both solvents, showing the expected lowering of solubility with an increase in symmetry of the ligand. Platinum acetylacetonate showed the highest solubility in both solvents, and was hence chosen as the precursor to be studied further. Platinum acetate was found to be unstable over extended periods of time or at higher temperatures and hence was excluded from consideration after a few initial experiments. After investigating platinum acetylacetonate, platinum hexafluoroacetylacetonate was explored in the hopes that the organic ligand from the precursor would be less likely to adsorb to the nanoparticles, since the precursor itself was a more polar molecule. The new precursor was also expected to be more soluble than platinum acetylacetonate in the solvents compatible with sodium napthalide, THF and diglyme. When the solubility of platinum hexafluoroacetylacetonate was tested, it was found to be more soluble than platinum acetylacetonate in these particular solvents. However, upon using this new precursor to synthesize PtPb nanoparticles, the resulting particles were hygroscopic and showed high amounts of sodium and fluorine (EDS) as well as characteristic fluoroacetylacetonate peaks (FTIR). The interference of this apparent sodium and fluorine complex was removed by subjecting the particles to a water/double MeOH wash. At this point the particles were no longer hygroscopic and did not contain the characteristic peaks of fluoroacetylacetonate in

the FTIR. However, the particles were highly polar to begin with (probably owing to Na/F containing polar/ionic species sticking to them) making their separation from the polar wash solvents very difficult and leading to extremely low yields. We believe that the lone, now highly acidic hydrogen, left on the hexafluoroacetylacetonate moiety is responsible for the hygroscopic property of the resulting nanoparticles. A per-fluorinated acetylacetonate may behave differently. However, this was not further pursued since the particles were not found to have any enhanced properties than the ones made from platinum acetylacetonate and our goal is to find a precursor convenient and simple to work with.

2.3.2 Synthesis of PtPb nanoparticles

Previous PtPb nanoparticles synthesized using dimethyl(1,5-cyclooctadiene)platinum and lead(II)2-ethylhexanoate showed higher electrocatalytic activity and larger domain size of PtPb when they were synthesized by injecting the precursors into a sodium napthalide solution at a higher temperature (135 ^{o}C) rather than room temperature injection followed by annealing at 135 ^{o}C in the solvent[2]. Accordingly, an initial series of reactions was done by injecting the precursors into a reducing agent solution stirring at the desired temperature. A stirring time of 30 min was maintained in each case to ensure good crystallization based on previous trends observed in the group[2], following which, the solvent was evaporated off (series 1). We expected the temperature of crystallization to be lower when $Pt(acac)_2$ was used, since acetylacetonate is anionic and the Pt-O bond is weaker than Pt-ene bonds. Surprisingly, the domain size variation with reaction temperature was not similar to that observed when dimethyl(1,5-cyclooctadiene)platinum was used as the Pt precursor. Neither was lowering of crystallization temperature observed. Reactions carried out at

temperatures above and below 120 ^{o}C resulted in pXRD patterns with low intensity and broad peaks, approximately matching the more intense peak positions of the PtPb structure. However, given the broad nature of the peaks, the presence/absence of other phases could not be established. Annealing the product, after sealing it in an evacuated silica tube and heating at 600 ^{o}C for 12h, showed PtPb as the only crystalline phase by pXRD with a mean crystal domain size of 30 nm. SEM images of the as-prepared samples showed a high degree of agglomeration. EDX analysis of the particles showed the presence of Pt and Pb in 1:1 ratio (+/- 5%) in multiple micron square regions along with the presence of some sodium (Figure 2.1).

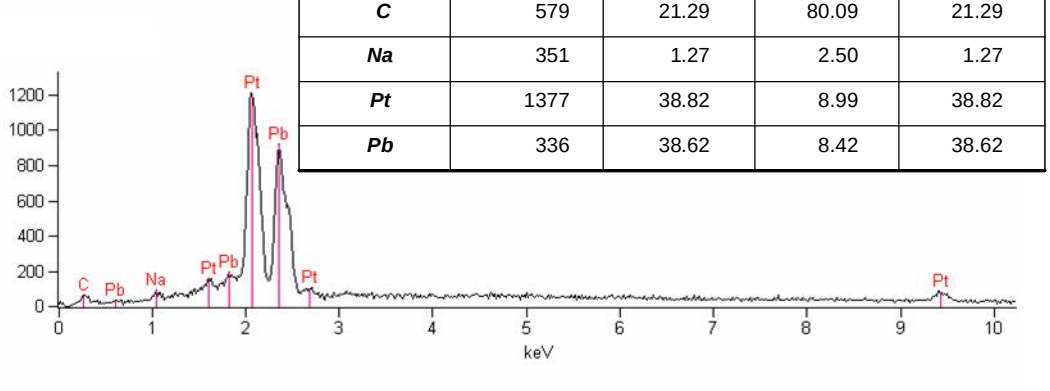

Element	*Net Counts*	*Weight %*	*Atom %*	*Compnd %*
C	579	21.29	80.09	21.29
Na	351	1.27	2.50	1.27
Pt	1377	38.82	8.99	38.82
Pb	336	38.62	8.42	38.62

Figure 2.1: EDX data of PtPb nanoparticles synthesized by injecting the precursors into reducing agent solution at 135 ^{o}C, followed by 30 min stirring at 135 ^{o}C.

For the reaction carried out at 120 ^{o}C, XRD patterns showed peaks which could be clearly indexed only to PtPb. The mean domain size calculated from the peak widths

using the Scherrer equation[19] was 8.4 nm. A domain size versus reaction temperature curve showed a sharp maximum around 120 ^{o}C (Figure 2.2).

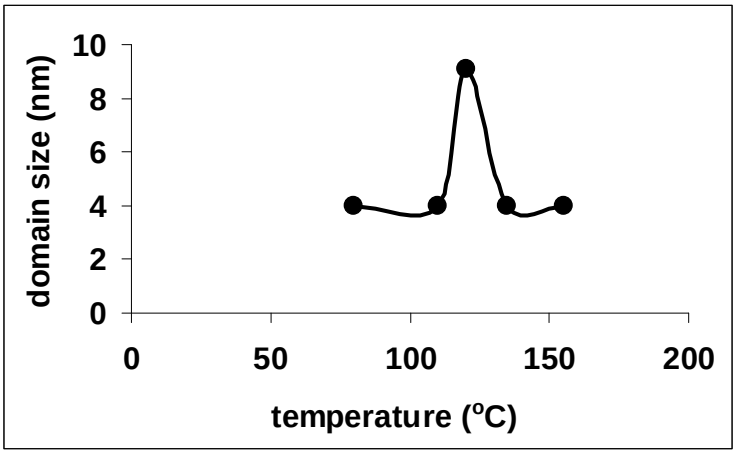

Figure 2.2: Domain size of PtPb nanocrystals synthesized by injecting the precursors into reducing agent solutions at different temperatures followed by stirring for 30 min at those temperatures.

EDX data again showed the presence of Pt and Pb in 1:1 ratio (+/- 5%) in multiple micron square areas along with the presence of some sodium. However, the amount of sodium present was negligible in this case. All EDX studies were done on dry samples on GaAs wafers to allow rough quantification of the amount of carbon present in the samples. Samples prepared at 120 ^{o}C showed lowest amount of carbon. A point to keep in mind here is the much higher molecular weights of the metals compared to carbon. Even a low weight % of carbon would indicate a considerable atomic ratio of carbon to the metals. Although absolute quantification of carbon using EDX is difficult owing to background signals, we used the carbon signal from nearby areas of

GaAs as a background correction. The background signal on GaAs was a small fraction of the total carbon signal (less than 0.1 wt %). In order to identify the source of the carbon content, ATR measurements were obtained from the solid powder samples. The acetylacetonate ligand on the PtPb surface could be clearly identified in the resulting spectra from asymmetric and symmetric ν_{coo-} stretching peaks at the 1600 -1400 cm^{-1} region in all samples except for the one prepared at 120 ^{o}C (Figure 2.3).

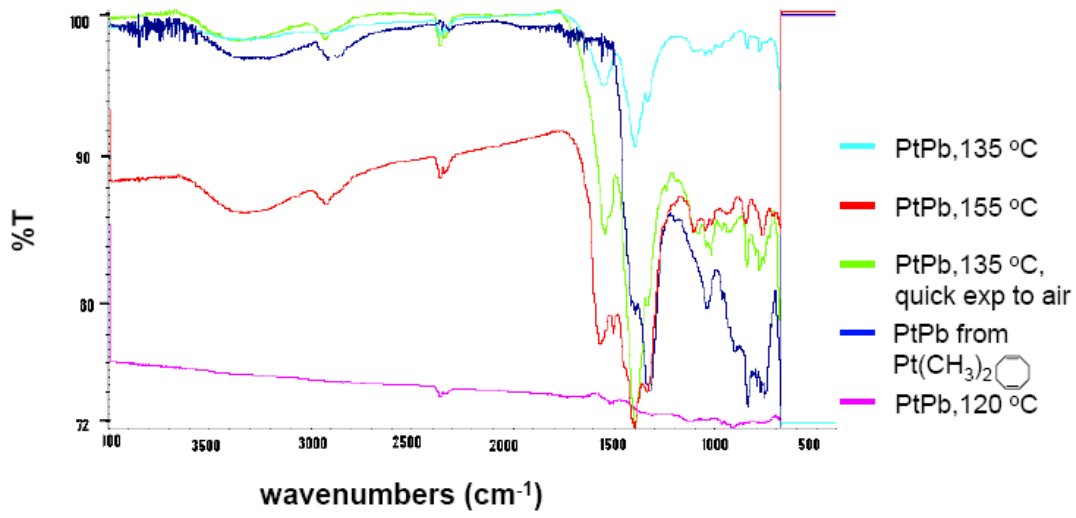

Figure 2.3: FTIR spectra of PtPb nanoparticle powders. Asymmetric and symmetric ν_{coo-} stretching peaks at the 1600 -1400 cm^{-1} region in all samples prepared from platinum acetylacetonate except for the one prepared at 120 ^{o}C. PtPb prepared from dimethyl(1,5-cyclooctadiene)platinum doesn't show the ν_{coo-} stretching peaks.

Aliphatic -C-H stretches were also observed (~2900 cm^{-1}), but no indication of ethylhexanoate (1735 cm^{-1} ester peak) from the lead precursor or sodium napthalide (aromatic –C-H stretching bands) was observed. We assume, therefore, that aromatic

groups are present only in insignificant amounts, if at all. SEM images of the samples, prepared at 120 ^{o}C gave clearly observable particles with sizes agreeing well with the calculated domain sizes from XRD. CBED patterns of this region confirm that the particles retain their crystallinity at the nano level (Figure 2.4 a, b).

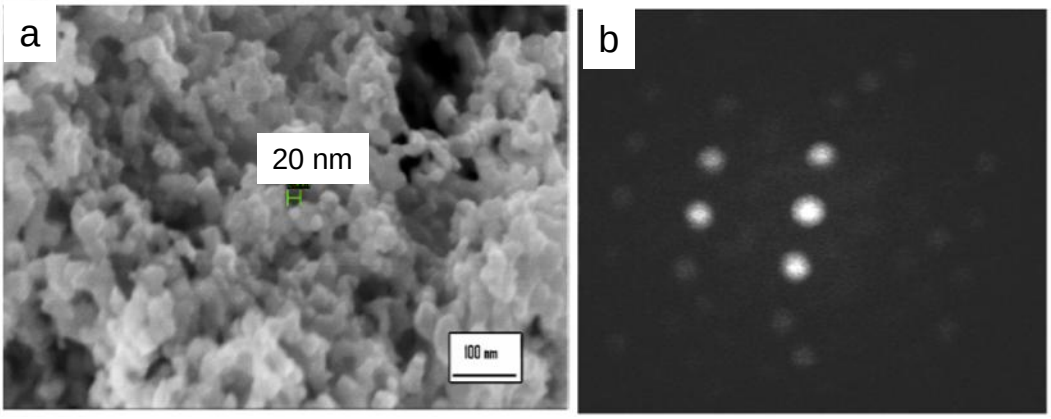

Figure 2.4: (a) SEM image of PtPb nanoparticles prepared from platinum acetylacetonate by injecting the precursors into reducing agent solution at 120 ^{o}C (b) CBED pattern of a PtPb nanocrystal from the same sample.

The particles, as expected, were seen to be highly agglomerated. Images of samples prepared at other temperatures also appeared as agglomerated networks, but smaller nanometer shapes were not identifiable under imaging conditions (Figure 2.5).

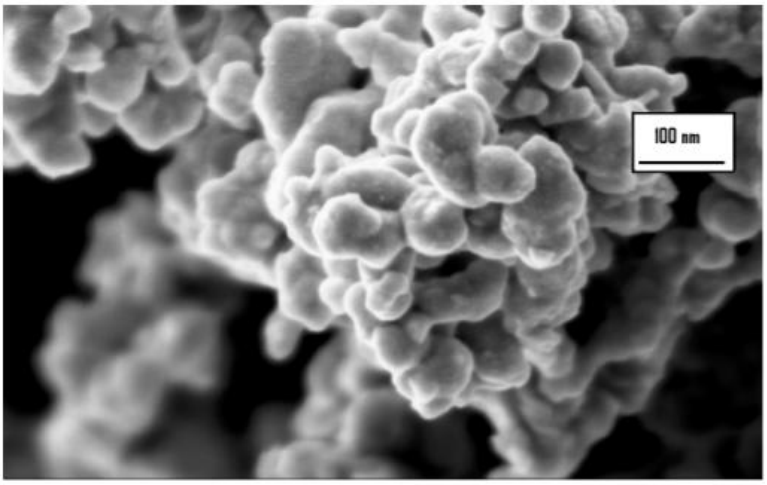

Figure 2.5: SEM image of PtPb nanoparticles synthesized from platinum acetylacetonate by injecting the precursors into the reducing agent solution at 135 ^{o}C.

As mentioned previously, all samples were found to contain sodium by EDX (sodium was also found on the walls of the tubes used for annealing). EDX confirms that the sodium could be completely removed by water. However, the IR spectra of the washed samples did not seem to be much different (figure 2.6), suggesting the presence of organics on the nanoparticles even after complete removal of the sodium. TGA of the samples done under nitrogen, showed up to 20% mass loss for the samples, with samples starting to loose mass at as low as 150 ^{o}C, again suggesting presence of organic species. The mass loss was the smallest for nanoparticles prepared at 120 ^{o}C, thus confirming the IR and EDX results. Thus, lower organic presence in the product is correlated with larger domain sized particles (Figure 2.7).

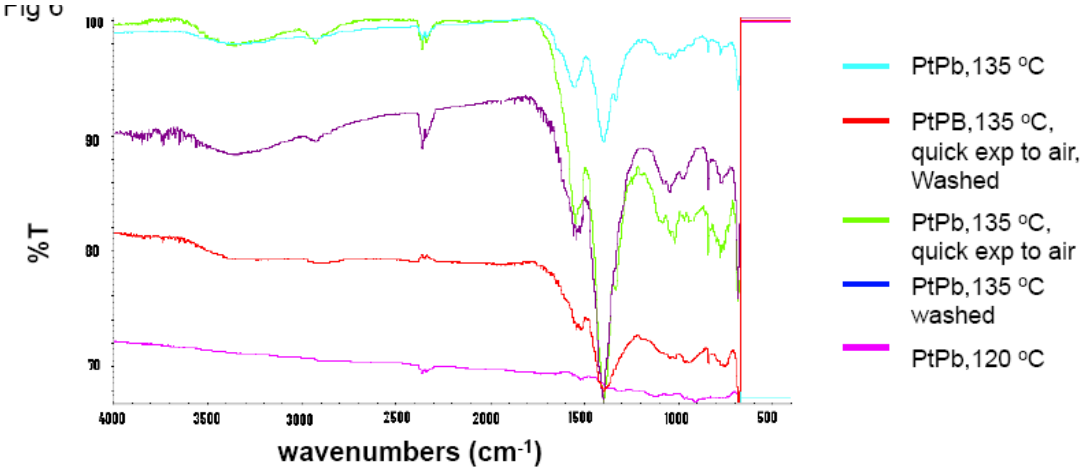

Figure 2.6: FTIR spectra of PtPb nanoparticle powders before and after water wash (particles were washed with water to remove the sodium initially detected on the particles by EDX). Asymmetric and symmetric ν_{coo-} stretching peaks at the 1600 - 1400 cm^{-1} region still observed, so water wash removes the sodium completely, but removal of sodium did not result in removal of the organics (at least not completely). The 'quick exp to air' refers to the samples exposed to air quickly (instead of slowly as described in the experimental section) post reaction and wash with solvents. It however seemed to have made little or no difference in terms of the organic material detected by FTIR on the nanoparticles.

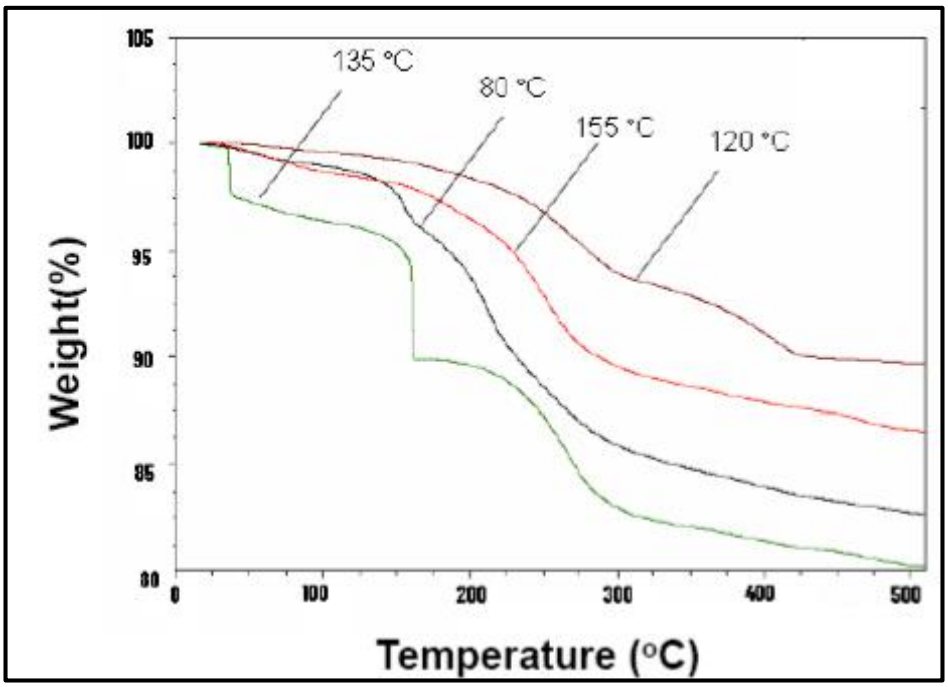

Figure 2.7: Thermogravimetric analysis plot of the PtPb nanoparticle samples prepared by injection of precursors into reducing agent solution at different temperatures showing mass loss (in %) of the samples with increasing temperature.

Following the unexpected results observed when the precursors were injected into the reducing solution stirred at temperatures up to 150 ^{o}C, another series of reactions was done by injecting the precursors into a reducing agent solution stirred at room temperature, followed by heating up to the desired temperature. This was done to check our hypotheses about the precursor itself undergoing changes when injected into a hot reducing agent solution (temperatures above 120 ^{o}C) in presence of the Pb precursor. If so, this might lead to new species being formed which were interfering with nanoparticle crystallization at higher temperatures.

Typically, the solution would take 10-15 min to heat up to the desired temperature, following which it would be stirred for 10 min at that temperature and the reaction

solvent would be evaporated off (series 2). The domain size variation with reaction temperature, in this case, looked much more familiar to previous observations (Figure 2.8).

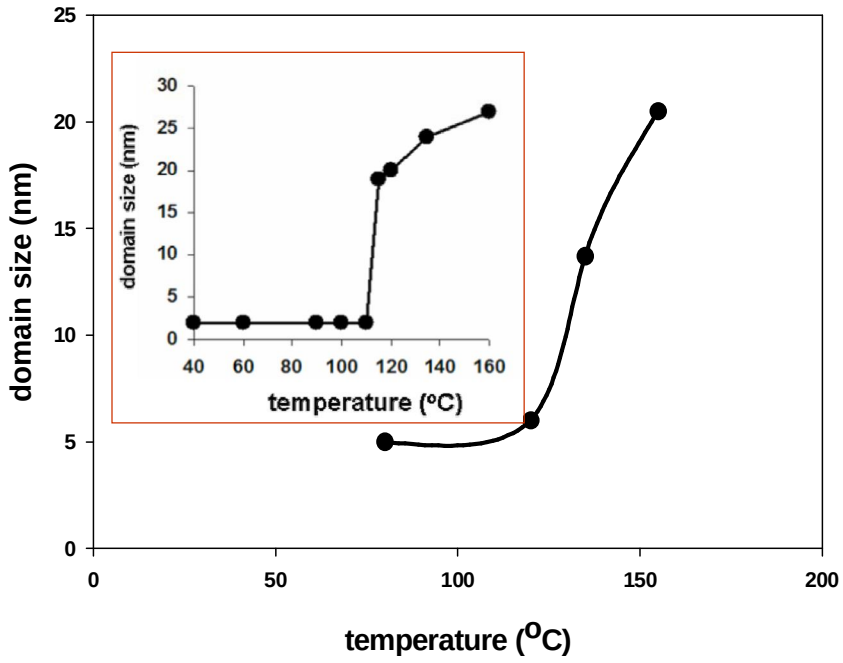

Figure 2.8: Domain size of PtPb nanocrystals synthesized by injecting the precursors into reducing agent solution at room temperature followed by heating up to different temperatures. Inset shows the similar domain size vs temperature trend observed with PtPb nanoparticles prepared from dimethyl(1,5-cyclooctadiene)platinum[12].

EDX data showed Pt and Pb to be present in a 1:1 ratio down to the nanoscale (20 nm X 20 nm regions) for all the samples. The amount of carbon and sodium observed on EDX remained almost constant irrespective of the domain size, but were much lower than the previous series (except for the 120 ^{o}C reactions, which were comparable). The

IR spectra of the samples again showed the presence of the acetylacetonate ligand on the nanoparticles. SEM images showed observable morphological changes suggesting gradual formation of the 'nanoparticles' with increasing reaction temperature (Figure 2.9 a,b,c).

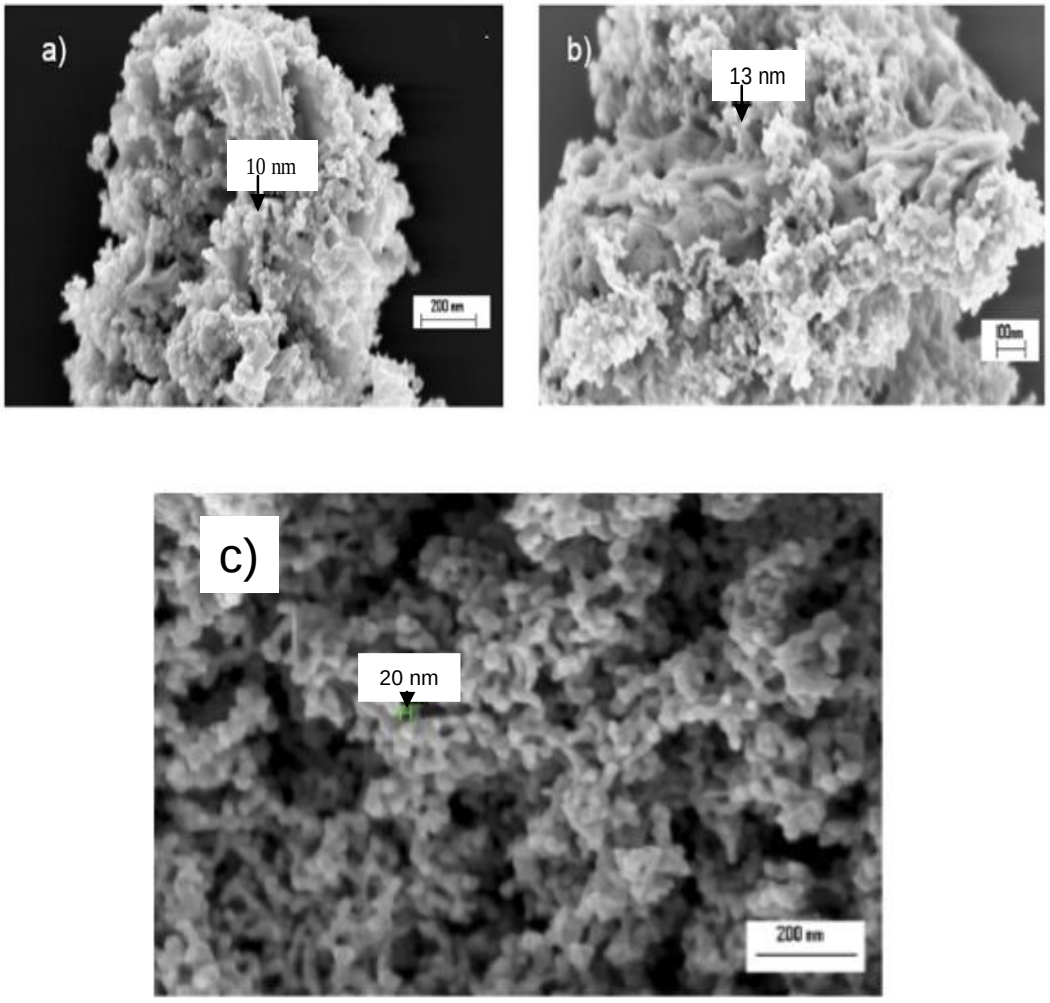

Figure 2.9: SEM images of PtPb nanoparticles prepared by injecting precursors into reducing agent solution at room temperature followed by heating up-to different temperatures (a) 120 ^{o}C (b) 135 ^{o}C and (c) 155 ^{o}C. The gradual formation of nanoparticles on going to higher temperatures can be observed in the images.

The smallest observable particles corresponded to the respective domain sizes calculated from Scherrer equation for all the samples. CBED patterns confirmed that the crystalline nature of the particles was retained at the nanoscale. The long time needed for solvent removal (diglyme took around 4 hr to evaporate off at 40 deg, ~150 mTorr) caused us to seek an alternative method of solvent removal. Interestingly, the properties of the resulting nanoparticles were significantly altered by changing this procedure. In this method, as described in the experimental section, post injection of precursors into the reducing agent solution (injection done at room temperature followed by heating up if necessary) and 15 min of stirring (typically), the mixture would be cannula transferred into a centrifuge tube, centrifuged and the supernatant would be syringed off. For this method, the mean domain size of the PtPb nanoparticles obtained by a room temperature reaction was 14 nm as determined by the Scherrer equation. The domain size variation with the temperature to which the solution was heated up to post injection, was minimal (Figure 2.10).

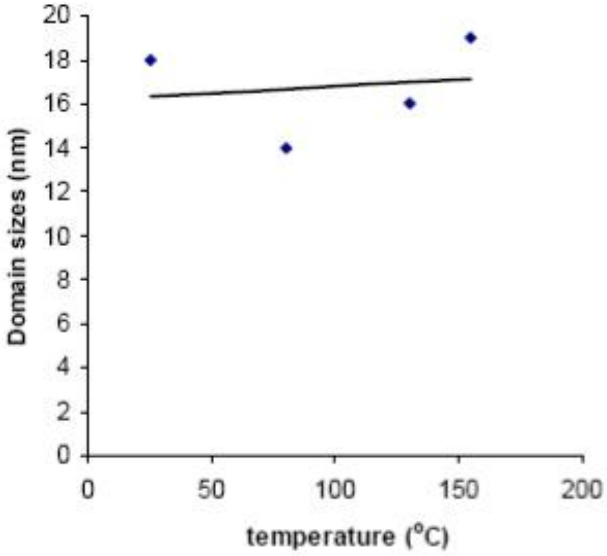

Figure 2.10: Domain size of PtPb nanocrystals synthesized by injecting the precursors into reducing agent solution at room temperature followed by heating up to different temperatures; solvent syringed off post reaction after precipitating out the nanoparticles. Domain size observed to be largely invariant of temperature, with clearly identifiable PtPb crystals (with mean domain size of 18 nm) was obtained for even the room temperature reaction.

Also, SEM images confirmed the domain sizes calculated from X-ray diffraction. Interestingly, this confirms that the organics present on these nanoparticles are on the surface and not trapped inside. Interesting changes were again observed in the nanoparticle shapes and agglomeration with increases in the reaction temperature (Figure 2.11a,b,c,d). A plausible explanation for crystallization at room temperature and the overall ease of crystal formation that was observed with this particular work-up procedure could be the removal of the reaction solvent and organic products.

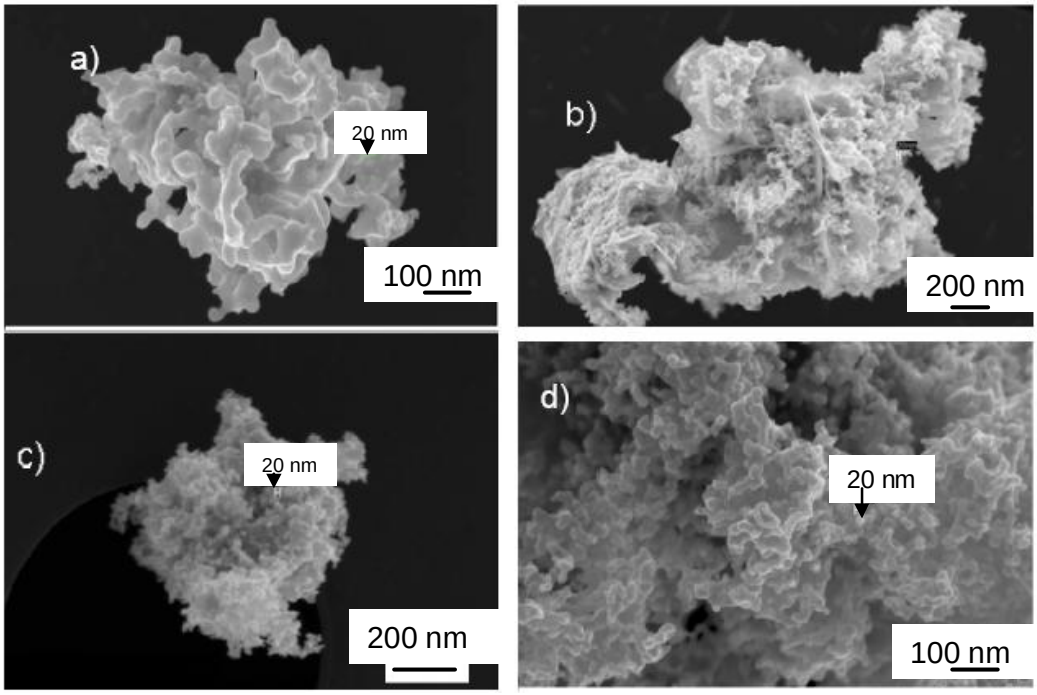

Figure 2.11: SEM images of PtPb nanoparticles prepared by injecting precursors into reducing agent solution at room temperature followed by heating up to different temperatures (a) room temp (b) 80 ^{o}C and (c) 130 ^{o}C and (d) 155 ^{o}C; solvent syringed off post reaction after precipitating out the nanoparticles. The gradual formation of nanoparticles on going towards higher temperature can again be very clearly observed. The observed morphological changes might be arising from compositional changes. If so, the temperature dependent property changes observed in all these materials can be explained.

Solvent removal by evaporation concentrates the organic product. This can be understood in terms of a ligand equilibrium between the reaction solvent and the solids in the system (L(solvent)↔L(solid)), which shifts towards more L(solid) when only the solvent is removed (by evaporation). Indeed the IR signal from acetylacetonate is

lowered following a THF wash. TEM studies done on microtomed sections (uniformly 60 nm in thickness) of the nanoparticles from the 80 ^{o}C reaction, showed darker and lighter regions. SAED confirmed that all regions studied were crystalline (Figure 2.12 a, b).

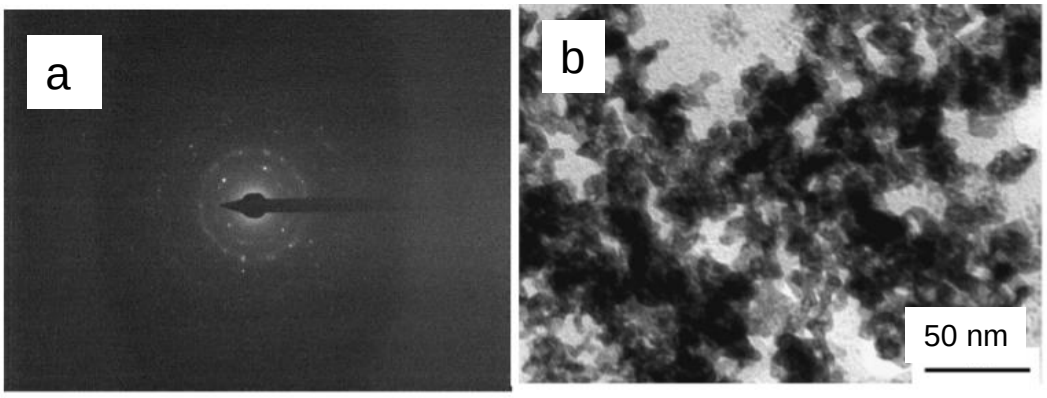

Figure 2.12: (a) SAED pattern of PtPb nanocrystal prepared by injecting precursors into reducing agent solution at room temperature followed by heating up to 130 ^{o}C; solvent syringed off post reaction after precipitating out the nanoparticles. (b) Microtomed section (of uniform 1 μm thickness) of the same sample.

For both series 2 and 3, TGA showed much lower mass losses (averaging around 9 %) than what was observed for series 1. This agrees well with the corresponding EDS studies. Also, for series 1 and 2 the TGA mass losses corresponded to the domain size variation with temperature (highest mass losses were observed for temperatures at which particle domain size found to be lowest and vice versa). For series 3, TGA mass loss is almost constant with respect to reaction temperature (as is the domain size variation) (Table 2.2). These observations fit in well with the model of surface-bound organics interfering with nanoparticle crystallization.

Table 2.2: Different method of synthesis followed for PtPb nanoparticles and associated observations.

Series	Method	Domain size variance with reaction temperature	TGA mass loss observed (around 150°C – 200°C)
Series1	Precursors injected into a reducing agent solution stirring at the desired temperature. Solvent evaporated off post reaction	Domain size falls on increasing/decreasing Reaction temperature from 120 °C	Lowest (120°C)- 10.03% Highest (155°C)- 19.91%
Series 2	Precursors injected into a reducing agent solution stirring at room temperature, solution then heated up to desired temperature. Solvent evaporated off post reaction	Domain size increases On increasing reaction temperature	Lowest (155°C)- 5.75% Highest (80°C)- 13.52%
Series 3	Precursors injected into a reducing agent solution stirring at room temperature, solution then heated up to desired temperature. Solution centrifuged post reaction, supernatant solvent syringed off.	Domain size remains constant with respect to change in reaction temperature. PtPb domain size measured to be 18 nm even on doing a room temperature reaction.	Lowest (155°C)- 8.64% Highest (r.t.)- 9.18%

2.3.3 Electrocatalytic activity

Electrocatalytic activity of the nanoparticles prepared by injecting precursors into the reducing agent solution at different temperatures and worked up by evaporating off the reaction solvent (series 1) toward the oxidation of formic acid was examined. The onset potential for PtPb nanoparticles is the same as that of all PtPb nanoparticles examined previously in the group (i.e. -0.2 V for PtPb nanoparticles prepared by both sodium borohydride and sodium napthalide reduction). Hence, to compare the electrocatalytic activity of the particles, the magnitude of current density at a potential positive of onset (+0.2V) was compared (Table 2.3).

Table 2.3: Mass activities of PtPb samples prepared by injection of precursors into reducing agent solution at different temperatures at onset potential of PtPb (-0.2 V).

Sample Injection at reaction temperature	Mean Domain Size (nm)	Mass activity at 0.2 V/ mA μg^{-1}
PtPb from $Pt(acac)_2$,80°C	4	0.036
PtPb from $Pt(acac)_2$,135°C	4	0.092
PtPb from $Pt(acac)_2$,120°C	**8.4**	**0.153**
PtPb from $Pt(acac)_2$,155°C	4	0.030

Higher mass activities at a given potential indicate a better catalyst. However, the values compared here in units of mA/μgm and need to be normalized with respect to the BET surface area (which would be different for each sample owing to different particle size and degree of agglomeration) for an absolute comparison. The highest mass activity is observed for the nanoparticles prepared at 120 ^{o}C. This mass activity

is much higher (>200%) than what was previously obtained from PtPb nanoparticles made by sodium napthalide reduction (using dimethyl(1,5-cyclooctadiene)platinum precursor) but is lower (<200%) than what was obtained from PtPb nanoparticles made by sodium borohydride reduction in the group.

The electrocatalytic activity of the nanoparticles prepared by heating up the solution to different temperatures post injection of precursors into a room temperature reducing agent solution and worked up by evaporating off the solvent (series 2) toward the oxidation of formic acid was measured by comparing the magnitude of current density at +0.2V (Table 2.4). Again, the highest mass activity was observed for the nanoparticles prepared at 120 ^{o}C. Also, the mass activity obtained for this sample was much higher than the PtPb nanoparticles made by high temperature injection of precursors into the sodium napthalide solution and is comparable to current densities obtained from PtPb nanoparticles made by sodium borohydride reduction. Again, for a more meaningful comparison, currents were normalized to the BET surface area of the respective catalysts. The current density obtained for the present PtPb product is the highest obtained to date. In terms of highest obtainable electrocatalytic activity, room temperature injection into a solution of the reducing agent solution followed by heating works better for platinum acetylacetonate than for platinum dimethyl cyclooctadiene.

Table 2.4: Mass activities of PtPb samples prepared by injection of precursors into reducing agent solution at room temperature followed by heating up to different temperatures at onset potential of PtPb (-0.2 V).

Sample Room temperature injection, followed by heating up	Mean Domain Size (nm)	Mass activity at 0.2 V / mA μg^{-1}
PtPb from $Pt(acac)_2$,80°C	5	0.051
PtPb from $Pt(acac)_2$,135°C	13.7	0.34
PtPb from $Pt(acac)_2$,120°C	**6**	**0.52**
PtPb from $Pt(acac)_2$,155°C	20	0.21

Similarly, the electrocatalytic activity of the nanoparticles prepared by heating the solution to different temperatures post injection, and worked up by centrifuging and syringing off the reaction solvent (series 3) toward the oxidation of formic acid was assessed by comparing the mass activity at a potential positive of onset(-0.2V). The highest mass activity was observed for the nanoparticles prepared at 135 ^{o}C (Table 2.5).

Table 2.5: Mass activities of PtPb samples prepared by injection of precursors into reducing agent solution at room temperature followed by heating up to different temperatures (solvent syringed off post reaction) at onset potential of PtPb (-0.2 V).

	Domain size in nm	MA/mAμg^{-1} at 0.2 V
PtPb from $Pt(acac)_2$,130°C	16	0.179
PtPb from $Pt(acac)_2$,80°C	14	0.0163
PtPb from $Pt(acac)_2$,155°C	19	0.064

Also, the highest mass activity obtained in this case is much lower than the highest obtained in the case of room temperature injection of precursors following drying of the reaction mixture under vacuum, but is comparable to the highest obtained by high temperature injection of precursor method (Table 2.6). Figure 2.14a, b shows the rotating disk voltammograms of the PtPb nanoparticles synthesized by different methods as well as for Pd black and PtRu alloy standards. The variation in current densities of PtPb particles prepared differently maybe due to different crystal planes exposed in different samples, different degree of agglomeration or different surface composition of the nanoparticles.

Table 2.6: Comparison of electrochemical data of PtPb samples prepared in group till date by various methods. Results from previous work in PtPb syntheses are compared (*, **, ***) to those synthesized in this work[1, 2, 12].

	Domain size in nm	MA/mAμg^{-1} at 0.2 V	MA/mAcm^{-2} at 0.2 V
PtPb from $Pt(acac)_2$,120°C, Series 1	9.1	0.153	2.43
PtPb from $Pt(acac)_2$,120°C Series 2	13.7	0.520	5.95
PtPb from $Pt(acac)_2$,130°C Series 3	16	0.179	1.73
PtPb (produced with H_2PtCl_6 and $Pb(MOEEAA)_3$, $NaBH_4$ reduction*)	**10.6**	**0.132**	5.5
PtPb (produced withH_2PtCl_6 and $Pb(C_2H_3O_2)_2$), $NaBH_4$ reduction***)	12	**0.441**	2.94
PtPb (produced with $PtMe_2$◯ and $Pb(C_2H_3O_2)_2$,135°C, 10 min), NaNp reduction**)	24	**0.045**	1.98

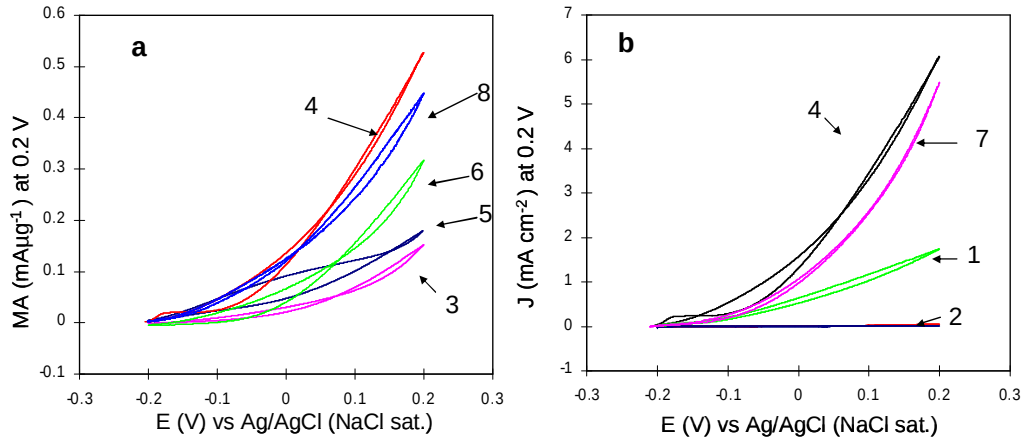

Figure 2.13: Rotating disk voltammograms showing mass activity (MA) and current density (J, current normalized with respect to the BET surface area of the catalysts) for formic acid oxidation on Pd Black(1), PtRu/C (2), 120 ^{o}C reaction, Series1 (3), 120 ^{o}C reaction, Series 2 (4), 135 ^{o}C reaction series 3 (5), PtPb prepared from PtPb (produced with dimethyl (1,5-cyclooctadiene) platinum and $Pb(C_2H_3O_2)_2$, sodium napthalide reduction (6), PtPb (produced with H_2PtCl_6 and $Pb(MOEEAA)_3$, $NaBH_4$ reduction (7), PtPb (produced with H_2PtCl_6 and $Pb(C_2H_3O_2)_2$), $NaBH_4$ reduction (8).

2.4 Conclusions

In conclusion, we have found a more convenient precursor (platinum acetylacetonate) for PtPb intermetallic syntheses using sodium napthalide (or similar reducing agents which would require inert techniques and etheral solvents). PtPb synthesized with this precursor has a higher specific activity for formic acid oxidation when compared to those prepared previously. Also, we have shown adsorbed organic fragments from the precursors to be one of the factors interfering with nanoparticle crystallization, and have been able to establish a method to minimize their effects after carefully varying

the various controlling factors (mode of precursor injection, reaction temperature and solvent removal). Interesting trends in particle morphology and electrochemical activity were observed but need further investigation. Research is ongoing in the group for further identification and characterization of the organic fragments sticking to the particles (MS, TGA and FTIR studies along with nanoscale EDS).We are also extending our work with this precursor towards syntheses of other platinum intermetallics starting with the Pt-Ti ones.

REFERENCES

1. Roychowdhury, C.; Matsumoto, F.; Zeldovich, V. B.; Warren, S. C.; Mutolo, P. F.; Ballesteros, M.; Wiesner, U.; Abruna, H. D.; DiSalvo, F. J., Synthesis, characterization, and electrocatalytic activity of PtBi and PtPb nanoparticles prepared by borohydride reduction in methanol. *Chemistry of Materials* **2006,** 18, (14), 3365-3372.

2. Alden, L. R.; Roychowdhury, C.; Matsumoto, F.; Han, D. K.; Zeldovich, V. B.; Abruna, H. D.; DiSalvo, F. J., Synthesis, characterization, and electrocatalytic activity of PtPb nanoparticles prepared by two synthetic approaches. *Langmuir* **2006,** 22, (25), 10465-10471.

3. Lamy, C. L., Leger, J. M., Srinivasan, S., *Direct Methanol Fuel Cells: From a Twentieth Century Electrochemist's Dream to a Twenty-first Century Emerging Technology*. New York: Kluwer Academic/Plenum: 2001; Vol. 34.

4. Shah, R. K.; Kandlikar, S. J. In *Fuel cell science, engineering and technology* American Society of Mechanical engineers, Rochester, NY, 2003; Rochester, NY, 2003; p 538

5. Liu, H. S.; Song, C. J.; Zhang, L.; Zhang, J. J.; Wang, H. J.; Wilkinson, D. P., A review of anode catalysis in the direct methanol fuel cell. *Journal of Power Sources* **2006,** 155, (2), 95-110.

6. Casado-Rivera, E.; Gal, Z.; Angelo, A. C. D.; Lind, C.; DiSalvo, F. J.; Abruna, H. D., Electrocatalytic oxidation of formic acid at an ordered intermetallic PtBi surface. *Chemphyschem* **2003,** 4, (2), 193-199.

7. Roychowdhury, C.; Matsumoto, F.; Mutolo, P. F.; Abruna, H. D.; DiSalvo, F. J., Synthesis, characterization, and electrocatalytic activity of PtBi nanoparticles prepared by the polyol process. *Chemistry of Materials* **2005,** 17, (23), 5871-5876.

8. Oana, M.; Hoffmann, R.; Abruna, H. D.; DiSalvo, F. J., Adsorption of CO on PtBi2 and PtBi surfaces. *Surface Science* **2005,** 574, (1), 1-16.

9. Volpe, D.; Casado-Rivera, E.; Alden, L.; Lind, C.; Hagerdon, K.; Downie, C.; Korzeniewski, C.; DiSalvo, F. J.; Abruna, H. D., Surface treatment effects on the electrocatalytic activity and characterization of intermetallic phases. *Journal of the Electrochemical Society* **2004,** 151, (7), A971-A977.

10. Casado-Rivera, E.; Volpe, D. J.; Alden, L.; Lind, C.; Downie, C.; Vazquez-Alvarez, T.; Angelo, A. C. D.; DiSalvo, F. J.; Abruna, H. D., Electrocatalytic activity of ordered intermetallic phases for fuel cell applications. *Journal of the American Chemical Society* **2004,** 126, (12), 4043-4049.

11. Blasini, D. R.; Rochefort, D.; Fachini, E.; Alden, L. R.; DiSalvo, F. J.; Cabrera, C. R.; Abruna, H. D., Surface composition of ordered intermetallic compounds PtBi and PtPb. *Surface Science* **2006,** 600, (13), 2670-2680.

12. Alden, L. R.; Han, D. K.; Matsumoto, F.; Abruna, H. D.; DiSalvo, F. J., Intermetallic PtPb nanoparticles prepared by sodium naphthalide reduction of metal-organic precursors: Electrocatalytic oxidation of formic acid. *Chemistry of Materials* **2006,** 18, (23), 5591-5596.

13. Doernickel, F. Z., *Anorg Chem* **1908,** 54, 358.

14. Mortimer, C. T., *Reviews in Inorganic Chemistry* **1984,** 6, (3), 233.

15. Keller, R. N., Platinum(Iv) Chloride. *Inorganic Syntheses* **1946,** 2, 253-255.

16. Basato, M.; Biffis, A.; Martinati, G.; Tubaro, C.; Venzo, A.; Ganis, P.; Benetollo, F., Reaction of platinum acetate with phosphines and molecular structure of trans-[Pt(OAc)(2)(PPh3)(2)]. *Inorganica Chimica Acta* **2003,** 355, 399-403.

17. Murugan, N. A.; Yashonath, S., Pressure induced orientational ordering in p-terphenyl. *Journal of Physical Chemistry B* **2005,** 109, (4), 1433-1440.

18. Prabhuram, J.; Zhao, T. S.; Tang, Z. K.; Chen, R.; Liang, Z. X., Multiwalled carbon nanotube supported PtRu for the anode of direct methanol fuel cells. *Journal of Physical Chemistry B* **2006,** 110, (11), 5245-5252.

19. Warren, B. E., *X-ray Diffraction*. 1st ed.; Dover Publications Inc.: 1990.

Chapter 3

SYNTHESIS OF Pt-Ti PHASES BY SODIUM NAPTHALIDE REDUCTION

3.1 Background

This work was started as continuation of Dr. Hideki Abe's work with Pt-Ti systems. As mentioned in the previous chapter, we were following the leads from our collaborators doing combinatorial research to identify potentially interesting combinations of metals as catalysts for small molecules. The Pt-Ti intermetallic compounds showed more negative onset potentials than Pt. Also, the high electropositivity of Ti leads to more challenging chemistry than for Pb and Bi, which has already been extensively explored[1]. Thus we decided to explore the potential of sodium napthalide to co-reduce Pt and Ti precursors, to determine how far this co-reduction method can be extended. Driven by the above objectives, Dr Hideki Abe (a then post-doctoral research fellow in the DiSalvo group) pursued the synthesis of Pt-Ti intermetallic phases by sodium napthalide reduction of suitable precursors[2]. Table 3.1 summarizes his reactions and observations. The co-reduction of Pt(1,5-cyclooctadiene)Cl_2 and Ti(tetrahydrofuran)$_2Cl_4$ by sodium naphthalide in tetrahydrofuran at room temperature resulted in the formation of atomically disordered Pt-Ti nanoparticles (FCC-type structure: *Fm*$\underline{3}$*m*; *a* = 0.39 nm; average particle size = 3 nm). The atomically disordered Pt-Ti particles were found to grow in size upon annealing in vacuum. On increasing the annealing temperature to 600 ^oC, atomically ordered Pt_3Ti nanoparticles (Cu_3Au-type structure: *Pm*$\underline{3}$*m*; *a* = 0.3898 nm; average particle size = 35 nm) were formed.

Table 3.1: Summary of previous reactions done in the group with the Pt-Ti system. All reactions were done in THF, at room temperature, 100 % excess of the reducing agent and stirring time 24 h.

Pt Precursor	**Ti precursor**	**Ratio of precursors Pt : Ti**	**Approx. Pt : Ti ratio from EDS**	**X-ray diffraction**	**X-ray diffraction after annealing at 600 °C**
$PtCODCl_2$	**$TiCl_4(THF)_2$**	**1 : 0.5**	**Not done**	**Disordered, broad peaks**	**Not done**
		1 : 1	**3 : 1**	**Disordered, broad peaks**	**Pt_3Ti**
		1 : 2	**3 : 1**	**Disordered, broad peaks**	**Pt_3Ti**
		1 : 3	**3 : 1**	**Disordered, broad peaks**	**Pt_3Ti**
$PtCODCl_2$	**$TiCl_3(THF)_3$**	**1 : 1**	**Not done**	**Disordered, broad peaks**	**Pt_3Ti**
$PtCODMe_2$	**$TiCl_3(THF)_3$**	**1 : 1**	**Not done**	**Disordered, broad peaks**	**Pt_3Ti**

Both atomically disordered and ordered Pt_3Ti nanoparticles showed lower onset potentials for the oxidation of both formic acid and methanol and lower affinity for CO adsorption than either pure Pt or Pt-Ru nanoparticles. Higher current densities were obtained with atomically ordered Pt_3Ti nanoparticles in the oxidation of both formic acid and methanol than with atomically disordered Pt_3Ti, pure Pt, or Pt-Ru nanoparticles. Although encouraging from the catalysis point of view, two important issues, not encountered for the Pt-Pb system, arose from these observations. Firstly, as determined by EDS in the UHV-STEM, the Pt:Ti::3:1 phase (Pt_3Ti) was obtained even thought larger amounts of Ti (Ti/Pt $\geq$ 1) were used. The loss of Ti from the system

was attributed at that point to the work up step involving a MeOH wash. We hypothesized that the Ti was being oxidized by reacting with the wash solvent to form titanium methoxide. Secondly, the ordered phase could only be obtained on annealing at high temperatures (600 ^{o}C) after the reduction reaction. As depicted in Table 3.1, all reductions were carried out at room temperature. One of the methods that led to the growth of nanoparticle size of the PtPb phase was in-situ heating of the reaction solution following the injection of precursors into the reducing agent. In-situ heating might also help in facilitating nucleation and growth of the desired Pt-Ti phases. In that case, the removal of Ti during washes with MeOH is expected to be limited to the surface of the particles. Additionally, if in-situ heating could form the ordered phases, no further annealing would be required. As discussed in Chapter 2, from our studies with the Pt-Pb system, $Pt(acac)_2$ had emerged as a convenient precursor which could possibly replace the previous Pt precursors employed. Combining the above two possible directions, reactions with $Pt(acac)_2$ as the Pt precursor were explored at different temperatures.

3.2 Reactions using $Pt(acac)_2$

3.2.1 Experimental

The procedure followed for co-reduction of Pt and Ti precursors with sodium napthalide closely mimics the ones described in the PtPb chapter. However, we present the details here for completeness.

Materials: Platinum acetylacetonate ($Pt(acac)_2$ where acac = acetylacetonate anion, $C_5H_7O_2^-$) was used as the platinum precursor for the reactions described in this section. The platinum acetylacetonate was obtained commercially from Aldrich. The

precursor for Ti, $Ti(THF)_2Cl_4$ where THF is tetrahydrofuran, was synthesized from $TiCl_4$ (Aldrich; 99.9% purity) and distilled tetrahydrofuran (Fisher) according to literature procedures[3]. The other precursor explored for Ti was $TiCp_2Cl_2$ (Cp = cyclopentadienyl anion, $C_5H_5^-$), which was obtained commercially from Aldrich. Sodium metal and all solvents were purchased from Aldrich. Naphthalene were purchased from Fisher. All other metal precursors were purchased from STREM chemicals Inc. Dry solvents (THF, Diglyme and hexanes) for the reaction was obtained using the solvent system.

Sodium Napthalide: Sodium napthalide solutions were prepared in either THF or diglyme (bis(2-methoxyethyl)ether, MW = 134.18) according to well known literature methods[4]. Stoichiometric amounts of naphthalene and sodium metal were weighed out in an argon atmosphere glovebox and added to a flask containing 40 ml of the solvent. The sealed flask was removed from the glovebox and stirred overnight under argon to produce a dark green sodium napthalide solution.

3.2.1.1 Single precursor reductions

The Ti or Pt precursor ($Ti(THF)_2Cl_4$ or $Pt(acac)_2$ respectively) was dissolved in THF (0.06 mmol in 10 ml THF) inside the argon atmosphere box. Sodium napthalide solution (0.72 mmol in 40 ml THF prepared the day before according to procedure described previously) was injected with this solution while rapidly stirring under argon. An immediate color change to black was observed suggesting reduction of the precursor. The solution was allowed to stir for 3 hr, and the solvent was evaporated off. After dispersing the solid black residue in hexanes (dry, from the solvent system) by sonicating for 10 min, the solution was transferred into a centrifuge tube and centrifuged. The clear solvent was removed with a syringe. For the reduction of Pt, an

additional wash with MeOH was performed. This step was skipped for the Ti precursor given the reactivity of Ti with MeOH. The product in each case was dried under vacuum and stored under argon. The Pt reaction product was exposed to air slowly by allowing air to diffuse through a needle that punctured the septum on the centrifuge tube. X-ray diffraction pattern was obtained on the Pt product after exposing it to air. The Ti product was pumped into the dry box and we attempted to obtain air free X-ray diffraction pattern by sealing the product in a sample holder with a film of mylar. Color change from black to lighter shades happened on air exposure under mylar within the time span of running the X-ray diffraction scan suggesting oxidation of the product by air diffusing through the mylar covering.

3.2.1.2 Co-reduction of Pt and Ti precursors

A precursor solution containing a 1:1 stoichiometric ratio of the precursors was prepared by dissolving Pt(1,5-cyclooctadiene)Cl_2 (0.06 mmol) and Ti$(THF)_2Cl_4$ (0.06 mmol) in 10 ml of distilled tetrahydrofuran (Fisher) under dry Ar atmosphere. The precursor solution was then transferred into a syringe, taken out of the dry box and injected into a freshly prepared sodium napthalide solution in THF (0.72 mmol in 40 ml when the reducing agent is used in 100 % excess) which was being stirred under argon. 100 % excess of the reducing agent was used to ensure complete reduction of the highly electropositive Ti^{4+}. The sodium napthalide solution turned dark-brown immediately upon injection. After stirring overnight, the solvent was distilled off at a reduced pressure to leave a dark-brown precipitate. Approximately 20 ml of anhydrous MeOH (degassed for 1 hr) was transferred into the flask, the products were re-suspended by sonication (2 min) and cannula transferred into a centrifuge tube under argon. The solution was centrifuged at 9000 rpm for 30 min, and the supernatant

was removed with a syringe. 20 ml of hexane (dry, from the solvent system) was washed added and the sonication and centrifugation steps were repeated. At each washing step, the precipitate was separated from the washing solvents by centrifugation without air exposure. The final precipitates were dried by evacuation at room temperature, following which the tube was backfilled with argon. In the very last step, the product was exposed to air slowly by puncturing the septa with a needle. The above procedure was slightly modified for heating the products in-situ.

The sodium napthalide solution was prepared in diglyme instead of THF. The higher boiling point of the former allowed in-situ heating of the products at temperatures up to ~160 ^{o}C. The precursors were dissolved in diglyme (solubility of the Ti precursor was found to be higher in diglyme than in THF) Following injection of precursors into the reducing agent solution, the reaction flask was heated up to 80 ^{o}C or 120 ^{o}C using an oil bath. Tetraglyme was used as a solvent when the reaction mixture was heated to 220 ^{o}C post injection. The experimental procedure for those reactions is described in the next section. After 24 hrs of stirring at these temperatures, the reaction mixture was allowed to cool down to 60 ^{o}C, and the diglyme was evaporated off to dryness under vacuum. The evaporation was carried out at 60 ^{o}C instead of room temperature in order to speed up the solvent removal process which is quite time consuming with high boiling solvents (boiling point of diglyme = 162 ^{o}C). The rest of the work-up procedure followed was identical to what is described above.

In an alternative work-up procedure for solvent removal, the reaction mixture was allowed to come down to room temperature following 24 hr of stirring (if the stirring was not at room temperature) and cannula transferred into a centrifuge tube. The mixture was centrifuged at 9000 rpm for as long as 60 min. If the product precipitated, the supernatant was removed with a syringe. For the room temperature reactions in THF, the solution would still be very dark with very little product precipitating out.

Removing the supernatant with a syringe and carrying out MeOH and hexane washes in such cases resulted in very low yields as significant amounts of product were lost in the very first step. This procedure was thus abandoned for future Pt-Ti room temperature reactions. However, we will discuss in detail in the future sections the causes and implications for this observation. For the reactions in diglyme (which were heated in-situ to 120 ^{o}C), centrifuging (9000 rpm, 30 min) would result in complete precipitation of the product. In such cases, the diglyme was syringed off and the product was washed in MeOH and hexane, dried and exposed to air slowly. To study the effect of varying the reducing agent excess and precursor concentration, reactions were carried out at room temperature following the procedure described above. For studying the former effect, the initial amount of sodium napthalide was varied keeping the solvent volume constant (40 ml THF) with different initial amounts of sodium napthalide (0.54 mmol for 50 % excess, 0.45 mmol for 25% excess). For the later effect, the initial solvent volume was changed from 40 ml to 80 ml keeping the amount of sodium napthalide same (0.72 mmol, 100 %excess). Precursor amounts were maintained at 0.06 mmol each, dissolved in 10 ml THF for all reactions.

In-situ heating to temperatures higher than 165 ^{o}C (boiling point of diglyme): For reactions in which the reaction mixture was to be heated to 220 ^{o}C (and later 270 ^{o}C), tetraglyme was used as the solvent. Initial reactions were carried out by preparing the sodium napthalide in tetraglyme itself. Typically dry solvents would be pumped into the argon atmosphere box in amounts to suffice a few reactions in a bomb flask since the sodium napthalide needed to be prepared inside the box. However, given the very high boiling point of tetraglyme, distilling the amounts required from a sodium benzophenone still (used to dry commercially obtained tetraglyme) into the bomb flask would typically take days. In order to bring down this time, the tetraglyme was dried on molecular sieves in the bomb flask (after cannula transferring it into the flask

from the commercial bottle equipped with sure seal) and pumped into the dry box. Titration was carried out by adding different amounts of sodium and naphthalene to a fixed volume of this tetraglyme until the dark green color of sodium napthalide was obtained and retained for extended period of time. The goal was to quench the impurities in the solvent and still have enough sodium napthalide left to carry out the reduction. To do this, we needed to ascertain the amount of sodium napthalide for the volume of tetraglyme to be used in the reaction that would guarantee sufficient excess after reacting with impurities in the solvent. From the results of the titration, 3.6 mmol each of sodium and naphthalene (500 % or 10 times in excess) was dissolved in 40 ml tetraglyme inside the argon atmosphere box. The sealed flask was removed from glovebox and left stirring overnight under argon. 0.06 mmol each of the precursors were dissolved in 10 ml tetraglyme and injected into the reducing agent solution the next day. Following the injection, the reaction vessel was heated up to 220 ^{o}C using a silicone oil bath. Once at 220 ^{o}C, the reaction was stirred for a definite amount of time (two different stirring times were tried: 15 min and 3.5 hr), and then cooled down to room temperature. The solution was then cannula transferred into a centrifuge tube, centrifuged (at 9000 rpm for 15 min). This resulted in complete precipitation of the products once the reaction mixture had been heated up to these temperatures in-situ. The solvent was syringed off, and the product was washed with degassed MeOH and dry hexane, dried under vacuum, and slowly exposed to air with a needle through the septum.

Given the very high excess of sodium napthalide being used in these reactions, not unexpectedly the products showed high amounts of sodium and organics (EDX and TGA). As will be discussed in the results and discussions sections, this could potentially interfere with the formation of the desired Pt-Ti phases and result in unwanted residues on the final products. Hence, a different method was tried to

counter this problem, in which the sodium napthalide was prepared in diglyme (0.72 mmol in 40 ml) and precursors in diglyme (0.06 mmol each in total 10 ml) were injected into it (100 % reducing agent excess). This solution was stirred at room temperature for 30 min to ensure complete reduction, and then 40 ml of tetraglyme was injected into it. The mixture was heated up to first 70 ^{o}C and then to 100 ^{o}C under vacuum to remove the diglyme. When the reaction solvent volume was reduced to approximately 40 ml, the flask was switched back under argon and heated up to 220 ^{o}C with silicone oil bath. Once at 220 ^{o}C, the reaction mixture was stirred for either 15 min or 3.5 hr, cooled down to room temperature and worked up as described above. Products from all reactions described above were collected after slow exposure to air and analyzed by X-ray diffraction, EDX and ATR.

Reactions with higher initial amounts of Ti: Lastly, a few experiments were done with excess of $Pt(acac)_2$ with respect to the $Ti(THF)_2Cl_4$, with 8:1 molar ratio of Pt:Ti. The procedure for these reactions were identical to those described above, with the preparation of sodium napthalide (100 % reducing agent excess), the preparation of precursor solutions in the glove box (precursors were dissolved in 10 ml THF), and injection of precursors into the reducing agent solution. The reaction mixture was stirred at room temperature (overnight), and worked up as described above. For reactions requiring in-situ heating to 80 ^{o}C and 120 ^{o}C, the sodium napthalide and precursor solution were prepared in diglyme (all other factors kept constant). The reactions were worked up following the procedure described above.

Reaction with $TiCp_2Cl_2$: Co-reduction of $Pt(acac)_2$ and $TiCp_2Cl_2$ was carried out following the same procedure for room temperature reactions described above. The sodium napthalide solution was prepared in THF (0.72 mmol in 40 ml THF) and precursors dissolved in THF (0.06 mmol each in 10 ml of THF) were injected into the reducing agent solution. After stirring overnight, the THF solvent was distilled off at a

reduced pressure to leave a dark-brown precipitate. Approximately 20 ml of anhydrous MeOH (degassed for 1 hr) was transferred into the flask, the products were re-suspended by sonication (2 min) and cannula transferred into a centrifuge tube under argon. The solution was centrifuged at 9000 rpm for 30 min, and the supernatant was removed with a syringe. 20 ml of hexane (dry, from the solvent system) was added and the sonication and centrifugation steps were repeated. The product was dried under vacuum and exposed to air slowly with a needle through the septum. The above reaction was repeated with a smaller amount of solvent - total solvent volume 30 ml (20 ml for sodium napthalide solution and 10 ml for dissolving the precursors) to study the effect of reagent concentration. Reducing agent excess was maintained at 100 %.

Washes and solvents: Although the washes described in above sections (one MeOH followed by one Hexane wash) were carried out for most of the reactions, experiments were done by varying the number and sequence of washes before deciding on the above. The MeOH wash removes the salt (NaCl) but MeOH reacts with the Ti. Hence the to decide on the optimum number of MeOH washes, products from reactions worked up with two MeOH and one Hexane wash, one MeOH and one Hexane wash, and washes with only hexane were compared (by XRD and EDS). Sonication times in MeOH for the MeOH washes were also varied (15 min, 10 min, 5 min and 2 min). 2 min sonication time was determined to be sufficient. As expected, for in-situ heating to 220 ^{o}C reactions, given the high amounts of sodium napthalide used, the final products would show high amounts of Na in EDS. Water washes were carried out on these products in order to remove the sodium after they had been exposed to air. To understand the effect of wash solvent (MeOH, hexane and water) and reaction solvents (THF, diglyme and tetraglyme) on the final composition of the recovered product, the

solvents were collected in small beakers after centrifuging to precipitate the products and evaporated off to dryness. The residue left behind was analyzed by EDS and ATR.

Annealing: Products from the above reactions were sealed in silica tubes under vacuum and annealed at high temperatures (up to 1000 ^{o}C) in box furnaces. The temperature and time was controlled using the furnace controllers. The tubes were opened after annealing and the annealed products were collected and analyzed (XRD and EDX).

Characterization: X-ray powder diffraction powder patterns (Scintag XDS 2000) were taken of the nanoparticles to confirm the composition and structure of the phase. The particle morphology and size was studied by scanning electron microscopy (SEM) using a LEO-1550 Field emission SEM (FSEM). Energy dispersive X-ray analysis (EDX) was also done on the particles on the same instrument. For EDX analysis, unless otherwise specified, particles in dry powder form were used on GaAs wafers. A JEOL 8900 EPMA Microprobe was used for preliminary EDX on most of the samples. For some samples, scanning TEM images and EDX data were collected on a VG HB501UX UHV STEM. Dry particles, in powdered form dispersed on ultra thin TEM grid, were used for STEM and SEM images. To measure the surface area of the samples, a Micromeritics ASAP 2020 was used to collect a partial adsorption isotherm at liquid nitrogen temperature (-196 ^{o}C) with krypton as the adsorption gas over the pressure range (P/P_0) range of 0.06 and 0.5. Prior to measurements, the sample was degassed under vacuum at room temperature for 48 h. The specific surface area was determined according to the Brunauer-Emmett-Teller (BET) method in the relative pressure range of 0.08 to 0.185. ATR spectra were obtained on dry powder samples using a Nicolet AVATAR 370 DTGS OMNI sampler.

3.2.2 Results and discussion

As discussed briefly in the introduction of this chapter, our goal while starting this work was to continue from the leads of Dr. Hideki Abe's work and our previous work with PtPb. We hoped to tackle the challenges experienced in the former with what we had learnt from the later. From what we then understood about the process, in-situ heating of the reaction mixtures after co-reduction are expected to nucleate and grow nanoparticles of the desired phases (as was observed with PtPb)[5]. Larger nanoparticle diameters (5-10 nm) should reduce Ti removal (leaching) during subsequent MeOH washes. $Pt(acac)_2$ was used instead of $PtCl_2COD$ because of its higher solubility and improved results with PtPb compared to the later[4]. However, we experienced challenges different from our expectations. Unlike Dr Hideki Abe's observations with different precursors, products from the above reactions couldn't be dispersed well in hexane after the reaction solvent (THF) was evaporated off. This required us to switch the washes: MeOH first and then hexane to transfer the products completely into a centrifuge tube from the reaction flask. This observation suggests the possible polar nature of the particles (presumably arising from charged or polar species sticking closely to the particle surfaces. Also, unlike in the case of PtPb, the products from for room temperature reactions (never heated up in-situ) couldn't be precipitated from the reaction solvent (THF) even with high speed centrifuging. This suggested that the particles were too small or polar or probably both. With higher temperature reactions (in-situ heating of the reaction mixture to 120 ^{o}C or higher), the particles would precipitate from the solvent (diglyme or tetraglyme) on centrifuging at 9000 rpm for 15 min. This suggests that some particle growth had taken place, although the exact nature of the particles is still unknown. However, when the reaction solvents (diglyme

and tetraglyme) were isolated from the precipitated particles and evaporated off, the residue showed the presence of Ti (Table 3.2).

Table 3.2: EDX data showing semi-quantitative atomic percentages of different elements found in residues obtained after evaporating off the reaction solvent. The remainder of the residue showed C and O.

Residue from reaction solvent:	**Pt at %**	**Ti at%**	**Na at%**	**Cl at%**
Diglyme	**0.4**	**4.5**	**0.4**	**1.8**
Tetraglyme	**0.0**	**0.2**	**0.0**	**0.0**

Loss of one element compared to the other at this stage (where the products were still not exposed to a protic solvent like MeOH) suggested the Ti to be either in a partially oxidized state or Ti^0 closely associating with oxygen containing species (given the high oxophilicity of Ti). This association with oxygen could very well also occur for the oxidized Ti. Either way, the above possibilities would result in the loss of Ti from the product in very early stages and would make the product very susceptible to Ti loss once MeOH is added to the system. EDX results for the reactions agreed with this (Table 3.3).

Table 3.3: EDS data showing atomic percentages of Pt and Ti in the final products obtained from Pt-Ti precursor reactions at different temperatures. For reaction at 220 ^{o}C, two different methods, differing in the reducing agent excess used, were followed.

	Room temp	120 ^{o}C	220 ^{o}C, 100 % excess NaNp	220 ^{o}C, 500 % excess NaNp
Pt (atm %)	**70.7**	**30.5**	**18.3**	**62.3**
Ti (atm %)	**1**	**1**	**1**	**1**

XRD of the as prepared products (with or without in-situ heating) showed broad peaks with peak maxima indexing close to that of cubic Pt, with a slight shift to higher angles (suggesting some alloying by Ti incorporation into the fcc Pt) (Figure 3.1).

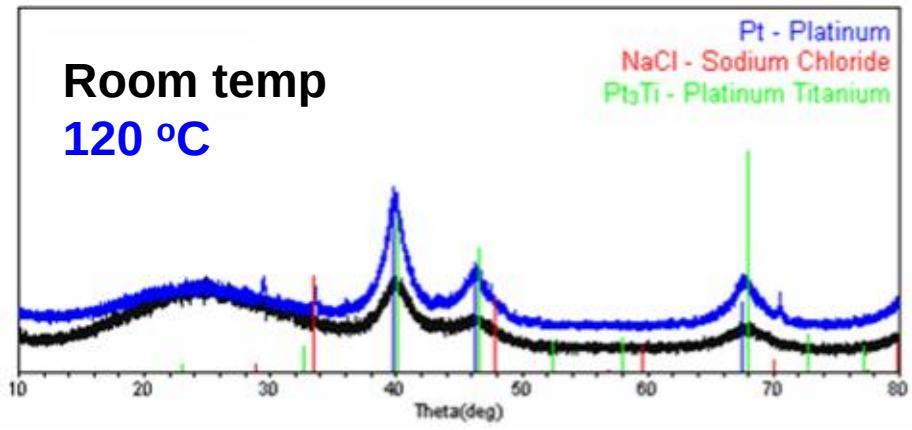

Figure 3.1: X-ray diffraction patterns of products obtained from co-reduction of $Pt(aca)_2$ and $Ti(THF)_2Cl_4$. Lines indicate expected peak positions for Pt (PDF # 01-070-2057), Pt_3Ti (00-017-0064) and NaCl (01-078-0751).

However, no ordering into any of the known Pt-Ti intermetallic phases was observed on either in-situ heating to as high as 220 ^{o}C (figure 3.2), or annealing to high temperatures after reduction (Figure 3.3). None of these observations were unexpected, given that the EDX showed in-sufficient Ti in the products. Given these observations, we surmised that $Pt(acac)_2$, which has a very polar oxygen containing anion like acetylacetonate, must strongly interact with Ti^0 or Ti cations and is not suitable for reactions with reactive elements like Ti.

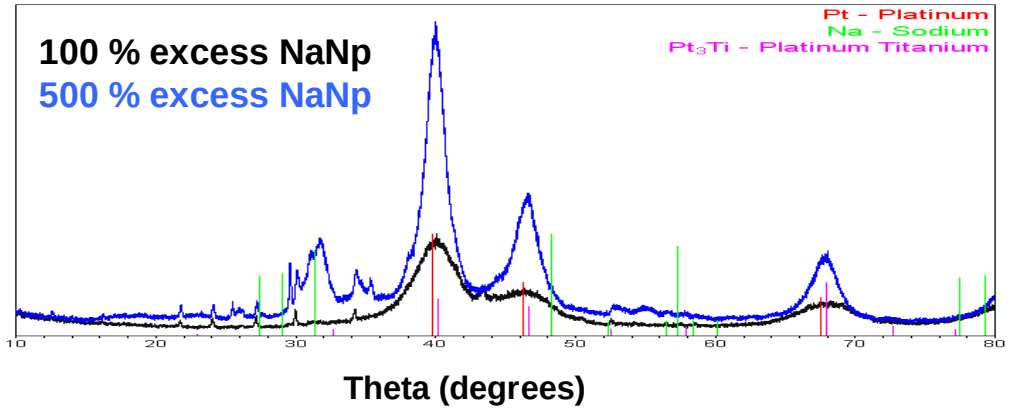

Figure 3.2: X-ray diffraction patterns of products obtained from co-reduction of $Pt(acac)_2$ and $Ti(THF)_2Cl_4$ at 220 ^{o}C. Lines indicate expected peak positions for Pt (PDF # 01-070-2057), Pt_3Ti (00-017-0064) and Na (01-071-4606).

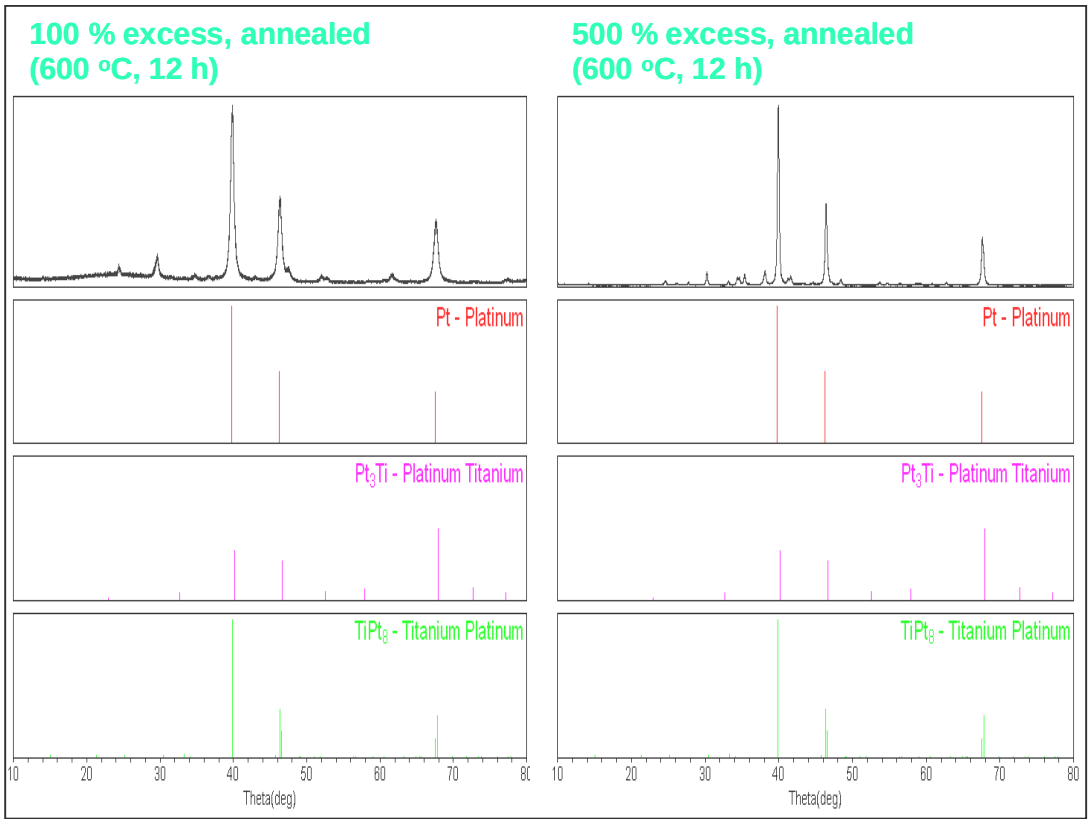

Figure 3.3: X-ray diffraction patterns of the products (from co-reduction of $Pt(acac)_2$ and $Ti(THF)_2Cl_4$ at 220 °C) after annealing to 600 °C. Lines indicate expected peak positions for Pt (PDF # 01-070-2057), Pt_3Ti (PDF # 00-017-0064) and Pt_8Ti (PDF # 04-007-1811).

Another valuable insight was obtained from reactions done with different sonication times in MeOH during the MeOH wash. The products which had been in MeOH sonicating for only 2 min, retained higher amounts of Ti than the ones sonicated for 10 min. The residue obtained after evaporating off the MeOH in latter case showed high amounts of Ti (Table 3.4). Also, in the later case, recovering the product completely from MeOH was found to be impossible. The reaction kinetics for the Ti

leaching out into MeOH was thus comparatively slow, but unfortunately for us, not slow enough. Also, the experiments from varying the number of MeOH washes showed that one MeOH wash was optimal. Products not washed with MeOH showed high amounts of by-product NaCl, which might interfere with particle growth. Products washed twice with MeOH showed almost no Ti, but most of the product stayed in solution after the second MeOH wash resulting in low yield.

Table 3.4: EDX data showing atomic percentages of Pt and Ti in the product recovered by precipitating out of MeOH and residue obtained by evaporating off MeOH for 10 min sonication time in MeOH. Residue obtained from evaporating the MeOH shows a large amount of Ti.

	Pt atm%	**Ti atm%**
Product recovered from MeOH (sonication time 10 min)	**30**	**1**
Residue from MeOH wash (sonication time 10 min)	**0.05**	**1**

Reactions were also carried out to study the effect of reducing agent excess and reagent concentration on the product. For the room temperature reactions, changing the reducing agent excess from 25% to 50% to 100% showed no definite effect on product composition or yield. However, larger particles were obtained with smaller reducing agent excess (Figure 3.4).

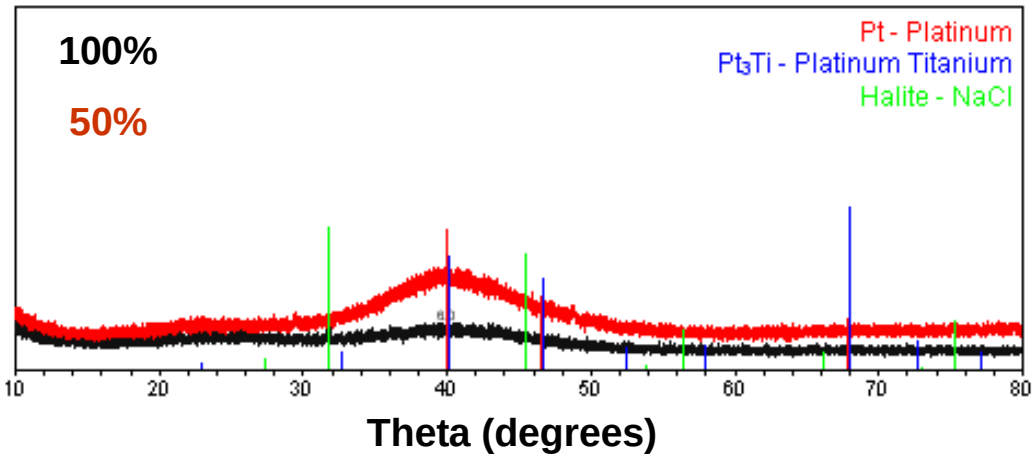

Figure 3.4: Comparison of X-ray diffraction patterns of products obtained with different reducing agent excesses. Lines indicate expected peak positions for Pt (PDF # 01-070-2057), Pt_3Ti (PDf # 00-017-0064) and NaCl (PDf # 01-078-0751).

For the reactions heated to 220 ^{o}C in-situ, less Ti was detected in the final product via EDS when significantly higher reducing agent excess was used (500 %) than when the reducing agent excess was maintained at 100 %. Also, the XRD showed extra peaks at the low angles for the former (figure 3.2). This issue will be discussed extensively in the next chapter. For now, we'll just say that sodium containing species could be responsible for these peaks. The same effect on particle size was observed for the 220 ^{o}C reactions, with particle sizes growing on cutting down the reducing agent excess to

25%. These observations suggested that sodium serves as a counter ion to the adsorbed anions (acetylacetonate or some derivative of its generated during the reaction would be strong candidates) forming charged double layers around the particles. Chloride ions present in the system (from the Ti precursor in this case), could be involved in a similar way. More support for this argument was obtained from the observation that sodium chloride peaks would grow stronger in the diffraction patterns of the annealed samples in cases where they were absent in the patterns from as prepared samples. The same was observed with in-situ heating. Thus, as the particles grew bigger on annealing or in-situ heating so did the sodium chloride crystals, with sodium and chlorine ions associated in the polar networks around metals now nucleating into NaCl crystals. Na was still left in the product even on complete removal of the sodium chloride crystals with MeOH washing (especially in the cases where a huge reducing agent excess had been used) and could only be removed by water washing. This was not unexpected, and reinforced the possibility of other sodium containing species forming in these reactions. Lastly, reactions with $TiCp_2Cl_2$ as the Ti precursor instead of $Ti(THF)_2Cl_4$ (with $Pt(acac)_2$ as the Pt precursor) confirmed that oxygen free precursors are better for either metal when dealing with Ti. Higher product yield (and ease of separation from MeOH after the MeOH wash), higher amounts of Ti in the product and X-ray diffraction patterns shifted significantly from cubic Pt to that expected for a 3:1 Pt:Ti alloy were observed for the reaction with $TiCp_2Cl_2$ as the Ti precursor.

The effect of reagent concentration was studied using the $TiCp_2Cl_2$ precursor. A 53 % decrease in yield was observed on changing the reagent concentration from 1.3 mM to 2.4 mM keeping all other factors constant. The decrease in yield with increasing concentration has been previously observed with some PtPb reactions (unpublished work in the group). However, the effect is not fully understood at this point. Typically,

high concentration reactions (lesser solvent volume) had larger amounts of Ti in the final product compared to the low concentration reactions.

The lessons learnt from this section are:

1. There is an optimal sequence and number of washes.
2. Short sonication times in MeOH are preferred.
3. Particle growth happens with in-situ heating.
4. $Pt(acac)_2$ as a precursor has detrimental effects on the final product composition.

The reactions with higher ratios of the Ti precursor ($Ti/Pt \geq 1$) are discussed in the results and discussions section of the next segment (3.3) although the precursors used were $Pt(acac)_2$ and $Ti(THF)_2Cl_4$ as the observations are more relevant to the discussion in that segment.

3.3 Reactions with $PtCl_2COD$

3.3.1 Experimental

Materials: The Pt(1,5-cyclooctadiene)Cl_2 ($PtCl_2COD$, COD = 1,5 -cyclooctadiene, C_8H_{12}) was obtained commercially from STREM chemicals incl. (99 % purity).

3.3.1.1 Co-reduction of Pt and Ti precursors

The co-reduction reactions with $PtCl_2COD$ were carried out; in each case (at room temperature, possibly followed by in-situ heating at 120 ^oC or 220 ^oC), following procedures identical to those described in section 3.2. The only difference was in the case of the higher temperature reactions (120 ^oC and 220 ^oC). In these cases, given the

very low solubility of the Pt precursor in diglyme and tetraglyme, the precursors were dissolved in THF inside the glove and injected into the reducing agent solution in diglyme or tetraglyme. Most reactions involving in-situ heating to 220 ^{o}C using this Pt precursor were carried out following the later procedure (reducing agent prepared in diglyme, diglyme evaporated off post injection of precursors, tetraglyme added and reaction then heated up to the high temperature). This was done to avoid using higher reducing agent excess than 100 %. Reducing agent excess and precursor concentrations were not varied for reactions with this precursor except for one reaction in tetraglyme, in-situ heating to 220 ^{o}C where a 500 % reducing agent excess was used (the sodium napthalide was prepared in tetraglyme). All reaction work-ups with this precursor involve one MeOH wash followed by one hexane wash. The Sonication time in MeOH was maintained at 2 min always. An additional reaction was carried out with this precursor where the reducing agent solution in diglyme was injected with the precursor solution, then the solution was stirred for 30 min and tetraglyme was added. Diglyme was evaporated off (following the procedure described in the previous sections). The reaction mixture was then heated up to 270 ^{o}C, stirred at that temperature for 3.5 hr and cooled down to room temperature. The reaction was then worked up as described previously and the product was exposed to air slowly with a needle through the septum.

3.3.2 Results and discussion

The final products obtained with $PtCl_2COD$ as a precursor showed much higher amounts of Ti in EDS analysis compared to the reactions using $Pt(acac)_2$. Co-reduction of $PtCl_2COD$ with $Ti(THF)_2Cl_4$ yielded products with 8 : 1 ratio of atomic percentages of Pt:Ti, while for co-reductions of $PtCl_2COD$ and $TiCp_2Cl_2$ (both

precursors free of oxygen) yielded 1 : 1 ratio of atomic percentages of Pt and Ti in the products. Also X-ray diffraction patterns of the as prepared samples showed significant shifts in the peak maxima from Pt in each case (Figure 3.5 a, b).

This further supports the importance of selecting both metal precursors to be oxygen free when dealing with a metal as oxophilic as Ti. It is shown with this work that much larger mole fractions of Ti can be obtained in the final products if oxygen free precursors are used. Oxygen containing groups most certainly play a role is closely associating with Ti in their nascent or derived forms, thus facilitating its oxidation and subsequent removal from the system during work up procedures. However, even with in-situ heating to temperature as high as 270 ^{o}C, no ordering peaks were observed in the as prepared samples. The only evidence of ordering that could be ever obtained with Pt-Ti systems was on annealing at temperatures as high as 600 ^{o}C (Dr. Hideki Abe's work) or at even higher temperatures like 1000 ^{o}C (in this work).

Annealing to temperatures like 1000 ^{o}C, not unexpectedly, caused the particles to sinter, giving particles with average domain size of 51 nm (calculated from the X-ray diffraction pattern using the Scherrer equation). Attempts to control this sintering by dispersing the particles on a C support (Vulcan) were then explored.

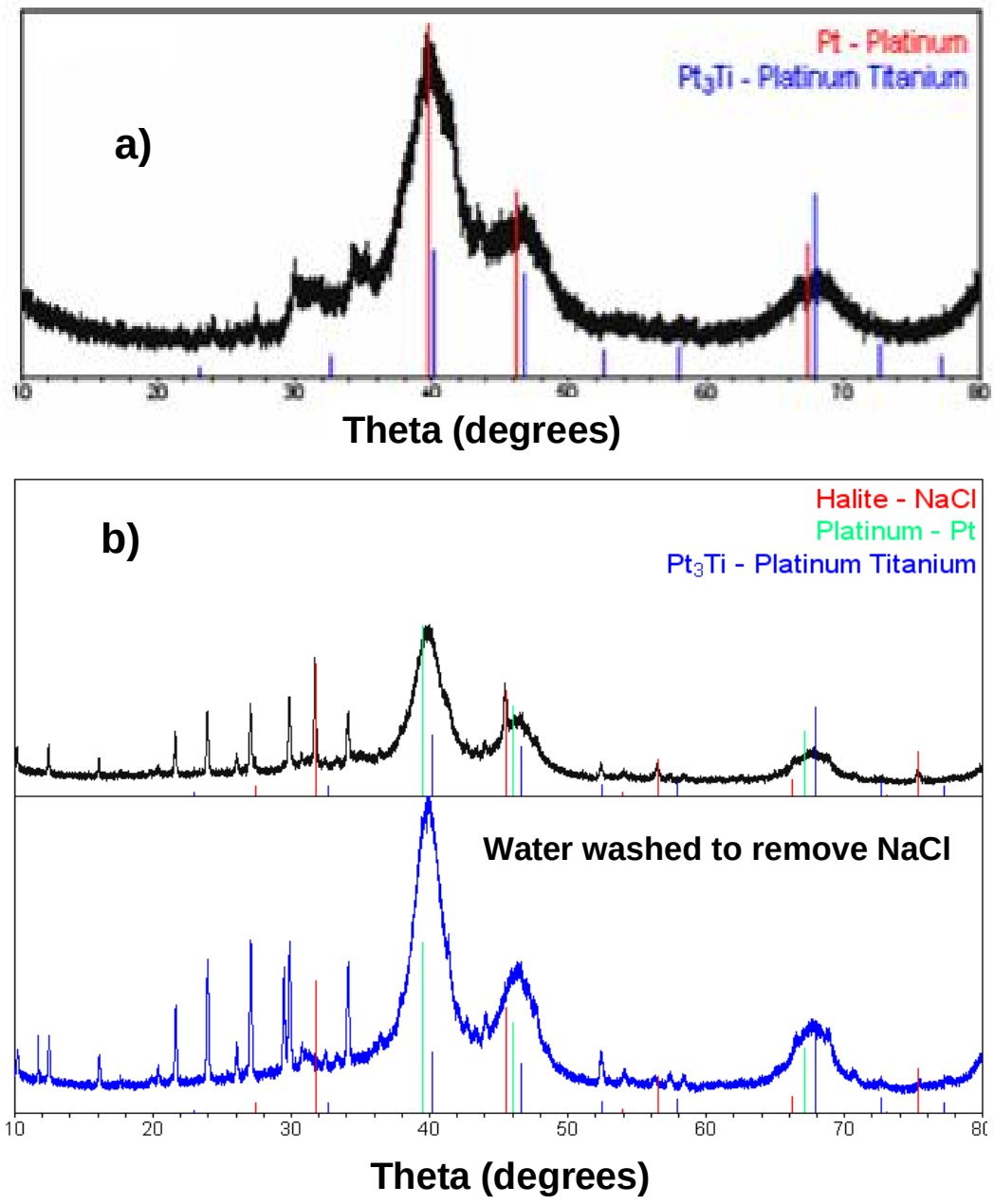

Figure 3.5: X-ray diffraction patterns of products from a) co-reduction of $PtCl_2COD$ and $TiCl_4(THF)_2$ and b) $PtCl_2COD$ and $TiCp_2Cl_2$ (before and after water wash to remove NaCl). Lines indicate expected peak positions for Pt (PDF # 01-070-2057), Pt_3Ti (PDF # 00-017-0064) and NaCl (PDF # 01-078-0751).

A solution containing the product (obtained from reduction of precursor) was sonicated with Vulcan for 1 hr and the product was isolated by centrifugation. This product was then annealed at 800 ^{o}C. Our idea in doing so was to try and control the particle sintering by separating the particles by using the Vulcan as a matrix. As will be discussed in the next chapter, this technique was successful with systems like Pt-Ni. However, with Pt-Ti, although lower domain sizes could be obtained, the ordering peaks couldn't be identified in the diffraction patterns for these C supported samples. Also important to note, the ordered phase obtained on annealing to 1000 ^{o}C was Pt_3Ti, in-spite of the EDS showing a 1: 1 Pt: Ti composition. These observations, and the fact that ordering could never be obtained by in-situ heating, suggested that at least some of the Ti was present in partially oxidized or oxygen associated states. Similar conclusions could be drawn from observations from reactions with high initial amounts of the Ti precursor (8:1::Ti:Pt molar ratio).In spite of the large amount of Ti was shown to be present in the products by EDS, X-ray diffraction patterns from as prepared samples showed broad peaks with maxima slightly shifted from Pt, while annealed samples showed Ti oxide phases and Pt. This is further supported through EDS on the individual particles using the STEM (UHV-STEM; VG HB501UX) at 120 kV. The atomic ratio of Pt:Ti on a small number of particle (Figure 3.6) was found to be different from that of a larger collective region (Figure 3.7), showing that Ti is present in other forms in and around the Pt containing particles. This explains why the ordered phases obtained on annealing would be the Ti poor ones (or just Pt and Ti oxide phases) in spite of much higher average Ti concentrations detected over larger regions of the samples.

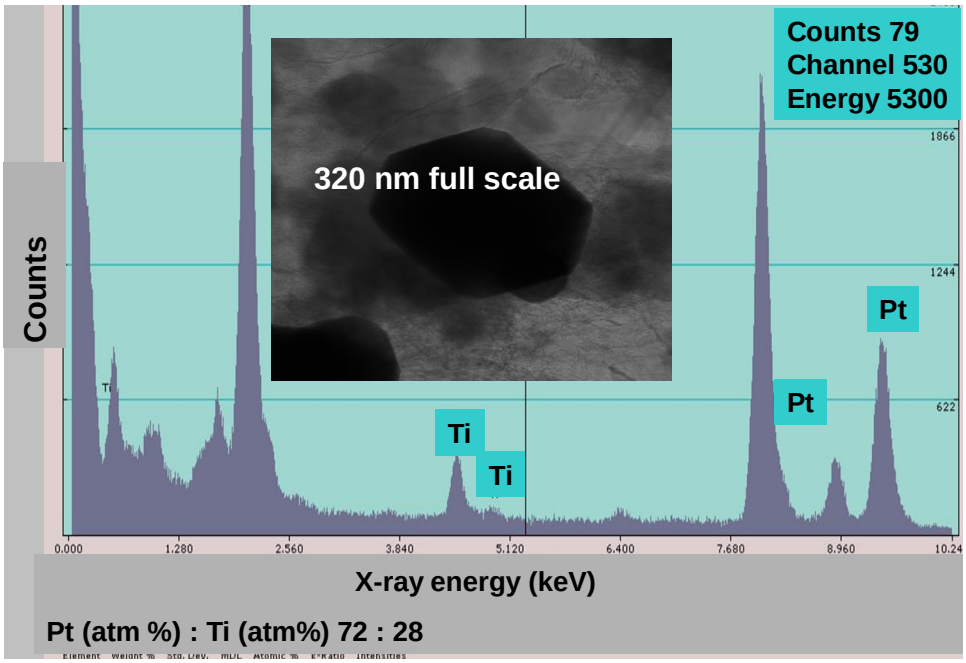

Figure 3.6: STEM images and EDS data of the Pt-Ti sample zoomed in on a particle.

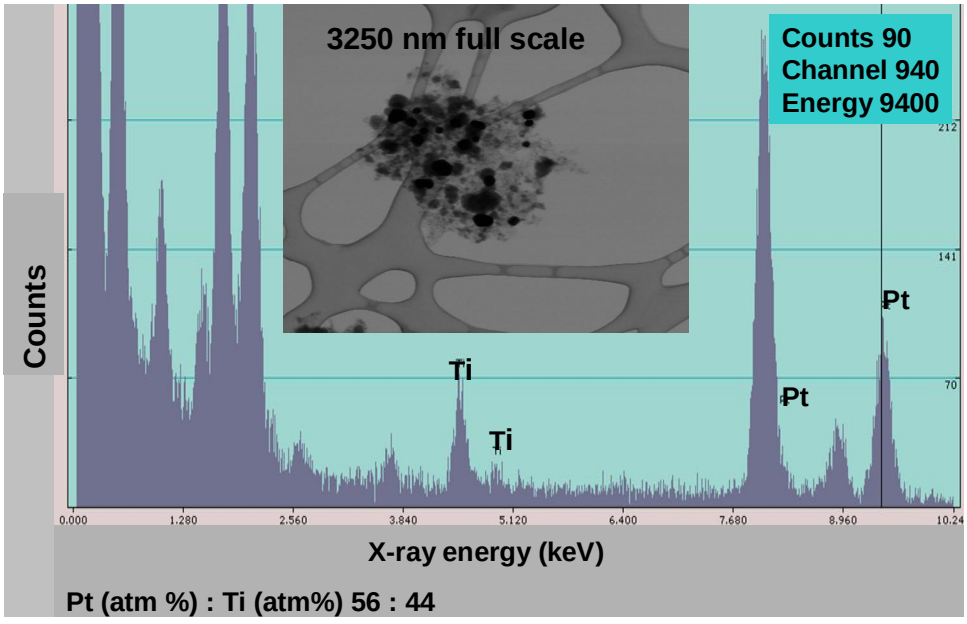

Figure 3.7: STEM images and EDS data of the Pt-Ti sample for the entire region.

3.4 Electrochemical activity

3.4.1 Experimental

Electrochemical characterizations of the products were performed by Dr. Futoshi Matsumoto in the Abruña group. For these experiments, 4 mg of the appropriate products were suspended in a mixture of 3.98 ml of distilled water (18 $M\Omega cm^{-2}$; Millipore Milli-Q), 1 ml of isopropyl alcohol, and 20 ml of a 5% w/w alcoholic solution of Nafion^{TM} (Aldrich; EW: 1100). Suspensions of pure Pt nanoparticles (Alfa Aesar; HiSPEC TM 1000; ADS = 2-3 nm; surface area = 2.7×10 m^2g^{-1}) and 50 wt % 1:1 Pt-Ru nanoparticles supported on a Vulcan XC-72R (E-TEK; total surface area of carbon and Pt-Ru nanoparticles = 1.07×10^2 m^2g^{-1}) were prepared in the same way. Each of the resultant suspensions was spread using a spin coater and dried to form a film on the polished surface of a glassy carbon (GC) electrode with a diameter of 3 mm. In each case, the catalyst loading was 70 μgcm^{-2}. The film containing the products was pretreated in a 0.1 M sulfuric acid solution for 30 minutes by applying a DC potential of -0.7 V before obtaining cyclic voltammograms. The films containing pure Pt nanoparticles and Pt-Ru nanoparticles were pretreated in a 0.1 M sulfuric acid solution by sweeping the potential between -0.2 and 0.2 V for 10 times at a sweep rate of 10 mVs^{-1}.

Cyclic voltammograms (sweep rate of 10 mVs^{-1}) were obtained in Millipore-water solutions of 0.1 M sulfuric acid (Sigma-Aldrich; 99.999% purity) that contained 0.5 M of fuel materials: formic acid (Mallinckrodt; 88% analytical reagent) or methanol (Burdick and Johnson; 99.9% purity). The rotation speed of the glassy carbon electrode was 2000 rpm during CV measurements. The electrode potentials were referenced to a saturated Ag/AgCl electrode. Mass activity obtained for the products

was normalized with respect to the surface area calculated (using the appropriate BET isotherm) to obtain the current densities.

3.4.2 Electrochemical results

Most of the products were found to be electrochemically inactive towards the oxidation of formic acid or MeOH. The best results obtained are compared to that obtained previously from Dr. Hideki Abe's samples (Table 3.5, 3.6 and 3.7).

Table 3.5: Catalytic activity of selected samples for MeOH oxidation compared to activity observed with samples prepared by Dr. Hideki Abe from $PtCl_2COD$ and $Ti(THF)_2Cl_4$[2]. The ordered Pt_3Ti was obtained after annealing at 600 ^oC[2].

	Onset Potential (V)	$mA\mu g^{-1}$ at 0.6 V	$mAcm^2$ at 0.4 V	BET surface area m^2/gm
Pure Pt	+ 0.40	0.00054	0.002	27
Pt-Ru	+ 0.18	0.025	0.036	70
Disordered Pt_3Ti	+ 0.04	0.026	0.024	110
Ordered Pt_3Ti	+ 0.08	0.0082	0.089	9.2
Product from co-reduction of $Pt(acac)_2$ and $TiCl_4(THF)_2$ at 220 ^oC, 500%excess of reducing agent, 15 min stirring	+0.3	0.00056	0.00066	83.9

Table 3.6: Catalytic activity of selected samples described in this chapter for formic acid oxidation.

Product description	Pre-treatment at -0.7 V for 30 min in 0.1 M H_2SO_4	Onset potential (V vs. Ag/AgCl)	Mass activity (mA/μg)	Current Density (mA/cm^2)	m^2/gm
Product from co-reduction of $Pt(acac)_2$ and $TiCl_4(THF)_2$ at 220 °C, 100% excess of reducing agent, 3 hr stirring	With pretreatment Without pretreatment	-0.15 -0.15	0.045 0.012	0.069	65.37
Product from co-reduction of $Pt(acac)_2$ and $TiCl_4(THF)_2$ at 220 °C, 500% excess of reducing agent, 3 hr stirring	With pretreatment Without pretreatment	-0.1 -0.1	0.033 0.0056	0.223	14.79
Product from co-reduction of $Pt(acac)_2$ and $TiCl_4(THF)_2$ at room temp, 100%excess reducing agent Overnight stirring		-0.125	0.080		
Product from co-reduction of $Pt(acac)_2$ and $TiCl_4(THF)_2$ at 120 °C,100 % excess reducing agent, overnight stirring		-0.125	0.044	0.152	29.01
Product from co-reduction of $PtCl_2$CODand $TiCl_4(THF)_2$ at 220 °C, 500% excess of reducing agent, 3 hr stirring		-0.1 -----	0.014 0.0005	0.172	8.16

Table 3.7: Catalytic activity of selected samples for formic acid oxidation compared to activity observed with samples prepared by Dr. Hideki Abe from $PtCl_2COD$ and $Ti(THF)_2Cl_4$[2]. The ordered Pt_3Ti was obtained after annealing at 600 ^oC[2].

Product description	Onset Potential (V)	$mA\mu g^{-1}$ at 0.2 V	$mAcm^{-2}$ at 0.2 V	BET surface area m^2/g
Pure Pt	- 0.09	0.0090	0.03	27
Pt-Ru	+0.20	0.0063	0.009	70
Disordered Pt_3Ti	-0.17	0.097	0.089	110
Ordered Pt_3Ti	-0.15	0.56	0.61	9.2
Product from co-reduction of $Pt(acac)_2$ and $TiCl_4(THF)_2$ at 120 ^oC,100 % excess reducing agent, overnight stirring Double MeOH wash	-0.2	0.045		
Product from co-reduction of $Pt(acac)_2$ and $TiCl_4(THF)_2$ at 220 ^oC, 500% excess of reducing agent, 3 hr stirring	-0.2	0.0059	0.29	20.4
Product from co-reduction of $Pt(acac)_2$ and $TiCl_4(THF)_2$ at 220 ^oC, 500% excess of reducing agent, 15 min stirring	-0.2	0.034	0.040	83.9

From Table 3.5 and 3.6 it can be seen that these products show good (low) onset potentials (best is -0.2 V, PtPb) for formic acid oxidation, but the observed activities are low (again, best is 5.5 mA/cm^2 for PtPb at 0.2 V). The overall performance of the materials synthesized in this work as electrocatalysts never reached that of PtPb, possibly due to the low amounts of Ti alloyed into the Pt. Another possible reason for the low activity observed could be presence of organic materials covering the catalyst surfaces. Evidence of the presence of organics was obtained from both EDX and TGA results. TGA experiments typically showed between 25-30 % product weight loss on heating. From this, a crude estimate can be made there are at least 3 carbon atoms per Pt atom in the samples. Annealing helps remove organics, but the annealed samples were also found to be inactive. This may be due to decomposition of the organics that occur before they sublime, this can lead to carbon coating of the products while annealing in sealed tubes. Especially on annealing to high temperatures (higher than 400 ^oC), a dark black coating covering the walls of the tubes is often visible (Figure 3.8). The same material is likely covering the surface of the annealed products causing them to be catalytically inactive. This could explain why other phases (discussed in Chapter 4) showed activity before annealing, but were rendered catalytically "dead" on annealing to high temperatures. A dynamic annealing process removes all the organics volatilized. Annealing in a temperature gradient so that the organics would sublime to the far end of the tube, or annealing under dynamic vacuum could possibly address this issue. If so, ordered phases with clean surfaces should show some activity.

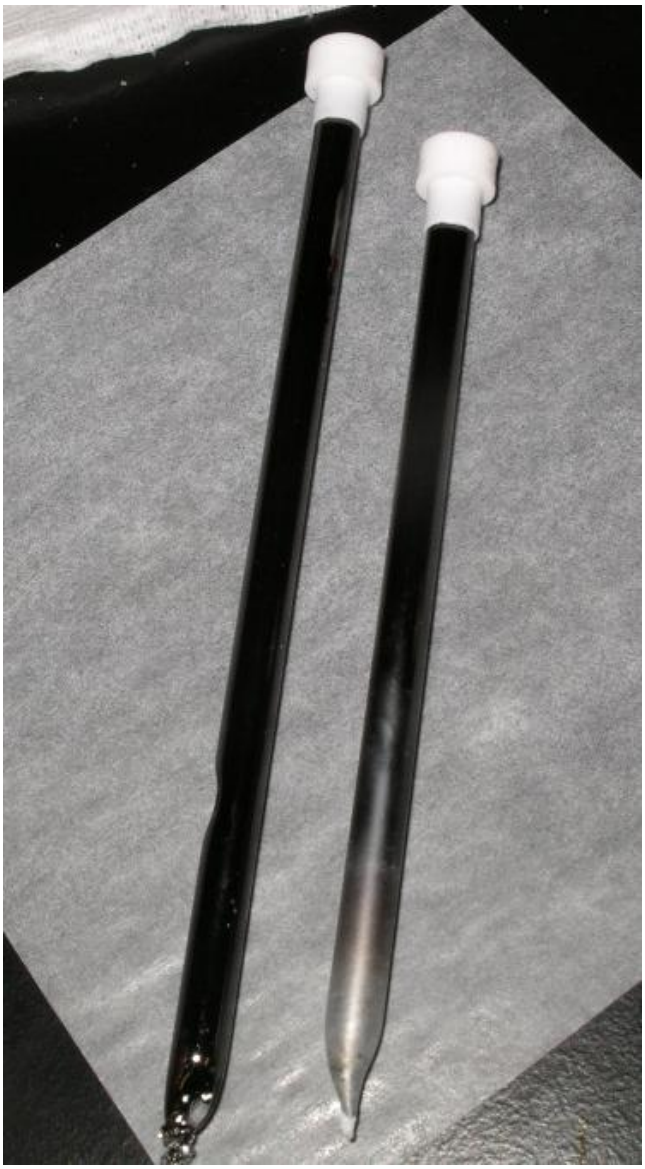

Figure 3.8: The tubes taken out of furnace after annealing the products at 600 ^{o}C showing black coating covering the walls. The tubes were cut open and capped after collecting the annealed product.

3.5 Conclusions

In this work, we discovered several outcomes that were different from our expectations. This made us rethink the differences between the Pt-Pb system and the Pt-Ti system, arising primarily from the high electropositivity, and more importantly, oxophilicity of Ti. The most important lesson learnt from this realization was the need to avoid oxygen (especially in form of polar reactive groups like acetylacetonate) in the precursors for a metal like Ti. The optimum number of MeOH washes and sonication time during the MeOH wash were found to play key roles. Composition control (by preventing the previously observed loss of Ti during washes) could be achieved in the as prepared samples with proper choice of precursors and proper work-up of the reduction products (1: 1 ratio of Pt: Ti observed in the products from co-reductions with 1: 1 ratio of precursors). However, keeping the Ti in a clean and un-oxidized form once reduced, so that it can bond to Pt and form the desired phases still remain a challenge. The role of reaction solvents, sodium and possibly chlorine in preventing nucleation and growth of nanoparticles has been identified and work is ongoing to devise methods to counter these impediments. Some of those approaches, such as exploring the use of Li reducing agents, are discussed in chapter 5. The electrochemical activity (specially the current density for fuel oxidation) for Pt-Ti catalysts prepared in this work fared very poorly compared to earlier results[2]. We learned that reproducibility is an issue when dealing with a metal like Ti as it is difficult to obtain the phases proven to be good electrocatalysts. After exploring the two extremes in terms of properties of the second metal (Pb vs Ti), the next viable step was to map out the scope of this method (sodium napthalide reduction) for synthesizing Pt alloys and intermetallics with elements across the periodic table. That is what we discuss in the next chapter.

REFERENCES

1. Alden, L. R.; Roychowdhury, C.; Matsumoto, F.; Han, D. K.; Zeldovich, V. B.; Abruna, H. D.; DiSalvo, F. J., Synthesis, characterization, and electrocatalytic activity of PtPb nanoparticles prepared by two synthetic approaches. *Langmuir* **2006,** 22, (25), 10465-10471.

2. Abe, H.; Matsumoto, F.; Alden, L. R.; Warren, S. C.; Abruna, H. D.; DiSalvo, F. J., Electrocatalytic performance of fuel oxidation by Pt3Ti nanoparticles. *Journal of the American Chemical Society* **2008,** 130, (16), 5452-5458.

3. Fackler, J. P., *Inorganic Synthesis*. Wiley and Sons: NY, USA, 1982; Vol. XXI.

4. Ghosh, T.; Matsumoto, F.; McInnis, J.; Weiss, M.; Abruna, H. D.; DiSalvo, F., PtPb nanoparticle electrocatalysts: control of activity through synthetic methods. *Journal of Nanoparticle Research* **2009,** 11, (4), 965-980.

5. Alden, L. R. Synthesis of platinum intermetallic compounds for fuel cell anode catalysts. Cornell University, 2006.

Chapter 4

Pt ALLOY AND INTERMETALLIC PHASES WITH V, Cr, Mn, AND Ni: SYNTHESIS AS NANOMATERIALS AND APPLICATION AS ACTIVE FUEL CELL CATALYSTS

In the last two chapters, synthesis of binary phases of Pt with Pb (quite noble in terms of electropositivity and oxophilicity) and with Ti (highly reactive or 'much less noble' in terms of electropositivity and oxophilicity) have been discussed. The challenges experienced in the latter case were very different from those in case of the former, making synthesis of the desired phases for the later in desirable sizes (possible only if the reaction, or post reaction annealing temperatures required for obtaining the ordered phases can be kept low) impossible with the method being following. Thus, a deeper look into identifying the alternatives by understanding and obeying the new constraints that arise in case of highly reactive metals like Ti (discussed in Chapter 3) is necessary. It is also necessary to explore the elements across the periodic table, intermediate to Pb and Ti in reactivity (electropositivity and oxophilicity); for some of these phases might be active catalyst materials, and define the scope of this method (co-reduction of precursors in solution by sodium napthalide in absence of surfactants to generate binary nanophases). In this chapter, we have discussed the work done to do explore this method for synthesis of Pt phases with V, Cr, Mn and Ni. We have defined general guidelines and limitations for successfully obtaining desired phases, showed the catalytic potential of these materials and outlined possible future directions for obtaining cleaner and smaller materials with further improved catalytic activity.

The work done for synthesis of Pt-Cu phases by Dr. Brian M. Leonard, a post doctoral researcher in the DiSalvo group has also been discussed in this Chapter given its relevance in understanding the arguments presented in this chapter for elements across the periodic table and establishing general guidelines. The electrochemical results discussed in this chapter were obtained by Dr. Qin Zhou, another post doctoral researcher in the DiSalvo group.
This chapter is partially adopted from a paper submitted for publication to the *Chemistry of Materials.*

4.1 Introduction

Developing sustainable energy technologies is important to reducing dependence on fossil fuels and to addressing environmental issues as well as global climate change. However, developing new, more affordable, durable and efficient materials, some with desired properties that are not as yet attained, remains the key issue in developing most of these technologies, particularly for fuel cells. While the efficiency of a fuel cell can in principle approach 100 % of the free energy of reaction, only 50-60 % efficiencies have been attained in hydrogen based fuel cells at reasonable power densities[1, 2]. That reduction in efficiency is due primarily to the slow kinetics of oxygen reduction at the cathode catalyst. For fuels other than hydrogen, slow oxidation kinetics and catalyst poisoning at the anode reduce the efficiencies even further[3]. Finally, the catalysts, catalyst supports and other materials used have poor durability and system costs are high[4]. These challenges must be overcome if fuel cells are to be widely adopted.

While there are different fuel cell technologies, polymer electrolyte membrane (PEM) fuel cells are receiving the most attention for transportation and small portable power source applications. Our interest in solving the material problems associated with PEM fuel cells led us to explore new catalysts (such as PtPb and Pt_3Ti intermetallics) and to synthesize them as high surface area nanomaterials[5, 6]. Previous work has ascertained the potential of these materials as anode electrocatalysts for small molecule fuels, like formic acid and methanol. However, as many more materials need to be explored in the search for even better catalysts, identifying the key challenges associated with synthesizing nanoparticles of these materials is vital.

Nanomaterials with narrow size distributions are generally synthesized successfully only using the bottom–up approach[3]. One common method is the chemical reduction of suitable precursors dissolved in an appropriate solvent and deposited on a conducting support. However, surfactants are used in many of the reported processes in order to keep the particles from agglomerating[7]. For catalyst applications in fuel cells, avoiding or perhaps subsequent removal of surfactants by thermal, chemical or electrochemical treatment is crucial due to their blocking access of the reactants to the catalyst surface. Often these methods involve high temperature processing, which can result in agglomeration and particle size growth which result in loss of surface area and subsequently give lower rates of reaction per unit mass of the catalyst. In current PEM fuel cells, catalyst particles are typically 3 to 5 nm in diameter and show an optimal performance per mass. Ideally a surfactant-free, low temperature synthesis applicable to a wide range of particle compositions is desired, so that complex alloys, ordered intermetallics and other classes of materials can be synthesized while still maintaining high surface area particles. Central to all these methods is the necessity for co-reduction of mixed precursors of different metals. This becomes more and more challenging as the differences in reduction potential of constituent metals becomes

large, and as one or more of the metals are reactive in the ambient environment (hydro- or oxo-philic).

So far we have focused on Pt-group metals as one of the components for our bimetallic catalysts nanoparticles. we have previously reported low temperature routes to prepare nanoparticles of PtPb with a relatively narrow size distribution and shown that these nanoparticle catalysts displays high activity for formic acid oxidation[8]. Additionally, we have shown that the identity of ligands and anions in metal precursors play an important role in synthesizing homogeneous products and in determining particle size and surface composition, which in turn effect the catalytic activity. Careful studies of the synthetic process suggested that ligands from precursors can remain bound to individual elements and the nucleating nano-particle surface, thus interfering with crystallization into well ordered and shaped (non-dendridic) nanoparticles. Not surprisingly, this becomes more and more challenging for a particular preparation scheme as the temperature of the reduction reaction is decreased. At room temperature, even relatively weak ligand or solvent interactions with the reduced metals or the nano-particle surfaces can interfere with the metal ordering and growth of a given nano-particle ensemble. Using PtPb as a model system, we varied the identity of the ligands, anions, solvents and reducing agents as well as the work up post reduction, and found that atomically ordered PtPb intermetallic nanoparticles could be prepared even at room temperature without heating/annealing. These studies allowed us to identify the general issues associated with solution phase synthesis of intermetallic nanoparticles (Scheme 4.1)[8]. However, on moving away from Pb, towards more electropositive and oxophilic elements, many of the interactions between the reduced metals and other components in the solvent become larger. The role of the particular precursors and work up procedures was recognized to be even more vital. Wash solvents used after reduction also have to be selected much

more carefully. It was also recognized that oxophilicity (affinity for oxygen) of the non-Pt element plays a central role in determining the outcome of a particular reaction scheme. At first we hypothesized that the differences in reduction potential played the deciding role, since simultaneous co-reduction with Pt is important. However, we have found that in general a strong reducing agent, such as sodium naphthalide, can address that issue, as we discuss further below.

Scheme 4.1**:** Key issues in the synthesis of intermetallic nanoparticles by chemical co-reduction of precursors.

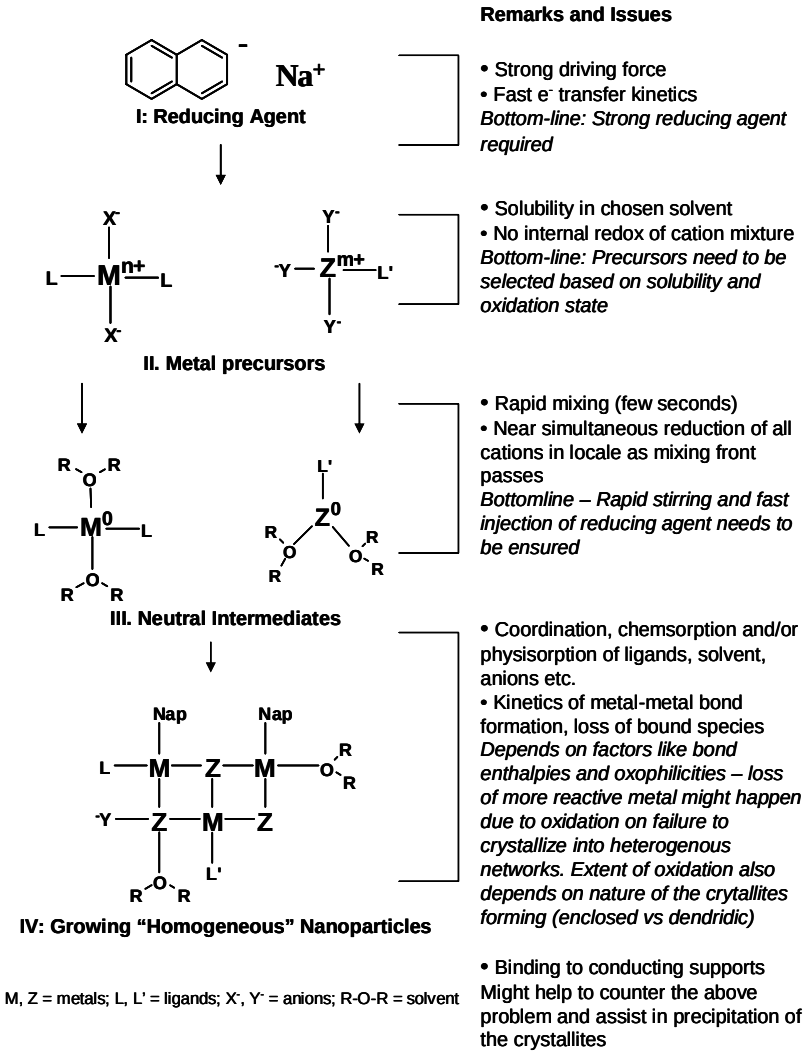

In this chapter, we outline and discuss the key issues as we investigated the challenges in synthesizing alloy and intermetallic nanoparticles which contain very electropositive metals such as Cr, Mn, and V. Using sodium naphthalide as a reducing agent, we have successfully synthesized Pt_3V, Pt_3Cr, Pt_3Mn, PtNi, and PtCu ordered intermetallic nanoparticles and alloy nanoparticles in each of these systems as well as the Pt-V system. We also detail the most successful synthetic routes obtained so far to prepare these alloy and intermetallics as nanometer size particles and discuss future modifications for further control of particle size and composition. Finally, we report on the catalytic activity of these materials toward the oxidation of formic acid.

4.2 Experimental

Materials: All reactants were used as received. Sodium metal, all solvents and VCl_3THF_3 (THF = Tetrahydrofuran) were purchased from Aldrich. Naphthalene was purchased from Fisher. All other metal precursors were purchased from STREM chemicals Inc. MeOH was first degassed for 1 h by bubbling Ar. The product was dried under vacuum, backfilled with argon. All reactants were pumped into and manipulated in an argon atmosphere glovebox. Dry solvents (THF, hexanes and diglyme) were obtained from a solvent system (custom built Seca solvent system by glass contour).

Sodium Napthalide: Sodium napthalide solutions were prepared in either THF or diglyme (bis(2-methoxyethyl)ether, MW = 134.18) according to well known literature methods[9]. Stoichiometric amounts of naphthalene and sodium metal were weighed out in an argon atmosphere glovebox and added to a flask containing 40 ml of the solvent. The sealed flask was removed from the glovebox and stirred overnight under argon to produce a dark green sodium napthalide solution.

Single precursor reductions with sodium napthalide: A significant challenge in this chemistry is finding solvents that are both non-reactive with strong reducing agents, such as sodium naphthalide, and finding a wide variety of soluble salts that will allow comparisons across a good part of the periodic table. The acetylacetonate salts of the appropriate metals were chosen as reactants, since they are all soluble in THF. A metal precursor solution ($Ni(acac)_2$,$Cr(acac)_3$, $Mn(acac)_3$, $Cu(acac)_2$, $CuCl_2$ or $Cu(C_2H_3O_2)_2$ where acac = acetylacetonate anion, $C_5H_7O_2^-$) (0.5 mmol in 20 ml THF) was injected into a flask containing freshly prepared sodium napthalide solution in THF(1.6 mmol, 30 ml for Cr and Mn and 1.1 mmol, 30 ml for Ni and Cu to maintain a constant 10 % excess of the reducing agent in all cases). The dark green sodium naphthalide solution immediately changed color to brown/ black and was stirred for 3 hr or overnight at room temperature. As will be discussed in detail in the following section, our goal was to try and isolate the reduced product (hopefully, the zero valent metal) from the reaction solvent before any kind of washing. Characterizing these isolated products would help us better understand the chemistry in more complex cases. In the case of PtPb, nanoparticles would spontaneously precipitate from the solvent or in some preparation schemes would require centrifuging in order to precipitate.

We first studied the reduction of Ni and Cr to explore methods to isolate the single metal product from the reaction solvent. First, the post reduction product mixture was transferred through a cannula into a centrifuge tube capped with a sealed septum and then centrifuged (9000 rpm, 30 min). Surprisingly nothing precipitated out for either metal, so the solutions were divided into portions. For each metal, one portion was allowed to stand overnight, followed by centrifuging at 9000 rpm for 30 min. Again nothing precipitated from the solution. Prolonged stirring of the second portion and subsequent centrifugation yielded partial precipitation of an amorphous product in the case of Ni, but not in the case of Cr. These reactions were repeated for both metal

precursors, but most of the THF was removed by evaporation under vacuum until products began precipitating. For Ni, the product crashed out once most of the THF was gone, for Cr, hexane needed to be added drop wise after most of the THF was evaporated off in order to obtain a precipitate. Of course, all non-volatile by-products remain mixed with the metallic product. Excess solvent was removed with a syringe, and the product was washed first with hexane (dry, from our solvent system) to remove hexane soluble by-products (naphthalene or neutral organic ligands not bound to metals or metal surfaces), and then with MeOH-hexane solutions (increasing the amount of MeOH gradually from 10% to 50% by volume) to remove ionic by-products such as NaCl or Na(acac), followed by a final hexane wash.

For Cr, no precipitate could be obtained once MeOH was added (as 10 % by volume MeOH solution). Rather, the solution separated into a very dark lower MeOH layer and a clear top hexane layer. In that case, the hexane layer was removed with a syringe, and the rest of the solution was pumped under vacuum until dry. The centrifuge tube was then backfilled with argon and pumped into the glove box. Given the extreme sensitivity of Cr to MeOH and air, one reaction was carried out with Vulcan (C black) suspended in the solvent to allow particle binding to that support. For this reaction, $Cr(acac)_3$ (0.5 mmol) and Vulcan (0.026 g, 50 wt % loading of Cr on Vulcan) were mixed together in 20 ml THF inside the argon atmosphere glove box and injected into the sodium napthalide solution (1.65 mmol, 30ml). Injection was followed by 3 hr stirring and then the solution was allowed to stand overnight. The solution (still completely dark) was transferred into a centrifuge tube, and centrifuged (9000 rpm, 30 min). Again nothing precipitated, even though pure Vulcan suspended in THF could be precipitated by this procedure. Consequently, the THF was evaporated off to dryness under vacuum. Washing with hexane and then with 10 % MeOH-hexane re-suspended the precipitate. The solvent was syringed off after

centrifuging (9000 rpm, 30 min). Once again, some product was soluble in the MeOH layer. A final hexane wash was performed; the dark colored product was pumped to dryness, backfilled with argon and taken into the glovebox.

Following the lead from the above experiments with Ni and Cr, a standard procedure was established and followed for Cu and Mn (and later for metal co-reductions). Three different precursors, $Cu(acac)_2$ $CuCl_2$ and $Cu(C_2H_3O_2)_2$ were used for Cu to determine the effect of utilizing different anionic ligands, if any. Injection of the precursors into the reducing agent solution immediately formed brown/black opaque solutions. The solution was stirred overnight, followed by transfer into a centrifuge tube. No precipitate was observed, so the THF was evaporated off under vacuum. A hexane wash, followed by a 10% MeOH in Hexane, a 50% MeOH in Hexane, followed by a neat MeOH wash was performed. After a final hexane wash, the tube was pumped to dryness, backfilled with argon and pumped into the argon atmosphere glove box. For Mn, excess reducing agent was varied from 10 -100%. This was because the although the solution turned black upon injection of the $Mn(acac)_3$ into the reducing agent, over time (in less than 30 sec) it changed to a light brown mocha color. Suspecting in-situ oxidation of the product, the reducing agent excess was increased, however the same was observed with 100% excess although the color change took longer to happen (about 5 minutes). It is possible that elemental Mn nanoparticles react with THF at room temperature. Work up was carried out in both cases following the standard procedure described above. Air free X-ray diffraction (XRD) patterns were obtained for the products pumped into the glove box. These and other characterization efforts will be discussed in the results and discussions section.

Pt alloys and ordered intermetallics: Stoichiometric amounts (0.5 mmol each) of metal precursor pairs ($Mn(acac)_3/Pt(acac)_2$, $Ni(acac)_2/Pt(acac)_2$, $V(THF)_3Cl_3/PtCl_2COD$ (COD = 1,5 -cyclooctadiene, C_8H_{12}), $V(Cp)_2Cl_2/PtCl_2COD$

(Cp = cyclopentadienyl anion, $C_5H_5^-$), $Cr(acac)_3/PtCl_2COD$), $CrCl_3/PtCl_2(COD)$, $Cu(acac)_2/Pt(acac)_2$) were dissolved in 20 ml THF in a scintillation vial inside the argon atmosphere box. The solution was brought out of the glove box in a syringe and quickly injected into a flask containing a freshly prepared dark green sodium napthalide solution in THF. The reducing agent excess was maintained at 10 %; however, in some cases mentioned below a 100 % reducing agent excess was used. Instantaneous color change from dark green to opaque dark brown/black was observed in every case. The solution was allowed to stir for 3 hr. In a few initial reactions, the reaction mixture was transferred into a centrifuge tube and centrifuged (9000 rpm, 30 min) in effort to precipitate the product out of the reaction solvent; however, since nothing precipitated out (except for co-reduction of $Pt(acac)_2$ and $Ni(acac)_2$ reactions, where some solid product was obtained), this step was omitted thereafter and the solvent was evaporated to dryness using a vacuum pump. The standard work-up procedure described in the above section for the Cu and Mn reductions was followed. The centrifuge speed required to precipitate the products depended on the reaction and the wash solvent (Hexane to MeOH ratio). For the more oxophilic metals like Cr, Mn and V; more often than not, the solution phase separated and the dark MeOH layer (lower) was removed completely under vacuum to prevent product loss (especially in cases where an oxygen containing precursor had been used for either metal). After a final hexane wash, the product was dried under vacuum until completely dry. Once the product was dry, the tube was backfilled with argon, and slowly exposed to air by putting a needle through the septum (in previous work, it was experienced that if the products were quickly exposed to air, they frequently "smoked" or burst into flame)[10]. XRD, EDS, Electron microscopic imaging (SEM, STEM, TEM – dark field and bright field), IR and TGA measurements were carried out on these products. Table 4.1 gives a summary of all the reactions done.

In a few cases, we used a different ethereal solvent, diglyme, to allow heating of the products directly in the mother liquor. For Pt-Ni, $Pt(acac)_2$ and $Ni(acac)_2$ (0.06 mmol each) were dissolved inside the glove box in 10 ml diglyme (dry, from solvent system) and injected into a freshly prepared sodium napthalide solution (0.36 mmol, a 50 % excess).The reaction flask was then heated in an oil bath to 120 ^oC and stirred for 3 h. After cooling, the product was transferred by cannula into a centrifuge tube. Some of the product precipitated quickly on centrifuging (9000 rpm, 30 min), the rest of the solution was transferred back into the reaction flask with a cannula and diglyme was removed under vacuum (since diglyme has a moderately high boiling point (162 ^oC), a higher surface area vessel is required for speedy removal of diglyme under a vacuum). The solid that had precipitated after centrifuging was collected separately and washed with hexane and MeOH: hexane solutions (sonicated for 2 min for each wash and product re-precipitated by centrifugation) and characterized by XRD. With the dried product in the reaction flask, the standard work up procedure described above was followed.

A co-reduction in presence of Vulcan was also carried out. A solution of $Pt(acac)_2$ and $Ni(acac)_2$ (0.5 mmol each) was mixed with Vulcan (0.126 g, 50 wt % loading of PtNi on Vulcan). The mixture was dispersed in 20 ml THF inside the glovebox and was injected into sodium napthalide solution (2.2 mmol, 30 ml) and stirred for 3 h. The work-up procedure was identical to what described above.

Table 4.1: Summary of different reactions attempted to in order to understand and achieve co-reduction of different metals with Pt.

Metals	Precursors (and other reagents)	Reaction conditions
Pt-Cu	$Pt(acac)_2$, $Cu(acac)_2$	In THF, 10 % excess of NaNp, Stirred at room temperature for 3h
Pt-Ni	$Pt(acac)_2$, $Ni(acac)_2$	In diglyme, 50 % excess of NaNp, Stirred at 120 ^oC for 3h
	$Pt(acac)_2$, $Ni(acac)_2$	In THF, 10 % excess of NaNp, Stirred at room temperature overnight
	$Pt(acac)_2$, $Ni(acac)_2$	In THF, 100 % excess of NaNp, Stirred at room temperature for 5 days
	$Pt(acac)_2$, $Ni(acac)_2$, Vulcan	In THF, 10 % excess of NaNp, 50 wt % loading of PtNi on Vulcan, Stirred at room temperature for 4 h
	$Pt(acac)_2$, $Ni(acac)_2$, Vulcan	In THF, 10 % excess of NaNp, 50 wt % loading of PtNi on Vulcan, Stirred at room temperature for 5 days, Precursors stirred with Vulcan in THF overnight before injection of reducing agent
Pt-Cr	$Pt(acac)_2$, $Cr(acac)_3$	In THF, 100 % excess of NaNp, Stirred at room temperature overnight
	$PtCl_2COD$, $CrCl_3$	In THF, 100 % excess of NaNp, Stirred at room temperature overnight
Pt-V	$PtCl_2COD$, VCl_2Cp_2	In THF, 100 % excess of NaNp, Stirred at room temperature overnight
	$PtCl_2COD$, VCl_3THF_3	In THF, 100 % excess of NaNp, Stirred at room temperature overnight
	$PtCl_2COD$, VCl_3	In THF, 100 % excess of NaNp, Stirred at room temperature overnight
Pt-Mn	$Pt(acac)_2$, $Mn(acac)_3$	In THF, 100 % excess of NaNp, Stirred at room temperature overnight
	$Pt(acac)_2$, $Mn(acac)_3$	In THF, 10 % excess of NaNp, 50 wt % loading of PtNi on Vulcan, Stirred at room temperature for 5 days, Precursors stirred with Vulcan in THF overnight before injection of reducing agent

The procedure described in the table for Pt-Cu was the standard method followed for all metal systems. For the other metal systems, only the variations to the standard method attempted are specified in the table.

Instrumentation: The sonicator used was a model 3150 Bransonic ultrasonic cleaner. All powder X-ray diffraction (pXRD) scans were taken on a Scintag XDS 200 powder X-ray diffractometer. pXRD patterns taken under inert conditions were prepared by loading the sample in an argon-filled glovebox into the sample holder and covering it with a mylar film before removing from the glove box to take the pXRD pattern. For TGA experiments, a Q50 instrument from TA instruments was used. The SEM and TEM imaging were done using a LEO-1550 Field Emission SEM (FE-SEM) and a TECNAI T-12 at 120 KV respectively. For imaging purposes, a solution of the nanoparticles was formed by suspending the particles in 5 ml of sonicated, degassed isopropyl alcohol and dropping the solution on a carbon coated copper grid. For EDS measurements on the SEM, TEM or STEM samples were prepared by transferring dry powder onto 300 mesh copper grids in order to avoid possible reaction of the electropositive metal with isopropyl alcohol affecting the composition.

Electrocatalytic activity: The electrocatalytic activity of the Pt_3Cr, PtNi and Pt_3V nanoparticles was tested for formic acid oxidation. Prior to each experiment, a suspension of the nanoparticle catalyst was prepared as follows: to 8 mg of the dried nanoparticle sample were added 3.98 mL of distilled water and 1 mL of isopropyl alcohol (Aldrich). Additionally, 20 μL of a 5% w/w Nafion solution in alcohols and water (Aldrich, EW: 1100) was added to this mixture. The resulting mixture was sonicated in a bath type ultrasonicator for 1 hour. Each nanoparticle suspension described above was coated onto a 4 mm diameter glassy carbon (GC) electrode. The GC electrode had been previously polished with diamond paste (METADI-Buehler, ø = 1μm) and ultrasonicated in Millipore water (18 MΩ cm^{-1}, Millipore Milli-Q) for 10 min. The electrode was then rinsed with Millipore water and allowed to dry in air. 140 μg cm^{-2} of the nanoparticle (10.8 μL of nanoparticle suspension) was coated onto the clean GC electrode. The coated electrode was then dried in air.

Formic acid oxidation on the nanoparticle-coated GC electrode was examined in a mixture of 0.5 M formic acid (Mallinckrodt, 88% analytical reagent) and 0.1 M sulfuric acid. A three-electrode electrochemical cell was used for all electrochemical measurements. The reference electrode was a sodium chloride saturated Ag/AgCl electrode, and the counter electrode was a platinum coil. All electrochemical experiments were carried out at room temperature with a Pine AFRDE2 potentiostat. All solutions were prepared with Millipore water and de-aerated with pre-purified argon for at least 15 min before each experiment.

4.3 Results and discussion

The goal of this work is to delineate factors that influence nanoparticle synthesis and to develop an understanding of, and possibly general guidelines for, solution phase syntheses of bimetallic nanoparticle phases by co-reduction. To achieve this, it is vital to minimize the interfering effects in solution of the by-products (ligands from reducing agent or precursors) so that the desired phases could be isolated from the reaction solvent (requiring that they have been able to grow sufficiently). If the other species present in the solution do not interact strongly with the metal particles post-reduction, the desired bimetallic phases should be able to nucleate and grow without in-situ heating or post-reaction annealing. Also, the side products would be easily removed from the reaction solvent, or by washing. If larger nanoparticles are obtained (larger than about 5 nm in diameter), removal of the more electropositive metal by reaction with MeOH (leaching) or by oxidation on exposure to air should occur only on the surface. However, it appears that strong association of the side products with the reduced metals keep the intermetallic phases from nucleating/growing in-situ, keep the products from precipitating out of the solution and result in significant loss of the

reactive metal (depending on its oxophilicity) during MeOH washes or on air exposure.

To address this challenge, two parallel routes have been explored: role of precursors in co-reduction and single precursor reductions. We began to explore the role of the precursors, since they produce some of the by-products in the reaction. Based on our experience with very electropositive and oxophilic metals like Ti, we examined the effect of oxygen containing vs. oxygen free precursors, and used that as a tool in controlling the final composition for the highly oxophilic metals.

Our choice of precursors is also limited by other factors. Sodium napthalide is compatible with only ethereal or glyme solvents, limiting our precursor choice to those with at least moderate solubility in these solvents. Metal chlorides and many organometallic compounds often have low or negligible solubility in ethers. However, precursors with both chloride and neutral or anionic organic ligands (e.g. $V(Cp)_2Cl_2$ or $Ti(THF)_3Cl_3$) are often suitable, as are metal acetylacetonates and ethylhexanoates (e.g. Cr(2-ethylhexanoate)$_3$). Generally precursor metals in their highest oxidation state are preferred to prevent internal redox reactions when the precursors are mixed, since this may lead to precipitation of one of the metals prior to reduction.

A second consideration in solvent choice is the ability to remove the side species associated with products (without affecting the reactive metal) by precipitating the product from the reaction or wash solvent, leaving the side products in solution. As described earlier, this would only be possible if these side products are not too strongly bound to the reduced metals. To better understand the nature of association of these species to the metals, single metal reductions, with smaller reducing agent excesses were studied – the objective was to simplify the number of species in solution. For this reason, metal acetylacetonates were the precursors of choice for most of these reactions, since only one anionic ligand is present in solution. The

phenomenon of ligands contaminating the nano-particle surface and their role in determining nanoparticle domain size and their electrochemical properties has been studied in the PtPb system[8]. To confirm and extrapolate our understanding to the case of metals more electrophilic than Pb, it's logical to first start by reducing that metal by itself. Our observations with PtPb suggested that products precipitated out the reaction solvent have less contamination than the products that were recovered by evaporation of the reaction solvent. As it can be concluded from combining these points, the objective in the single precursor reductions was to determine conditions under which the product could be isolated from the reaction solvent (THF) post-reduction.

4.3.1 Single precursor reductions

It is apparent even in the single precursor reductions that the by-products remaining in the solution indeed play a significant role in determining the properties of the final product, such as nanoparticle size and precipitation behavior. The product nanoparticles remain very small (2 nm or less) and they are very difficult to precipitate from the solvent. In case of oxophilic metals, the small size compounds the problem of the reactive metal being oxidized and solubilized by reacting with wash solvents such as MeOH. Centrifuging at 9000 rpm for 30 min after the reduction (injection of precursors, 3 h or overnight stirring) did not produce a precipitate for any of the metals (Ti, V, Cr, Mn, Ni and Cu). Occasionally the metal nanoparticles would precipitate out upon vacuum removal of most of the THF, but typically the solutions were evaporated to dryness then worked up using a methanol/hexane wash. The metals are discussed below in the order of increasing oxophilicity.

Three different copper precursors ($Cu(acac)_2$ $CuCl_2$ and $Cu(C_2H_3O_2)_2$) were used to study the effect of ligands on the formation of nanoparticles. Cu was chosen because it

is the least electropositive metal being studied here, and thus least reactive with solvents, water and air once reduced. For all precursors, no solid precipitations was seen upon centrifuging, so the THF was evaporated off completely, and product was worked up following the standard procedure described in the experimental section. However, no significant effect of the ligands could be inferred from these experiments with Cu as all products had similar particle sizes and behaved similarly in terms of precipitation. Thus for the other metals, only one type of precursor, acetylacetonate salts, was explored.

For Ni, some product (as discussed later, complete identification of the product was not possible in the case of single precursor reductions) could be precipitated out of THF by concentrating the solution until most of the THF was gone. The product was silvery grey and turned green (color of NiO) on exposure to air.

The Mn system showed unusual behavior upon reduction. Excess reducing agent was varied from 10-100% and for each reaction the solution would turn dark brown or black upon injection of the $Mn(acac)_3$ solution indicating reduction of the metal. In all cases the solution would then change from black to a light brown color. Initially this was suspected to be the oxidation of the particles since metal nanoparticle solutions are inevitably black and oxidation of the metal generally results in lighter colors. Increasing excess reducing agent would slow the color change but even with 100% excess, the solution would turn light brown within 5 minutes of addition of the reducing agent. The light product was collected by removing all of the THF under vacuum and washing with hexanes and methanol.

The observations with Cr were very similar to those seen with Ni, except, that precipitating out the product was more difficult in case of chromium, and required addition of significant amounts of hexane after evaporating off most of the THF. Also, once MeOH was added to the system, no solids could be recovered, showing the high

reactivity of MeOH with electropositive oxophilic systems (Ti and V showed similar results). For the more electropositive elements, MeOH apparently reacts with the metals to produce metal alkoxides, thus loosing the elemental metal. Attempts to counter this reactivity by using different wash solvents, such as propylene carbonate, were also unsuccessful. There were initial difficulties in drying the product post propylene glycol washes, which were overcome by washing multiple times with THF, however, sodium carbonate was found in the final product. In a parallel effort, Cr was reduced in the presence of Vulcan, a carbon support material, which should make the product more robust towards washes and easier to precipitate and recover from solvents. Contrary to expectations, nothing precipitated post-reaction on standing or centrifuging and once again, most of the THF had to be evaporated off to crash out the product. Also, a considerable amount of the Cr product was lost in MeOH washes in spite of the presence of the carbon support as seen by a very dark methanol supernatant. The recovered product that precipitated out of methanol was found to contain chromium particles dispersed on the carbon support as confirmed by TEM brightfield and darkfield imaging and subsequent EDS (Figure 4.1 a & b). However, the possibility of the chromium existing as oxide or carbon containing compounds couldn't be excluded with the available experimental means.

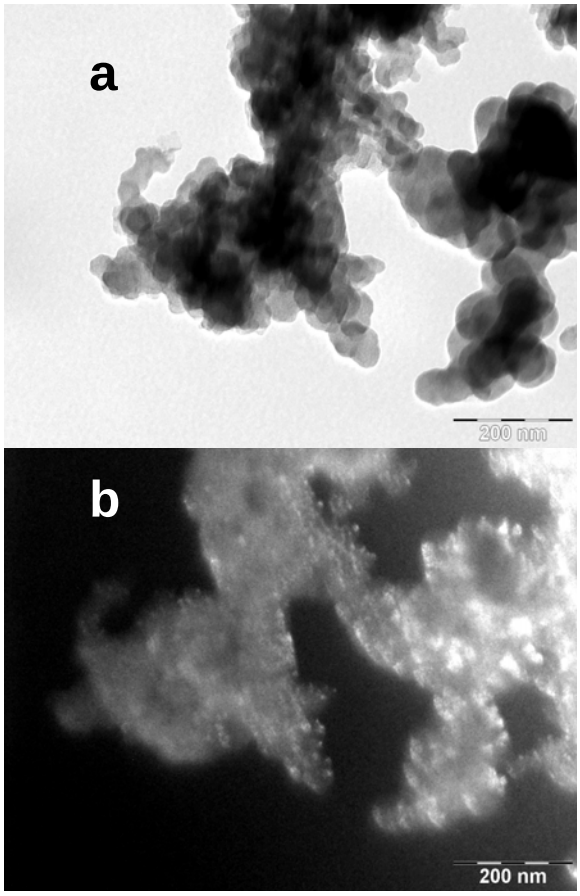

Figure 4.1: TEM a) brightfield and b) darkfield images of Cr/Cr containing particles dispersed on carbon support.

The products recovered from these single metal reactions were pumped into an argon filled glovebox and air free XRD patterns were obtained. For all the metals, XRD of the unannealed sample were inconclusive due to small particle size or amorphous/unclean material coupled with a large background signal from the mylar film. However, on exposing the powder to air they quickly change color to something similar to the respective oxide phases, for example the Mn changed from a brown

powder to a dark gray/green consistent with MnO or Mn_2O_3. Annealing the product in sealed, evacuated silica tubes to 600 ^oC, without exposing the sample to air, to obtain larger particles resulted in relatively sharp diffraction peaks. In the case of Cu, those peaks matched the Cu pattern for all Cu precursors, with little or no copper oxides visible. For most of the annealed products, the silica tubes were coated internally with a black film, which likely resulted from the decomposition of organic materials in the product. TGA on the products also showed significant weight loss consistent with presence of organic materials. With Mn, an X-Ray pattern with broad peaks near those expected for MnO was obtained on annealing. The Ni and Cr products were not annealed, since we had already determined from the end members (Cu, Mn) how sensitive the metals particles were to oxidation.

It was inferred from these experiments that very small (2 nm or less domain size) nanoparticles were formed upon reduction of the precursor as evidenced by the color change. However the particles did not grow or agglomerate, most likely due to ligands and ligand derivatives bound to the nascent particle surfaces. EDS confirmed the presence of sodium in all cases and weight loss was observed in TGA experiments corresponding to an organic residue being removed. Since Na(acac) by itself is soluble in THF, we concluded that acac must have some affinity for the neutral metal surfaces. These surface bound species curtail particle growth at room temperature, but not at elevated temperatures. Apparently these surface species also solubilize the small particles, preventing them from crashing out of THF, even under high speed centrifuging. MeOH /hexane washes were not sufficient to remove all the materials adhering to the nanoparticles. No specific trends with oxophilicity or electropositivity of the metals in terms of their precipitation behavior could be inferred.

We hoped that the presence of a second metal like Pt would alter this behavior by stabilizing the particles enough that a product could be obtained and characterized.

The observations with co-reductions are discussed below starting with the least reactive metal, Cu.

4.3.2 Co reduction with Platinum (Pt:M reactants are all 1:1 atomic ratio)

Pt-Cu: The platinum copper system has a relatively low affinity for oxygen, reflected in the positive reduction potential of both metals, produces nanoparticles with good yield and low temperature intermetallic formation. Acac precursors were used for both the Pt and Cu source due to better solubility and since the there was less concern for the formation of copper oxides. Upon injection of the metal precursors, the solution immediately turns black indicating reduction of the metal ions. The 1:1 product did not precipitate out of the solution with centrifugation, so THF was removed by vacuum and the product was washed with hexanes followed by hexanes/methanol mixtures. The resulting black powder was dried under vacuum and exposed to air slowly overnight by inserting a needle through the septum. The as-made powder showed a shift in the X-ray diffraction pattern from that of Pt to a smaller cubic lattice constant, consistent with significant alloying (Figure 4.2). Atomic ordering of the as-made sample could not be confirmed due to the small particle size giving broad diffraction peaks.

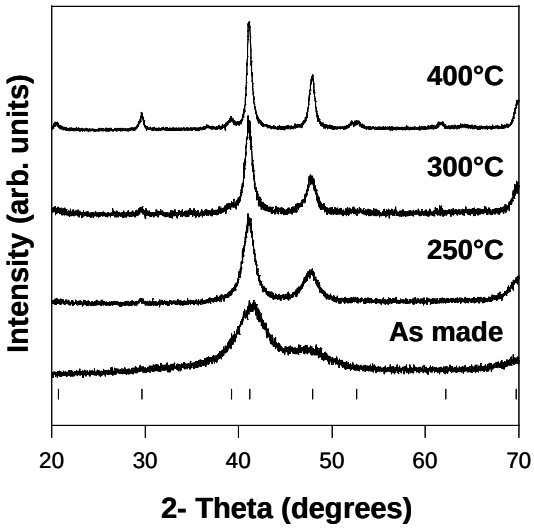

Figure 4.2: pXRD of CuPt nanoparticles as made and annealed to 250, 300, and 400°C. The as-made sample shows a significant shift from the Pt lattice due to the incorporation of Cu. Upon annealing the sample at 250°C, the intermetallic phase is formed as seen by the ordering peaks at 20.7°, 29.6°, 52.6° and 62.1° 2-Theta (PDF # 00-042-1326).

Annealing the powder at 250°C caused some growth of the particle size from 6.2 nm to 14.5 nm as determined by the Scherrer equation, and the ordered intermetallic phase PtCu could then be observed by the super-lattice peaks in the diffraction pattern. Further annealing caused more sintering and particle growth as seen by sharper diffraction lines. Figure 4.3 shows TEM images of the CuPt particles prior to annealing with small 3-5 nm particles and the annealed sample shows some aggregation and sintering. Selected Area electron diffraction (SAED) also shows broad diffuse diffraction pattern for the as prepared sample and sharper rings for the annealed pattern, consistent with the XRD data. EDS for both as-made and annealed samples confirmed the 1:1 composition (+/- 5%).

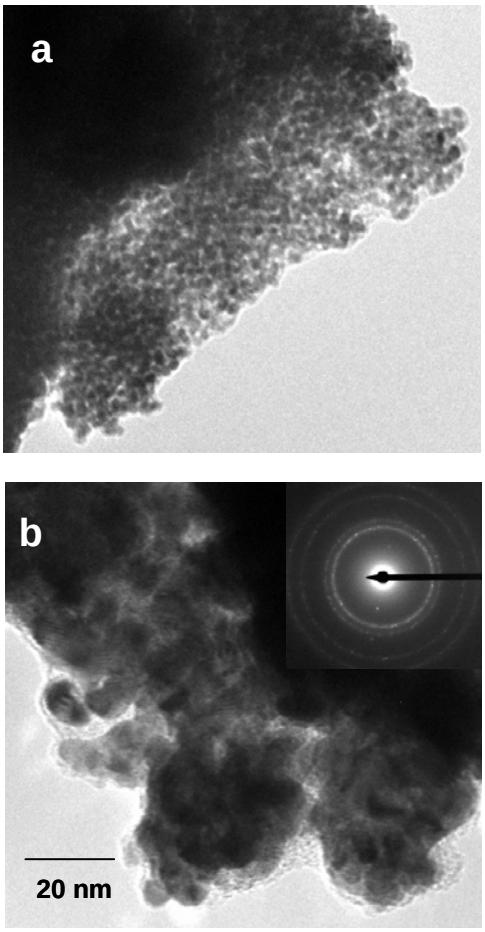

Figure 4.3: TEM images of CuPt nanoparticles a) as synthesized and b) after annealing at 250°C. Electron diffraction is inset in each picture showing a diffuse cubic pattern for the as synthesized sample and more crystalline ordered tetragonal pattern for the annealed sample.

Pt-Ni: Referring to Table 4.2 (low Ni oxophilicity and reduction potential) which agrees with single precursor reduction experience (less/no reactivity with MeOH), Ni was expected to co-reduce with platinum about as well as Cu and form the desired alloy and intermetallic phases. Acetylacetonate precursors were expected to be appropriate for the same reasons. However, as evident from the Pt-Ni phase diagram,

the tetragonal intermetallic PtNi phase might be difficult to obtain since it exists only within a narrow range of temperature.

Table 4.2: Reduction potential and bond enthalpy (with O) data for different metals as obtained from the CRC handbook for physics and chemistry[11].

Metal	Oxidation states	Correspondig reduction potentials ($E^{o}r_{ed}$)	Bond enthalpy M-O(Kcal/mol) (used for apprehending oxophilicity)
Aluminium	3+	-1.66	122
Titanium	3+	-1.37	157
	2+	-1.63	
	3+ to 2+	-0.9	
	4+ to 3+	-0.055	
	4+ to 2+	-0.502	
Manganese	2+	-1.185	96
	3+ to 2+	1.54	
Vanadium	2+	-1.17	150
	3+ to 2+	-0.225	
Chromium	3+	-0.74	102
	2+	-0.913	
	3+ to 2+	-0.407	
Iron	2+	-0.44	93
	3+ to 2+	-0.037	
Zinc	2+	-0.76	38
Gallium	3+	-0.55	85
Cobalt	2+	-0.28	92
Nickel	2+	-0.26	91
Tin	2+	-0.14	127
	4+ to 2+	0.15	
Lead	2+	-0.13	91
Copper	2+	0.34	64
Platinum	2+	1.18	94

As expected, the room temperature co-reduction of platinum and nickel acetylacetonates with sodium napthalide, yielded a final product of composition Pt:Ni of 1:0.6 +/- 5% (atomic ratio). The Ni content is a little low, even considering the semi-quantitative nature of the EDS measurement; so some Ni might have reacted with MeOH during the work-up. XRD suggested a cubic alloy phase of Pt with broad peaks that were shifted towards higher angles due to incorporation of Ni in the lattice. XRD the product obtained after heating in the TGA (product heated up to 550 ^{o}C) showed Pt and NiO. Annealing the product in a tube sealed under vacuum at 600 ^{o}C for 4 h gave single phase intermetallic PtNi, with a 20.5 nm domain size as determined by the Scherrer equation, and trace amounts of unknown impurities (Figure 4.4). The annealing tubes were coated with a black film, indicating that the sample contained some organic species before heating. Annealing at a higher temperature for longer times (670 ^{o}C, 48 h) yielded the $Pt_{0.5}Ni_{0.5}$ alloy predominantly which is to be expected based on the phase diagram.

Next we investigated the Pt-Ni system by reaction and subsequent heating in diglyme mother liquor. Heating to 120 ^{o}C in diglyme following injection of the Na naphthalide produced a large amount of precipitate on standing. However, some product could not be precipitated even in a centrifuge and could be recovered only by evaporating off the diglyme. The XRD for the product that precipitated had many low intensity peaks which were difficult to index. The product collected from the supernatant showed very broad diffraction peaks.

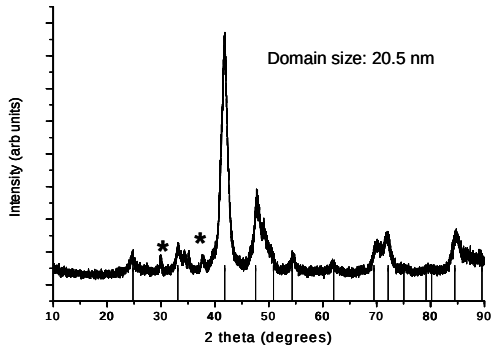

Figure 4.4: pXRD image of PtNi ordered tetragonal phase (PDF # 03-065-9446) obtained by co-reduction of $Pt(acac)_2$ and $Ni(acac)_2$, followed by annealing at 600 ^oC for 4h. * unknown impurity peaks.

On annealing this sample (670 ^oC, 48 h), sharp peaks indexing on the tetragonal cell of PtNi was obtained. EDS showed the composition to be Pt:Ni of 1:0.7 +/- 5 %(atomic ratio). Another reaction was allowed to stir for 5 days post injection at room temperature to attempt to precipitate out the product. The product, though bulkier, crashed out of THF on centrifuging, but was still an alloy phase as observed as broad peaks with no evidence of ordering in the XRD pattern. On annealing (600 ^oC, 4 h), unlike the previous room temperature reaction, the cubic PtNi alloy and not the tetragonal intermetallic phase was obtained. Co-injection of the precursors into the reducing agent solution with Vulcan (to form supported Pt-Ni phases) was successful, yielding a cubic PtNi alloy on annealing, but with much less aggregation than the unsupported sample seen by broader peaks in the XRD data (Figure 4.5a, b), and smaller particles in the brightfield and darkfield TEM images (Figure 4.6a, b). This shows the promise of co-reductions in presence of carbon nanoparticles to obtain

supported and smaller particles even with annealing at high temperatures which can be precipitated comparatively easily out of polar solvents.

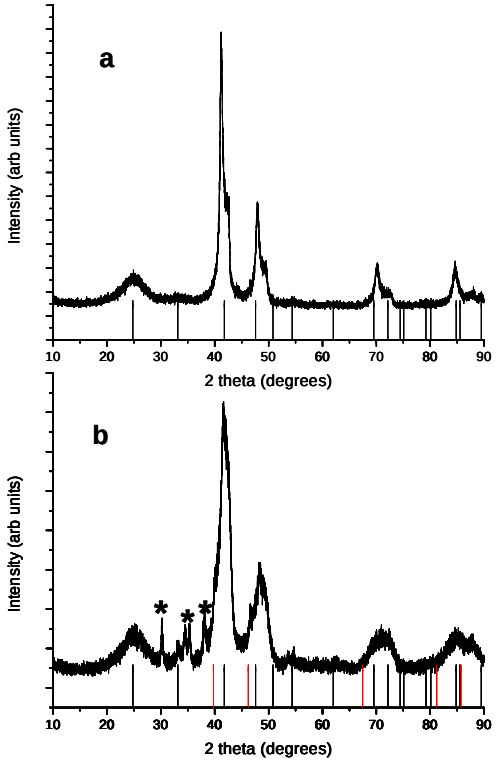

Figure 4.5: pXRD patterns of PtNi (PDF # 03-065-2797, indicated by the black lines) phases from co-reduction of precursors in presence of C black (Vulcan) after annealing at (a) 800 ^{o}C and (b) 670 ^{o}C. Particle agglomeration is seen to be less in the presence of C support. * Unknown impurity peaks, | shows 2 theta positions for the Pt phase (PDF # 04-001-2683).

Pt-Cr: In the case of co-reduction of platinum and chromium acetylacetonates, the EDS data showed the composition of the product to be mostly Pt (Pt:Cr was about

8:1). Thus oxygen free precursors were used in order to obtain the desired composition in the final product. $CrCl_3$ and $PtCl_2COD$ was the first oxygen-free precursor combination tried for Pt-Cr systems. Room temperature reduction yielded a product with a Pt:Cr atomic ratio of 1:0.8, and XRD showed very broad peaks indexing close to cubic Pt, but shifted slightly towards higher angles. On annealing in a tube sealed under vacuum at 500 ^oC for 48 h or 800 ^oC for 24 h, cubic Pt-Cr alloy phases were obtained. However, annealing at 700 ^oC for 24 h gave the Pt_3Cr ordered intermetallic phase (Figure 4.7).

Similar to the previous samples, all the annealing tubes were coated with a black film on the inside from the decomposition of organic species in the sample. Also, the XRD showed presence of significant amount of NaCl, which was expected in cases where chloride precursors have been used. This further emphasizes the need for a better wash solvent/ washing technique. TEM images showed particles with average size < 20 nm even after annealing at 500 ^oC and Pt and Cr were confirmed by the subsequent EDS analysis (Figure 4.8a, b). The background material in seen in the TEM image couldn't be identified, but given the presence of Na detected in EDS, a sodium salt with organic materials might be present surrounding the particles. This matter is further discussed in a following section.

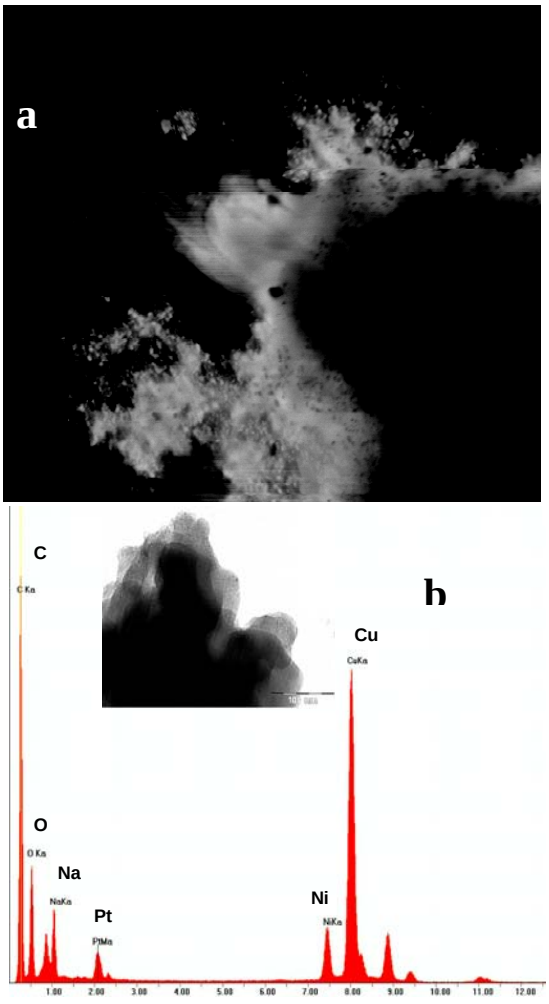

Figure 4.6: a) Darkfield TEM image (full scale = 3 μm) and b) showing high Z elements as white specks on the C support and EDS data of the PtNi obtained from co-reduction of precursors in presence of C black. Inset shows the region on which EDS data was obtained. The Cu signal comes from the TEM grid.

PtV: Vanadium is the most oxophilic of the metals used, and once again required looking into oxygen free precursors for products that contained significant amounts of V. Co-reduction of VCl_2Cp_2 and $PtCl_2COD$ at room temperature in THF yielded product with a Pt : V atomic ratio of 1:1 +/- 5 % by EDS, and XRD showed relatively

broad peaks with maxima shifted to higher angles compared to Pt. In an attempt to target the ordered PtV phase, the product was annealed at 1100 oC, 24 h (refer to phase diagram), however, ordering peaks weren't observed in the XRD. At this temperature there is significant attack of the silica tube, presumably by the V. Room temperature co-reduction of VCl_3THF_3 with $PtCl_2COD$ yielded Pt: V atomic ratio 3:1 (EDS).

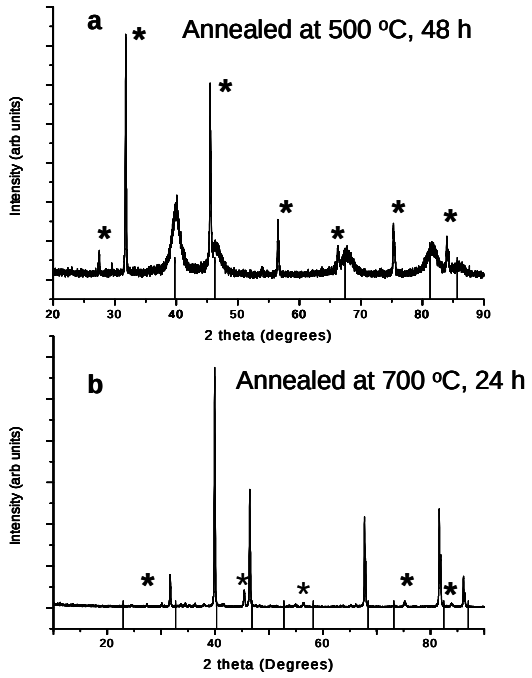

Figure 4.7: pXRD patterns the $PtCl_2COD$ and $CrCl_3$ reduction reaction annealed at different temperatures. a) shows peaks with maxima close to the pure Pt phase (PDF # 04-001-2683), but shifted (especially at higher angles) suggesting alloying of Cr into the pt phase. b) shows the ordered Pt_3Cr phase (PDF # 04-003-3551), the shifting of peaks might be due to compositional variation (Pt-Cr phase diagram shows that the Pt_3Cr phase can have significant compositional width).The ordered Pt_3Cr phase was obtained only from annealing at 700 ^oC. * shows the NaCl peaks.

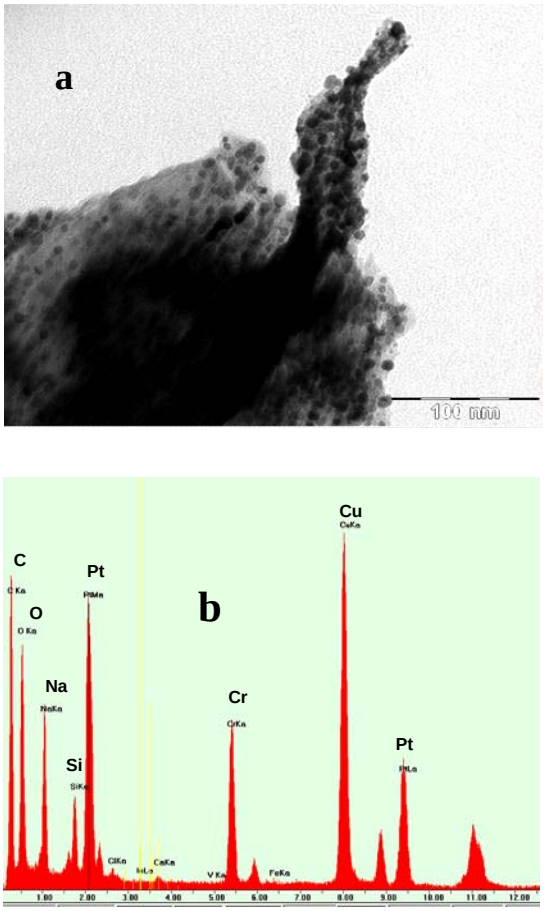

Figure 4.8: (a) TEM image of Pt-Cr particles from co-reduction of $PtCl_2COD$ and $CrCl_3$, annealed at 500 ^oC for 48 h. (b) EDS spectra of this region, the Cu signal typically comes from the TEM grid, other impurities are also detected in minor amounts which might from contamination from the TEM sample holder. The background material seen in a) might be sodium and organics known to be present in the samples.

The decline in the amount of vanadium retained in the final product on moving to a precursor containing oxygen (VCl_3THF_3 vs. VCl_2Cp_2) was indeed what was expected. XRD showed broader peaks with maxima close to cubic Pt. The product was annealed

in silica tubes sealed under vacuum to 700 ^{o}C for 4 h and 750 ^{o}C for 24 h in efforts to obtain the ordered Pt_3V phase. EDS analysis using the nanoprobe mode in the TEM microscope on individual particles showed the Pt: V ratio to be closer 5:1 (Figure 4.10). This suggests the presence of the rest of vanadium (as observed from EDS on broader regions) as a second phase, perhaps partially oxidized or closely associated with contaminant species (most probably oxygen containing), and thus unable to form Pt-V species. This might be the reason why ordered phases are not always observed on annealing in spite of the seemingly right composition of the elements required. The last reaction tried with Pt-V system was a co-reduction of VCl_3 and $PtCl_2COD$ – again, an oxygen free system, and not unexpectedly, Pt: V atomic ratio in the product was shown to be 1: 1 by EDS.

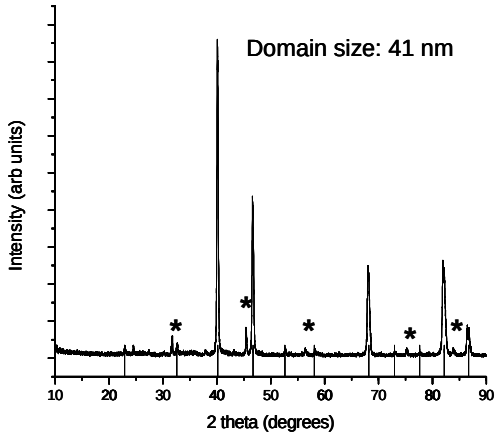

Figure 4.9: pXRD pattern of the ordered Pt_3V phase (PDF # 04-004-6343) from co-reduction of VCl_3 and $PtCl_2COD$, followed by annealing at 750 ^{o}C for 24 h. * shows the NaCl peaks.

The product was annealed at 750 ^{o}C for 24 h and the ordered Pt_3V cubic phase with domain size of 41 nm (from Scherrer equation) could be obtained. Shifting of peaks observed might be due to compositional width (the composition range over which the ordered phase can exist gives rise to a number of reported Pt_3V cubic ordered phases with peaks significantly shifted from each other).

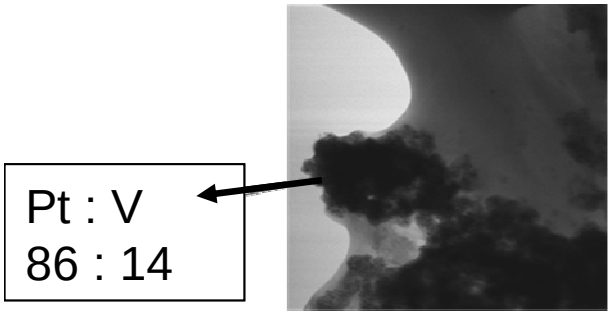

Figure 4.10: TEM image of Pt-V particles from co-reduction of VCl_3THF_3 and $PtCl_2COD$. Inset shows composition data from EDS.

Pt-Mn: Mn is intermediate between Ni and Cr in its oxiphilicity (Table 4.2). Once again, $Mn(acac)_3$ was chosen as the starting precursor. Co-reduction of platinum and manganese acetylacetonates at room temperature proceeded similar to the other metals, but the product was harder to recover post MeOH/hexane wash. To increase the yield an ethanol/hexanes wash was also employed and precipitated out a larger amount of sample. However, XRD showed a significant amount of unknown impurities. EDS showed the product composition to have a Pt:Mn atomic ratio of nearly 1: 1. XRD showed broad peaks with the maxima shifted from the pure Pt cubic phase, suggesting an alloy phase. The ordered Pt_3Mn phase was obtained on annealing

the product in a tube sealed under vacuum (800 ^{o}C for 24 hr, domain size 46 nm). Smaller particle sizes were achieved by annealing at lower temperature (600 ^{o}C for 24 hr, domain size 22.3 nm) (Figure 4.11). The presence of minor impurities was observed in both cases; however, contrary to expectations, the impurity peaks did not index to manganese oxide phases. As always in these systems, upon high temperature annealing, a black film formed on the inside of the silica tube.

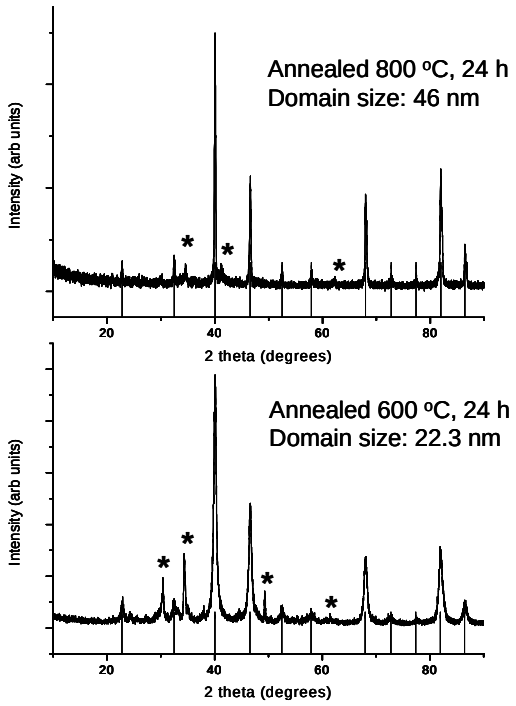

Figure 4.11: pXRD patterns of ordered Pt_3Mn (PDF # 03-065-3260) nanoparticles obtained by co-reduction of $Pt(acac)_2$ and $Mn(acac)_3$ followed by annealing at 800 ^{o}C and 600 ^{o}C respectively. * denotes unknown impurity and/or NaCl peaks.

4.3.3 Selection of precursors

In previous unpublished work in the group, it was observed that due to the high oxophilicity of the early transition metals, the presence of oxygen containing anionic or neutral ligands (e.g., $Pt(acac)_2$ or $Ti(THF)_4Cl_2$) often resulted in products containing oxygen while precursors such as $PtCODCl_2$ or $TiCP_2Cl_2$ produced cleaner products. In the former case, the oxygen containing species from precursors would either bind strongly to the reduced oxophilic metals such as Ti^0 or they directly react to re-oxidize Ti, thus removing some Ti from being available to bind with Pt. In such state, Ti will either be removed during post reduction wash (giving platinum rich or solely Pt end products) or be oxidized to Ti oxide species on annealing the samples. Either way, this made it impossible to obtain ordered Pt-Ti phases or even alloys with the desired Ti content reproducibly. Cr, V and Mn were expected to behave similarly to Ti given their reduction potential and oxophilicity (Table 4.2). Hence, avoiding oxygen in the precursors is desirable for these elements. The results described in the above sections confirm this. Higher contents of the second element (Cr and V) in the end product were obtained from the co-reductions of the respective metal chlorides and $PtCODCl_2$ than from the co-reductions of $Pt(acac)_2$ and the metal acetylacetonate precursors. However, as the oxophilicity of the metal decreased on going from Ti to Mn, it became easier to obtain the desired composition as an isolated product. Thus precursor selection based on the guidelines discussed in this paper is vital for achieving desired phases. Up to Mn (in the order of oxophilicity), oxygen containing precursors meeting other (solubility and oxidation state) criteria can be used. Going above that, chlorides and alkyl chlorides need to be used as precursors for both metals. It needs to be mentioned here that for these studies, only commercially available precursors were used since the goal was to look at as many different metals as possible

and to discover general principles and guidelines. Once the desirable properties for the precursors have been outlined, we can synthesize appropriate ligands for the metals if they are not commercially available. A quick summary of precursor choice and related observations is given in table 4.3.

Table 4.3: Summary of precursors selected for different metals based on desired criterion and final composition of products obtained as a result.

Second metal	Precursor used for the second metal	Is the precursor oxygen free?	Solubility in THF	Is metal at its highest (or high) oxidation state?	Pt: X by EDS (where X is V, Cr, Mn, Ni or Cu)
V	$V(DCP)_2Cl_2$	yes	ok	Yes	1:1
	$V(DCP)_2Cl$	yes	------	Yes	….
	VCl_3	yes	Poor	Yes	1:1
	$V(THF)_3Cl_3$	No	Good	Yes	3:1
Cr	$CrCl_3$	yes	Poor	Yes	1:0.8 * “
	$Cr(acac)_3$	No	Excellent	Yes	8:1
	$Cr(ethylhexanoate)_3$	No	Good	Yes	.....
Mn	$MnCl_3$	Yes	Poor	Yes	….
	$Mn(acac)_3$	No	Excellent	Yes	1:1 * “
	$Mn(ethylhexanoate)_3$	No	Good	Yes	….
Ni	$Ni(acac)_2$	No	Excellent	N/A	0.6:1 * “ #
Cu	$Cu(acac)_2$	No	Excellent	N/A	1: 1

* Ordered phase achieved, “ C supported reactions explored, # Higher temperature reactions explored, … stands for not done yet. Cr and Mn ethylhexanoate precursor reactions weren’t completely analyzed as the precursors come commercially as solutions in hexane and were difficult to purify and handle.

4.3.4 Looking into the contaminants, the role of Na

As mentioned in the above sections, obtaining a clean final nanoparticle product was not possible directly from room temperature reactions. Multiple washes and the use of MeOH reduced but did not eliminate the contaminants but resulting in product loss. Before high temperature annealing, low index peaks would be observed in the XRD, which did not index to known salts or oxides. EDS analyses always showed the presence of sodium in the final products. These observations strongly suggest that sodium is present in close association with some organic moiety on or near the nanoparticles, increasing their polarity. This is consistent with the observed difficulty in precipitating the products out of even weakly polar solvents. Such a surface contamination would also significantly hinder particle growth through agglomeration, until sufficiently high temperatures were used in annealing. Finally, products containing small (2 nm) dendridic particles would likely be highly reactive with most of the metal atoms accessible to reactive solvents such as MeOH. Thus the more oxophilic of these metals reacted with and were leached out of the product when washed with MeOH. If annealed before washing, larger particles were obtained and the reactive metal could only be removed from the top few monolayers of the product, as is observed in typical de-alloying experiments in bulk or thin film samples.

Considerable support for this hypothesis was obtained from STEM analyses of the nanoparticle samples. In the particular case for the Pt-V reaction with VCl_3 as the precursor, needle like structures could be identified which were shown by EDS to consist of only sodium and carbon (Figure 4.12 a, b). A background spectra obtained in the immediate vicinity showed much less carbon and no sodium (Figure 4.12c).

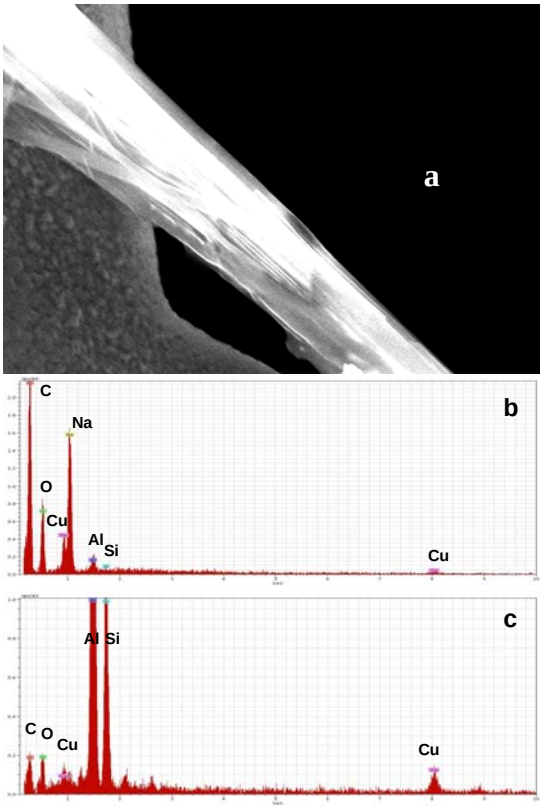

Figure 4.12: (a) STEM image of needle like structures observed in the $PtCl_2COD$ and VCl_3 co- reduction. (b) EDS spectra obtained right on the needle and (c) EDS spectra of the immediate background. Although quantification of C is not possible by EDS measurements, the huge difference in the total count for C observed between the two cases suggest that significant amount of carbon is present in the former region.

The identification of these sodium species suggest the possibility that on complete removal of these, much lower annealing temperatures would result in the desired phases and loss of the reactive metal could also be prevented or reduced. Multiple water washes followed by composition analyses showed that the sodium could be removed. However, water wash (especially on unannealed samples) cause oxidation of

the reactive metals, hence a balance needs to be found between the washing and annealing steps, to obtain the desired phase at low annealing temperatures or, more desirably, at room temperature.

4.3.5 Electrocatalytic activity

Figure 4.13 shows the rotating disk electrode voltammograms for formic acid oxidation on three different nanoparticle catalyst electrodes: Pt_3Cr, PtNi and Pt_3V. In comparing the relative activity of these electrocatalysts, we find that two parameters are of significance: onset potential (which reflects thermodynamic aspects) for fuel oxidation and current density (which reflects kinetic aspects) at a given potential. Thermodynamically, the onset of formic acid oxidation should occur near -0.2 V (vs NaCl-saturated Ag/AgCl electrode). Good catalysts are those with low overpotentials for oxidation, so that high oxidation currents occur at potentials only slightly more positive than -0.2 V. Therefore, the higher the current density at a given potential, the better the catalyst. For formic acid oxidation, Pt_3Cr and PtNi nanoparticle electrodes exhibited onset potentials of -100 and -40 mV, respectively, while Pt_3V is essentially inactive (Table 4.4). These values suggest that nanoparticles of Pt_3Cr and PtNi have superior electrocatalytic activity, especially when compared to Pt black[6]. Table 4 also lists the current densities (in terms of mA cm^{-2}) of the three catalysts at four specific potentials. This value is a direct measure of electrocatalytic efficiency. In this study, all the electrocatalyst materials examined had different particle sizes and, consequently, different surface areas and specific surface areas. Furthermore, electrochemical protocols for the measurement of the specific surface area for these novel intermetallic nanoparticles have not been established. This is in contrast to Pt, for which methods are well-established (e.g., Coulombic integration of hydrogen

adsorption). To make the most-meaningful comparison of the raw current data collected, we normalized currents to the measured BET surface area of the respective catalysts. The resulting surface area normalized current densities appear in plots and in the table as mA cm^{-2} (where cm^2 is the BET surface area for the catalyst coated on the GC electrode). From the values presented in Table 4.4, for formic acid oxidation, it is evident that Pt_3Cr and PtNi have activities that are far superior to that of Pt black. Pt_3Cr, in particular, exhibits a current density that is much higher (>20 times) than Pt black, the commercially available electrocatalyst. Pt_3Mn was also found to be catalytically active towards oxidation of formic acid. The mass activity measured for Pt_3Mn was 0.005 mA/μg compared to 0.022 mA/μg for Pt_3Cr and 0.013 mA/μg for PtNi, the current densities (normalized with respect to measured surface area) for which are shown in Figure 4.13. However, the surface area measurements could not be completed on the samples and hence the data for Pt_3Mn is not included in the figure or the table since the current observed couldn't be normalized to the measured surface area.

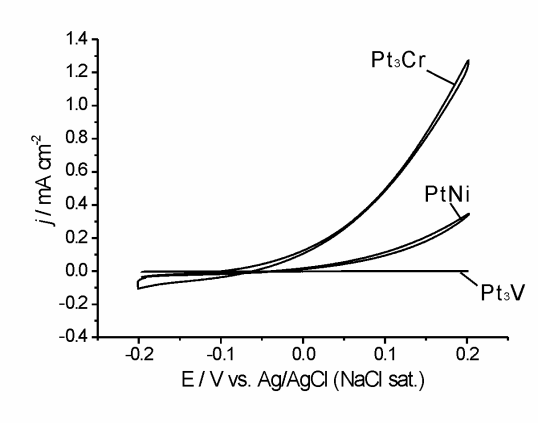

Figure 4.13: Rotating disk voltammograms for formic acid oxidation on Pt_3Cr, PtNi and Pt_3V nanoparticles. All data measured in a 0.5 M formic acid, 0.1 M sulfuric acid solution (electrode rotation rate: 2000 rpm, potential scan rate: 10 mV s^{-1}).

The BET surface area measured for all these materials was pretty low (for e.g 3.6 m^2/gm for PtNi and 1.7 m^2/gm for Pt_3Cr which as expected, further decreases on annealing) and thus the high current densities. This shows that increasing the surface area of these nano-phases (cleaner materials/smaller domain size materials) could give us very promising catalysts.

Table 4.4: Onset Potentials and Current Densities at Different Voltages for Pt_3Cr, PtNi and Pt_3V Nanoparticles for Formic Acid Oxidation (all specified potentials are vs Ag/AgCl (NaCl sat.)).

catalyst	onset potential (mV)	current density (mA cm^{-2})			
		-100 mV	0 mV	+100 mV	+200 mV
Pt_3Cr	-100	0.001	0.124	0.503	1.272
PtNi	-40	0	0.018	0.115	0.347
Pt_3V	200	0	0	0	0.001
Pt black*	0	0	0.003	0.018	0.05

* For Pt black, see reference[6]

4.4 Conclusions

Through the above synthetic explorations, we have been able to understand and control several key issues for achieving the desired composition (alloy and intermetallic phases) and particle size for a wide range of metals from Cu to V. Oxophilicity of the metal and the composition of the ligands and solvents (especially the presence of oxygen) are very important in determining the nature of the products. For example, although Mn is much more electropositive than vanadium, $Mn(acac)_3$ co-reduction yielded reasonable results and the Pt_3Mn ordered phase with a domain size as small as 10 nm could be obtained. However, with vanadium, even VCl_3THF_3 resulted in less V inclusion, presumably V(0) reacts with the THF and that product is

washed away by THF and especially MeOH. The same appears to be true for chromium, but to a smaller extent. In the end, the balance between having clean surfaces of the metal species in the system (washes) and mixing them well /promoting diffusion while their surface is clean (perhaps including in-situ heating and stirring/annealing) after the precursors are reduced is vital for the nanoparticles to grow and order.

If only a dendridic product is formed before washes with MeOH, the more reactive metal is more vulnerable to be removed by reaction with the washing solvents. Further, such products are too small to precipitate out of the reaction/wash solvent. Such dendridic products are also very air and water sensitive. On the other hand, if the metals are able to form well crystallized nanoparticle with sizes greater than about 5 nm, they appear to be much less reactive.

Further optimization of reactant precursors and processing conditions is required in order to process the materials at lower temperature and to reliably produce smaller nanoparticles (in the 5 to 10 nm range). But the point to note and the reason to be very interested in these materials is the reasonable activity observed in-spite of the low surface area showing the underlying catalytic potential that can be reached if these nano phases can be synthesized as cleaner/lower domain size materials. We know of the presence of sodium and organics in these products, which we are working on minimizing/removing completely (as discussed extensively in this work, which should simultaneously lead to better size control). Achieving this, thus, will give us some very active catalyst materials.

In spite of the challenges remaining, our work here has provided a route for obtaining nanometer sized alloys and intermetallics of Pt with very reactive metals which are active catalysts for formic acid oxidation. Also, identifying, understanding and outlining the key issues is the first step that will lead to higher yield synthetic schemes

giving materials with higher activity and stability, something we believe we have achieved through this work Research is ongoing to address the remaining challenges, however, the fact that these materials are active catalysts, ought to generate significant interest and support for further research in this direction in order to access the full potential of these vital materials.

REFERENCES

1. Lamy, C. L., Leger, J. M., Srinivasan, S., *Direct Methanol Fuel Cells: From a Twentieth Century Electrochemist's Dream to a Twenty-first Century Emerging Technology*. New York: Kluwer Academic/Plenum: 2001; Vol. 34.

2. Shah R. K., K., S.J. In *Fuel cell science, engineering and technology* American Society of Mechanical engineers, Rochester, NY, 2003; Rochester, NY, 2003; p 538

3. Liu, H. S.; Song, C. J.; Zhang, L.; Zhang, J. J.; Wang, H. J.; Wilkinson, D. P., A review of anode catalysis in the direct methanol fuel cell. *Journal of Power Sources* **2006,** 155, (2), 95-110.

4. Borup, R.; Meyers, J.; Pivovar, B.; Kim, Y. S.; Mukundan, R.; Garland, N.; Myers, D.; Wilson, M.; Garzon, F.; Wood, D.; Zelenay, P.; More, K.; Stroh, K.; Zawodzinski, T.; Boncella, J.; McGrath, J. E.; Inaba, M.; Miyatake, K.; Hori, M.; Ota, K.; Ogumi, Z.; Miyata, S.; Nishikata, A.; Siroma, Z.; Uchimoto, Y.; Yasuda, K.; Kimijima, K. I.; Iwashita, N., Scientific aspects of polymer electrolyte fuel cell durability and degradation. *Chemical Reviews* **2007,** 107, 3904-3951.

5. Abe, H.; Matsumoto, F.; Alden, L. R.; Warren, S. C.; Abruna, H. D.; DiSalvo, F. J., Electrocatalytic performance of fuel oxidation by Pt3Ti nanoparticles. *Journal of the American Chemical Society* **2008,** 130, (16), 5452-5458.

6. Roychowdhury, C.; Matsumoto, F.; Zeldovich, V. B.; Warren, S. C.; Mutolo, P. F.; Ballesteros, M.; Wiesner, U.; Abruna, H. D.; DiSalvo, F. J., Synthesis, characterization, and electrocatalytic activity of PtBi and PtPb nanoparticles prepared by borohydride reduction in methanol. *Chemistry of Materials* **2006,** 18, (14), 3365-3372.

7. Schaak, R. E.; Sra, A. K.; Leonard, B. M.; Cable, R. E.; Bauer, J. C.; Han, Y. F.; Means, J.; Teizer, W.; Vasquez, Y.; Funck, E. S., Metallurgy in a beaker: Nanoparticle toolkit for the rapid low-temperature solution synthesis of functional multimetallic solid-state materials. *Journal of the American Chemical Society* **2005,** 127, (10), 3506-3515.

8. Ghosh, T.; Matsumoto, F.; McInnis, J.; Weiss, M.; Abruna, H. D.; DiSalvo, F., PtPb nanoparticle electrocatalysts: control of activity through synthetic methods. *Journal of Nanoparticle Research* **2009,** 11, (4), 965-980.

9. Connelly, N. G.; Geiger, W. E., Chemical redox agents for organometallic chemistry. *Chemical Reviews* **1996,** 96, (2), 877-910.

10. Alden, L. R.; Roychowdhury, C.; Matsumoto, F.; Han, D. K.; Zeldovich, V. B.; Abruna, H. D.; DiSalvo, F. J., Synthesis, characterization, and electrocatalytic activity of PtPb nanoparticles prepared by two synthetic approaches. *Langmuir* **2006,** 22, (25), 10465-10471.

11. Carper, J., The CRC Handbook of Chemistry and Physics. *Library Journal* **1999,** 124, (10), 192.

Chapter 5

OTHER REDUCING AGENTS EXPLORED FOR CO-REDUCTION OF METAL PRECURSORS TO OBTAIN NANO PHASE ALLOYS AND INTERMETALLICS

As discussed in the previous chapters extensively, a bottom-up approach with chemical co-reduction of the metal precursors in solution is one of the very few viable methods available to obtain metallic phases as nanomaterials. However, in our attempts do to so (without using any surfactants in order to have materials usable as catalysts), we found that the reducing agent (sodium napthalide) plays an inhibiting role in the nucleation and growth of the desired nanoparticles. Sodium from the reducing agent was found in the products, especially when oxygen containing ligands were used. It appears that Na participates in polar double layer that adhere to the metal particles. Low angle peaks in the XRD (X-ray diffraction patterns) and EDS (energy dispersive X-ray spectroscopy) showed the presence of organics and sodium in the products. Although the exact composition and structure of these species are still unknown, it is highly likely that they are responsible for the challenges faced in preparing the targeted nanoparticles. These species keep the reduced metal particles separated from each other (making the more reactive metal more vulnerable to oxidation and subsequent removal from the system during washes) and dispersed in polar solvents (causing loss of yield, and again, mostly of the more reactive metal). The need for washing with polar solvents also arises from the fact that side products formed with sodium (e.g. NaCl when chloride containing precursors were used) can not be removed otherwise. Even after those washes, some sodium remains in the products – most probably as organic salts. All the above require the products to be annealed before the crystalline phases can be achieved, which in turn affects size

control. Also, the as prepared and the high temperature annealed materials appear to have carbon contaminants on their surfaces, making it difficult to determine its intrinsic activity as a catalyst material. Although naphthalene hasn't been identified on the products; it is very likely that it is also contributing to the problem, since it is known that unsaturated organics interact strongly with neutral or oxidized Pt[1] as discussed in chapter 2.

All this could be countered, if an alternative to sodium napthalide could be found, especially if side products were easily removable by washing with appropriate solvents. This prompted us to look into other possible options for reducing agents, and we describe those efforts in this chapter.

5.1 Reducing agents for the chemical co-reduction method: options and limitations

The task described above, is easier said than done, since we are limited by certain needs while looking for alternative reducing agents. Firstly, $NaBH_4$ (which fitted the need for easily removable side products well) is able to reduce Fe, Co, Ni but some B may be included in the products[2]. More electropositive metals, such as Cr, Mn, V and Ti, need stronger reducing agents. Hence, stronger reducing agents are necessary for extending the search for better catalyst materials to phases with highly electropositive metals. Table 5.1 gives a list of reduction potentials of metals compared with that of possible reducing agents for co-reduction[3]. This limits us to sodium bases with aromatic counter anions, super hydrides, sodides and other electrides or lithium bases (like alkyl lithiums and lithium napthalides and derivatives). Additionally, the base in consideration needs to be commercially available, easy to synthesize or at the very least, stable for extended periods once synthesized. Lastly, extremely hazardous materials cannot be used, otherwise, the application would be limited. In previous yet

unpublished results from the DiSalvo group, sodides and electrides were eliminated from consideration as they were found to be extremely difficult to handle. Reactions and observations with some of the other reducing agents are described below.

Table 5.1: Reduction potential of metals (in H_2O) and reducing agents[4, 5].

Metal	Oxidation states	E^o_{red}	Reducing agent	E^o_{red}
Al	3+	-1.66	Na (in THF, glyme)	-3.04
Ti	3+	-1.37	$NaC_{10}H_8$	-2.73
Mn	2+	-1.185	Li $(NH_3)_x$	-2.64
V	2+	-1.17	Na $(NH_3)_X$	-2.25
Cr	3+	-0.74	nBuLi	-2.05
Zn	2+	-0.76	$NaBH_4$ (basic)	-1.24
Ga	3+	-0.55	$NaBH_4$ (acidic/neutral)	-0.481
Fe	2+	-0.44		
Co	2+	-0.28		
Ni	2+	-0.26		
Sn	2+	-0.14		
Pb	2+	-0.13		
Bi	3+	0.32		
Cu	2+	0.34		
Pt	2+	1.18		

5.2 Reductions with $LiAlH_4$

Lithium aluminum hydride ($LiAlH_4$) has a lower reduction potential than sodium borohydride, and although reaching to very electropositive metals like Ti would not be possible, it could give us some leeway beyond sodium borohydride on metals and is quite easy to handle.

5.2.1 Experimental

Materials: $LiAlH_4$ was obtained commercially from Aldrich. $Pt(acac)_2$ was purchased from Aldrich and Lead(II)2-ethylhexanoate was purchased from STREM Chemicals Inc. Because of the high viscosity of lead(II)2-ethylhexanoate, 0.05M stock solutions were prepared by dissolving 2.496 g in 100 mL THF.

5.2.1.1 Reduction of $Pt(acac)_2$ with $LiAlH_4$

A single precursor reduction of just $Pt(acac)_2$ was also performed with $LiAlH_4$. $LiAlH_4$ (1.5 mmol) was weighed out in a 3-necked flask inside the argon atmosphere box. To this 40 ml of THF (dry, from solvent system, pumped into the box in a bomb flask) was added, the flask was fitted a condenser and an adapter on one arm, a stopper in the second arm and a septum on the third and was brought out of the box. The assembly was hooked up to the Schlenck line and the mixture was stirred under argon. $Pt(acac)_2$ solution (0.25 mmol in 5 ml THF) was prepared inside the glove box and injected into the reducing agent solution in THF. The mixture was allowed to stir for 30 min, and the THF was evaporated off completely under vacuum. 40 ml of isopropyl alcohol (degassed for 1 hr) was added into the flask, the suspension was cannula transferred

into a centrifuge tube and centrifuged at 2000 rpm for 10 min. The supernatant isopropyl alcohol with white cloudy lithium oxides and hydroxides was syringed off. The product left behind was exposed to air slowly with a needle left through the septum overnight. 30 ml of saturated Na_2SO_4 solution was added to remove the side products as Li and Al sulfates. After this wash, glassy crystals were observed on the black nanoparticles, which could be removed by subsequent water washes. A final wash was performed with 20 ml of acetone and the product was dried under vacuum. X-ray diffraction pattern of the product was obtained.

5.2.1.2 Co-reduction of Pt and Pb precursors with $LiAlH_4$

$LiAlH_4$ (1.5 mmol) was weighed out in a 3-necked flask inside the argon atmosphere box. To this 40 ml of THF (dry, from solvent system, pumped into the box in a bomb flask) was added, the flask was fitted a condenser and an adapter on one arm, a stopper in the second arm and a septum on the third and was brought out of the box. The assembly was hooked up to the Schlenck line and the mixture was stirred under argon. Inside the glove box, $Pt(acac)_2$ (0.25 mmol) was weighed out into a scintillation vial and 4.9 ml of the stock Pb(2-ethylhexanoate)$_2$ solution (0.05 M in THF) was added to it. The solution was drawn into a syringe, taken out of the glove box and injected into the stirring $LiAlH_4$ solution in THF. The previously ash colored solution turned dark black immediately with agglomerated nanoparticles appearing. The mixture was allowed to stir for 30 min, and the THF was evaporated off completely under vacuum. Work-up procedure identical to that described in the above section was carried out. The final product was obtained after washing with 20 ml acetone and drying under vacuum. The product was characterized by x-ray diffraction.

5.2.1.3 Electrochemical experiments

The activity of the materials for formic acid oxidation was tested in the Abruna group by Dr. Futoshi Matsumoto. The procedure followed for these experiments were identical to those described in Chapter 2.

5.2.2 Results and discussion

The XRD pattern obtained from Pt-Pb reduction (Figure 5.1) showed Pt-Al phases (mainly Pt_3Al along with Pb). Also, Na_2SO_4 peaks could be identified. On repeated washing, the Na_2SO_4 could be removed, however, several low intensity peaks indexing to a number of mixed phases like Li_4PbO_4 appeared. It was thus evident that side products of the reaction couldn't be removed completely with the technique employed and weren't as easy to wash off as expected. Further optimizations could be attempted to counter this, however, the main drawback of this reagent laid elsewhere. The Pt-Al bond enthalpy is much higher than that of Pt-Pb and hence, with this reagent, Pt-Al phases would form predominantly over others. If Pt-Al phases were found to be of interest catalytically, this method could be very useful. Thus electrochemical testing was done on the products and is discussed below.

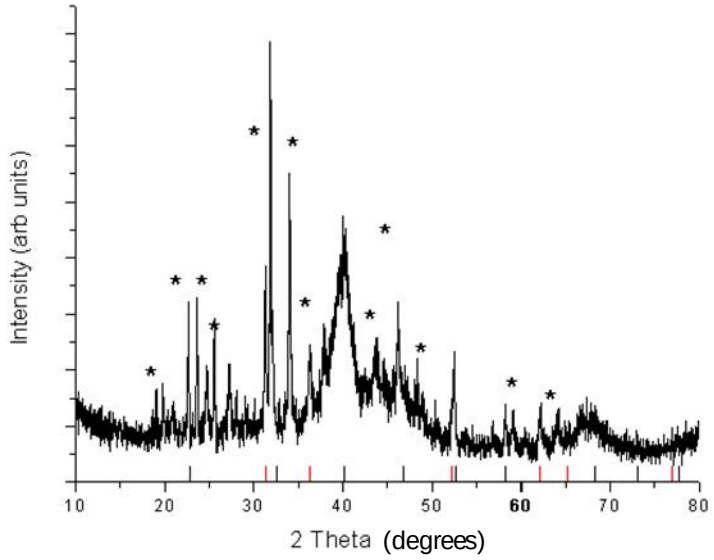

Figure 5.1: X-ray diffraction pattern of the products obtained from the co-reduction of Pt and Pb precursors with $LiAlH_4$.Black and red lines denote Pt_3Al (PDF # 04-001-3490) and Pb (PDF # 01-072-6646) phases respectively, while * shows the peaks from Na_2SO_4 (PDF # 01-075-1979).

Catalytic activity of the products: The activities observed from the products for the oxidation of formic acid are summarized in Table 5.2. Activity was observed in the product from the co-reduction reaction. However, in order to ensure that the observed activity was coming from the Pt-Al phases and is not due to the Pb present in the sample, a reaction was carried out in absence of Pb (reduction of $Pt(acac)_2$ only with $LiAlH_4$). As depicted in the table, a significant decline of activity was observed, suggesting that the previously observed activity was from the proximity of the Pb present in the sample (PtPb has the best activity till date for formic acid oxidation).

Table 5.2: Electrocatalytic activity of different $LiAlH_4$ reduction products towards formic acid oxidation with and without pretreatment.

Sample description	MA/ mAμg-1 at 0.2 V
Pt-Al, no Pb (Without pretreatment)	0.016
Pt-Al, no Pb (Pretreatment at -0.7 V for 30 min)	0.0095
Pt-Al, Pb (Without Pretreatment)	0.20
Pt-Al, Pb (Pretreatment at -0.7 V for 30 min)	0.087

Summarizing the above discussions, $LiAlH_4$ lacks the capacity to be a universal reducing agent for the purpose of co-reduction of metal precursors with Pt, since Pt-Al phases form predominantly. It would be a useful route to pursue if Pt-Al phases were desired (in our case: if they had high activity). However, since no such evidence was obtained, this route was abandoned for the purpose of this work. If in the future, ternary phases with Pt and Al are desired, this method can be further explored.

5.3 Reductions with $Li_2C_{10}H_8.2TMEDA$

In the continuing search for strong reducing agent with soluble side products, Li bases would be strong contenders given their highly negative reduction potentials. Prof. Galen Stucky and his research group had reported isolation of the Lithium salt of the naphthalene dianion as its TMEDA (*N, N, N', N'*-tetramethylethylenediamine) complex in crystalline form[6]. Their reported synthesis looked simple enough to

attempt in our laboratory since the base would have very high reducing power (highly negative reduction potential). Also, since complexes of permethylated amines with main group halides are known to be highly soluble in organic solvents and lithium halide complexes with different ligands have been studied extensively (often crystallized from hexanes) [7-9], solubility of the possible side products from this base (lithium halide complexes, given that chlorides and alkyl chlorides are used as the metal precursors) should be high in THF and hexanes. Synthesis and reduction efforts with this base are discussed in the following section. Also, since; to our knowledge, the reduction potential of this base hasn't been measured previously, attempts were undertaken to do the same.

5.3.1 Experimental

Materials: TMEDA, Napthalene and *n*-BuLi (1.6 M solution in hexanes) were obtained commercially from Aldrich. Initially, 1,4 dihydronapthalene was synthesized in laboratory following a reported procedure[10] given its limited commercial availability. The synthesized product was purified by distillation. For later reactions, commercially obtained 1,4 dihydronapthalene (Tokyo Kasei) was used.

5.3.1.1 Synthesis of the base

The procedure reported by the Stucky group was followed for synthesizing this base[11]. 0.85 g (6.5 mmol) of 1,4 dihydronapthalene was added to a 300 ml flask containing 200 ml hexane and 1.5 g (13 mmol) of TMEDA inside the argon atmosphere glove box. 8.1 ml of *n*-BuLi solution in hexanes (1.6 M, 13 mmol) was added to this slowly with a syringe. The solution was left to stir for 12 hr inside the glove box. After 12 hr,

the product (purple crystals) were filtered, washed with hexanes, dried on the filter paper and stored in scintillation vials in the glove box. Problems encountered during the above procedure will be discussed in the next section.

5.3.1.2 Reduction of precursors

Two platinum precursors: $Pt(acac)_2$ and $PtCl_2COD$ were reduced individually using this base and the results were compared. For each reduction 0.75 mmol of the reducing agent was dissolved in THF (30 ml) inside the glovebox, and 0.25 mmol of the precursor (so 50 % reducing agent excess was used) dissolved in 20 ml THF and was injected into this solution. An immediate color change to dark black on injection suggested successful reduction. The mixture was stirred for 30 min, and brought outside the box in a sealed reaction apparatus (3-neck round bottom with condenser and adapter). The primary goal here was to try and isolate the side products, which, if characterized successfully, would provide clear understanding of what was going on in-situ, a process which has been impossible to do with sodium napthalide. So the reaction vessel was hooked up to the Schlenck line and the mixture was cannula transferred into a centrifuge tube, however, even on centrifuging at 9000 rpm for 40 min, the product did not precipitate out of THF. Thus, the THF was evaporated off completely, Degassed MeOH (20 ml) was added to the tube, and the mixture was sonicated and centrifuged. The supernatant was syringed of and collected for characterization attempts. 30 ml of hexanes (dry, from the solvent system) was added and the above steps were repeated. The product was dried under vacuum, exposed to air slowly and characterized by XRD and WDS (in order to detect nitrogen). Commercially obtained boron nitride was used as the standard for WDS experiments.

5.3.1.3 Experiments to determine the reduction potentials of the base in THF

Although the Stucky group had crystallized the naphthalene dianion as its dilithium salt co-ordinated with TMEDA and determined its structure by X-ray diffraction, very few reports could be found on studies of its thermodynamic reduction potential. This is because, although chemical reduction of these aromatic species could be easily achieved with alkali metals in several solvents (e.g. in dry THF), electrochemical reduction giving stable di-ions for these species require comparatively sophisticated techniques. For example, observed potentials are often from irreversible processes due to protonation reactions from impurities in the solvent or from species derived from supporting electrolytes. Hence, we undertook some efforts to obtain the reduction potential of this base ($Li_2C_{10}H_8$.2TMEDA). The initial experiments involved obtaining cyclic voltammograms in 0.1 M TBAP $(C_4H_9)_4NH_2PO_4$, tetrabutylammonium phosphate: commercially obtained, stored in argon atmosphere box) / THF (dry, from solvent system) to check the potential window. Potentials were measured with respect to Ag/Ag^+ (50 mM $AgClO_4$). Following initial experiments, the TBAP had to be recrystallized to obtain a supporting electrolyte that was non-reactive in the desired potential window of 0 to -3 V (vs Ag/Ag^+). After establishing the potential window, cyclic voltammograms were obtained with 100 mM solution of the base at scan rate 10 mV/s on a glassy carbon electrode. Comparative voltammograms with 100 mM solutions of naphthalene were also obtained. These electrochemical experiments were performed by Dr. Futoshi Matsumoto in the Abruna group.

5.3.2 Results and discussion

Although a reported procedure was being followed for the synthesis of the base, the product yield was low (12.7%). Contrary to what was described in the literature, we couldn't get the crystals to grow large enough to recover all of it by filtration. The filtrate was dark purple even after multiple passes, and seemed to contain very fine crystals. The filtrate was recovered, concentrated and allowed to stand and some more of the product was recovered from the second crop, however, we still failed to obtain high product yield. We also encountered issues with stability of the base, as on drying, the crystals would often change color from purple to yellow inside the argon atmosphere box. The same was observed on adding THF (clean and dry, from solvent system) and thus, the base was titrated with THF (adding small amounts of the former to fixed volume of THF until dark purple color is retained) to determine what amount of the base in a given volume of THF would ensure sufficient excess of the former present to reduce the metal precursors. 0.0051 g (0.014 mmol) of the base would be required for 3 ml THF to obtain a dark purple solution, and it appeared stable over extended time period. This required at least 0.21 mmol of the base for 45 ml of THF (the amounts used for typical reduction reactions). This means that although 0.75 mmol of the base was used for each reduction reaction, the actual excess of the reducing agent present was less than 50 % (the desired excess) since some of it was reacting with presumed impurities in the THF. Also, a possible reaction with THF could be replacement of the TMEDA in the complex by THF, causing the color change. If so, the reagent should still be able to reduce the metal precursors. Unless the released TMEDA molecules adhered very strongly to the reduced metals (which would cause problems similar to those with sodium napthalide) this reagent should successfully accomplish our desired goals. If the above was indeed occurring and the

TMEDA was found to interfere, a similar reducing agent could be synthesized using TMCDA (tetramethylcyclohexane-1,2-diamine), which is known to be more stable to the above kind of replacement reactions. Also, the reduction reactions could be done in a solvent other than THF, or since the rate of such a reaction should be dependent of solvent order, the THF amount could be reduced by mixing in other solvents. Amongst these possible routes, in order to decide a path, the speculations needed to be tested by proving or disproving the role of TMEDA. This could be done if side products from the reaction could be isolated and characterized (one of our initial reasons for selecting this reagent) or if the chemical analysis of products isolated showed nitrogen. In our attempts to do this, we did several experiments with the hexane collected from the washes for the reduction of $PtCl_2COD$ with the $Li_2C_{10}H_8.2TMEDA$. Our initial goal was to collect the THF post reduction as a supernatant and analyze it. However, it was not possible to obtain THF as supernatant, since the products couldn't be precipitated from THF. We would need to always evaporate the THF off in order to collect the products. For these reactions, the MeOH wash step was skipped, since MeOH could remove chlorides and amines from the system while our goal was to get them to crystallize as Li salts and identify them. If this could be done successfully, they should be soluble in hexane, which would allow us to skip the MeOH step altogether. This would be highly beneficial while dealing with electropositive metals (see chapter 3 and 4 for detailed discussion on the topic).The hexane supernatant was collected in and divided into halves. Half of it was refrigerated in order to crystallize possible Li salts. The other half was allowed to dry under air. Although no crystals could be obtained from the first half, yellow crystals were collected from the second (hexane evaporated under air) and crystallographic analysis was attempted. Unfortunately the crystals were ~0.1 mm size while at least 0.3 mm crystals were required for successful analysis. So the procedure was repeated and this time, slower evaporation of hexane

was attempted to allow the crystals to grow bigger. However, we failed to isolate a larger crystal. In order to identify the crystals, they were washed carefully with small amounts of hexane and dissolved in distilled H_2O. $AgNO_3$ was added to this solution to identify presence of Chloride (expected side products would be (LiHal)n.(xL)n crystals, where L is THF or TMEDA). However, no whitish color was observed, instead, the $AgNO_3$ dissolved to give a clear solution. This suggested absence of chlorine in the crystals, or if present, the concentration of chlorine was lower than the detection limit with this test. In other reactions tried (reductions of $Pt(acac)_2$ and $PtCl_2COD$ respectively), a MeOH wash was performed. The supernatant was collected in each case The products from the $Pt(acac)_2$ couldn't be precipitated completely from the MeOH, suggesting similar role of precursor ligands (especially of acetylacetonate) in forming charged layers adhering to the particles preventing their precipitation from polar solvents. In contrast, the products from $PtCl_2COD$ reduction precipitated out of MeOH with ease giving a clear and almost colorless supernatant. EDS was performed on the products and on the residues left behind on evaporating off the MeOH supernatants (Table 5.2). Chlorine was absent on the product, but was present in the residue from the MeOH wash, suggesting that the chlorine (in whatever form it was present post reaction), could be removed by MeOH wash.

Table 5.3: EDS data showing atomic percentages of Pt and Cl in the residue from MeOH wash and the product from reduction of $PtCl_2COD$ and $Pt(acac)_2$ with $Li_2C_{10}H_8.2TMEDA$. The remainder of the products and residues showed C and O.

product	$PtCl_2(COD)$	$Pt(acac)_2$
Pt	30.4	24.6
Cl	0.0	Should not have Cl

MeOH wash	$PtCl_2(COD)$	$Pt(acac)_2$
Pt	0.0	1.5
Cl	0.53	Should not have Cl

TGA on the product and MeOH residue for the $PtCl_2COD$ reduction showed 6% vs. 30 % weight loss respectively (Figure 5.2) suggesting removal of most of the other volatile side products (containing C, H and possible N) in the MeOH wash, presumably assisted by the chloride ions forming salts soluble in MeOH (easy precipitation of the products out of MeOH in this case vs. in the case of reduction of $Pt(acac)_2$). Presence of chloride in high concentrations in the MeOH wash residue from the reduction of $PtCl_2COD$ was also confirmed by the $AgNO_3$ test. EDS of the residue from the $Pt(acac)_2$ reduction showed significant amounts of Pt, which was not unexpected since the products couldn't be precipitated out completely. The MeOH supernatant remained very dark when syringed off. WDS on the products in either case showed no presence of nitrogen, suggesting TMEDA in nascent or derived form is not sticking on to the products. So, although the side products couldn't be identified

with this reagent, its ability to reduce $PtCl_2COD$ to give clean products was promising. Even though yield was lost during MeOH wash with $Pt(acac)_2$ as the precursor, absence of nitrogen on the final product that could be recovered from MeOH (by precipitation) was also encouraging. However, against our hopes, MeOH wash, once again was found to be vital in each case, as otherwise chlorine (for $PtCl_2COD$ as the Pt precursor) was detected on the products and the crystals isolated from the hexane wash didn't test positive for chloride. There is a possibility that with $Pt(acac)_2$ (a chloride free precursor) all side products will be removed from the products with just hexane wash. However, ligands of polar nature were found to adhere strongly to the products in making them polar (the products didn't precipitate out of MeOH). The possibility of obtaining completely clean products with just hexane wash was slim, and wasn't explored.

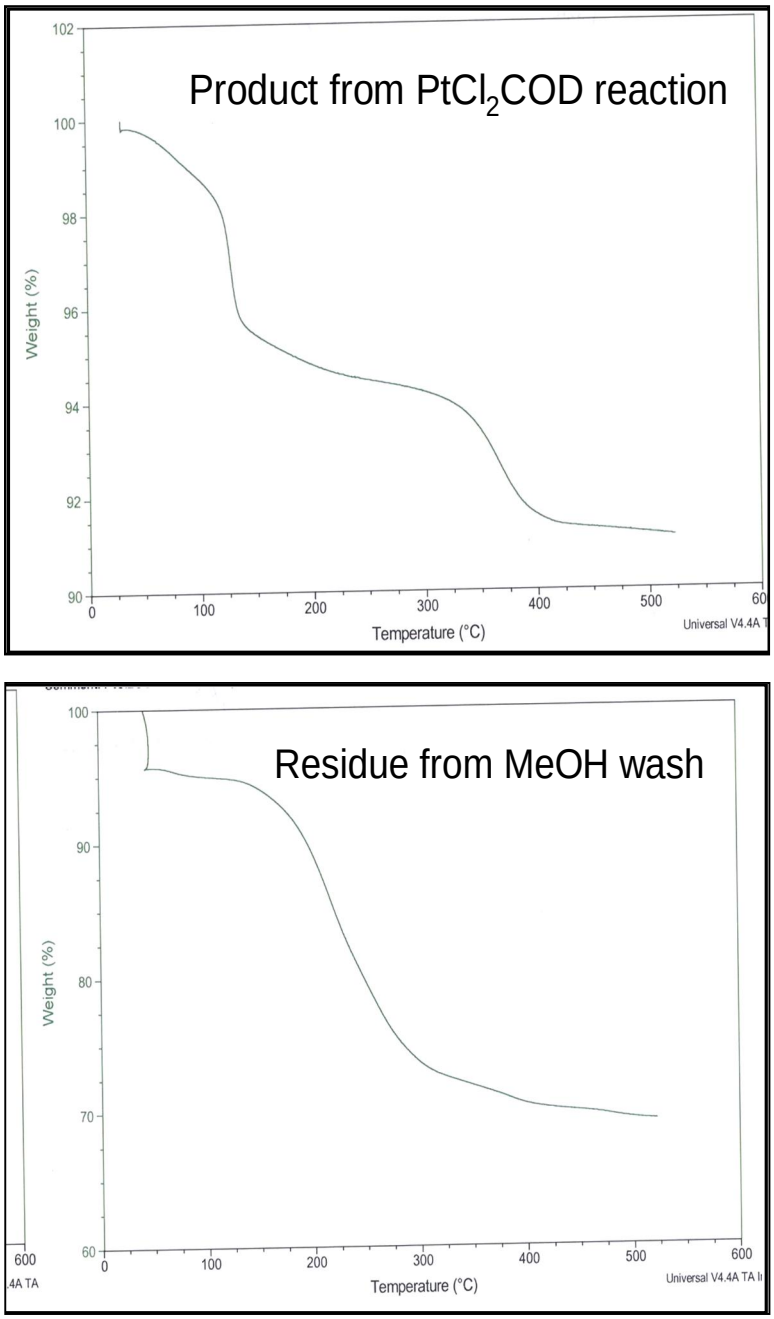

Figure 5.2: TGA data of product and MeOH wash residue from reduction of $PtCl_2COD$ with $Li_2C_{10}H_8.2TMEDA$.

If 1,4 dihydronapthalene is obtained commercially, synthesis of the reagent ($Li_2C_{10}H_{8.}2TMEDA$) becomes an one step process. However, given the low yield and instability on storing we decided to abandon this route.

Electrochemical experiments with $Li_2C_{10}H_{8.}2TMEDA$: Efforts of measuring the thermodynamic reduction potential of the base weren't very successful. Firstly, although a 100 mM solution of the base was prepared for the experiments, the solution was found to loose color (going from purple to brown to yellow) on adding TBAP and standing, suggesting reactions of the base with impurities in THF or TBAP. This makes it impossible to determine the true concentration of the base during the electrochemical experiments. Also, literature reports [12] with this base showed that due to the high reactivity of the dianion, only the first reduction potential could be measured reversibly (-2.53 V), but with methyl amine (MA) and dimethyl amine (DMA) as solvents and tetrabutyl ammonium bromide as the supporting electrolyte. Because of their extremely low electrophilicity, these solvents make it possible to measure the reduction potentials without side reactions, allowing several aromatic dianions to be generated reversibly within the timescale of slow sweep cyclic voltammetry. The literature also suggests that the tetrabutyl ammonium salts are stabilized in the amine solvents against possible Hoffman eliminations, which can occur in solvents like THF, thus resulting in protonated species participating in side reactions. However, even with the extremely negative cathodic limits that could be obtained with these solvents (-3.3 V vs Ag/AgCl for MA and -3.4 V vs Ag/AgCl for DMA), the literature reports the second reduction potential to be beyond the cathodic limit for naphthalene, and only the monoanion formation could be observed. This effect has been explained by the extra energy penalty that has to be paid for the second reduction in naphthalene anion since it attains an anti aromatic character[13]. This agreed with what we observed from our experiments with TBAP/THF. Literature reports exist

on using highly purified and super dried THF and $NaBPh_4$ for reversible generation of highly charged anions[14] and on use of liquid ammonia as solvent for electrochemical experiments with aromatic dianions[15]. However, these techniques would require significant sophistication, expertise and time. Thus, we were unwilling to go further until we had confirmed the synthetic utility of this base for our purposes.

5.4 Reductions with n-BuLi

We have established in the previous chapters and in the earlier sections of this chapter the need for a 'strong' (to be able to reduce electropositive metals beyond those for which sodium borohydride is sufficient) and 'clean' (so there's no interference from by-products coming from the reducing agent or precursors so that the desired phases can form easily) reducing agent. Additionally, from our experience with synthesis of the $Li_2C_{10}H_8.2TMEDA$ and previous work done in the group with sodides, something commercially available or something that can be synthesized easily would be highly desirable. N-butyl lithium fits the above criterion well. Also, since it is available commercially as solution in hexanes (of different concentrations) or as a neat liquid, a desired amount can be injected into the precursor solution. This allows us to use higher volume of solvents for dissolving the precursors. Earlier, we were injecting the precursors into the reducing agent solution, and hence were limited by syringe volume and injection speed. Injecting very high volumes (> 20 ml) of precursor solutions into the reducing agent wouldn't be very reasonable from speed and efficiency point of view. There's also the need to limit the total solvent volume of the reaction so that a reasonable reagent concentration is maintained. In a typical reaction, a sodium napthalide solution would contribute 40 ml to the total solvent volume compared to a few µ- or milli- liters (depending on the solution strength) of n-butyl lithium.

This advantage might allow us to use metal chlorides, or mixed metal chlorides (or halides) as precursors, which would be ideal for minimizing side products (only metal halide salts should form as side products), but could seldom be used before because of their limited solubility in THF. Even if alkyl chloride precursors are used, side products should be limited to salts or simple organics which should all be soluble in hexanes (Scheme 5.1). Lastly, *n*-butyl lithium (nBuLi) is safer to handle than its close cousins like *t*-butyl lithium. Even then, all reactions to be discussed in this section were done inside an argon atmosphere box for safety reasons.

Scheme 5.1: Possible products resulting from different metal precursors co-reduced with nBuLi in presence of THF as the solvent.

MCl_x / MR_yCl_x + THF + BuLi + $M'R'_{y'}Cl_{x'}$ = M-M' / M-M/M'-M' + LiCl + Different organics with R,R' and Bu which should all be soluble in hexanes

Na_xMCl_y + $M'Cl_{x'}$ + BuLi + THF = M-M' (etc) + LiCl + NaCl + simple alkanes, should be soluble in hexanes

Where M,M' – Metals, R,R' – Alkyl/THF

5.4.1 Experimental

Materials: nBuLi was obtained commercially from Aldrich (1.6 M solution in hexanes). THF and hexanes were obtained from the solvent system (custom built Seca solvent system by glass contour). All precursors were obtained commercially from Aldrich. The $Na_2PtCl_6.6H_2O$ salt was obtained commercially (Alfa Aesar) and heated up under vacuum in a sealed quartz tube to obtain in anhydrous form (by Dr. Brian

Leonard in the DiSalvo group). However, some amount of water might have been left in the final product and obtaining it in completely anhydrous form was not possible.

Single precursor reductions: 0.06 mmol of the desired precursor ($CrCl_3$, $Ti(THF)_2Cl_4$, $TiCp_2Cl_2$, VCl_3, $Mn(acac)_3$) was dissolved in 18 ml (in a scintillation vial) THF inside the argon atmosphere box. nBuLi solution; stored in the box in a refrigerator, was allowed to warm up to room temperature for 15 min. The desired volume (10 % excess of reducing agent was used for each injection) was then drawn out in a 1 ml glass syringe, and injected into the precursor solution. Immediate observations were noted, additional amounts of nBuLi (always 10 % excess at a time) were injected until no further change was observed on injection and the solution was allowed to stand for a few days. Observations were noted. No attempts to isolate and characterize the products were made in the case of the single precursor reductions. With $CrCl_3$ and $TiCp_2Cl_2$, reactions were repeated with a higher solvent volume (the precursor was dissolved in 125 ml THF in a 250 ml 2 necked round bottom flask) keeping everything else the same to study the effect of solvent volume, if any, on reduction of metal precursors by nBuLi.

Co-reductions of metal precursors: 0.06 mmol each of precursors were dissolved in pairs in 18 ml THF ($CrCl_3$/$PtCl_2COD$, VCl_3/$PtCl_2COD$, $TiCl_2Cp_2$/$PtCl_2COD$). For $Ti(THF)_2Cl_4$/$Na_2PtCl_6.6H_2O$ and VCl_3THF_3/$Na_2PtCl_6.6H_2O$, 0.25 mmol each of the precursors were dissolved in 18 ml THF. A large scale reaction, with 0.5 mmol each of $TiCl_2Cp_2$ and $PtCl_2COD$ dissolved in 40 ml THF was also done. In all cases, 10 % excess of nBuLi (as a 1.6 M solution in hexanes) was injected into the precursor solution. The reactions were allowed to stir for 20 min in most cases and allowed to stand overnight. For the reactions with $Na_2PtCl_6.6H_2O$, the reactions were stirred for 3 h and allowed to stand overnight. The products were recovered in most cases by concentrating the THF to 50 % of the initial volume, adding equal amount of hexanes

and then centrifuging at 9000 rpm for 30 min. The supernatants remained dark in most cases and the rest was recovered by evaporating off the solvent to dryness under vacuum. In each case, the products were washed repeatedly with hexanes. The products were then dried under vacuum, exposed to air slowly, X-rayed and annealed in sealed silica tubes. In one case, the large scale reaction with $TiCl_2Cp_2$ and $PtCl_2COD$, the product was recovered by pouring the reaction solution into an Erlenmeyer flask containing large amount of hexanes (200 ml), causing the product to precipitate. The product was then recovered by decantation, washed repeatedly with hexanes, and annealed in sealed silica tubes at different temperatures without ever being exposed to air.

5.4.2 Results and discussion

5.4.2.1 The single precursor reductions

The single precursor reductions were performed to see what precursors can be reduced successfully by nBuLi and identify other issues that might arise with nBuLi method while keeping the system simple. Scheme 5.1 gives a possible scenario with this method, but there are several possible issues hidden within this simplistic depiction. Issues like reaction between nBuLi and THF (or solvation of nBuLi by THF), alkylation reactions by nBuLi with the organic groups in the precursors, formation of mixed metallic phases of the metals with Li are some of the possible processes which might effect the end product. The rates of these processes, how the rates change with temperature and solvent (THF) order would ultimately decide the end result. Also, if, as depicted in scheme 5.1, only salts and simple organics (soluble in hexanes) are formed as side products, with no side species adhering strongly to the reduced metals,

the desired metallic phases would be able to nucleate, grow, and agglomerate and should crash out of the reaction solvent easily. Thus, immediate reduction observed on injection of nBuLi into the precursor solution under different conditions, followed by eventual precipitation of black material would indicate a) the reduction process predominates under those conditions over other possible parasitic processes, b) by-products are not interfering significantly in the nucleation and growth of the desired phases after the initial rapid reduction. Single precursor reductions, with only one precursor in question, will offer greater chance of observing behaviors like these and identifying other possible reaction routes. Table 5.4 gives a summary of observations for the different precursors injected with nBuLi. We discuss the observations and conclusions that can be drawn from these observations in the order in which they are given in the table.

Table 5.4: Observations on injecting 1.1 * x * y equivalents of nBuLi (where x is the valency of the metal and y is number of times x * 1.1 equivalents of nBuLi was injected) into solution/suspension of different metal precursors in THF.

Precursor	Solvent volume	Solution/ Supension	Observation on Injection of nBuLi	Equivalents of nBuLi required to get to a constant state	Observation After a few days
$CrCl_3$	18 ml THF	suspension	Reduction obs	3*1.1 eqv BuLi	Solution turned green
$CrCl_3$	125 ml THF	suspension	Reduction obs but immediate change follows	3*3*1.1 eqv BuLi	Cloudy ppt appears Supernatant retains yellow color
$TiTHF_2Cl_4$	18 ml THF	Solution	Reduction obs but immediate change follows	4*1.1 eqv BuLi	Solution color stays constant
$TiCp_2Cl_2$	18 ml THF	solution	Reduction obs	4*1.1 eqv BuLi	Black particles settle down, clear (but colored) supernatant
$TiCp_2Cl_2$	125 ml THF	solution	Reduction not obs	Even with 2*4*1.1 eqv BuLi	Solution turned red/black
VCl_3	18 ml THF	suspension	Reduction obs	3*1.1 eqv BuLi	Black particles settled down
$Mn(acac)_3$	18 ml THF	solution	Reduction obs, But needs excess BuLi for completion	6*3*1.1 eqv BuLi	Black particles settled down

$CrCl_3$ (0.06 mmol) does not appreciably dissolve in 18 ml of THF; rather a suspension of fine particles is obtained. An immediate color change to dark black from a purple suspension occurs on injection of 10 % in excess nBuLi and the color stayed constant with time. However after a couple of days, the solution color changed to green (color of Cr_2O_3). No precipitation of product was observed at any time. $CrCl_3$ dispersed in 125 ml of THF showed no observable change from a purple suspension on the first injection of nBuLi (in 10 % excess). On the second injection of the same amount of

nBuLi, a series of color change occurred within a total time period of 5 min, the color change processes then slowed down. No black particles were seen to be formed at any stage. After 2 days, a yellow solution with a cloudy precipitate was obtained. The precipitate was collected and the solution was evaporated off to obtain a residue. TGA and EDS analysis was done on these materials. However, no significant information could be obtained from either, except for the presence of Cr detected by EDS in the residue from the solution suggesting that Cr existed in some form other than the precursor $CrCl_3$ (purple crystals, detected in small amounts in the cloudy precipitate, since $CrCl_3$ doesn't dissolve in THF), reduced Cr metal (would result in black nanoparticles) or Cr_2O_3 (green). This would mean that the precursor suspended in the THF reacted with nBuLi (or with THF and nBuLi when the later was added) and went through several intermediary steps (suggested by the fast and various color changes of the solution observed) before forming the final yellow solution. The residue obtained by evaporating off the yellow solution was yellow in color and soluble in THF and H_2O, while the precipitate was white and insoluble in THF and H_2O. Both TGA and EDS showed presence of significant amounts of organics. Chlorine was also detected in both materials by EDS. X-ray analysis showed these materials to be amorphous. Although these materials couldn't be identified completely, this experiment suggested that the reaction of $CrCl_3$ with nBuLi definitely depends on THF order, since the results were dramatically different with different THF volumes. The reaction results also showed that with smaller volume of THF, $CrCl_3$ can be successfully reduced by 10 % excess of nBuLi.

The next precursor to be studied was $Ti(THF)_2Cl_4$. 0.06 mmol dissolved in 18 ml of THF showed immediate color change to black suggesting reduction on injection of 10 % excess nBuLi. However, within a few seconds, the solution color cleared up significantly to give an almost orange solution (Figure 5.3). No further change was

observed on a second injection of same amount of nBuLi. These results suggest that the reduced Ti reacts with THF or possibly with the butyl group.

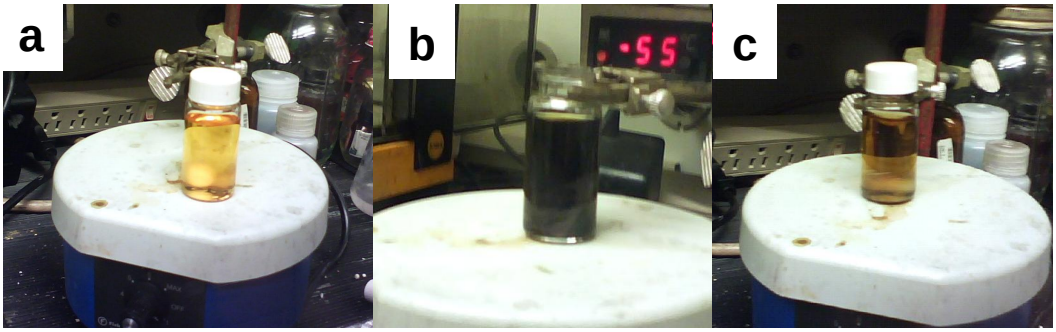

Figure 5.3: $TiCl_4(THF)_2$ solution in THF a) before, b) immediately after and c) few minutes after injection of 10 % excess nBuLi.

$TiCp_2Cl_2$ was tried next. It showed immediate reduction on the first addition of nBuLi. The dark black color of the solution stayed constant with time and a black product crashed out leaving a clear, but colored supernatant over a period of 2 days. Since this precursor showed the ideal behavior with a small solvent volume, the experiment was repeated with 125 ml of THF to check if the effect of solvent volume was a general one, or one restricted to certain metals/precursors (like $CrCl_3$). The observation suggested the former, since no reduction was observed in this case, the solution turned green on injection and yellow on further stirring. No further change was observed on a second injection of nBuLi, but the solution changes to red-black color over a period of 2 days.

VCl_3 and $Mn(acac)_3$ (0.06 mmol dissolved in 18 ml THF) both showed immediate reduction on addition of nBuLi with black particles precipitating out over a period of 2 days. For $Mn(acac)_3$ however, 5 injections of nBuLi (10 % excess each time) were

required for completion of reduction (until no further color change could be observed), since with each injection solution turned darker and darker (Figure 5.4).

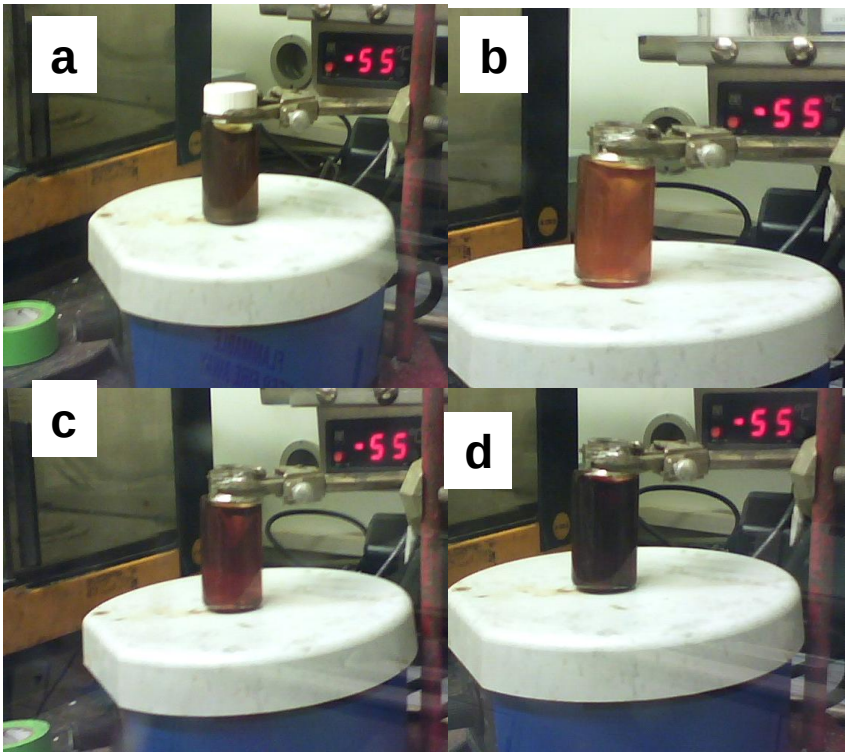

Figure 5.4: $Mn(acac)_3$ solution in THF a) before, b) after 1^{st} injection, c) after 2^{nd} injection and d) after 6^{th} injection of 10% excess nBuLi.

These observations lead us to make the following conclusions about the nBuLi method:

- nBuLi can reduce Cr, Ti, V and Mn. Solubility issues remain with Cr and V chlorides.
- The reaction depends on volume of THF (observed both for $CrCl_3$ and $TiCp_2Cl_2$).

- The reaction appears to depend on the ligands in the precursor ($TiCl_4THF_2$ different from $TiCp_2Cl_2$, $Mn(acac)_3$ needed much more nBuLi for complete reduction).
- The reaction is not simple in the case of high solvent volume – so salts with reasonable solubility in THF are required.

So the question remains: are nanoparticles of these metals kinetically stable in pure THF and/or do they react with impurities in the THF.

5.4.2.2 Co-reduction of metal precursors

As discussed in the experimental section, both co-reductions of $CrCl_3/PtCl_2COD$ and $VCl_3/PtCl_2COD$ resulted in some product that could be recovered by precipitation from the mother solvent (to be referred to as PtCr-ppt and PtV-ppt respectively). The rest of the products in each case were recovered by evaporating off the mother solvent completely (to be referred to as PtCr-THF evap and PtV-THF evap respectively). X-ray analysis of the products from the Pt-Cr reaction showed the former product (PtCr-ppt) to give extremely broad peaks, while the later (PtCr-THF evap) showed peaks indexing closely to LiCl and the PtCr tetragonal intermetallic phase (Figure 5.5). This was quite remarkable, since these materials were never heated up, and room temperature crystallization of Pt phases with highly electropositive metals like Cr was not observed before. This also showed that LiCl is formed as a side product, and since it was detected in the product obtained by evaporating off THF and not on the precipitate, it had to be quite soluble in THF. This was also promising, showing that with this method, we are at last forming side products which can be easily removed without washes with highly protic solvents like MeOH and H_2O: definite good news for targeting phases with highly electropositive elements.

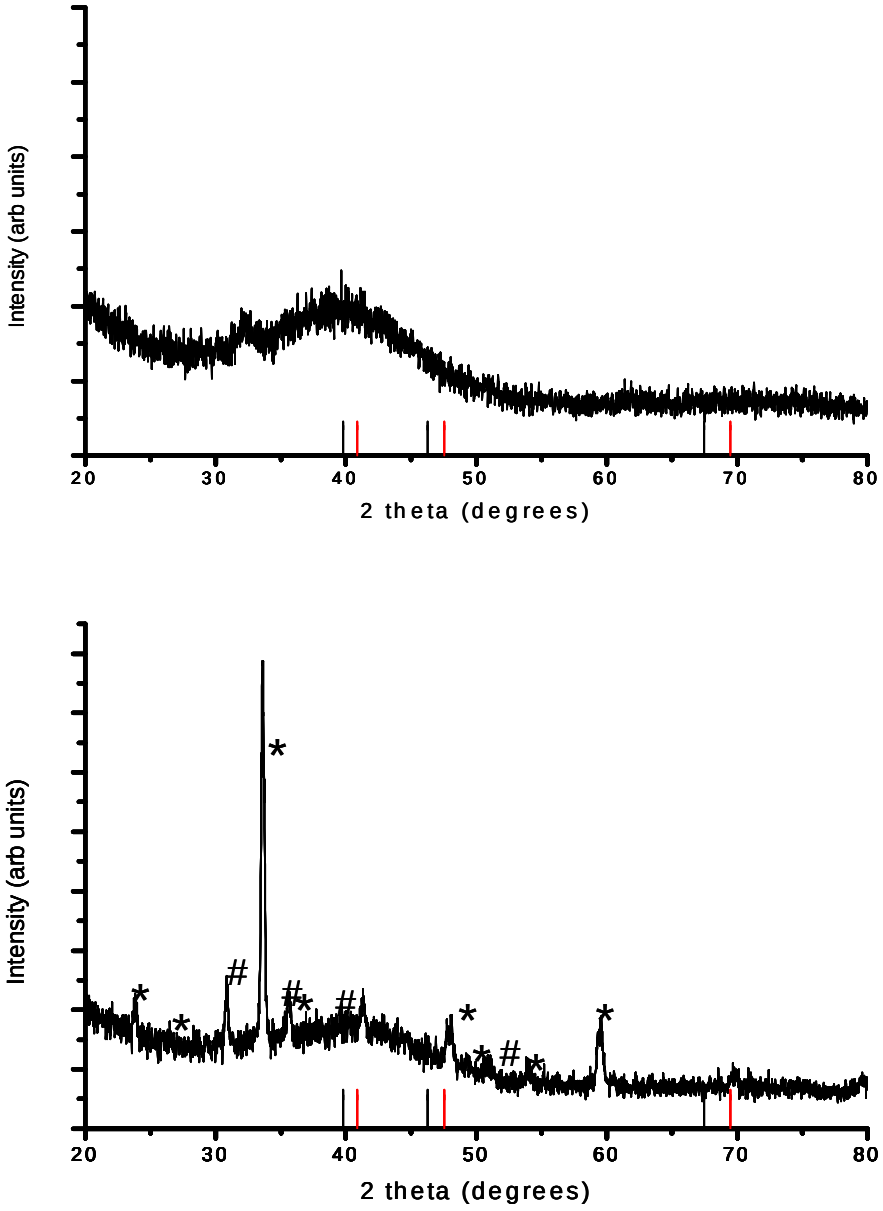

Figure 5.5: Products obtained as precipitate (top) and on evaporating off solvents (bottom) from co-reduction of $CrCl_3$ with $PtCl_2COD$. The black and red lines mark the Pt (PDF # 01-070-2057) and PtCr (PDF # 03-065-4629) peak positions respectively, the * denotes peaks from $LiCl(H_2O)$ (PDF # 01-073-1273) and # denotes LiCl (PDF # 01-074-1181) peaks.

For the Pt-V reaction, the PtV-ppt product showed peaks indexing close to the PtV phase, while the PtV-THF evap product showed broad peaks and LiCl (Figure 5.6).

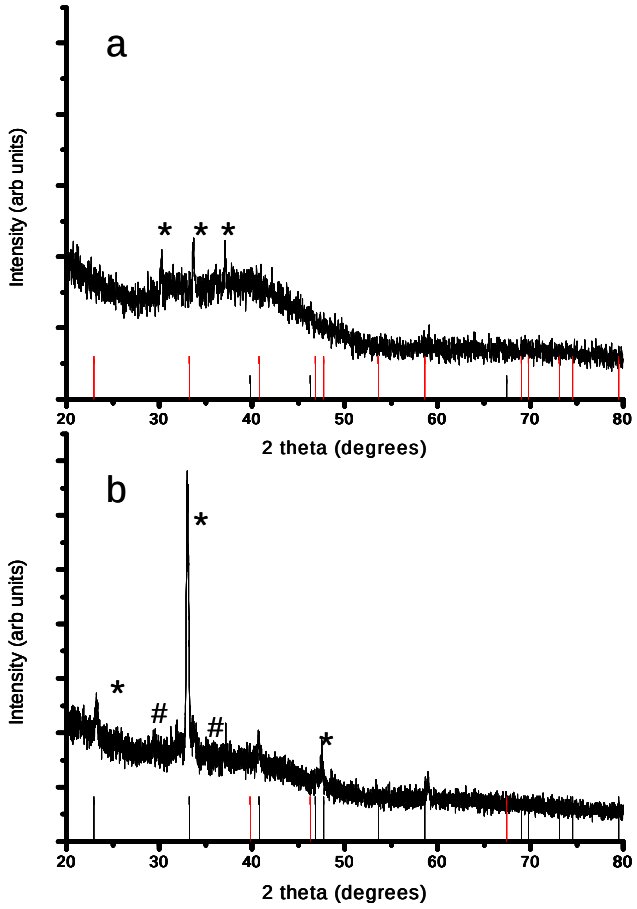

Figure 5.6: Products obtained a) on evaporating off solvents and b) as precipitate from co-reduction of VCl_3 with $PtCl_2COD$. In a) the black and red lines mark the Pt (PDF # 01-070-2057) and PtV (PDF # 01-072-3010) peak positions respectively, the * denotes LiCl peaks. In b) the black lines denote Pt peak positions, the red lines denote PtV peak positions, * denotes peaks from $LiCl(H_2O)$ (PDF # 01-073-1273) and # denotes LiCl (PDF # 01-074-1181) peaks.

EDS analysis on these materials showed presence of the electropositive element (Cr or V) in amounts equivalent to Pt (Table 5.5), while in previous observations (with our previous methods), a 1:1 precursor ratio would give products with 3:1::Pt:X at best, where X is a reactive metal like Ti, Cr or V). TGA analysis showed the presence of organics in smaller amount in the products obtained by precipitation (PtCr-ppt and PtV-ppt) than in the products obtained by evaporating off solvent (PtCr-THF evap and PtV-THF evap) (Figure 5.7). The products from Pt-Cr and Pt-V reactions were annealed at 700 ^{o}C for 24 h and 750 ^{o}C for 24 h respectively. The annealed products did not reveal any further information, as X-ray diffraction patterns from the products indexed to a cubic Pt phase. This may be due to reaction of the Cr and V with the silica tube. Evidence for this could be seen by attack on the inner walls of the tube. Blackening of the walls of the annealing tubes, similar to what was observed with sodium napthalide reduction products, was observed in these cases.

Table 5.5: EDS data showing ratio of atomic % of different elements in the unannealed products obtained by co-reduction of $PtCl_2COD$ with $CrCl_3$ and VCl_3 respectively. PtX ppt and PtX THF evap (where X is Cr or V) refer respectively to product obtained as precipitate or by evaporating off THF post reduction. Note the large amount of organics (data obtained from dry products dispersed on plasma cleaned Al stubs) detected.

Atm% of :	Pt	Cr	C	O	Cl
PtCr ppt	1.51	1.02	49.83	42.73	3.07
PtCr THF evap	2.31	3.20	32.88	44.35	16.02
	Pt	V	C	O	Cl
PtV ppt	0.58	4.25	13.33	41.37	14.16
PtV THF evap	0.94	0.77	34.57	57.78	5.51

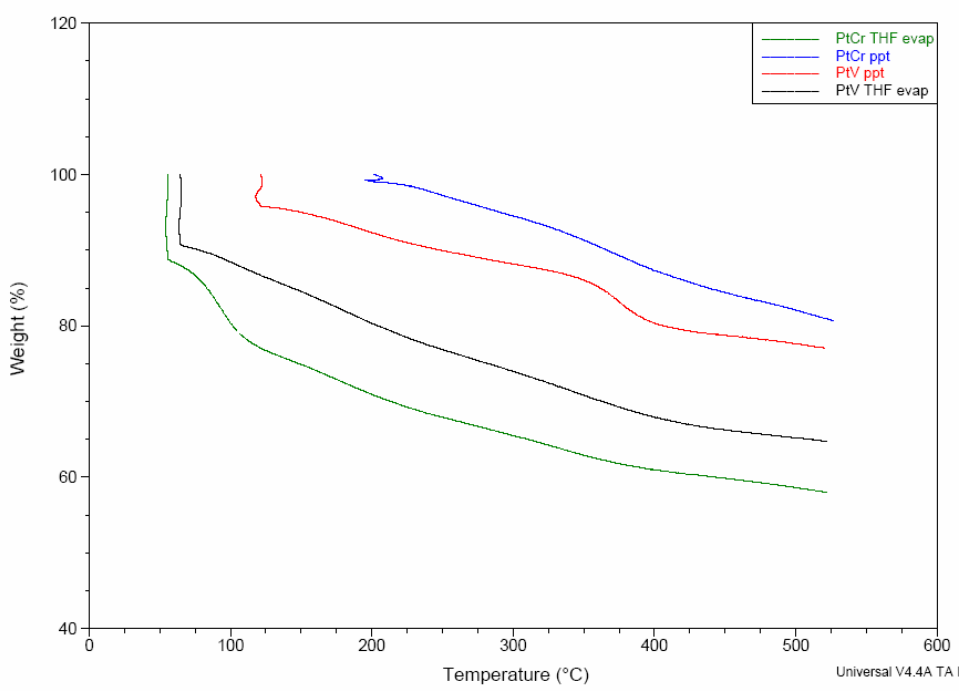

Figure 5.7: TGA data of different products obtained from co-reduction of $PtCl_2COD$ with $CrCl_3$ and VCl_3 respectively. PtX ppt and PtX THF evap (where X is Cr or V) refer respectively to product obtained as precipitate or by evaporating off THF post reduction.

Co-reduction of $TiCp_2Cl_2$ and $PtCl_2COD$ in 18 ml THF showed immediate reduction, with the product crashing out of THF on standing overnight. EDS analysis showed the product to have unprecedented amounts of Ti (Figure 5.8), and SEM imaging showed agglomerated material (Figure 5.9). However, X-ray diffraction patterns from the as prepared material indexed closely to Pt_3O_4 (Figure 5.10). This was very puzzling, since Ti was the element expected to be oxidized of the two if oxidation was to happen, but no Ti oxide peaks were detected. Perhaps this similarity is accidental, for example,

there may be a Pt-Ti-O phase with very similar lattice parameters, although none have been reported.

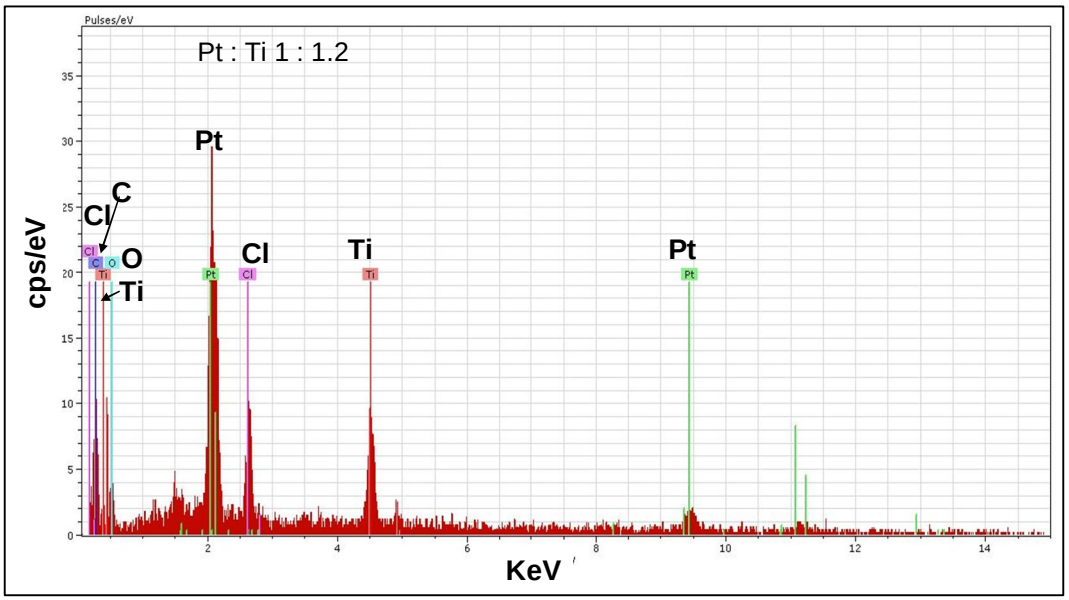

Figure 5.8: EDS spectra and atomic % ratio of Pt:Ti of the $TiCp_2Cl_2$ and $PtCl_2COD$ co-reduction product.

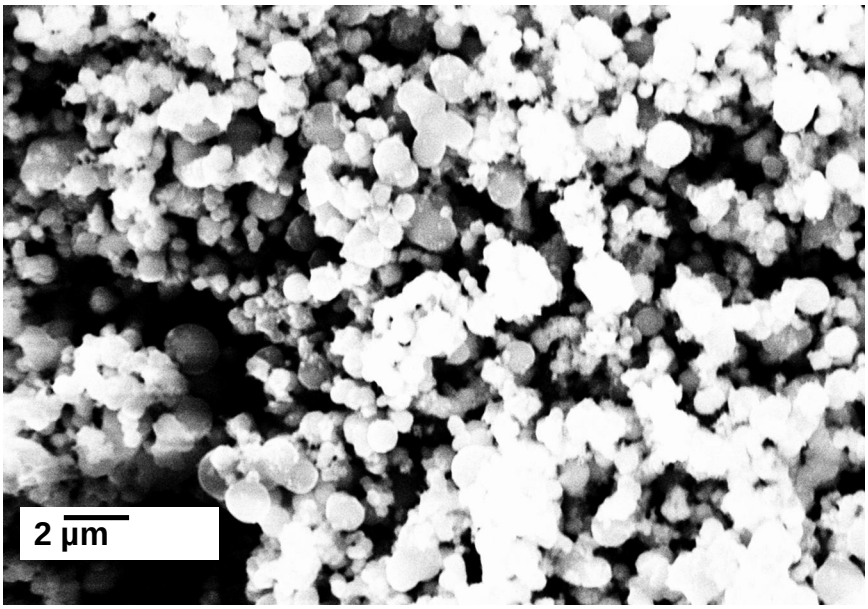

Figure 5.9: SEM image of the $TiCp_2Cl_2$ and $PtCl_2COD$ co-reduction product.

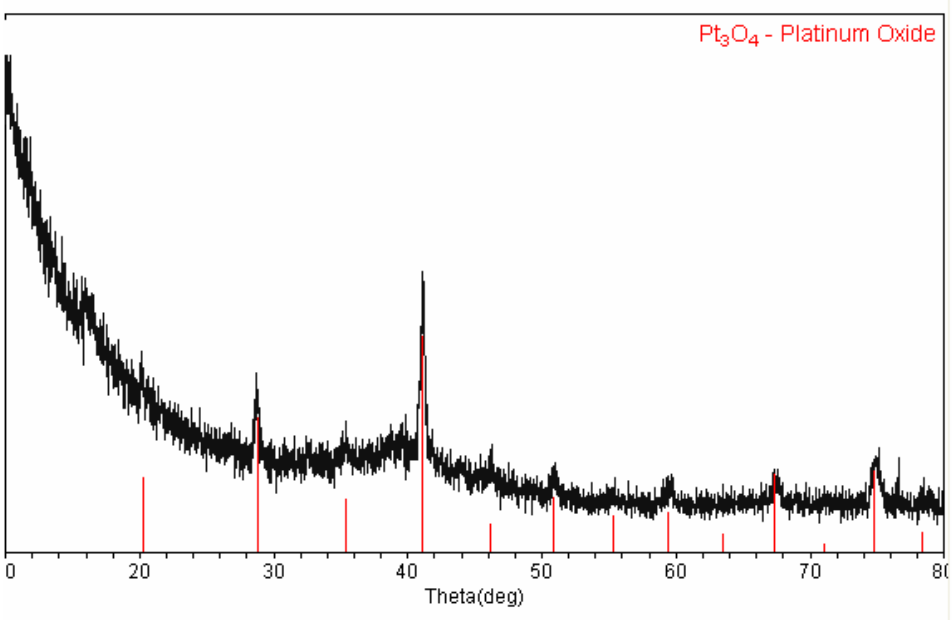

Figure 5.10: X-ray diffraction pattern of the $TiCp_2Cl_2$ and $PtCl_2COD$ co-reduction product (as prepared, before annealing). Red lines indicate the peak positions for the Pt_3O_4 phase (PDF # 04-007-2455)

The sample was then annealed at 600 ^{o}C for 12 h. The X-ray diffraction pattern of the annealed product showed familiar relatively broader peaks, with maxima indexing close to cubic Pt peaks. This reaction was scaled up and repeated and the product was annealed at several different temperatures (300 ^{o}C, 500 ^{o}C and 700 ^{o}C) for 12 h without exposing to air at any step. The X-ray patterns showed broad peaks indexing close to Pt, but EDS analysis showed presence of almost twice the mole fraction of Ti than Pt (Table 5.6). This again was quite surprising. Disappointing too, as although the final products showed much more Ti with this method than previously possible, evidence of ordered (or even alloy phases with peaks significantly shifted from Pt) could still not be obtained by X-ray diffraction analysis. Blackening on the walls of the tubes (the usual indication of C present) was found to increase with the annealing tem[perature. The 300 ^{o}C tube showed no blackening whatsoever on the walls of the tube, the 400 ^{o}C tube showed a faint layer of soot like deposits on its walls, while walls of the 700 ^{o}C tube were completely blackened. SEM images of these samples (especially the one annealed at 500 ^{o}C) showed presence of morphologically different and interesting structures, which couldn't be yet identified (Figure 5.11).

Table 5.6: Ratio of atomic % of Pt:Ti (from EDS) in as prepared and annealed products of the $TiCp_2Cl_2$ and $PtCl_2COD$ co-reduction (annealed at 300 ^{o}C for 12 h and annealed at 500 ^{o}C for 12 h without ever being exposed to air).

Atm% of:	Pt	Ti
As prepared	1	2
300 ^{o}C	1	1.9
500 ^{o}C	1	1.8

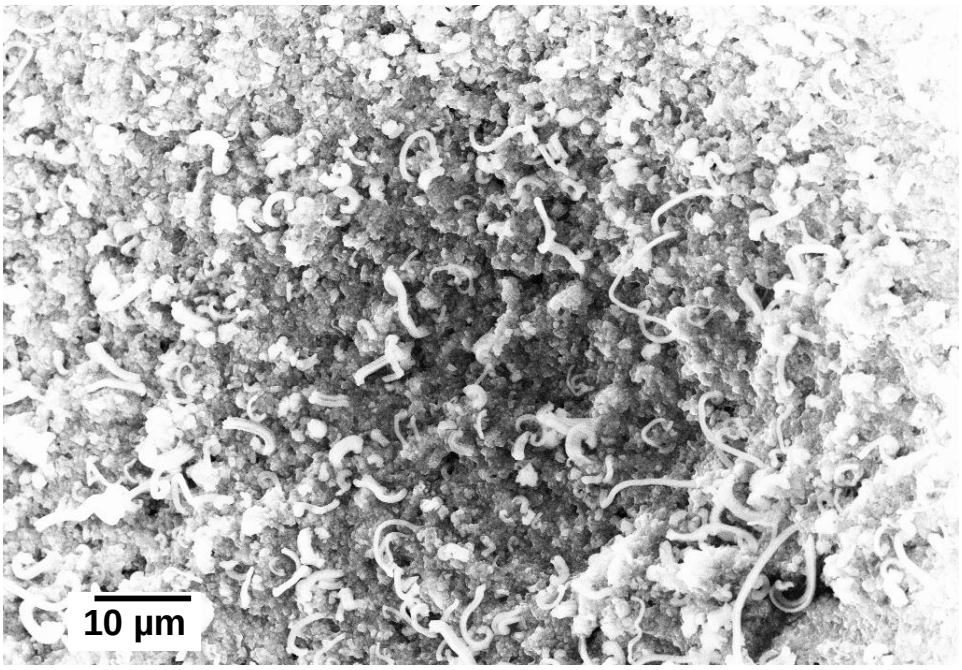

Figure 5.11: SEM image of the product of co-reduction of $PtCl_2COD$ and $TiCp_2Cl_2$ after annealing at 500 ^oC for 12 h. Morphologically interesting structures can be seen.

Co-reductions of $Ti(THF)_2Cl_4$ and $V(THF)_3Cl_3$ respectively with $Na_2PtCl_6.6H_2O$ showed immediate reduction on injection of nBuLi. It should be mentioned here that some initial cloudiness was observed on mixing the precursors which cleared off on stirring for 10 min (Figure 5.12). This might indicate reaction of Ti and V with H_2O present in the Pt salt. Obtaining the later in completely anhydrous form was not possible.

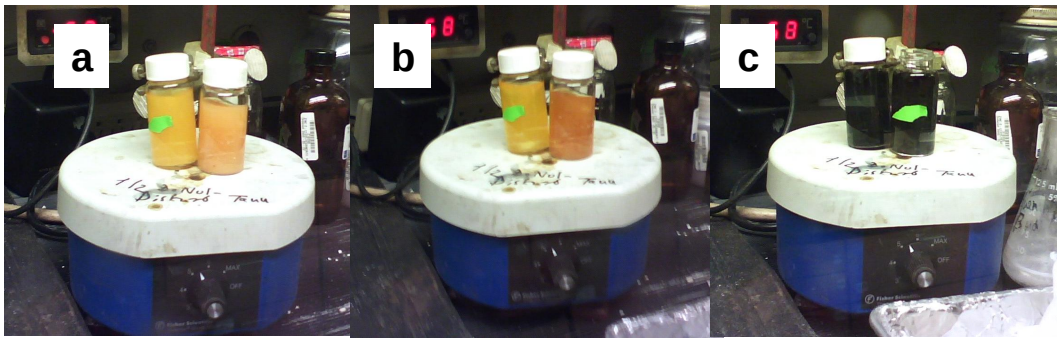

Figure 5.12: Solutions of $Na_2PtCl_6.6H_20$ and $TiCl_4(THF)_2$ and $VCl_3(THF)_3$ in THF a) immediately on mixing b) few minutes after and c) after injection of nBuLi.

These reactions also gave two products each – recovered by precipitation and recovered by evaporating off the solvents All four products were annealed at 400 ^oC for 48 h without ever exposing to air and X-ray diffraction patterns were obtained. The products obtained as precipitates in each case showed the presence of significant amounts of NaCl by X-ray diffraction (Figure 5.13). In the case of the Pt-Ti broader peaks with maxima close, but shifted from Pt were also observed. SEM images also confirmed the presence of a lot of salt in these samples.

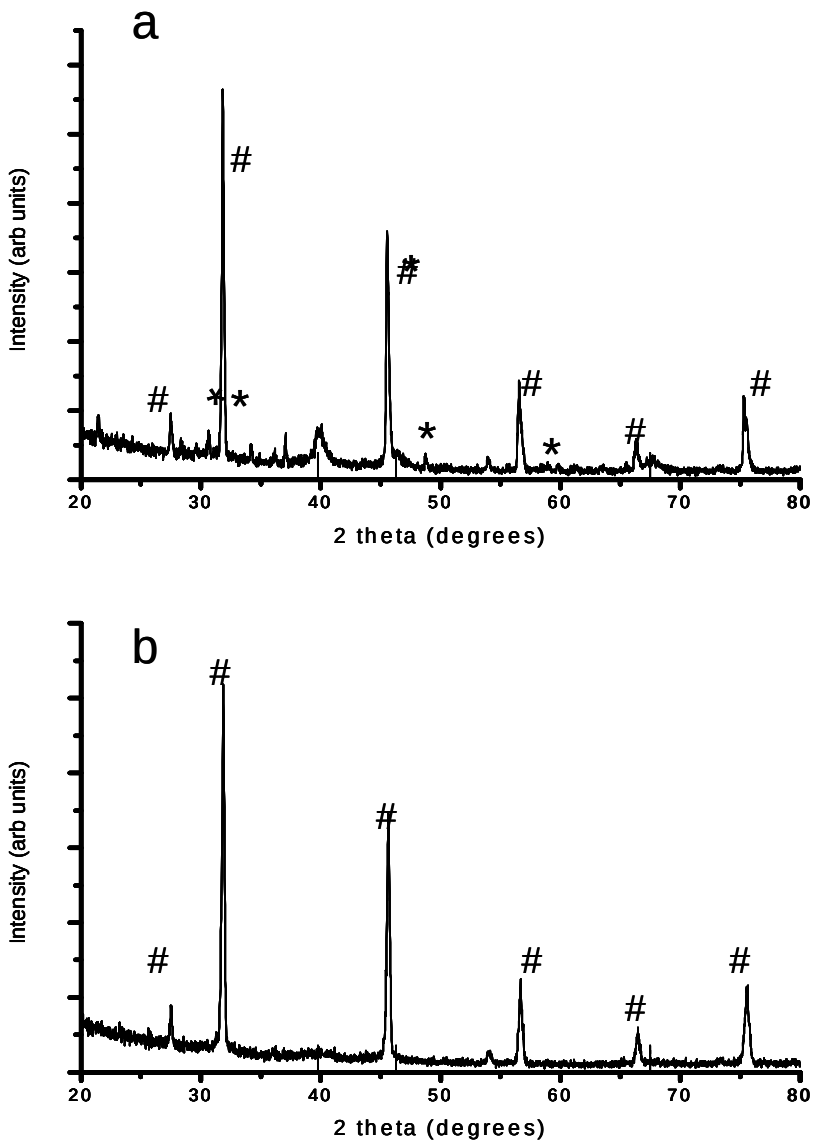

Figure 5.13: X-ray diffraction patterns of the products obtained as precipitates from co-reduction of a) $TiCl_4(THF)_2$ and b) VCl_3THF_3 with $Na_2Cl_6.6H_2O$. Black lines mark Pt peaks (PDF # 01-070-2057) and # shows NaCl peaks. * denotes unidentified peaks in a).

For the Pt-V reaction, the product obtained by evaporating off solvents showed peaks indexing to PtV phases, LiCl and some broader regions close to where Pt peaks would index (Figure 5.14). The one from Pt-Ti reaction showed broad peaks indexing close to Pt. However, one point to note here would be the NaCl detected on the precipitates proving its formation and insolubility in THF. This might become a potential drawback of using mixed metal salts with Na. Thus, while exploring mixed metal salts for higher solubility in THF and cleaner precursors, Li salts would be preferable. EDS data showed presence of the electropositive metals in ratios comparable to Pt in the products (Table 5.7). This is more promising than sodium napthalide reduction, since loss of the reactive metal (probable cause discussed extensively in Chapter 4) was a significant challenge for the latter.

Also promising was the fact that the walls of the tubes in which all these products were annealed were completely clean and showed no indication of carbon deposition (Figure 5.15).

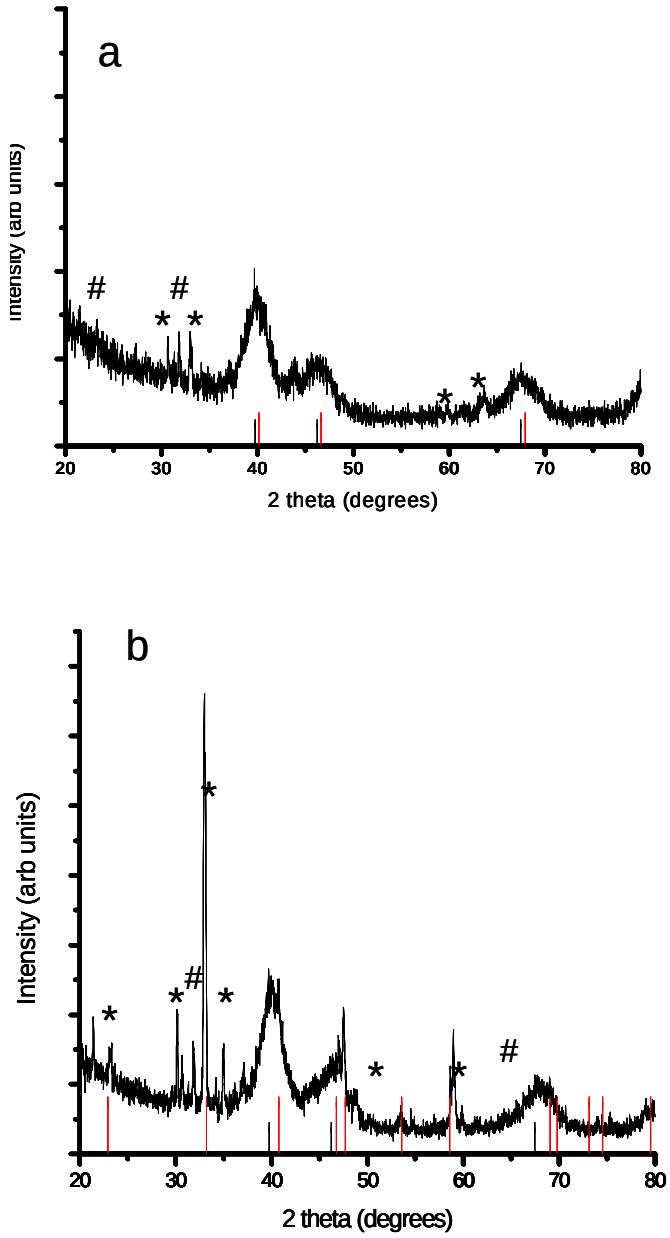

Figure 5.14: X-ray diffraction patterns of the products obtained on evaporating off the solvents after co-reduction of a) $TiCl_4(THF)_2$ and b) VCl_3THF_3 with $Na_2Cl_6.6H_2O$. Black lines mark Pt peaks and * denotes LiCl/LiCl(H_2O) peaks and # denotes unidentified peaks. The red lines denote the Pt_3Ti (PDF # 00-017-0064) and PtV (PDF # 01-072-3010) peak positions respectively in a) and b).

Table 5.7: EDS data showing ratio of atomic % of different elements in the products obtained by co-reduction of $TiCl_4(THF)_2$ and VCl_3THF_3 with $Na_2Cl_6.6H_2O$. PtX ppt and PtX THF evap (where X is Ti or V) refer respectively to product obtained as precipitate or by evaporating off THF post reduction.

At % of:	Pt	Ti
PtTippt	1.9	1
PtTi THF evap	1.2	1
At% of:	Pt	V
PtV ppt	1	2.3
PtV THF evap	Not done	Not done-

Figure 5.15: Tubes of Pt-V and Pt-Ti reactions taken out of the furnace after annealing at 400 ^oC for 48 h. No black deposits were seen on the walls.

5.5 Conclusions

In conclusion, several different alternatives to sodium napthalide for co-reducing metals across the periodic table has been tried and tested. Alkyl lithiums (nBuLi primarily) seem to be the most promising of them so far. The advantages of nBuLi have already been discussed in the introductory sections of this chapter. Additionally, high contents of electropositive and highly reactive elements were recovered in the products (with possibilities of ordered phases in some cases) of nBuLi reductions and impurities observed were simple salts or hydrated salts. Further work with this method to obtain cleaner products is worth trying and may be promising.

Keeping in mind the necessity of finding salts soluble in THF or other ethereal solvents, mixed metal salts of Pt and other elements with alkali metals like Li and Na are being synthesized by others in the group. Li is preferred over Na since NaCl is a by-product formed in the later case which doesn't dissolve in THF. Out intention is to co-reduce the salts and characterize the products. The products discussed in this chapter will be tested for electrochemical activity. Hopefully, promising outcomes from the above measures will lead to the development of the nBuLi reduction methods that will prove more versatile than the sodium napthalide method.

REFERENCES

1. Mortimer, C. T., *Reviews in Inorganic Chemistry* **1984,** 6, (3), 233.

2. Schaak, R. E.; Sra, A. K.; Leonard, B. M.; Cable, R. E.; Bauer, J. C.; Han, Y. F.; Means, J.; Teizer, W.; Vasquez, Y.; Funck, E. S., Metallurgy in a beaker: Nanoparticle toolkit for the rapid low-temperature solution synthesis of functional multimetallic solid-state materials. *Journal of the American Chemical Society* **2005,** 127, (10), 3506-3515.

3. Connelly, N. G.; Geiger, W. E., Chemical redox agents for organometallic chemistry. *Chem. Rev.* **1996,** 96, 877-910.

4. Carper, J., The CRC Handbook of Chemistry and Physics. *Library Journal* **1999,** 124, (10), 192-+.

5. Murphy, D. W., Intercalation chemistry. *Advances in the synthesis and reactivity of solids* **1991,** 1, 237-272.

6. Brooks, J. J.; Rhine, W.; Stucky, G. D., Pi Groups in Ion-Pair Bonding - Stabilization of Dianion of Naphthalene by Lithium Tetramethylethylenediamine. *Journal of the American Chemical Society* **1972,** 94, (21), 7346-&.

7. Barr, D.; Snaith, R.; Wright, D. S.; Mulvey, R. E.; Wade, K., Reactions of Ammonium-Salts with Butyllithium and with Lithium Hydride - New Routes to Fully Anhydrous Inorganic Lithium Complexes. *Journal of the American Chemical Society* **1987,** 109, (25), 7891-7893.

8. Hoffmann, D.; Dorigo, A.; Schleyer, P. V.; Reif, H.; Stalke, D.; Sheldrick, G. M.; Weiss, E.; Geissler, M., The Bicyclic Structure of a Novel Tmeda-Solvated Lithium-Chloride Tetramer [(Licl)(4).3.5tmeda](2) - X-Ray Structural-Analysis and Mo Investigations. *Inorganic Chemistry* **1995,** 34, (1), 262-269.

9. Moser, W. R.; Langer, A. W., *Catalysis in organic syntheses* **1978**.

10. Menzek, A.; Altundas, A.; Gultekin, D., A new, safe and convenient procedure for reduction of naphthalene and anthracene: synthesis of tetralin in a one-pot reaction. *Journal of Chemical Research-S* **2003**, (11), 752-753.

11. Stucky, G. D.; et. al, *Journal of the American Chemical Society* **1965,** 87, 655.

12. Meerholz, K.; Heinze, J., Multiple Reversible Electrochemical Reduction of Aromatic-Hydrocarbons in Liquid Alkylamines. *Journal of the American Chemical Society* **1989,** 111, (6), 2325-2326.

13. Melero, C.; Guijarro, A.; Yus, M., Reactivity in the upper limits of the reduction potential in solution: arene dianion intermolecular carbolithiation of alkenes. *Tetrahedron Letters* **2006,** 47, (35), 6267-6271.

14. Mortensen, J.; Heinze, J., Tetraanions of Acepleiadylene and Pyrene - an Electrochemical Study. *Tetrahedron Letters* **1985,** 26, (4), 415-418.

15. Demortie.A; Bard, A. J., Electrochemical Reactions of Organic Compounds in Liquid-Ammonia .1. Reduction of Benzophenone. *Journal of the American Chemical Society* **1973,** 95, (11), 3495-3500.

Chapter 6

PREPARATION AND ELECTROCHEMISTRY OF Pt-Cd AND Pt-Hg NANOPARTICLES

6.1 Background

As discussed in Chapter 1, need for good electrocatalysts is our underlying motivation for understanding the mechanism of nano phase syntheses of alloys and intermetallic compounds. In this goal we work in collaboration with the CFCI combinatorial sub-group. We follow their lead in exploring potential catalysts whenever promising activity is reported. In this chapter, we look away from the mechanistic work we have done (and are continuing to do) in understanding co-reduction method for nanomaterials synthesis. Instead, we discuss a few catalytically interesting phases synthesized following combinatorial leads. Pt-Cd and Pt-Hg phases were synthesized and studied as nanomaterials (and in bulk form). The results from the combinatorial group that lead us to explore these phases are discussed in brief in the next section. This is just to offer some perspective, full discussion and analysis of the combinatorial methodologies and studies[1-3] is beyond the scope of this work. We then discuss the syntheses methods explored and the phases obtained. Lastly, electrochemistry showing catalytic activity of these phases is presented. The combinatorial work mentioned in this Chapter was done by John Mathew Gregoire, and the electrochemical tests were carried out by Dr. Quin Zhao, graduate and post doctoral students respectively in the present DiSalvo group. We plan to publish this work in one of the major journals in this field in the near future and are currently preparing for submission.

6.2 Combinatorial leads generating interest in Cd and Hg phases

The combinatorial group in the CFCI investigated the improvement of electrochemical activity of Pt by adding different alloying elements. In particular, they used the flourescence profiles for MeOH oxidation of thin films to choose the optimal composition/processing. Figure 6.1 shows that several elements can be alloyed into fcc Pt to improve its activity. The $E_{1/2}$ values shown in the figure are from curve fitting flourescence profiles of MeOH oxidation. The minima of each curve are approximately the solubility limit of the element in Pt. Cd, not shown on this curve (given its toxic nature, sputtering experiments were not done with Cd) has a higher solubility limit in Pt (41 % at low temperatures)[4]. Therefore, significant improvement of catalytic activity of Pt should be observed on alloying Cd into Pt. Figure 6.2 shows maximum % change in Pt lattice constant (calculated from diffraction data and solubility limits[4]) plotted against maximum electron transfer per atom for several elements (calculated using Miedema model[5] and solubility limits) with the color scale depicting the flourescence activity for MeOH oxidation (red equals highest activity). Of the elements shown in the figure, only 4 elements were not tested by the combinatorial method (Ga – melts too low so couldn't be sputtered, Os – oxide is toxic, Ir and Cd). Given that the position of Cd on the plot is very different from the others, Pt-Cd catalysts would be potentially very interesting as bulk or nano-materials (alloy or intermetallic with Pt). Of the group 12 elements, Zn has already been explored (Figure 6.2, shows high activity) as thin films with Pt and nano-materials. So, both Cd, Hg, which are too toxic to be explored by sputtering were explored as alloying elements for Pt using our co-reduction method to prepare nano materials and by high temperature methods to produce bulk materials.

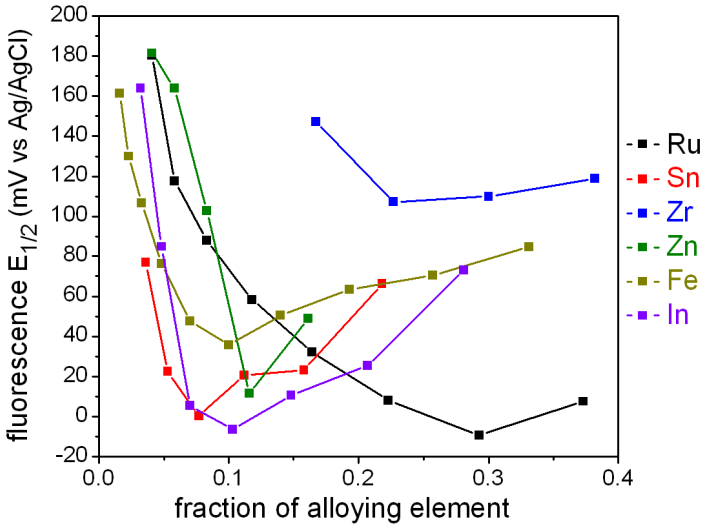

Figure 6.1: Alloying of different elements into Pt to improve its activity towards MeOH oxidation. Value obtained by curve fitting flourescence profiles of MeOH oxidation.

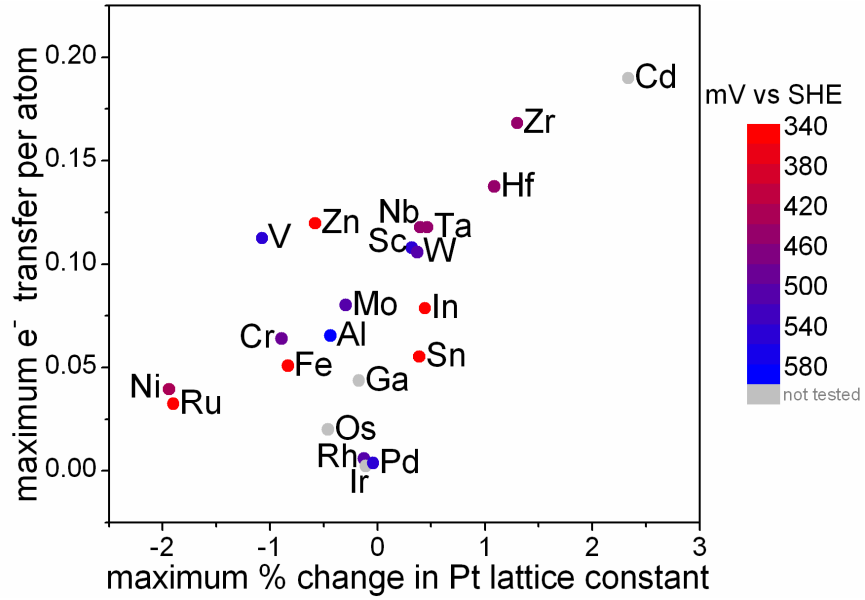

Figure 6.2: Maximum % change in Pt lattice constant plotted against maximum electron transfer per atom plotted for several elements. Color scale indicates flourescence activity for MeOH oxidation of the alloy with red standing for highest activity.

6.3 Experimental

6.3.1 Synthesis

Both sodium napthalide and sodium borohydride reductions of Pt, Hg and Pt, Cd precursors were carried out. The reason for using two different reducing agents is discussed in section 6.4. Bulk phase synthesis of the Pt-Hg phases was also used to compare the activity with nanoparticles of the same composition.

6.3.1.1 Sodium borohydride reductions

Materials: Hexachloroplatinic (IV) acid (H_2PtCl_6) was obtained from Strem Chemicals. Potassium hexachloroplatinate (K_2PtCl_6) was synthesized in the laboratory[6]. Cadmium (II) chloride ($CdCl_2$) and mercury (II) chloride ($HgCl_2$) (Aldrich) were used as Cd and Hg precursors. Anhydrous methanol (Alfa Aesar) was used as the solvent. $NaBH_4$ (Aldrich) was used as the reducing agent. Degassed distilled water and acetone (Aldrich) were used to wash the final products.

Experimental: For each reaction, 50 ml MeOH was degassed for 2 h. 1.4 mmol each of the Pt and Cd or Pt and Hg precursors were dissolved in 40 ml of the degassed MeOH in a 2 necked round bottom flask (required stirring for some time) under argon. 20 equivalents of $NaBH_4$ (1.4 * 20 mmol) were dissolved in the rest of MeOH (vigorous bubbling observed) and was poured through the 2^{nd} neck of the flask into the precursor solution. Immediate reduction and vigorous evolution of hydrogen gas was observed. The second neck of the flask was closed with a stopper once the bubbling subsided (the other neck was used all the time to purge the flask with argon). The reaction was allowed to stir overnight after which the product was allowed to settle down. The product was isolated by decantation.

In some cases, centrifugation was necessary to completely precipitate out the product. If so, the solution was concentrated by evaporating off some of the solvent under vacuum. This would allow us to accommodate the reaction mixture in a centrifuge tube. The mixture was transferred into a Teflon centrifuge tube with a cannula and centrifuged. The product was isolated and washed repeatedly with deionized water, and finally with acetone. After the acetone wash, the product was dried under vacuum, backfilled with argon and exposed to air slowly by piercing the septum with a syringe needle. For Pt-Hg, several more reactions were carried out targeting the other PtHg

phases (Hg_4Pt, Hg_2Pt and alloy phase of 90 % Pt with 10% Hg). For these reactions, only the initial ratio of the Pt:Hg precursors was varied depending on the desired phase (e.g. for the Hg_2Pt phase, 0.9 mmol of K_2PtCl_6 and 1.8 mmol of $HgCl_2$ was dissolved in MeOH) everything else was kept the same as the above described procedure. The reducing agent excess was always maintained at 20 equivalents with respect to the Pt precursor. X-ray diffraction patterns, SEM images and EDS data were obtained in each case.

Similar reactions were attempted for Pt-Cd to Pt rich alloy phases as nano-materials. For these reactions, 1 : 9 equivalents of Cd : Pt (for a 90% Pt 10 % Cd alloy) and 2 : 8 equivalents of Cd : Pt (for a 80 % Pt 20 % Cd alloy) of the Cd and Pt precursors ($CdCl_2$ and K_2PtCl_6) were dispersed in 40 ml THF. To each of these suspensions (K_2PtCl_6 is not very soluble in MeOH, so obtaining is clear solution is often not possible), 9 * 20 equivalents of $NaBH_4$ (dissolved in 10 ml MeOH) were added. The reactions were stirred overnight, the products were isolated by decantation (and centrifugation if necessary), washed repeatedly with deionized water and finally with acetone. The products were then dried under vacuum and exposed to air slowly, as above.

6.3.1.2 Sodium napthalide reductions

Materials: Naphthalene was purchased from Fisher. Sodium metal and diglyme were purchased from Aldrich. THF and diglyme were freshly distilled over sodium prior to use. Sodium napthalide was prepared freshly for each reaction following the procedure described in section 2.2.3. Platinum acetylacetonate ($Pt(acac)_2$), cadmium acetylacetonate ($Cd(acac)_2$) and mercury (II) acetate ($Hg(CH_3CO_2)_2$) were all purchased from Aldrich.

Experimental: 0.5 mmol each of the Pt and Cd or Pt and Hg precursors were dissolved in 20 ml THF inside the glove box and taken out in a syringe and injected into the freshly prepared sodium napthalide solution (2.2 mmol sodium napthalide in 30 ml THF). An immediate color change from light yellow to black was observed in each case. The Pt-Cd products were stirred overnight, while the Pt-Hg reaction was stirred for 4 h. After completion of the stirring times, the reaction mixture was allowed to stand to allow precipitation of the product. However, in neither case complete precipitation could be achieved by doing so, and the supernatants remained very dark. Therefore, the reaction solvent (THF) was completely evaporated off under vacuum, 20-30 ml of dry hexanes was added and the slurry was cannula transferred into centrifuge tubes. The mixture was sonicated and then centrifuged (5000 rpm, 10 min). For the Pt-Cd reaction, one wash was tried with a mixture of 5ml MeOH and 30 ml hexanes, however, the MeOH layer remained dark even after multiple centrifugation efforts and only partial recovery of the product was possible. The MeOH wash was skipped altogether for Pt-Hg, since in one trial of adding 1 ml of MeOH to the hexane solution produced a product that did not precipitate out on centrifuging. A final wash with just hexanes was done in both cases and the product was dried under vacuum. The centrifuge tube was backfilled with argon and the product was exposed to air slowly by putting in a needle through the septum. X-ray diffraction patterns, SEM images and EDS data were obtained.

6.3.1.3 Annealing the products and bulk phase syntheses

Experimental: The 1:1 reaction samples obtained from sodium borohydride and sodium napthalide reductions were annealed to obtain the ordered phase (for Pt-Cd) or to obtain a single phase material (for Pt-Hg) at 600 ^{o}C and 400 ^{o}C respectively for 12 h

in silica tubes sealed under vacuum. Lower annealing temperature (300 ^{o}C, 12 h) were tried for the Pt-Cd reaction. Some of the product from the Pt-Hg, $NaBH_4$ reduction and the product from the Pt-Hg, sodium napthalide reduction were also annealed at 300 ^{o}C for 12 h and quenched by taking the tube out of the furnace at 300 ^{o}C and dropping it in a beaker of cold water. A part of the product from the Pt-Hg, $NaBH_4$ reduction was also annealed at 150 ^{o}C for 12 h. These different conditions were explored in an effort to try to obtain other (Pt rich) ordered Pt-Hg phases. The products from the sodium napthalide reduction of Pt-Cd were annealed at 500 ^{o}C for 12 h, again, to obtain the ordered phase. Annealing steps to obtain specific phases were decided on input from the EDS data showing ratio of Pt : Cd or Pt:Hg present in the product and from the Pt-Cd and Pt-Hg phase diagrams (Figure 6.3)[4]. This discussed in detail in the results and discussions section.

Bulk phase syntheses of Pt-Hg phases were carried out by weighing out stoichiometric amounts of Pt and Hg (200 Mesh Pt (99.99%, Engelhard) and Hg (99.999%, Alfa Aesar)) into a silica tube, sealing the tube under vacuum and annealing at 380 ^{o}C for 72 h and finally, cooling the tube down over a period of 24 h to room temperature. Since the boiling point of Hg is only 356.73 ^{o}C, higher temperatures that could lead to explosion of the tubes were avoided.

6.3.2 Characterization

X-ray powder diffraction powder patterns (Scintag XDS 2000) were taken of the products to confirm the composition and structure of the phases. The particle morphology and size were studied by scanning electron microscopy (SEM) using a LEO-1550 Field Emission SEM (FE-SEM). EDX data was obtained using the same

microscope. Dry powder sample of nanoparticles dispersed on Al stubs were used for SEM.

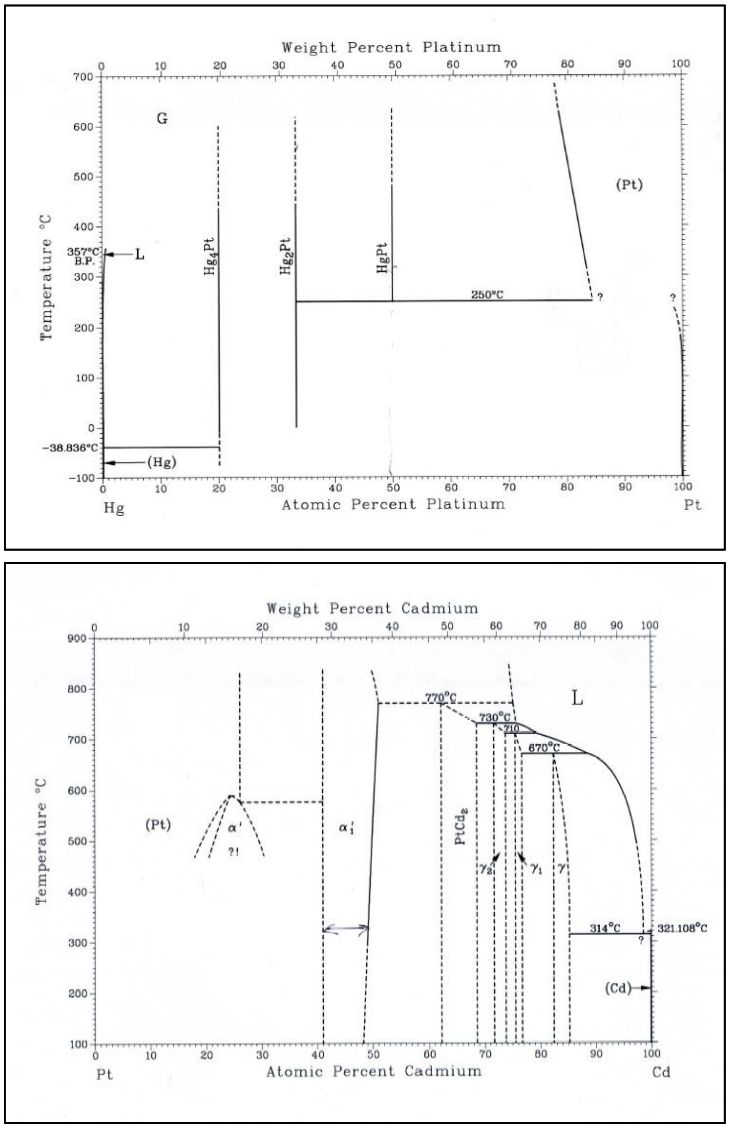

Figure 6.3: Phase diagrams for Pt-Hg and Pt-Cd systems[4].

6.3.3 Electrochemical experiments

The electrocatalytic activity of the Pt-Cd and Pt-Hg nanoparticles and bulk materials for oxidation of methanol and formic acid were examined. Prior to each experiment, a suspension of the nanoparticle catalyst was prepared as follows: to 8 mg of the dried nanoparticle sample were added 3.98 mL of distilled water and 1 mL of isopropyl alcohol (Aldrich). Additionally, 20 µL of a 5% w/w Nafion solution in alcohols and water (Aldrich, EW: 1100) was added to this mixture. The resulting mixture was sonicated in a bath type ultrasonicator for 1 hour. Each nanoparticle suspension described above was coated onto a 4 mm diameter glassy carbon (GC) electrode. The GC electrode had been previously polished with diamond paste (METADI-Buehler, ø = 1µm) and ultrasonicated in Millipore water (18 MΩ cm^{-1}, Millipore Milli-Q) for 10 min. The electrode was then rinsed with Millipore water and allowed to dry in air. 140 µg cm^{-2} of the nanoparticles (10.8 µL of nanoparticle suspension) was coated onto the clean GC electrode. The coated electrode was then dried in air.

Methanol oxidation on the nanoparticle-coated GC electrode was examined in a mixture of 0.5 M methanol (Burdick and Johnson, 99.9% purity) and 0.1 M sulfuric acid. Similarly, formic acid oxidation on the nanoparticle-coated GC electrode was examined in a mixture of 0.5 M formic acid (Mallinckrodt, 88% analytical reagent) and 0.1 M sulfuric acid. A three-electrode electrochemical cell was used for all electrochemical measurements. The reference electrode was a sodium chloride saturated Ag/AgCl electrode, and the counter electrode was a platinum coil. All electrochemical experiments were carried out at room temperature with a Pine AFRDE2 potentiostat. All solutions were prepared with Millipore water and de-aerated with pre-purified argon for at least 15 min before each experiment.

6.4 Results and discussion

6.4.1 The borohydride reductions

Pt is known to form several intermetallic line phases (Hg_4Pt, Hg_2Pt, HgPt and a high temperature Pt rich phase with some composition width) with Hg, of which the two Hg rich phases are known to be stable at room temperature[4]. Cd too is known to form a number of ordered phases with Pt including the 1:1 phase (with some composition width) which should be stable at room temperature[4]. Our initial goal was therefore to synthesize the 1:1 (PtHg and PtCd) phases as nanoparticles using the co-reduction technique. In earlier work with electropositive elements, we found that the electropositive metal reacted with protic wash solvents during the work up processes (discussed in Chapter 3 and 4). The samples obtained from co-reduction of a solution containing a 1:1 ratio of metal precursors with sodium napthalide (necessary for reducing the electropositive metal) were either disordered phases or comprised of very small particles (a few nm). After MeOH wash and annealing the product formed Pt rich phases with domain size between 20 – 40 nm depending on the annealing temperature. As discussed in detail in the earlier chapters, the reactant ligands (anions or neutral electron donors) or even the reaction solvent in the early stages of the co-reduction interfere with the nucleation and growth of the desired phases. The less noble metal is thus easily leached from the product during work-up with protic solvents. These issues were not as significant for PtPb and PtBi, Pb and Bi do not react with MeOH and the by-products from the precursors could be easily washed off with a protic solvent[6-9].

Keeping in mind all these factors, Cd and Hg were thought suitable for co-reduction with Pt using $NaBH_4$ (Table 6.1). Nevertheless, we wanted to compare the products

obtained from using sodium borohydride as the reducing agent to those obtained from sodium napthalide. So we used both reducing agents in different reactions to obtain nanoparticles of the ordered 1:1 phases at room temperature.

Table 6.1: Reduction potentials and metal oxygen bond enthalpies for Cd, Pt and Hg compared to reduction potential of sodium borohydride and sodium napthalide[10].

Metal	Oxidationstates / Conditions	E^0_{red}	Reducing agent	E^0_{red}	Bond enthalpy with O (Kcal/mol)
Cd	2+ to 0	-0.4	$NaBH_4$ Basic	-1.24	56.3
	$Cd(OH)_2$ to Cd (0)	-0.8	Acidic/ Neutral	-0.481	
Hg	2+ to 0	0.85	NaNp	-2.73	52.8
	1+ to 0	0.796			
	2+(Basic) to 0	0.09			
Pt	2+ to 0	1.18			94

The X-ray diffraction patterns of products obtained from a 1:1 precursor ratio of Pt:M (M = Hg or Cd) showed very different behavior for Pt-Hg and Pt-Cd. For Pt-Hg, the X-ray diffraction pattern indicated the presence of ordered Hg_4Pt (of domain size 27.2 nm, calculated using the Scherrer equation) with some broad peaks indicating the presence of a second, probably Pt rich, disordered phase (Figure 6.4). The EDS analysis showed Pt:Hg atomic ratio in the product to be 1.6:1. These data suggest that a multi phase product was obtained. In order to produce a single phase product, the product was split into batches and several annealing experiments were tried. One batch was annealed at 300 ^oC for 12 h followed by quenching to obtain the HgPt phase. The phase diagram for the bulk material indicated that HgPt has a lower peritectoid

temperature of 250 ^{o}C and slow cooling would lead to separation into Hg_2Pt and some Pt rich alloy. Another batch was annealed to just 150 ^{o}C, for 12 h to increase the diffusion rate nucleation and growth of a single phase. In both cases, the X-ray pattern showed the end product to be mixture of HgPt, Hg_2Pt and Pt. A single phase material couldn't be obtained by annealing a 1:1 starting composition (Figure 6.5).

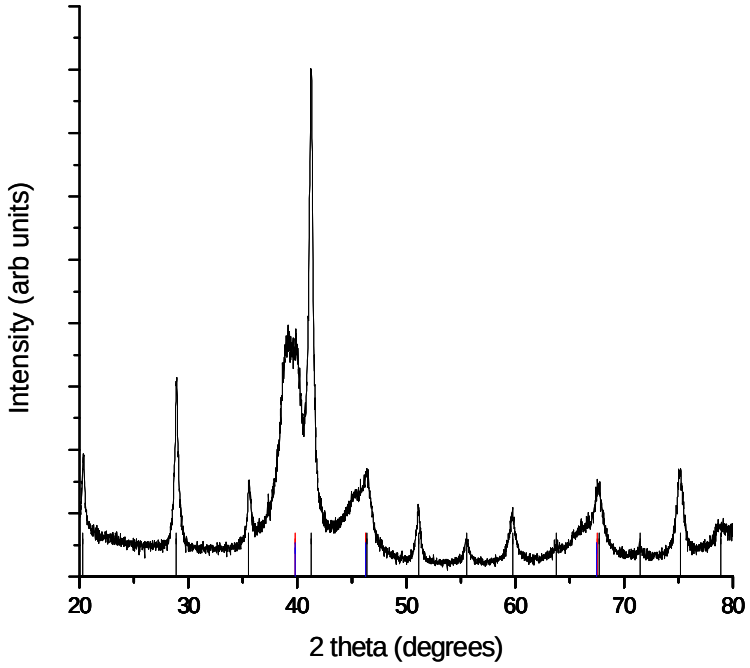

Figure 6.4: X-ray diffraction pattern of product obtained by co-reducing K_2PtCl_6 and $HgCl_2$ in 1:1 ratio. The black lines mark the Hg_4Pt phase (narrow peaks) PDF # 04-004-7276, the blue and red lines mark the Pt (PDF # 01-070-2057) and $Pt_{0.75}Hg_{0.25}$ (alloy, PDF # 04-001-2909) phases respectively (broader peaks).

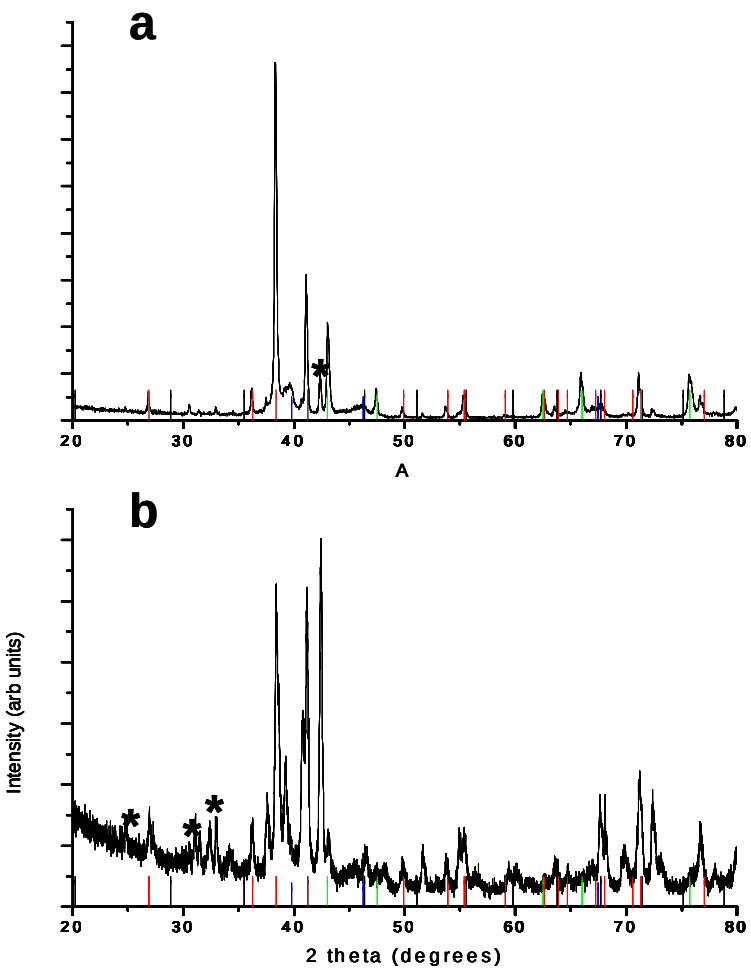

Figure 6.5: X-ray diffraction patterns of the products from co-reduction of K_2PtCl_6 and $HgCl_2$ (in 1:1 ratio) with $NaBH_4$ after annealing at a) 150 ^oC and b) 300 ^oC . HgPt, Hg_2Pt, Hg_4Pt and Pt peak positions are shown by the red, green, black and blue lines respectively (PDF #s 03-065-9987, 04-004-7277, 04-004-7276 and 01-070-2057 respectively). The products are found to be mixtures of the first three phases. * denotes unidentified, possible impurity peaks.

For the1:1 Pt-Cd reaction, the 1:1 reduction with sodium borohydride reaction, the product showed comparatively broad peaks in the X-ray diffraction pattern with peak maxima close to those for fcc Pt (Figure 6.6). EDS data showed Pt:Cd atomic ratio close to 1:1. The product was annealed at 600 ^{o}C for 12 h to see if the ordered PtCd phase forms. While the attempt was successful, and we obtained the ordered CdPt phase, the domain size was quite large (71.1 nm). The annealing was repeated a lower temperature (300 ^{o}C) to obtain the phase with smaller domain size, resulting in the CdPt phase with domain size 18.9 nm (Figure 6.7). The peak shifts from the reported patterns may be due to different compositions allowed in the broad phase width of the CdPt phase: $Cd_{1-x}Pt_x$ with $x < 0$.

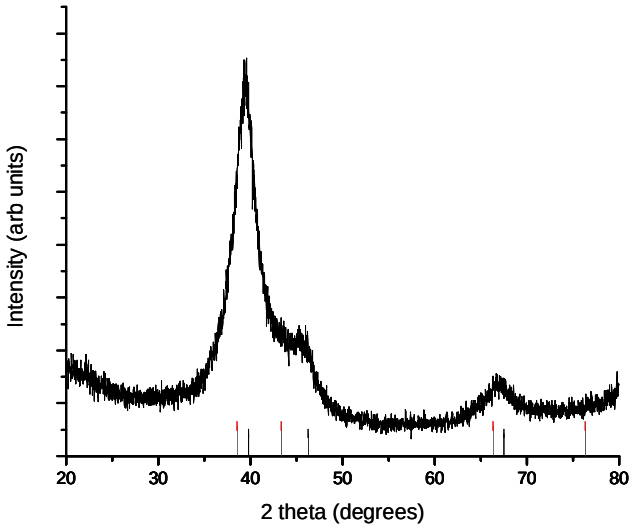

Figure 6.6: X-ray diffraction pattern of the product from co-reduction of K_2PtCl_6 and $CdCl_2$ (in 1:1 ratio) with $NaBH_4$. The black and red lines show the Pt (PDF # 01-070-2057 and PtCd (PDF # 03-065-8872) peak positions respectively.

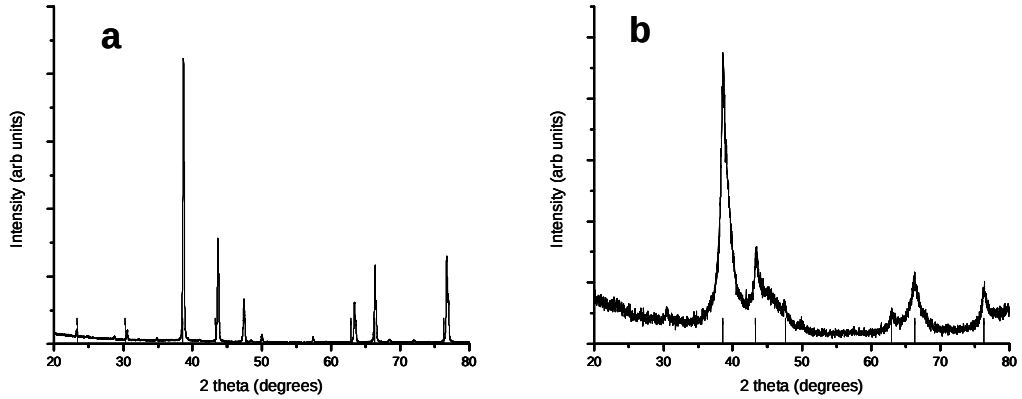

Figure 6.7: X-ray diffraction patterns of the products from co-reduction of K_2PtCl_6 and $CdCl_2$ (in 1:1 ratio) with $NaBH_4$ a) after annealing at 600 ^oC and b) after annealing at 300 ^oC. The black lines denote the peak positions expected for the PtCd phase (PDF # 03-065-8872).

For the Pt-Hg system, since we couldn't obtain a single phase material from co-reduction of precursors in a 1:1 ratio, we attempted to synthesize the phases known to be stable at room temperature, Hg_2Pt and Hg_4Pt, as nanomaterials. Accordingly, stoichiometric amounts of the precursors (2 Hg:1 Pt and 4 Hg:1 Pt precursor ratio) were reduced with sodium borohydride. However, in the case of the 4 Hg:1 Pt reaction, the X-ray diffraction patterns showed the products to be a mixture of Hg_4Pt (ordered) and HgCl. For the 2 Hg:1 Pt reaction, the product showed peaks corresponding to ordered Hg_4Pt. In each case, there is evidence of a second phase of disordered, small particle size material in the sample as well (Figure 6.8 a, b).

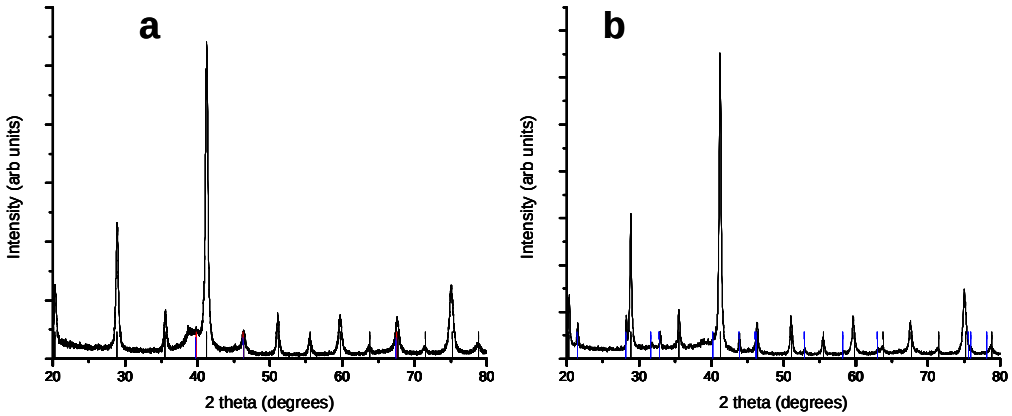

Figure 6.8: X-ray diffraction patterns of the products from co-reduction of K_2PtCl_6 and $HgCl_2$ in a) 1:2 and b) in 1:4 ratio with $NaBH_4$. In a), the black, blue and red lines shows peaks of Hg_4Pt, Pt and $Pt_{0.75}Hg_{0.25}$ phases respectively (PDF #s 04-004-7276, 01-070-2057 and 04-001-2909 respectively). In b), black lines show the Hg_4Pt while the blue lines show the HgCl phase (PDF #s 04-004-7276 and 00-004-0581 respectively).

The atomic ratio of Hg:Pt observed by EDS was 1.9:1 and 2.6:1 for the 2 Hg:1 Pt and 4 Hg:1 Pt products respectively.

The reaction to prepare a 90% Pt/10 % Hg alloy phase yielded two morphologically different products. Some of the product was comprised of significantly larger particles, which crashed out of the reaction solvent completely. This product could be completely isolated from the reaction solvent by decantation. However, the supernatant still had very fine black suspended particles, which could only be isolated by centrifugation. The former (big particles) were found be primarily Hg_4Pt (ordered) by X-ray diffraction. Presence of broader peaks with maxima corresponding to the fcc Pt showed presence of some Pt, or a Pt alloy of composition Pt0.75Hg0.25, which is

almost indistinguishable from pure Pt by X-ray diffraction analysis given the proximity of the peaks corresponding to this phase to those of pure Pt. The later product (smaller particles) showed only peaks corresponding to Pt or a Pt rich alloy (Figure 6.9 a, b).

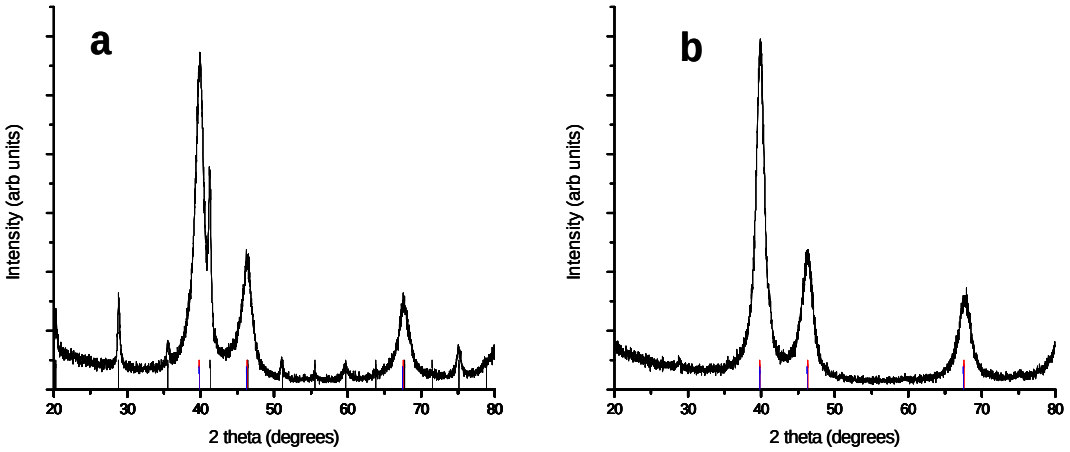

Figure 6.9: X-ray diffraction patterns of the products from co-reduction of K_2PtCl_6 and $HgCl_2$ in 9:1 ratio with $NaBH_4$. a) Shows the pattern from the product consisting of particles that precipitated and were recovered by decanting the reaction solvent. b) Shows the product that were precipitated by centrifugation from the decanted reaction solvent. Black lines show the line positions expected for the Hg_4Pt phase while the blue and the red lines show the Pt and $Pt_{0.75}Hg_{0.25}$ phases respectively (PDF #s 04-004-7276, 01-070-2057 and 04-001-2909 respectively).

EDS analysis on these materials showed the precipitation product (Figure 6.9 a) to have an average composition of 9:1::Pt:Hg (which is the exact ratio of precursors used for this reaction). There was also an isolated region found on this material showing 90 Pt:6 Hg (ratio of the atomic % of these metals). This, along with X-ray diffraction

result shows that this material is not phase pure and is comprised of a Pt rich (or pure Pt phase) phase along with the Hg_4Pt intermetallic. The later product (figure 6.9 b) showed a composition of 52 Pt:1 Hg – a composition suggesting the product is primarily Pt. However, in this product also, an isolated region was detected with the composition 72 Pt:26 Hg (ratio of atomic percentages) – a composition close to the Pt0.75Hg0.25 alloy. This, along with the X-ray diffraction patterns suggests that this material is a Pt rich alloy phase.

For the Pt-Cd system, synthesis of Pt rich alloy phases (90%Pt-10 %Cd and 80 % Pt - 20 % Cd) as nanomaterials was also attempted. The entire product from the first reaction could be isolated by decantation. The second reaction (80% Pt, 20% Hg), however, gave two morphologically different products comprising of larger (isolated by decantation) and smaller (isolated by centrifugation) particles. X-ray analysis for all three products showed relatively broad peaks with maxima corresponding to Pt or Pt alloys (Figure 6.10 a, b, c). The EDS analysis showed that the first two materials (product from 90% Pt -10 % Cd reaction and the bigger particles from 80 % Pt - 20 % Cd reaction) contain only Pt (besides some C and O from organic contaminants). However, EDS analysis on the third product (smaller particles from the 80 % Pt - 20 % Cd reaction) showed an average composition of 6 Pt:1 Cd (atomic %).

It is important to point out here, that K_2PtCl_6 (the Pt precursor used for all $NaBH_4$ reduction reactions) had very low solubility in MeOH while the Cd and Hg precursors dissolved completely in the same. Hence the rate of reduction of the two metals (Pt vs Cd or Hg) was expected to be different. This might be responsible for the inhomogeneity observed in some cases (for example, Figure 6.4, 6.8 a, b and 6.9 a, b). However such observations were not general and single phase products could be obtained in the other cases.

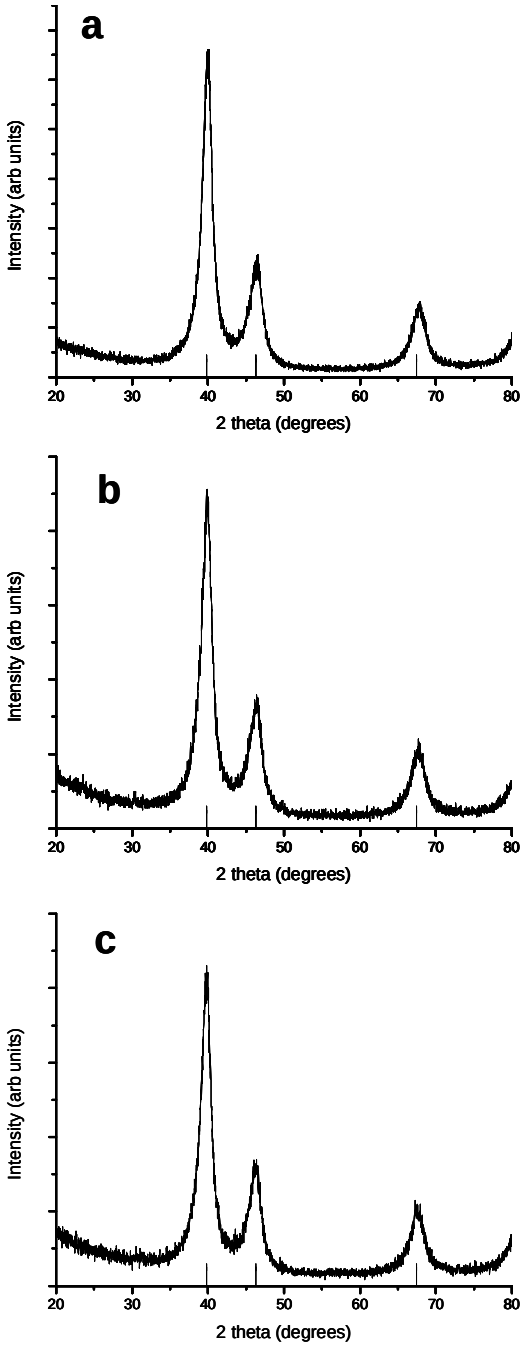

Figure 6.10: X-ray diffraction patterns of products obtained by co-reducing K_2PtCl_6 and $CdCl_2$ with $NaBH_4$ a) 8:2 ratio, b) 9:1 ratio, product recovered by decantation (bigger particles) and c) 9:1 ratio, product recovered by centrifugation (smaller particles). The lines show the Pt (PDF # 01-070-2057) peak positions.

Thus, for less electropositive elements like Hg and Cd, the $NaBH_4$ reduction method provides products that are relatively easy to isolate either by direct precipitation or centrifugation. For Pt-Hg, the products were mixtures of several binary alloy and intermetallic phases as clean nano-materials. However these materials In the Hg-Pt system, Hg_4Pt appears to nucleate and grow preferentially. However, when the reactant ration Hg:Pt::4:1 was used, the product, while containing majority of Hg_4Pt, was not phase pure.

6.4.2 The sodium napthalide reductions

Sodium napthalide reductions were also undertaken to see if any phase pure product could be obtained as the 1:1 ordered phases for either the Pt-Cd or the Pt-Hg system. One reason to do so was to try a stronger reducing agent, especially for Pt-Cd where sodium borohydride might not suffice to ensure rapid co-reduction of both metals. More importantly, we thought it would be interesting to compare the two methods side by side to see if the preparation method influenced the products obtained or their electrochemical properties. Given that the reagents and solvents used are very different in the two cases, we'll be able to further explore our hypotheses about the role of the side species involved in the process of co-reduction.

The first point to note was the products, for both Pt-Cd and Pt-Hg, in the case of sodium napthalide reduction would not precipitate out of a MeOH wash (even when only 5 ml MeOH was used along with 30 ml hexanes). The products from the sodium borohydride reductions not only precipitated out of MeOH (which was the reaction solvent), but also precipitated out of the de-ionized H_2O they were washed with. This suggests that the particles obtained by sodium napthalide reduction are not only very small, but are prevented from agglomeration by surface coatings that are formed by

strong adsorption of neutral species such as naphthalene or THF or charged species such as acetylacetonate. For this reason, the crystallites remain too small to precipitate out of solution or to be identified by X-ray diffraction. Charged particles are much less likely to precipitate from polar solvents. If acetylacetonate binds to the particles, the reduced particles are rendered charged. The X-ray diffraction patterns obtained for the Pt-Cd and Pt-Hg products with sodium napthalide reduction and subsequent solvent removal by evaporation showed very broad peaks (Figure 6.11). The very small particles are chemically labile – most of the reduced metals are at or near the particle surface. Thus, reactions with solvents, wash solvents, water and air are more likely than for larger particles. For larger particles, leaching or oxidation may be confined to the particle surface, which becomes enriched in Pt.

The EDS data showed for the precursor Pt:Cd::1:1, the Pt : Cd atomic ratio to be 1:1.3 , so we attempted to obtain the ordered phase by annealing. The product was annealed at 500 ^{o}C for 12 hr and the tetragonal PtCd phase was obtained (Fig 6.12). For the 1:1::Pt-Hg reaction, the Pt: Hg atomic ratio was shown to be 1 : 1 by EDS, so this product was also annealed at 300 ^{o}C, 12 h followed by quenching in an attempt to obtain a metastable HgPt phase. Diffraction pattern of the product showed it to be a mixture of the HgPt, Hg_2Pt and Pt (present in very small amount) phases (Figure 6.13). Apparently the rate of quenching is too low to prevent the peritectoid decomposition of HgPt.

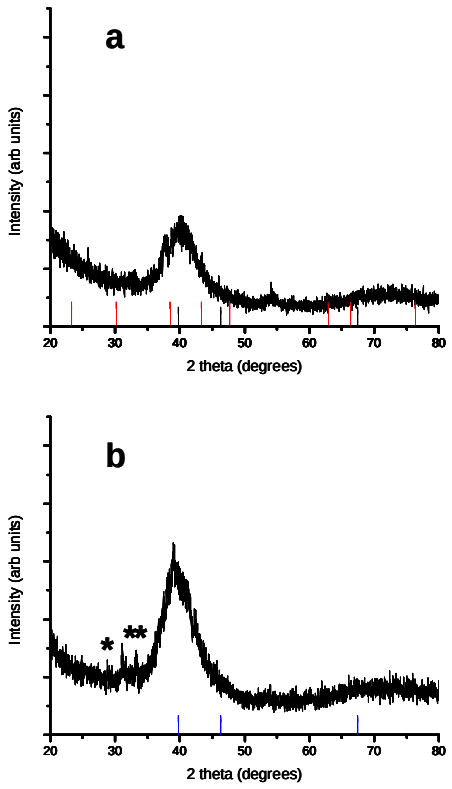

Figure 6.11: X-ray diffraction patterns of products of sodium napthalide reduction of $Pt(acac)_2$ with a) $Cd(acac)_2$ and b) $Hg(CH_3CO_2)_2$ (ratio of precursors 1 : 1 in each case). In a) the black and red lines mark the peak positions of Pt (PDF # 01-070-2057) and PtCd (PDF # 03-065-8872) phases respectively while in b) the lines show Pt (PDF # 01-070-2057) peak positions.

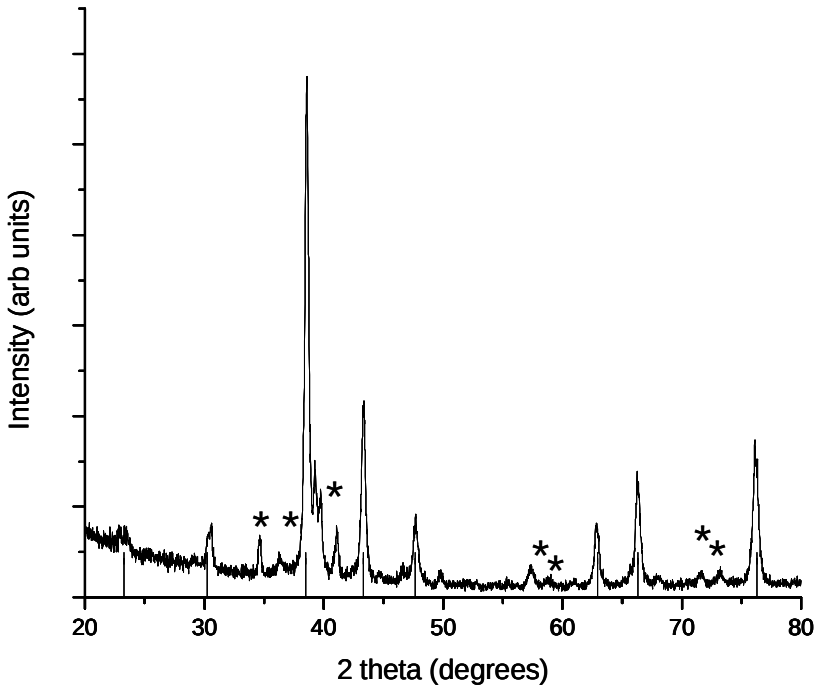

Figure 6.12: X-ray diffraction pattern of the product of the sodium napthalide reduction of $Pt(acac)_2$ with $Cd(acac)_2$ (1 : 1 ratio) after annealing at 500 ^oC. The black lines mark the PtCd phase (PDF # 03-065-8872) while * denotes unidentified, possible impurity peaks.

However, the X-ray pattern showed several additional small peaks at the low angles which could not be indexed. This once again, is a typical observation in products from sodium napthalide reduction suggesting presence of organic containing side products or impurities.

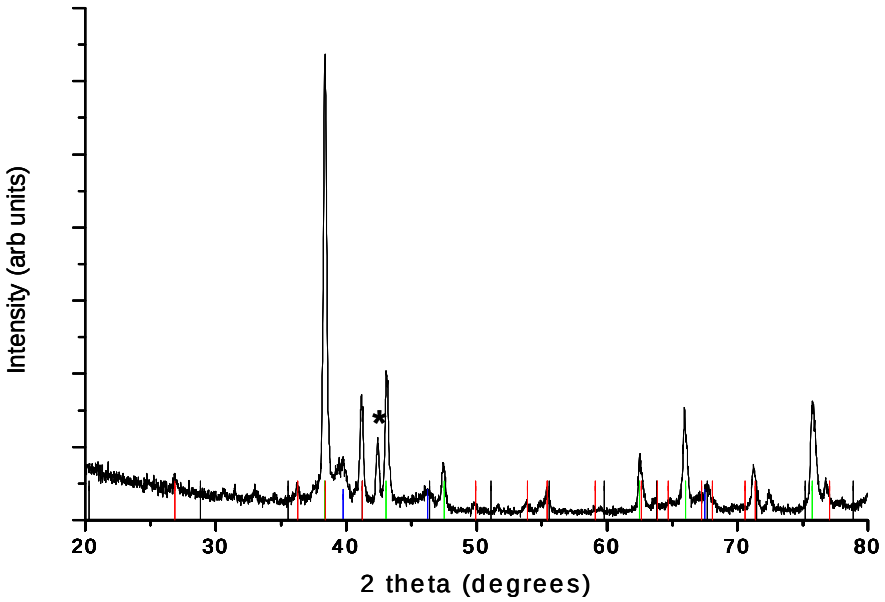

Figure 6.13: X-ray diffraction pattern of the product of the sodium napthalide reduction of $Pt(acac)_2$ with $Hg(CH_3CO_2)_2$ (ratio of precursors 1 : 1) after annealing at 300 ^oC. HgPt, Hg_2Pt, Hg_4Pt and Pt peak positions are shown by the red, green, black and blue lines respectively (PDF #s 03-065-9987, 04-004-7277, 04-004-7276 and 01-070-2057 respectively). The product is a mixture of the first three phases. * denotes an unidentified peak.

6.4.3 Bulk phase reactions

As discussed in the introduction to this chapter, our inspiration for exploring these particular phases was a suggestion that enhanced electrocatalytic behavior could be expected; however, the initial products from the above reactions discussed showed no electrocatalytic activity. Although this could very well be because of the inherent

inactivity of these materials, it could also be due to side products sticking to the surface of nano-materials causing them to be inactive (especially for the sodium napthalide reduction products). Even for annealed samples, it is possible that some of organic materials decompose on the particle surfaces, instead of being removed, deposit back on the nanoparticles, poisoning their surface (since we anneal the particles in sealed tubes). This issue has been discussed in section 3.4.2. The best way to eliminate the later possibility would be to synthesize these phases as bulk materials and test their electrocatalytic activity. If still inactive, the synthesis of these phases as cleaner nanomaterials should not be further pursued.

In the case of Hg:Pt::4:1 reaction, the product is comprised of Hg_4Pt and Hg_2Pt intermetallic phases, with the former being predominant. In the case of Hg : Pt 2 : 1 reaction, the product comprised of again comprised of Hg_4Pt and Hg_2Pt intermetallic phases with the later being predominant. For the Pt:Hg::1:1 reaction, the Hg_2Pt phase, with small amounts of Pt resulted, while for the Pt:Hg::9:1 reaction, the product was found to be a mixture of HgPt, Hg_2Pt and Pt (or $Pt_{0.75}Hg_{0.25}$ alloy – indistinguishable from Pt by X-ray diffraction pattern) of which the first two were predominant. Thus, completely pure single phase materials could not be obtained by bulk phase reactions. Figure 6.14 shows the X-ray diffraction patterns for the four reaction products.

Even though not single phase, all the products were tested electrochemically for catalytic activity towards small molecules such as formic acid and methanol. If one of the phases were very active, we would detect that activity here and be then motivated to pursue different methods to obtain single phase products.

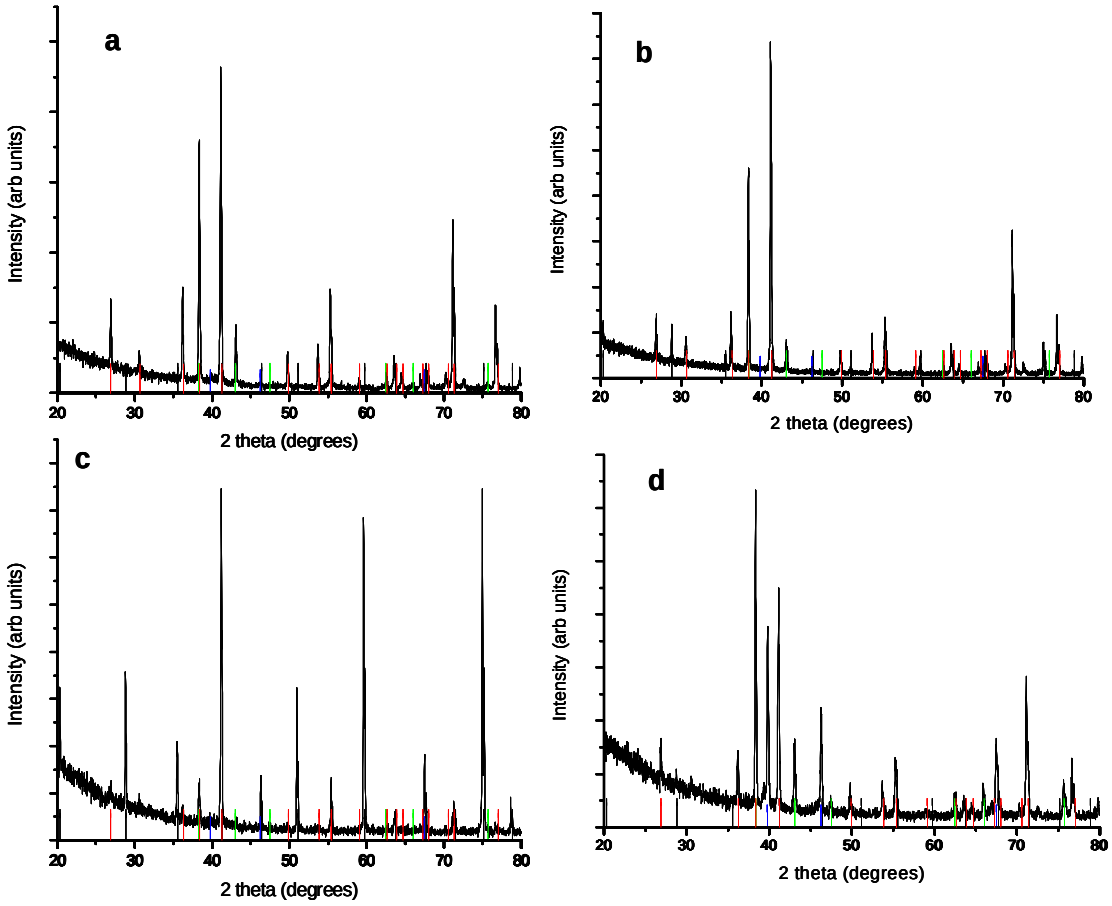

Figure 6.14: X-ray diffraction patterns of the products from bulk phase reaction of Pt and Hg in ratios a) 1:1, b) 1:2, c) 1:4 and d) 9:1. HgPt, Hg_2Pt, Hg_4Pt and Pt peak positions are shown by the green, red, black and blue lines respectively (PDF #s 03-065-9987, 04-004-7277, 04-004-7276 and 01-070-2057 respectively).

6.4.4 Electrochemical activity of PtHg and PtCd phases

Of the Pt-Hg phases described above, only those obtained from $NaBH_4$ reduction of $HgCl_2$ and K_2PtCl_6 in ratios 1:9 (done with the intention to obtain an alloy phase rich in Pt) showed activity for formic acid oxidation. Of the two products obtained from that reaction, the one with larger particles showed higher activity (Figure 6.15) with mass activity and current density at +0.2 V (normalized with respect to BET surface area measured) of 0.026 mA/µg and 0.278 mA/cm^2 respectively. The onset potential was measured to be -0.15 V. This is not as good as PtPb, which has an onset of -0.2 V and current density of 5.5 mA/cm^2 at +0.2 V. Since other samples that contain Hg_4Pt are not active, we conclude that the Hg-Pt alloy produced is the active species. However, there are many factors, such as surface contamination that are not controlled in these experiments.

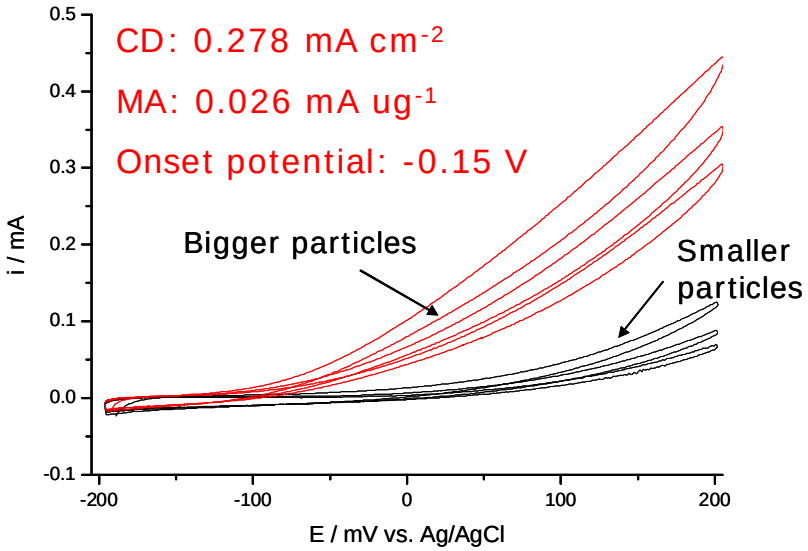

Figure 6.15: Cyclic voltammograms of the Pt-Hg phases obtained by co-reduction of K_2PtCl_6 and $HgCl_2$ with $NaBH_4$ in 9:1 ratio in 0.5 M formic acid, 0.1 M H_2SO_4 at electrode rotation rate of 2000 rpm and scan rate 10 mV/sec.

Of the PtCd products, the product obtained (unannealed) by co-reduction of $CdCl_2$ and K_2PtCl_6 (in 1:1 ratio) with $NaBH_4$ was to found to be active towards formic acid oxidation. The activity was found to increase in the product annealed at 300 ^oC, but decreased in the product annealed at 600 ^oC. This might be due to the two different factors in play on going from as prepared unannealed product to materials annealed at different temperature. Compared to the as prepared product, the annealed products contain ordered phases. However, with the increase in annealing temperature particle domain size and hence surface area decreases. Figure 6.16 shows the voltammograms while table 6.2 shows the BET surface areas measured for these three samples.

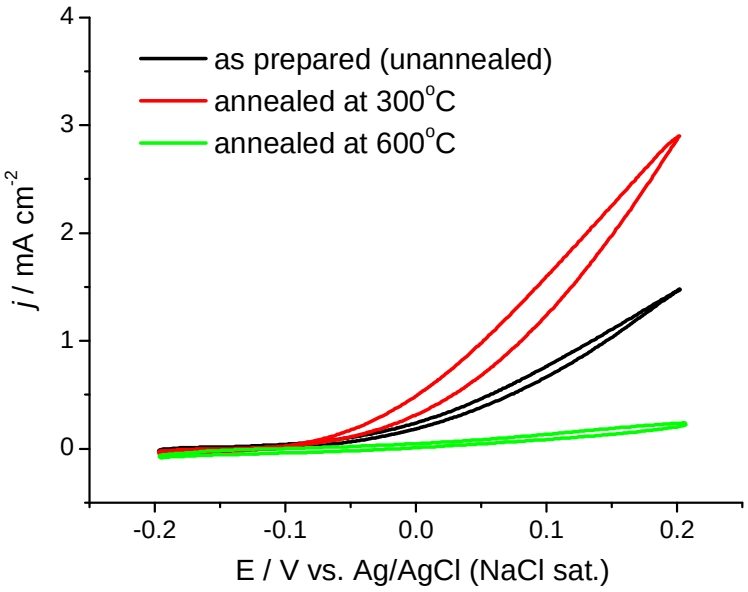

Figure 6.16: Cyclic voltammograms of the Pt-Cd phases obtained by co-reduction of K_2PtCl_6 and $CdCl_2$ with $NaBH_4$ in 1:1 ratio in 0.5 M formic acid, 0.1 M H_2SO_4 at electrode rotation rate of 2000 rpm and scan rate 10 mV/sec.

Again, the surfaces of the samples annealed at the higher temperature, 600 ^{o}C, may be coated with organic decomposition products.

Table 6.2: BET surface area of the Pt-Cd samples synthesized by co-reduction of $CdCl_2$ and K_2PtCl_6 in 1:1 ratio with $NaBH_4$.

PtCd	BET SA(m^2 g^{-1})
Unannealed	5.06
Annealed at 300 ^{o}C	3.44
Annealed at 600 ^{o}C	0.62

Activity towards formic acid oxidation was also observed for the PtCd samples obtained by co-reduction of the precursors (in 1:1 ratio) with sodium napthalide. The activity observed for the annealed sample (annealed at 500 ^{o}C) was higher than that for the unannealed one (Figure 6.17). These observations suggest that the PtCd is an active catalyst material for formic acid oxidation with the ordered tetragonal phase having higher activity than the disordered alloy phase with a 1:1 composition. The higher activity observed from materials obtained by sodium borohydride reduction compared to materials obtained by sodium napthalide reduction is not unexpected, since we have established that the surface contamination with side species (mainly

organics) in the later case is much higher resulting in cleaner materials with the former method.

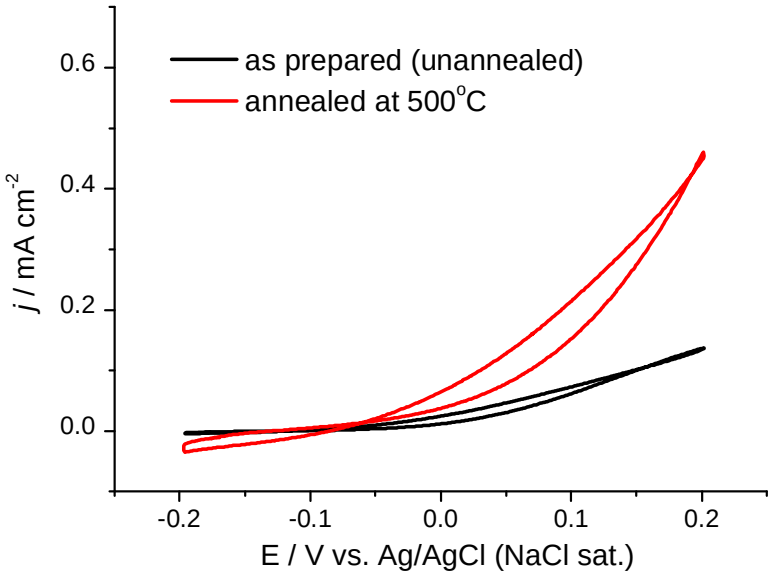

Figure 6.17: Cyclic voltammograms of the Pt-Cd phases obtained by co-reduction of $Pt(acac)_2$ and $Cd(acac)_2$ with sodium napthalide in 1:1 ratio in 0.5 M formic acid, 0.1 M H_2SO_4 at electrode rotation rate of 2000 rpm and scan rate 10 mV/sec.

High activity towards formic acid oxidation was also observed with Pt-Cd alloy phases synthesized by co-reduction of K_2PtCl_6 and $CdCl_2$ with $NaBH_4$ in ratios 9:1 and 8:2. As discussed in the results and discussions section, the former reaction gave two products comprising of the smaller and bigger particles. The product with larger particles, showed to contain the highest amount of Cd by EDS, was the one to show highest activity amongst all Pt-Cd samples (Figure 6.18). Stability over multiple cycles was also improved in these materials compared to the earlier ones. This results are consistent with the expectations from the combinatorial studies that Pt rich alloys

with Cd (with high Pt %) should be reasonable catalysts for oxidation of small molecules was accurate. These materials are now being tested for MeOH oxidation and the same Pt –Hg sample found active for formic acid oxidation has also shown MeOH oxidation activity in the preliminary experiments.

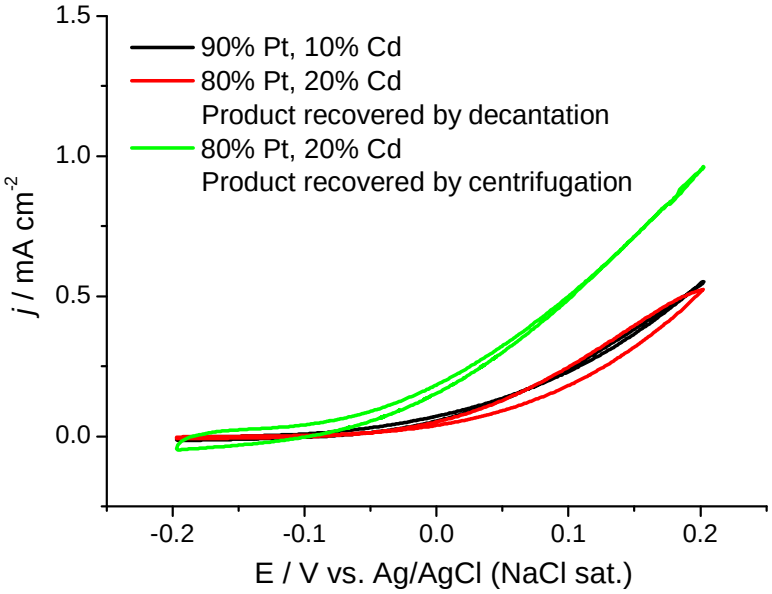

Figure 6.18: Cyclic voltammograms of the Pt-Cd phases obtained by co-reduction of K_2PtCl_6 and $CdCl_2$ with $NaBH_4$ with high Pt precursor ratio in 0.5 M formic acid, 0.1 M H_2SO_4 at electrode rotation rate of 2000 rpm and scan rate 10 mV/sec.

6.5 Conclusions

We have been able to synthesize intermetallic and alloy Hg-Pt and Cd-Pt nano-phases and have shown that some of them are active catalysts. In the Pt-Hg system, Hg_4Pt and Hg_2Pt: were always found to form with the syntheses schemes studied in this work.

The active catalysts obtained were found to be Pt rich. Hence exploring ways to generate single phase, Pt rich nanomaterials would be the next step for the Pt-Hg system.

For the Pt-Cd system, the synthesis of ordered PtCd as a single phase could be demonstrated by both sodium napthalide and sodium borohydride reduction. Obtaining Pt rich single phase alloys was also possible, and activity obtained from all the Pt-Cd materials was good, but not as good as PtPb. Addressing the stability issues (refer to the voltammograms) would be the next step for the Pt-Cd catalysts. We have also demonstrated that metals co-reduced with Pt by $NaBH_4$ form intermetallic phases as nano-materials. These nucleate and grow to a point where they can be characterized by diffraction at room temperature, or by annealing at temperatures as low as 300 ^{o}C. This in-turn gives us size control – vital for catalyst materials. These studies pave the way for further pursuit of reducing agents like nBuLi (discussed in Chapter 5) for devising a generalized method that could work for elements across the periodic table for synthesizing clean nanomaterials at low temperatures. This work provides a side by side comparison of the sodium borohydride and the sodium napthalide methods, from synthesis to electrochemical testing of the materials. This is valuable for understanding solution phase co-reduction of metal precursor for synthesis of binary (or multi-component) nano-phases.

REFERENCES

1. Gregoire, J. M.; Kostylev, M.; Tague, M. E.; Mutolo, P. F.; van Dover, R. B.; DiSalvo, F. J.; Abruna, H. D., High-Throughput Evaluation of Dealloyed Pt-Zn Composition-Spread Thin Film for Methanol-Oxidation Catalysis. *Journal of the Electrochemical Society* **2009,** 156, (1), B160-B166.

2. Gregoire, J. M.; Lobovsky, M. B.; Heinz, M. F.; DiSalvo, F. J., Resputtering phenomena and determination of composition in codeposited films. *Physical Review B* **2007,** 76, (19).

3. Gregoire, J. M.; van Dover, R. B.; Jin, J.; DiSalvo, F. J.; Abruna, H. D., Getter sputtering system for high-throughput fabrication of composition spreads. *Review of Scientific Instruments* **2007,** 78, (7).

4. Okamoto, H., *Desk handbook: Phase diagrams for binary alloys*. Illustrated ed.; ASM International.

5. Miedema, A. R.; Dechatel, P. F.; Deboer, F. R., Cohesion in Alloys - Fundamentals of a Semi-Empirical Model. *Physica B & C* **1980,** 100, (1), 1-28.

6. Roychowdhury, C. Intermetallic nanoparticles for fuel cell applications: syntheses and characterization studies. Cornell University, 2008.

7. Roychowdhury, C.; Matsumoto, F.; Zeldovich, V. B.; Warren, S. C.; Mutolo, P. F.; Ballesteros, M.; Wiesner, U.; Abruna, H. D.; DiSalvo, F. J., Synthesis, characterization, and electrocatalytic activity of PtBi and PtPb nanoparticles prepared by borohydride reduction in methanol. *Chemistry of Materials* **2006,** 18, (14), 3365-3372.

8. Roychowdhury, C.; Matsumoto, F.; Mutolo, P. F.; Abruna, H. D.; DiSalvo, F. J., Synthesis, characterization, and electrocatalytic activity of PtBi nanoparticles prepared by the polyol process. *Chemistry of Materials* **2005,** 17, (23), 5871-5876.

9. Alden, L. R.; Roychowdhury, C.; Matsumoto, F.; Han, D. K.; Zeldovich, V. B.; Abruna, H. D.; DiSalvo, F. J., Synthesis, characterization, and electrocatalytic activity of PtPb nanoparticles prepared by two synthetic approaches. *Langmuir* **2006,** 22, (25), 10465-10471.

10. Carper, J., The CRC Handbook of Chemistry and Physics. **1999,** 124, (10), 192.

Chapter 7

INTERMETALLICS AND Pt MONOLAYER DEPOSITION BY UPD: POTENTIAL FOR PROMISING ORR CATALYSTS

7.1 Introduction

Several ordered Pt intermetallics have been shown to be better catalysts for small molecule oxidation by research groups in CFCI (e.g. PtPb for formic acid oxidation)[1, 2]. As described in the previous chapters, the challenges associated with obtaining these intermetallics as nanoparticles (which is critical for application in real fuel cells), are numerous. As discussed in the previous chapters, these challenges were explored and addressed from several directions. At the same time, in the combinatorial effort at CFCI, a constant search for even higher activity and lower cost catalysts is ongoing. Simultaneously, given the higher electrochemical stability of the ordered intermetallics, their possible applications as cathode catalysts also need to be explored. Thus, when an opportunity to work with the Adzic group at Brookhaven National Laboratories (our longtime collaborators in the CFCI) arose, I chose to explore the catalytic potential of intermetallic compounds for the oxygen reduction reaction (ORR). The Adzic group in BNL, has reported for a long time significant increases in activity of the existing catalysts by deposition of a single monolayer of Pt on their surface.

If the starting catalyst is Pt free (as in the alloy Pd-Fe systems explored in the Adzic group) this method could result in significant reduction of catalyst cost along with improvement of activity. Now, if we started with ordered intermetallics, and were able to obtain good activity by depositing Pt monolayer on their surface, we could possibly add 'stability' to the above equation. In this chapter the initial exciting results from a combination of the two very powerful approaches mentioned above are discussed.

This chapter is partially adopted from a paper submitted for publication to the *Journal of the American Chemical Society.*

7.2 Choice of the intermetallic compounds to be explored

Pt phases: PtPb was the first choice for the Pt intermetallic to be explored because it is the phase whose syntheses in nanoparticle form, characterization and activity for methanol and formic acid oxidation has been the most explored and documented[1-4]. Also, single crystals of the PtPb intermetallic compound are available (synthesized in Stockbarger furnace) for future experiments that would be necessary to study the surface of the catalyst. Pt_3Cr (a cubic intermetallic phase) and PtNi (tetragonal intermetallic phase) were also explored, since nanoparticle samples were available (Chapter 4). However, for these two phases, only initial experiments could be carried out owing to time constraints.

Pd phases: Pd compounds would be more desirable in terms of cost as starting point catalysts than Pt compounds. The current (8/9/09) cost of Pd is $275/oz while that of Pt is $1265/oz. PdFe was chosen as a base since the Adzic group had worked extensively with Pd-Fe alloys and they have showed promising results[5, 6]. Pd-Ni and Pd-Co, other alloys being investigated in the Adzic group[7], would also be interesting. Unfortunately, however, Pd is not known to form ordered compounds with Co and Ni.

At first, Pb and Cu systems with Pd were not considered since these metals leached out of the alloy at high potentials (~ +0.8 V). Pd –Cr/Ti/V might be promising. However, previous experience with nanoparticle synthesis involving Cr, V and Ti compounds has shown that these reactions are extremely difficult to control (Chapter 4). These issues have been discussed in Chapter 3 and 4. However, if our initial results obtained were encouraging, it would open a huge area to explore and the synthetic complexities might be worth enduring. We describe some work with PdPb at the end of this Chapter which was started after the success with PtPb. Table 7.1 summarizes the different Pd systems (alloys/intermetallics) that can be explored.

7.3 Synthesis of the intermetallics

7.3.1 Experimental

7.3.1.1 Napthalide reduction

Materials: Naphthalene was purchased from Fisher. Sodium metal and diglyme were purchased from Aldrich. THF and diglyme were freshly distilled over sodium prior to use. Lead(II)2-ethylhexanoate was purchased from STREM Chemicals Inc. Because of the high viscosity of lead(II)2-ethylhexanoate, 0.05M stock solutions were prepared by dissolving 2.496 g in 100 mL THF.

Table 7.1: Summary of standard reduction potentials of different elements for consideration of co-reduction with Pd. The parentheses depict the oxidation state for which the reduction potential is given, When nothing is specified, the potential is for conversion to the zero valent metal from the most common oxidation state.

Metal 1	E red	Metal 2	E red	Ordered phases exist?
Pd	0.951	Fe	-0.44 (+2)	Yes
			-0.037 (+3)	
			0.77 (+3 to +2)	
		Pb	-0.13	Yes
		Cu	0.34	Yes
		Zn	-0.76	Yes
		Bi	0.317 (+3)	
			2 (+5)	
		Ni	-0.23	No
		Co	-0.28	No
		Re	1.72 (+6)	No
			0.276 (+4)	
		Cr	-0.74 (+3)	yes
			-0.913 (+2)	
		V	-1.17(+2)	yes
		Ti	-1.37	yes
		Ta	-0.81 (+5)	
		W	-0.119 (+4)	
			-0.090 (+6)	
		In	-0.33 (+3)	yes
			-0.126 (+1)	

Synthesis of PtPb nanoparticles: A solution of sodium napthalide was prepared by weighing out stoichiometric amounts of naphthalene (0.1923 g, 1.50 mmol) and sodium metal (0.0345g, 1.50 mmol) in an argon atmosphere glovebox and loading these reactants into a flask containing 50 mL diglyme or THF. The flask was sealed and removed from the glovebox and stirred overnight under argon to produce a dark green sodium napthalide solution.

Platinum acetylacetonate (0.0988 g.0.25 mmol) was dissolved in a 5.0 mL aliquot of a 0.05 M stock solution of lead(II)2-ethylhexanoate in diglyme (0.25 mmol lead(II)2-ethylhexanoate). Meanwhile, an argon purged flask containing the freshly prepared sodium napthalide was connected to a water cooled condenser. The aliquot of metal precursors was injected into the dark green sodium napthalide solution which immediately became black and opaque. Following the injection, the flask was stirred for 30 min at room temperature. The reaction mixture was cannula transferred into a centrifuge tube and was centrifuged for 10 min at 2000 rpm. The diglyme was syringed off leaving a black residue. 40 mL of degassed ethanol was added to the flask, which was then sonicated in an immersion bath sonicator for 10 min. The supernatant (colored yellow) was removed and 40 mL of hexanes were distilled into the black precipitate. The tube was sonicated for 10 min and centrifuged again. The supernatant (usually colorless) was removed and the black precipitate was dried under vacuum. The tube was then backfilled with argon, and was left overnight with a needle in the septum to allow slow exposure of the nanoparticles to air[4].

7.3.1.2 Synthesis of PdFe nanoparticles

A reported procedure from Ray Schaak group[8] for other Pd alloys was followed for PdFe nanoparticle synthesis. Precursors used were $PdCl_2$ and $FeCl_2.4H_2O$. 0.034

mmol each of the precursors along with 120 mg of poly(vinylpyrrolidone) (PVP, MW = 40000) were added to 25 ml degassed MeOH. The mixture was stirred for 30 min under Ar, 25 ml of 0.01 M $NaBH_4$ solution was added to it and stirred for 3 h. The product was isolated by centrifugation, washed with MeOH repeatedly and dried. The reaction was repeated by substituting stirring of the mixture with sonicating to ensure more efficient mixing (in some cases, metallic Fe or FePd can stick to the magnetic stir bar, which was avoided by using a sonicator.).The resulting product was characterized by XRD and annealed to different temperatures to target the different intermetallic phases of Pd-Fe system.

7.3.1.3 Synthesis of the nanophase PdPb

0.9 mmol each of $Pb(C_2H_3O_2)_2.3H_2O$ and $Na_2PdCl_6.4H_2O$ was dissolved in 40 ml of degassed methanol (degassed with argon for 1 hr) in 2 necked round bottom flask. The solution was stirred under argon. 1.8 mmol of $NaBH_4$ was dissolved in 10 ml of the degassed MeOH and was poured into the precursor solution through the side arm of the flask. Immediate reduction was observed along with vigorous bubbling. The bubbling was allowed to subside, and the arm was closed with a stopper. After 15 min, black mass was found to be settling down at the bottom of the flask. The solution was stirred overnight under argon and the black particles were collected the next day. After repeated washing with de-ionized water, the particles were rinsed with acetone and dried under vacuum. The product was characterized by X-ray diffraction. The sample was then annealed in a silica tube sealed under vacuum at 300 ^oC for 12 hr to obtain ordered phases. The annealed sample was also characterized by X-ray diffraction (Figure 7.1). The annealed product was found to be a mixture of Pd_3Pb and Pd_5Pb_3 intermetallics.

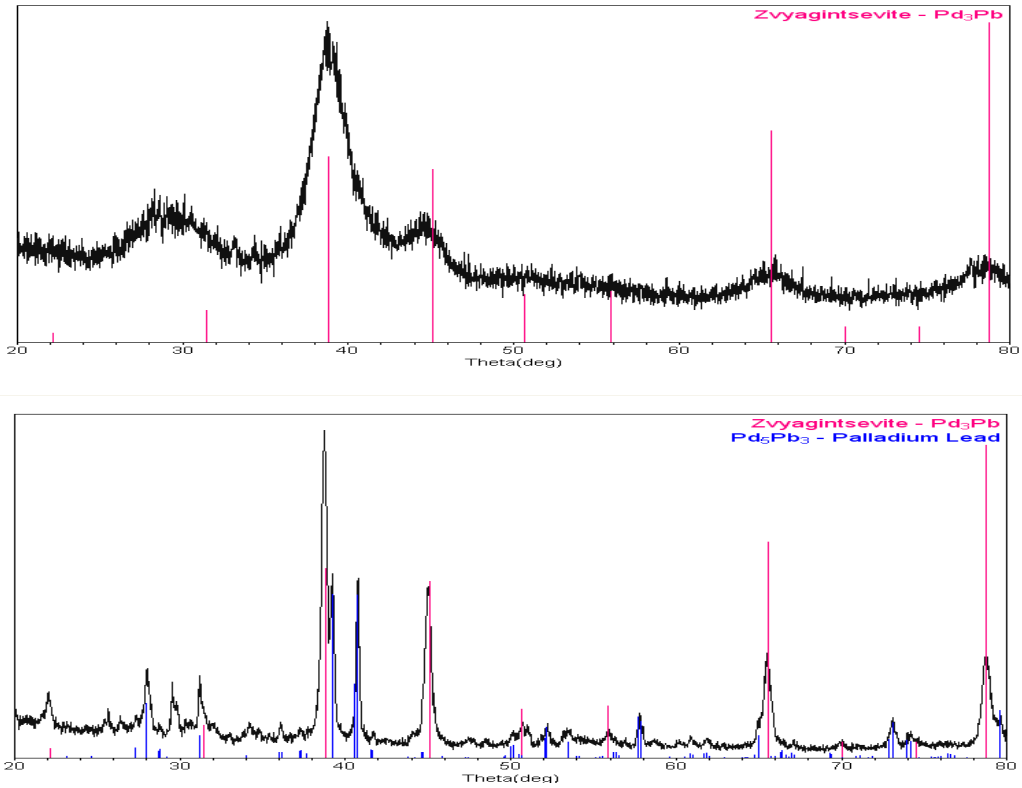

Figure 7.1: X-ray diffraction patterns of PdPb phases synthesized. (Top) product obtained at room temperature, (bottom) product obtained after a 12 hr, 300 ^{o}C anneal. Lines indicate the peak positions for Pd_3Pb (PDF # 00-020-0827) and Pd_5Pb_3 (PDF # 00-026-1151).

7.3.1.4 Characterization

XRD, SEM, TEM, EDS, BET and IR were done on the PtPb sample. The data is summarized in table 7.2. XRD, SEM, EDS and IR were done on the PdFe sample, and the data is summarized in table 7.3. The instruments specifications and sample preparation techniques for each of these have been described in Chapter 2, 3 and 4.

Table 7.2: Characterization data for PtPb sample used.

PtPb	EDS Pt: Pb ratio (at %)	BET surface area (m^2/gm)	Domain size (nm, Scherrer equation)	XRD
	1: 1	7.3	18	Single phase PtPb

7.3.2 Discussions on synthesis

The various aspects of PtPb synthesis have been discussed extensively in Chapter 1. Since the synthesis of ordered (or disordered) Pd-Fe phases were not attempted in the DiSalvo group before, in this section, we will discuss some key observations from Pd-Fe synthesis efforts. It's worthwhile to mention here that the synthesis of Pd-Fe phases discussed in this Chapter were physically undertaken at BNL in the Adzic group, as were the electrochemical experiments, although the other characterizations methods were used at Cornell University. The absence of a Schlenck line and argon atmosphere box in the Adzic group at BNL limited the use of sophisticated air free techniques while targeting these phases. That is why only sodium borohydride reduction method was undertaken. Electrochemical experiments along with XRD suggested presence of impurities.

Since polyvinylpyrrolidone (PVP) was used during the syntheses, IR (ATR) was taken on the solid samples to identify possible impurities. While no evidence of PVP was found on any of the annealed samples, the as prepared samples did show evidence of PVP. It is likely that PVP decomposes on annealing. The IR for annealed samples (550 ^{o}C and 700 ^{o}C) showed strong absorption in the finger print region, which could not be ascribed to particular organic species.

Table 7.3: Summary of characterization data for as prepared and annealed PdFe samples synthesized using stirring or sonication as the method of mixing the precursors during the reaction. The rest of the product in each case was detected as C and O.

PdFe	EDS Pd: Fe ratio (atm%)	Domain size (nm,Scherrer equation)	XRD pattern shows:
Stirring, as prepared	16 :20	17.9	Pd (cubic)
Stirring, Annealed 550 ^{o}C, 4 hr	24 : 36	37.4	Pd_3Fe cubic alloy phase, some ordering peaks might be present (intermetallic)
Sonication, as prepared	11 : 39	23.2	
Sonication, 300 ^{o}C, 12 h	18 : 28		Pd (cubic) with peak maxima shifted suggesting Fe incorporation
Sonication, 550 ^{o}C, 4 hr	18 : 36	36	Pd_3Fe cubic alloy phase, some ordering peaks might be present (intermetallic)
Sonication, 700 ^{o}C, 4 hr	17 : 36	58.8	Pd_3Fe cubic alloy phase, some ordering peaks might be present (intermetallic)

EDS on Pd-Fe samples showed them to be iron rich, but XRD indicated otherwise. It is likely that this is due to the semi-quantitative nature of results obtained with powders rather than flat, polished solid angles. Small unidentifiable peaks in XRD might also suggest organic salts present. SEM images (Figure 7.2 a, b, c, d) showed the presence of morphologically different crystallites.

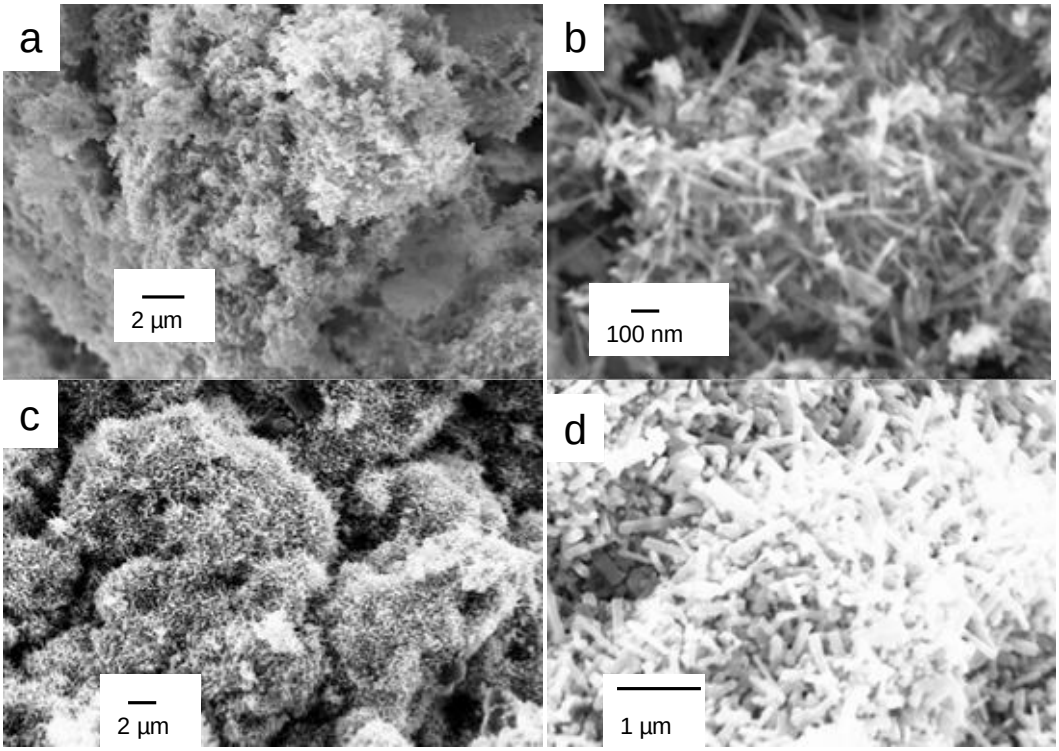

Figure 7.2: SEM images of PdFe samples annealed to 550 ^{o}C (a, b) and 700 ^{o}C (c, d) respectively. For each sample, (b) and (d) are the images taken at higher magnifications.

7.4 Electrochemical experiments

7.4.1 Experimental

Thin film electrodes with nano-electrocatalysts were prepared by placing definite amounts of a nanoparticle suspension in H_2O (1 mg ml^{-1}) onto a flat glassy carbon electrode (5 mm diameter, Pine instrument). For some experiments, the electrode with the nanocatalyst was kept in 1 mM $PdCl_2$ and K_2PtCl_4 solutions for 1 hr to obtain irreversible electro-less adsorption of Pd and Pt respectively. However, no significant changes in surface area were observed on the cyclic voltammograms obtained post this process, suggesting the incorporation of the noble metal from this process, if any, was not significant, and hence has not been included in the calculation of Pt/noble metal loading. These samples are depicted as Pd(el)/PtPb and Pt(el)/PtPb respectively. In some cases a Pt/Pd monolayer was added after the electroless adsorbtion by galvanic replacement of an underpotentially deposited (upd) Cu monolayer on the catalyst (PtPb, Pt(el)/PtPb, Pd(el)/PtPb, PdFe) electrode with Pt atoms. After UPD of Cu from a 50 mM H_2SO_4 + 50 mM $CuSO_4$ solution, the thin film electrode covered with a Cu monolayer was rinsed and kept in a 1.0 mM K_2PtCl_4 + 50 mM H_2SO_4 solution for about 3 min to complete the replacement of Cu with Pt. These samples are depicted as M*(ML)/PtPb and M'(ML)/PtPb with * and ' standing for Pd and Pt electro-less deposition, respectively, attempted prior to deposition of the M monolayer, M being either Pt or Pd (M(ML) = M monolayer). M(el)/PtPb on the other hand depicts the sample where only electro-less deposition was attempted on the PtPb with M solution, M again being either Pt or Pd. For the ORR measurements the electrode was covered with a thin layer of Nafion by placing 5 µL of 5 wt % Nafion solution on the electrode followed by drying in a dessicator.

7.4.2 Results and discussion

The PtPb catalyst suspension was placed on the electrode, and modifications such as Pt or Pd monolayer deposition, electro-less adsorption of Pt or Pd or a combination of these were undertaken and the catalyst systems were then tested for ORR activity. Catalyst performance and activity was found to differ in each case. The same is true for Pd-Fe systems. Table 7.4 summarizes step by step modifications done on each catalyst system tested along with the notations used to refer to them.

As mentioned in the experimental section, in the cases where the electrode with the nanocatalyst was kept in 1 mM $PdCl_2$ and K_2PtCl_4 solutions for 1 hr no significant change in surface area were observed on the cyclic voltammograms obtained. This lack of depositions of Pt or Pd suggests a high stability of the surface of the intermetallic, or a lack of metallic Pb in the surface layer. Since no significant change in surface area was observed post this process, the incorporation of the noble metal from this process, if any, is not significant, and hence has not been included in the calculation of Pt/noble metal loading.

Figure 7.3 shows the ORR polarization curve obtained with the Pt'/PtPb/C and Pt(ML)/PdPb as a thin film RDE . A high activity of the first catalyst is indicated by $E_{1/2}$ = 900 mV; Pt mass activity of 0.03 A/mg based on a calculated Pt monolayer coverage and the initial Pt contained in the PtPb.

Table 7.4: Summary of different catalyst modifications attempted and corresponding notations used to refer to them.

PtPb	Suspension of PtPb in H_2O (1µg/µL) dispersed on electrode
Pt(ML)/PtPb	Pt monolayer placed by galvanic displacement of underpotentially deposited Cu monolayer (Cu upd) with Pt atoms on the PtPb
Pt(el)/PtPb	Electroless deposition of Pt on PtPb attempted by immersing the later in Pt^{2+} solution
Pt'(ML)/PtPb	Electroless deposition of Pt^{2+} attempted, then Pt monolayer deposited (by Cu upd) on the PtPb
Pt*(ML)/PtPb	Electroless deposition of Pd^{2+} attempted, then Pt monolayer deposited (by Cu upd) on the PtPb
Pt(ML)/Pd*(ML)/PtPb	Electroless deposition of Pd^{2+} attempted, then first Pd and then Pt monolayer was deposited (by Cu upd) on the PtPb
Pt(ML)/PdFe(550)	Pt monolayer Cu upd on the PdFe, annealed at 550 ^oC sample
Pt(ML)/PdFe(700)	Pt monolayer Cu upd on the PdFe, annealed at 700 ^oC sample

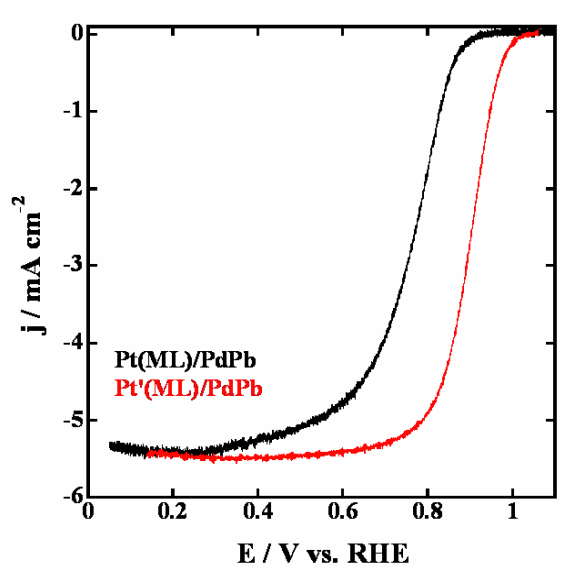

Figure 7.3: Polarization curves for the ORR on Pt'(ML)/PtPb and Pt(ML)/PdPb (inset) in 0.1 M $HClO_4$ solution; sweep rate 20 mV/sec.

Pt/PtPb systems were found to give currents as high as 2.7 mA/cm^{-2} (normalized to the geometric surface area of the electrode) at 0.9 V. Table 7.5 summarizes the results. The highest activity in terms of half wave potential was observed for the Pt'(ML)/PtPb (Pt(ML) = Pt monolayer) system. Owing to the initial higher loading of the catalyst (PtPb), the mass activities are low in spite of high specific activity. To counter this problem, for the best system, the experiments were repeated with lower initial loading of just PtPb and PtPb dispersed on carbon support (Vulcan XC-72).

Table 7.5: Comparison of electrochemical characteristics of the PtPb- and Pd-Fe-based electrocatalysts.

	Half wave potential(V)	J_k (0.9 V) μA/cm^2	mass activity wrt total Pt A/mg
PtPb	**846**	**1391**	**0.03**
Pt(ML)/PtPb	**869.5**	**1938**	**0.04**
Pt(el)/PtPb	**862**	**2241**	**0.03**
Pt'(ML)/PtPb	**899.4**	**5385**	**0.06**
Pt*(ML)/PtPb	**818.3**	**468**	**0.01**
Pt(ML)/Pd*(ML)/PtPb	**808.6**	**1031**	**0.02**
Pt(ML)/PdFe(550)	**848.2**	**2171**	**0.54**
Pt(ML)/PdFe(700)	**779.7**	**130**	**0.13**

The later should ensure higher dispersion even with lower loading and prevent the activity from being affected. Table 7.5 also includes the summary of activities observed for the best Pd-Fe catalysts. Pt mass activity for these systems are off course much higher, given Pt is only deposited in as a monolayer on the Pd-Fe system for these catalysts.

Stability of the catalysts was tested by applying potential steps between 1132 mV and 594 mV at 10 sec intervals. The unsupported catalysts showed no loss of activity after 6000 cycles. Loss of activity was observed in the corresponding supported catalyst, which suggests carbon corrosion or other problems related to the support to be responsible for activity loss. Figure 7.4 compares the activities of the different electrocatalysts towards the ORR at 0.9 V before and after application of the potential steps. After 16,000 cycles, the unsupported catalysts showed activity loss, but entire activity could be recovered by cycling for 20 cycles at 50 mV sec^{-1} in a fresh

electrolyte solution (0.1 M $HClO_4$). This suggests contamination of the electrode surface by spectator species in the solution to be causing the loss of activity observed. Figure 7.5 gives the polarization curves for the Pt'(ML)/PtPb system showing the above results.

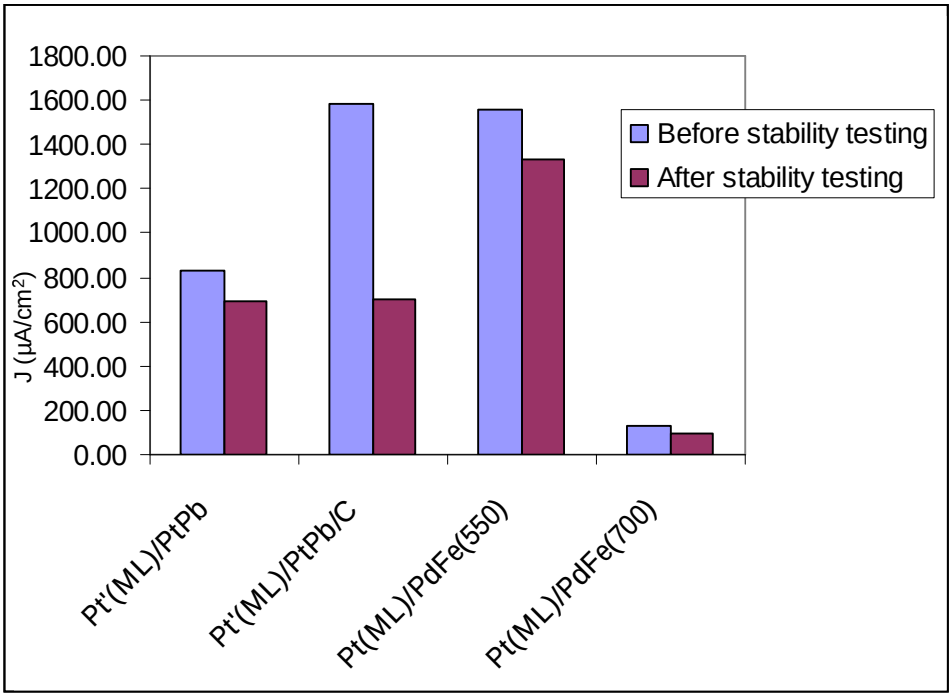

Figure 7.4: Comparison of current densities (normalized with respect to the geometric surface area of the electrode) of the PtPb and PdFe electrocatalysts before and after stability testing by applying 6000 potential steps between 1132 mV and 594 mV at 10 sec intervals.

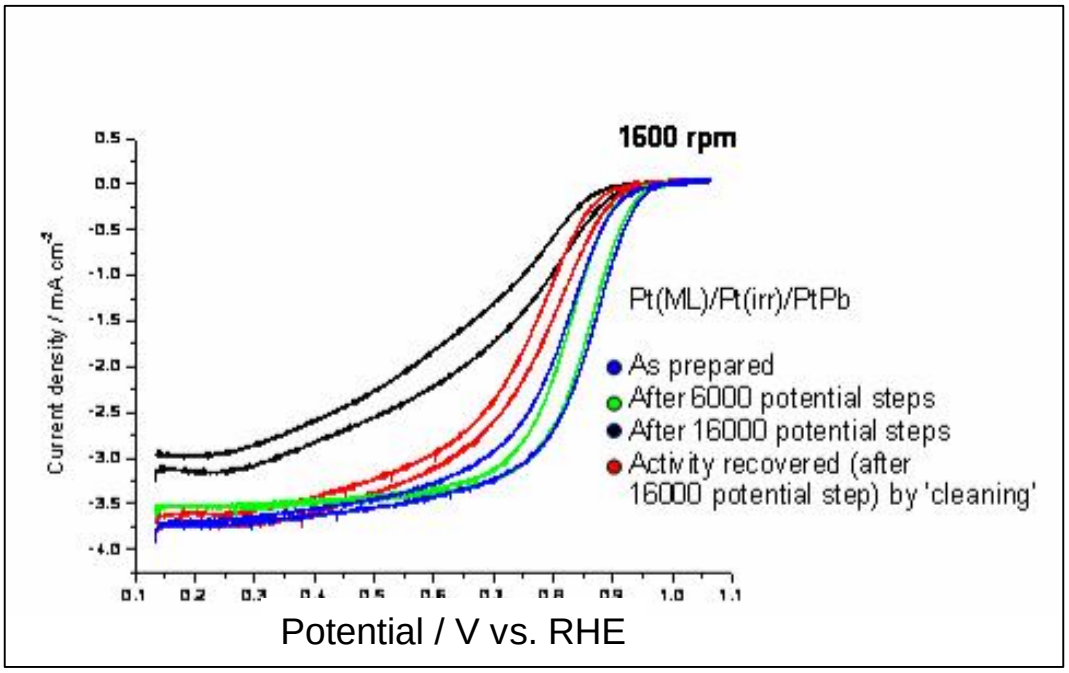

Figure 7.5: Comparison of the polarization curves for the ORR on Pt'(ML)/PtPb before and after applying potential steps (between 1132 mV and 594 mV at 10 sec intervals) in 0.1 M $HClO_4$ solution. Activity lost after 16000 potential steps could be recovered by cycling at 50 mV/sec for 20 cycles in 0.1 M $HClO_4$ solution between -0.2 V and 0.85 V(described as 'cleaning') suggesting surface contamination by spectator species playing a role in the observed activity loss.

The Pd-Fe catalysts were reasonably stable with little or no decline in activity following 5000 cycles of stability testing.

Pt_3Cr and PtNi intermetallics were also tested for oxygen reduction activity (unsupported) – both with and without Pt monolayer deposition by Cu UPD. The activity and hydrogen absorption area from the CVs were found to be very low in all cases. The probable cause is insufficient dispersion of the catalysts in H_2O in the mother solution resulting in much lower solution strength than what was intended and

assumed (1 µgm/µl). Consequently, actual catalyst loading was much lower than what was intended. Most of the catalyst could not be dispersed even after 2 to 4 h of sonication. The data are summarized in table 7.6. The Pt amount from loading would not be accurate and hence, is not included. The next step with these systems would be to use additives like alcohols or dilute acids which should help in achieving higher dispersions. Experiments with C supported systems also need to be done.

Table 7.6: Summary of electrochemical observations for Pt_3Cr and PtNi catalysts.

	Surface area from CV (cm^2)	Half wave potential (mV)	µgm of Pt from UPD	Pt from initial loading of catalyst (µgm)	Total Pt (µgm)
PtNi	**0.27**	**No activity**		**15.4**	**15.4**
PtNi/Pt(ML)	**0.35**	**No activity**	**0.2**	**15.4**	**15.6**
Pt_3Cr	**0.02**	**No activity**		**18.4**	**18.4**
Pt_3Cr/Pt(ML)	**0.02**	**No activity**	**0.2**	**18.4**	**18.6**

Alkaline media experiments with PtPb: Cyclic voltammograms for the PtPb (unsupported) was obtained in alkaline media (0.1 M NaOH solution, freshly prepared) by cycling between potentials from -1.2 V to 0.8 V. CVs (at different sweep rates) were obtained on the same electrode (without washing) in 0.1 M $HClO_4$ after it was removed from the alkaline media. However, no significant information was obtained from these curves as noticeable changes weren't observed by alkaline cycling.
Additional experiments with PdFe systems: PdFe samples investigated showed interesting morphologies under the SEM and suggested the presence of additional surface species (CV and ATR). The cyclic voltammograms obtained for PdFe showed

evidence of Fe dissolution at the initial potential. To understand this effect further, additional experiments were done by obtaining subsequent voltammograms starting at the same or different potentials. The oxygen reduction activity of the catalyst was measured after running these cyclic voltammograms by employing the same electrode (in a fresh electrolyte solution) for testing ORR activity. Some activity loss was observed, but as in the case of PtPb catalysts, the catalyst could be reactivated after 20 cycles (sweep rate 50 mV/sec, scan rate 1600 rpm, between – 0.2 and 0.8 V). Although interesting, the information obtained from these observations are not completely understood at this point, and more experiments remain necessary.

Additional discussions for PdPb: Although PdPb was not an initial system of interest (discussed in the 'choice of intermetallics to be explored' section), given the high stability showed by the PtPb catalyst systems, our hopes were raised about lead containing systems. Also, a viable way to counter the low Pt mass activity problem would be starting with the exact system, just without Pt. Combining the above factors, with the fact that Pd and Pb forms a number of ordered phases, PdPb systems were targeted to be explored. Initial voltammetry of PdPb nanoparticles showed dissolution of Pb. This subsided after several cycles indicating the presence of Pd in the surface layer (Figure 7.6).

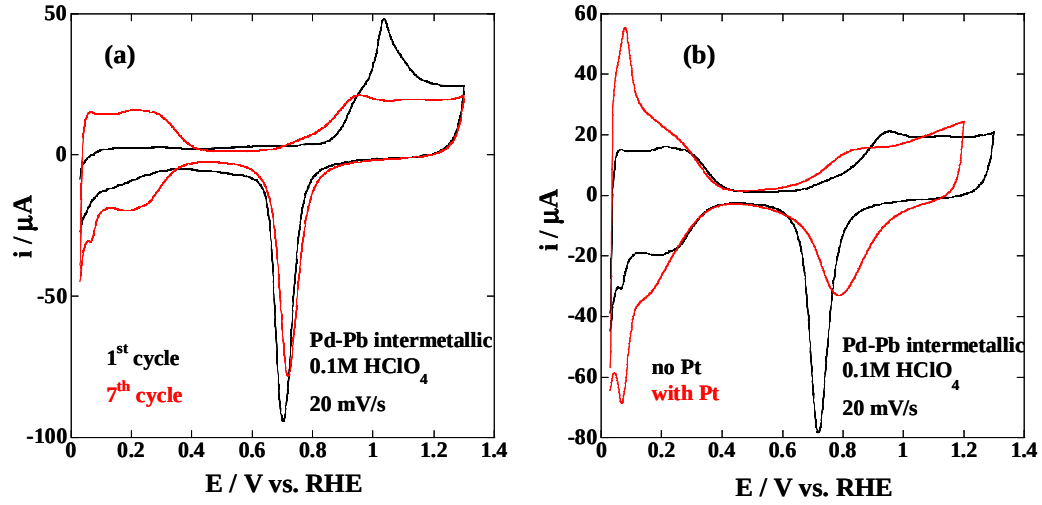

Figure 7.6: a) Cyclic voltammograms of the PdPb intermetallic in 0.1 M $HClO_4$, sweep rate 20 mV/s. The stable CV of the PdPb intermetallic is obtained after 7 cycles between -0.03 V and 1.30 V.b) Cyclic voltammograms of the PdPb intermetallic with and without Pt monolayer deposited.

Voltammetry of a Pt/PdPb/C catalyst showed the onset of PtOH formation at quite negative potential, more negative than that observed for Pt nanoparticles. This implies that the surface will not be a very active ORR catalyst, which was observed in the polarization curve (Figure 7.3). Although the surface layer contains Pd atoms; they are apparently expanded as a consequence of the larger lattice and atomic size of Pb. The electronic properties of a Pt monolayer, particularly the shift of the weighted d-band center, which depends on the cumulative contributions of lattice strain and ligand effect, is likely to account for this phenomenon[9], since the d-band center of metal monolayers is directly linked to the adsorption energies and activation barriers for reactions. The electrochemical experiments with PtPb were done by Adzic group member, Dr. Miomir B. Vukmirovic at the Brookhaven National Laboratory.

7.5 Correlation studies for UPD (underpotential deposition) shift and enthalpy of formation of intermetallic compounds

7.5.1 Background

The term ‘underpotential deposition (upd)’ refers to the electrochemical formation of up to a monolayer of the adsorbate at potentials more positive than the reversible Nernst potential for its bulk deposition. Upd has been observed for a wide variety of substrate/adsorbate combinations, and is very well established. The mechanism and forces behind upd however, although studied extensively, still awaits complete understanding. The academic motivations behind studying upd are many. The very fact that upd exists shows that the chemical potential of atoms deposited at the underpotentials differ from that of the bulk metal and the adatoms are more strongly bound to the surface of the foreign surface than the surface of its own species. Understanding why that is so, may lead to possible prediction of upd shifts (defined variedly, but in simple terms, the potential difference between the bulk and monolayer stripping peaks), and to measures of the binding energy for the pairs in consideration. For example, this attraction between the adatom and substrate was measured by the magnitude of the upd effect (upd shift) and has been used to determine the binding energies of the substrate and adsorbate atoms[10]. A more general definition for upd shift, defined at a given degree of coverage for a substrate adsorbate system is the equilibrium potential of the substrate/adsorbate system at a given coverage, measured with respect to an electrode of the same metal M, both in equilibrium with the same solution containing M^{z+} ions[11]. In such a case, measurement of potentials at different coverage degrees by the adsorbate may deliver direct information about binding of the

adsorbed atoms. These tasks however, are easier said than done, and numerous studies have been undertaken till date in this direction, we discuss some of them below.

Starting with the idea that electrostatic interactions have to play a dominant role is the upd phenomena, electronegativity was considered for correlating to the upd shift measured ($\Delta\Phi_{upd}$) for polycrystalline substrates in aqueous and non-aqueous solutions by Kolb, Przasnyski and Gerischer[12-14]. Since the work functions of solids are known more accurately than electronegativities, and are linearly related to Pauling's electronegativities of the corresponding atoms[15, 16], the substrate/adsorbate work function difference was plotted against $\Delta\Phi_{upd}$ by Kolb *et al.*[12] Another treatment by Trasatti at the onset of upd (degree of coverage, $\Theta = 0$)predicts a linear relationship of unit slope between underpotential shift and work function differences based on the argument that the bond between the substrate and adsorbate is fully ionic in this limit[17]. These treatments work well for polycrystalline substrates but break down for upd on single crystal faces[18], particularly for more compact faces where interactions between the adatoms are expected to be large. In a more general way, from a thermodynamic point of view, the upd shift is related to chemical potential (or binding free energy change) difference between S/M (where S and M stands for the substrate and adsorbate respectively) and M/M pairs[19, 20]. These terms (binding free energy change) have solvent effects included and is purely dependent on work function only when the bonding is purely ionic and adatom-adatom interactions can be neglected (e.g. Trasatti 's treatment at low coverage with the adion assumption). The upd shift has also been treated in terms of electron and ion core properties by neglecting solvent effects and considering the free energy of the substrate/adsorbate system as a function of two constituents: metal ion cores and valence electrons. The resulting equation has been used for obtaining information about ion cores for substrate adsorbate systems by expolating results from solid/vacuum interface to the electrochemical system[11]. Other

treatments include phenomenological analysis for both aqueous and non-aqueous systems (acetonitrile, propylene carbonate) which takes into account solvent effects and was used to estimate upd shifts with good agreements to the experimental data using work function differences, lattice co-ordination numbers and adsorption energies of solvent dipoles. This treatment showed linear variation of upd shift with Θ, where the intercept and slope depends on the free energy change for water desorption, work function differences and enthalpies of S-M and M-M bonds for chosen solvents[21].

The density functional method has proved to be a very powerful tool for the electronic structure of complex solids. A density functional theorem (dft) jellium model for polycrystalline surfaces accounted for higher UPD shifts with higher work function difference and forecast the role of surface energies. The model was extended to single crystal surfaces[22-24]. In general, density functional approaches are useful for understanding the general trends of upd phenomena. Binding energies, upd shifts, lattice constants of adsorbates, induced image charges and related properties can be calculated. But so far sensible results are limited to sp metals. Detailed discussions on any of the treatments mentioned above are beyond the scope of this work. The interested reader should refer to the references for further understanding of the upd phenomena and its implications.

What we set to do here, is to try another approach towards understanding the upd phenomena – by correlating the upd shifts (experimental) of a substrate/adsorbate pair to the calculated enthalpies of formation of an intermetallic phase between them (calculated using the Miedema model). Since electronegativity (related to the work function) difference is considered to be the major factor contributing towards the enthalpy of formation of intermetallic compounds between two elements, a correlation should exist between the later and the upd shift. The enthalpies calculated using the Miedema model contains work function and electron density terms and depends on the

stoichiometry of the compounds (to be discussed in the next section). Hence, the nature of the correlation should provide information about factors controlling upd shifts and binding at the surface. We intend to start with data from aqueous systems and extend to other solvents if possible. Density functional calculations will be done following the initial work to further the analysis by students in the DiSalvo group.

7.5.3 Results and discussion

This work is currently at a very primary stage with no significant results to be discussed. Initial enthalpy calculations using the Miedema model[25] shows some correlation between the relative binding energies (calculated from experimental upd shift values in aqueous media[12], and enthalpies of formation of intermetallic compounds of the metal pairs studied (Figure 7.7).

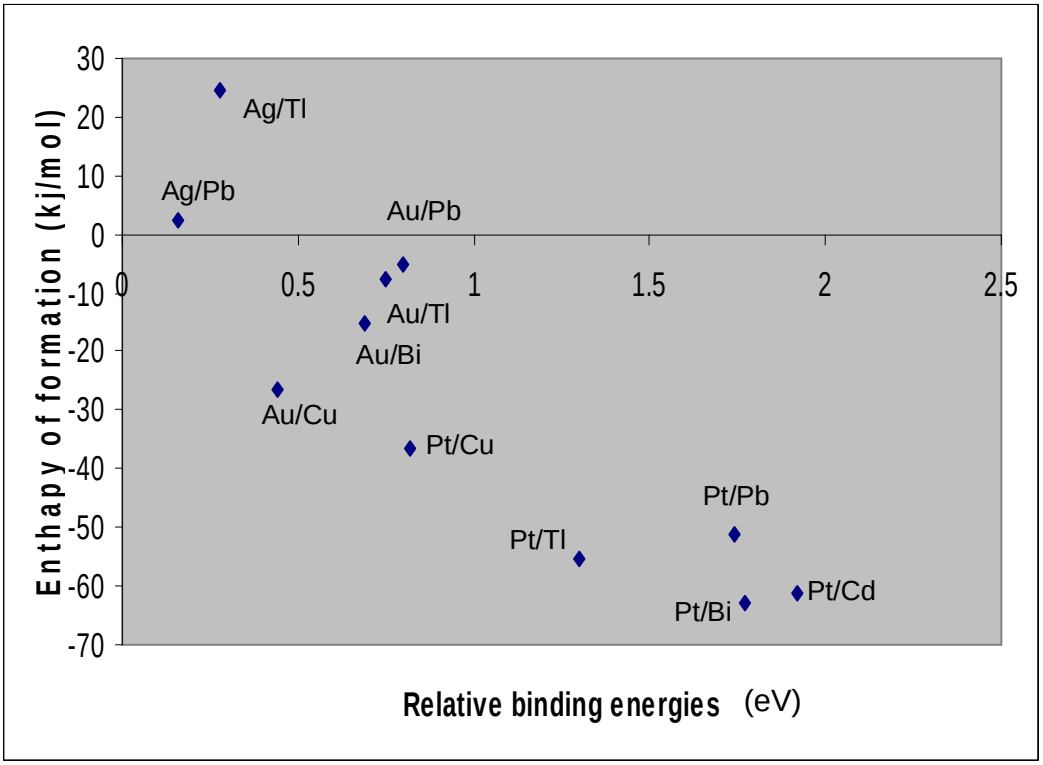

Figure 7.7: Enthalpies of formation of intermetallic compounds for different metal-metal pairs plotted with respect to their relative binding energies calculated from upd shifts[12].

7.6 Conclusions

In conclusion, in this section we have demonstrated the formation of a new class of core-shell electrocatalysts for the ORR comprising a Pt monolayer shell and ordered intermetallic compound cores. We have coupled highly stable, less expensive intermetallics with a Pt monolayer (high activity, low metal content). These electrocatalysts exhibit high activity and very high stability. Our data indicate strategies suitable for selecting the types of intermetallic compounds as the support for

a Pt monolayer. We consider that this fabrication method holds excellent potential for creating efficient fuel cell electrocatalysts. For further work in this topic, more experiments need to be done, especially on bulk (single crystal) surfaces in order to understand the surface phenomena for PdFe and also for PtPb. These studies would provide significant insight towards the electrochemistry observed with these materials before and after monolayer deposition. Lastly, preliminary correlation studies of the bulk enthalpy of formation and the upd described in the last section need to be complimented with density functional calculations.

REFERENCES

1. Roychowdhury, C.; Matsumoto, F.; Zeldovich, V. B.; Warren, S. C.; Mutolo, P. F.; Ballesteros, M.; Wiesner, U.; Abruna, H. D.; DiSalvo, F. J., Synthesis, characterization, and electrocatalytic activity of PtBi and PtPb nanoparticles prepared by borohydride reduction in methanol. *Chemistry of Materials* **2006,** 18, (14), 3365-3372.

2. Alden, L. R.; Roychowdhury, C.; Matsumoto, F.; Han, D. K.; Zeldovich, V. B.; Abruna, H. D.; DiSalvo, F. J., Synthesis, characterization, and electrocatalytic activity of PtPb nanoparticles prepared by two synthetic approaches. *Langmuir* **2006,** 22, (25), 10465-10471.

3. Roychowdhury, C.; Matsumoto, F.; Mutolo, P. F.; Abruna, H. D.; DiSalvo, F. J., Synthesis, characterization, and electrocatalytic activity of PtBi nanoparticles prepared by the polyol process. *Chemistry of Materials* **2005,** 17, (23), 5871-5876.

4. Ghosh, T.; Matsumoto, F.; McInnis, J.; Weiss, M.; Abruna, H. D.; DiSalvo, F., PtPb nanoparticle electrocatalysts: control of activity through synthetic methods. *Journal of Nanoparticle Research* **2009,** 11, (4), 965-980.

5. Shao, M. H.; Sasaki, K.; Liu, P.; Adzic, R. R., Pd3Fe and pt monolayer-modified Pd3Fe electrocatalysts for oxygen reduction. *Zeitschrift Fur Physikalische Chemie-International Journal of Research in Physical Chemistry & Chemical Physics* **2007,** 221, 1175-1190.

6. Shao, M. H.; Sasaki, K.; Adzic, R. R., Pd-Fe nanoparticles as electrocatalysts for oxygen reduction. *Journal of the American Chemical Society* **2006,** 128, (11), 3526-3527.

7. Shao, M. H.; Huang, T.; Liu, P.; Zhang, J.; Sasaki, K.; Vukmirovic, M. B.; Adzic, R. R., Palladium monolayer and palladium alloy electrocatalysts for oxygen reduction. *Langmuir* **2006,** 22, (25), 10409-10415.

8. Schaak, R. E.; Sra, A. K.; Leonard, B. M.; Cable, R. E.; Bauer, J. C.; Han, Y. F.; Means, J.; Teizer, W.; Vasquez, Y.; Funck, E. S., Metallurgy in a beaker: Nanoparticle toolkit for the rapid low-temperature solution synthesis of functional multimetallic solid-state materials. *Journal of the American Chemical Society* **2005,** 127, (10), 3506-3515.

9. Greeley, J.; Mavrikakis, M., Alloy catalysts designed from first principles. *Nature Materials* **2004,** 3, (11), 810-815.

10. Gerischer, H.; Kolb, D. M.; Sass, J. K., Study of Solid-Surfaces by Electrochemical Methods. *Advances in Physics* **1978,** 27, (3), 437-498.

11. Leiva, E., Recent developments in the theory of metal upd. *Electrochimica Acta* **1996,** 41, (14), 2185-2206.

12. Kolb, D. M.; Przasnys.M; Gerische.H, Underpotential Deposition of Metals and Work Function Differences. *Journal of Electroanalytical Chemistry* **1974,** 54, (1), 25-38.

13. Gerische.H; Kolb, D. M.; Przasnys.M, Chemisorption of Metal Atoms on Metal-Surfaces in Correlation to Work Function Differences. *Surface Science* **1974,** 43, (2), 662-666.

14. Kolb, D. M.; Gerischer, H., Further Aspects Concerning Correlation between Underpotential Deposition and Work Function Differences. *Surface Science* **1975,** 51, (1), 323-327.

15. Gordy, W.; Thomas, W. J. O., Electronegativities of the Elements. *Journal of Chemical Physics* **1956,** 24, (2), 439-444.

16. Trasatti, S., Work Function, Electronegativity, and Electrochemical Behaviour of Metals .2. Potentials of Zero Charge and Electrochemical Work Functions. *Journal of Electroanalytical Chemistry* **1971,** 33, (2), 351-&.

17. Trasatti, S., Development of Work Function Approach to Underpotential Deposition of Metals - Application to Hydrogen Evolution Reaction. *Zeitschrift Fur Physikalische Chemie-Frankfurt* **1975,** 98, (1-6), 75-94.

18. Schultze, J. W.; Dickertmann, D., Potentiodynamic Desorption Spectra of Metallic Monolayers of Cu, Bi, Pb, Tl, and Sb Adsorbed at (111), (100), and (110) Planes of Gold Electrodes. *Surface Science* **1976,** 54, (2), 489-505.

19. Schmickler, W., A Model for the Adsorption of Metal-Ions on Single-Crystal Surfaces. *Chemical Physics* **1990,** 141, (1), 95-104.

20. Leiva, E., *Current topics in electrochemistry* **1993,** 2, 269.

21. Sudha, V.; Sangaranarayanan, M. V., Underpotential deposition of metals - Progress and prospects in modelling. *Journal of Chemical Sciences* **2005,** 117, (3), 207-218.

22. Lang, N. D., Theory of Work-Function Changes Induced by Alkali Adsorption. *Physical Review B* **1971,** 4, (12), 4234-&.

23. Leiva, E.; Schmickler, W., A Model for the Adsorption of a Monolayer of a Metal on a Foreign Metal-Substrate. *Chemical Physics Letters* **1989,** 160, (1), 75-79.

24. Lehnert, W.; Schmickler, W., A Model for the Adsorption of a Commensurate Layer of Metal-Ions on a Single-Crystal Substrate. *Journal of Electroanalytical Chemistry* **1991,** 310, (1-2), 27-37.

25. Miedema, A. R.; Dechatel, P. F.; Deboer, F. R., Cohesion in Alloys - Fundamentals of a Semi-Empirical Model. *Physica B & C* **1980,** 100, (1), 1-28.

Chapter 8

CONCLUSION AND FUTURE DIRECTIONS

The work discussed in this dissertation addresses the synthesis and applications of alloy and intermetallic (ordered compounds) catalyst nanomaterials. Prior to this work, nano-phase synthesis of these materials for catalyst applications without using surfactants was explored for only a few systems (Pt-Pb, Pt-Bi and Pt-Ti). Although encouraging catalytic activities were observed with the synthesized products, not all the challenges were identified and overcome. The synthetic methods were not extended to all metals across the periodic table, rather the focus was on Pt compounds with Bi and Pb. Lastly, catalytic applications of the synthesized materials were limited to oxidation of small molecules only.

In this work, I started with the already explored phases and tried to improve the synthesis techniques. For PtPb, where obtaining the desired phase by sodium napthalide reduction was possible with low temperature annealing (~110 ^{o}C), I tried to obtain the phase at room temperature. The objective was to have higher control on the size distribution as well as cleaner surfaces. Together, we hoped this would increase the catalytic activity of the PtPb nanoparticles. Indeed I was successful in this quest (Chapter 2).

I next tried to improve the sodium napthalide method, since it is a stronger reducing agent, able to possibly reduce group IV through XV metals. As discussed in Chapter 2, I succeeded in this goal by exploring new Pt precursors and changing the post reaction work up techniques. For Pt-Ti, I tried to understand the underlying factors causing the system to behave differently from PtPb to address the two major challenges faced: high temperature (above 700 ^{o}C) annealing was required to obtain ordered phases, and

loss of Ti from the final product during work-up. The work described in Chapter 3 identifies these factors.

After Pb and Ti, I explored the 3d elements in-between for co-reduction with Pt (or even to be reduced by themselves) to give nano phase materials. In Chapter 4, I discussed the challenges that I have identified through this work, and methods to counter the challenges and limitations that still remain. I have been able to synthesize binary alloy and intermetallic compounds of Pt with Cr, V, Mn, and Ni. Most of these materials have shown at least some electrochemical activity for the oxidation of small molecules.

Most importantly, through the above work, the previously unidentified factors that need to be addressed have been recognized. Doing so has enabled us to consider alternative reducing agents. Some of these have even been explored and their own limitations have been identified. For others, preliminary work has been completed and future research directions have been identified. These alternative reducing agents were discussed in Chapter 5.

As a continuation of the work with different metals across the periodic table, other phases with Cd and Hg have been synthesized, both nano and bulk materials using sodium napthalide as well as sodium borohydride methods. Along with generating some new catalysts, this work provided a side by side comparison of properties of the phases synthesized by different methods. Chapter 6 discusses this work and its implications.

Lastly, these materials and PdPb phases were used as supports for core-shell cathode catalysts in collaboration with the Adzic group at the Brookhaven National Laboratories. The success of this work has broadened the application of these materials from just anode catalysts for oxidation of small molecules to catalysts for the oxygen reduction reaction. In Chapter 7 I discussed this work and possible future

research directions for generating improved catalysts for fuel cell cathodes using these materials.

However, challenges still remain for synthesizing clean, nano (5-10 nm) particles of ordered intermetallic materials at as low a temperature as possible without using surfactants so that the particles remain clean and active. But through this dissertation, the challenges have been identified and addressed wherever possible (Pb, Hg and Cd). In other cases (especially with very reactive metals like Ti, V, Cr and Mn) further research is necessary and has been started in the directions identified in this work. Most importantly, I have been able to explain and predict the observations based on the properties of the non-Pt metal in question.

Last, but not the least, several new catalysts have been successfully synthesized and tested through the work described in this dissertation – doing justice to our motivation for starting this work.